CONTRACTOR REPORT

SAND81-8192/3
UC-62d
Unlimited Release

Alternate Central Receiver Power System, Phase II Volume III—Molten Salt Materials Tests

Martin Marietta Corporation

Prepared by Sandia National Laboratories, Albuquerque, New Mexico 87185 and Livermore, California 94550 for the United States Department of Energy under Contract DE-AC04-76DP00789.

Printed January 1984

Printed in the United States of America
Available from
National Technical Information Service
5285 Port Royal Road
Springfield, VA 22161

NTIS price codes
Printed copy: A02
Microfiche copy: A01

MCR-81-1707
CONTRACT SANDIA-18-6879C

May 1981

FINAL REPORT

ALTERNATE CENTRAL RECEIVER POWER SYSTEM, PHASE II

VOLUME III: MOLTEN SALT MATERIALS TESTS

MARTIN MARIETTA CORPORATION
Denver Division
P.O. Box 179
Denver, Colorado 80201

FOREWORD

This report is submitted by the Martin Marietta Corporation to Sandia Laboratories in accordance with the provisions of contract Sandia No. 18-6879C. This final report consists of the following volumes:

Volume I - Executive Summary

Volume II - Molten Salt Receiver

Volume III - Molten Salt Materials Tests (this volume)

The contract was under the technical direction of Mr. William C. Peila of Sandia Laboratories, Livermore, California. The following organizations have contributed to this work:

1)	Martin Marietta Corporation (Denver)	Program management and overall responsibility for the design, fabrication, and test phases of the Subsystem Research Experiments (SRE's), and for the refinement of the conceptual design of a commercial receiver.
2)	Badger Energy, Inc. (Cambridge)	Selection of critical molten salt components, control system engineering, and structural design of the molten salt system piping. Provide engineering expertise in the areas of design, manufacturing, and operation of molten salt components and subsystems.
3)	Arizona Public Service Company (Phoenix)	Utility observer of the test program at CRTF and contributor to the final report.

TABLE OF CONTENTS

TABLE OF CONTENTS (Continued) Page

LIST OF FIGURES

LIST OF FIGURES (continued) Page

LIST OF FIGURES (continued

LIST OF FIGURES (Continued) Page

LIST OF TABLES

LIST OF TABLES (continued) Page

I. INTRODUCTION & SUMMARY

The objective of the Phase II Alternate Central Receiver program was to demonstrate the feasibility of the molten salt central receiver power system by conducting a series of experiments and using the results to update the commercial-scale design developed during Phase I of the program. The experiments were directed at two levels of inquiry: the systems-level testing of a 5 MW_{th} molten salt receiver---hereafter referred to as the receiver SRE; and the investigation of molten salt chemistry and the compatibility of selected materials with molten salt. Detailed discussion of the receiver testing are contained in Volume II of this report, while the materials tests are the subject of this volume.

The materials and salt chemistry research experiments were designed to answer important questions on the use of molten salt mixtures of sodium and potassium nitrate in solar receiver applications.

The experiments were conducted to provide data in the areas of molten salt stability and materials compatibility which could be used in designing a commercial molten salt solar central receiver power system with a lifetime of 30 years or more. Specific questions addressed in designing these experiments were:

- What materials of construction could meet the design requirements for a solar receiver in a molten salt environment?
- Will molten salt stability be adequate for long term solar use?
- How can the molten salt be repurified or regenerated if degradation occurs?
- What effects may commercial salt impurities have on construction materials?
- Will material surface preparation or finish have an effect on molten salt compatibility?
- Do the mechanical properties of metal alloys change when exposed to molten salt?
- Does a material transport mechanism exist in a flowing molten salt system with a thermal gradient?

Four different categories of tests were conducted: (1) materials compatibility; (2) materials mechanical properties; (3) dynamic testing; and (4) salt chemistry tests. The first two categories were static materials immersion tests. The dynamic testing was conducted in a pumped molten salt loop covering a thermal gradient of 566°C (1050°F) to 288°C (550°F). The molten salt chemistry tests were carried out in test vessels with controlled thermal and atmospheric environments.

Specific questions not addressed in these tests include long term thermal stability of molten salts, thermal cycling effects on mechanical properties of construction alloys, methods of inhibiting or passivating surfaces to prevent salt corrosion, and the effect of incremental temperature and atmospheric changes on salt stability. These and other areas should be addressed in future work.

The results indicate the Incoloy 800 and RA330 are acceptable materials for long-term, high-temperature service [up to 580°C (1075°F)], and that 316 and 316L stainless may be acceptable subject to the results of further study. The results of tests on carbon steel indicate that it is acceptable for low temperature molten salt applications [up to 288°C (550°F)]. None of the low-nickel alloys tested were found to be acceptable for intermediate-temperature service [up to 400°C (750°F)].

We found the stability of the molten salt to be adequate for long-term solar use provided the carbonates and hydroxides are controlled (either with a CO_2/water vapor scrubber, or by regenerating the salt with NO_2).

There were no indications that the effects of surface preparation on mild steel material behavior are significant, and there does not seem to be any direct effect of molten salt exposure on materials properties. We did not find any thermal gradient-induced materials transport mechanisms in the salt flow loop. There are several areas requiring further investigation, and these are detailed in Chapter VII, Conclusions and Recommendations. Included among these are the search for an intermediate-temperature alloy, possibly in the low-chromium ferritic steel family (2-1/4 Cr, 1 Mo). We also need to further investigate the deposits found in the intermediate-temperature sections of the molten salt flow loop.

The remainder of this report is divided into six chapters. Chapters II through V contain descriptions and results of each test conducted. Chapter VI is a discussion of all the results in light of their impact on solar central receiver design, and Chapter VII is a collection of conclusions from the tests and recommendations for future work.

II. SALT CHEMISTRY TESTS

A. ENVIRONMENTAL EFFECTS TESTS

The objective of this test was to determine the long-term deleterious effects of gaseous carbon dioxide and/or water vapor on molten nitrate salt mixtures at 593°C (1100°F). Additional information was gained on the solubilities of carbonate and hydroxide reaction products in molten salt and also on metal alloy (Incoloy 800) compatibility with molten nitrate salts which have been exposed to carbon dioxide and/or water vapor.

1. Test Methods

Reaction vessels containing molten salt at 593°C (1100°F) were exposed to known amounts of carbon dioxide and water vapor over selected test periods according to the test matrix presented in Table II-1. Series A tests consisted of molten salt mixtures which were exposed to ultrapure carrier grade air (Air Products and Chemicals, Inc., Allentown, Pa). This mixture contained less than 2.0 parts per million (ppm) water and less than 0.5 ppm carbon dioxide.

Series B tests exposed molten salt to ultrapure carrier grade air which had first been humidified by passing it through a gas washing bottle containing distilled, deionized water. The gas washing bottle was thermally equilibrated at 31°C (88°F).

Series C tests exposed molten draw salt to dry carrier grade air containing 1% carbon dioxide, and Series D tests exposed the salt to humidified air containing 1% CO_2.

A gas inlet tube was used to bubble the gas mixture through the salt sample in each Incoloy 800 test vessel (Figure II-1). Special test ovens were constructed to maintain the salt samples at the required test temperature. The top part of the vessels extended above the oven lid and were kept below the freezing point of the salt to prevent the salt from creeping out of the container.

Test vessels were cleaned and passivated with molten salt at 593°C (1100°F) for 120 hours prior to test. The test apparatus was assembled as shown in the flow schematic (Figure II-2), and the vessels and all fittings were bubble leak checked prior to use. Figure II-3 is a photograph of the oven arrangement and a CO_2/H_2O test vessel. Thermocouple wires were placed on the outside of each test vessel to measure the degree of temperature variation between the eight individual vessels.

The location of each of the eight test vessels in the high temperature oven, and their respective thermocouple readouts at the beginning of each test is in Figure II-4. The 28-week exposure test was performed in test vessels 8, 2, 3, and 6, and the 1-week, 5-week and 15-week tests were performed in vessels 1, 7, 4, and 5.

Table II-1 Environmental Effects Test Matrix

TEST	GAS PURIFIED AIR	COMPOSITION H_2O	VOL % CO_2	TEST TIME
A1	100%	0	0	1 Wk
A2	↓	↓	↓	5 Wk
A3	↓	↓	↓	15 Wk
A4	↓	↓	↓	6 Mo
B1	BALANCE	100% R.H.	0	1 Wk
B2	↓	↓	↓	5 Wk
B3	↓	↓	↓	15 Wk
B4	↓	↓	↓	6 Mo
C1	BALANCE	0	1.0%	1 Wk
C2	↓	↓	↓	5 Wk
C3	↓	↓	↓	15 Wk
C4	↓	↓	↓	6 Mo
D1	BALANCE	100% R.H.	1.0%	1 Wk
D2	↓	↓	↓	5 Wk
D3	↓	↓	↓	15 Wk
D4	↓	↓	↓	6 Mo

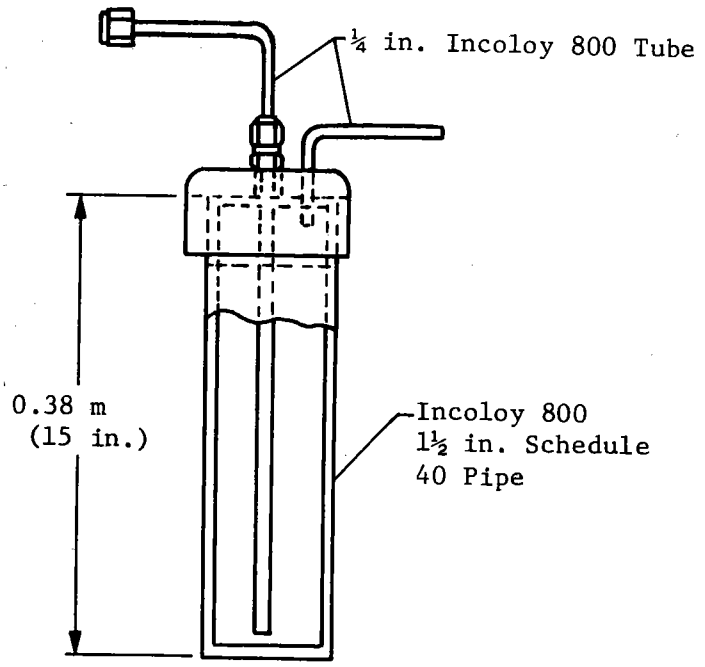

Figure II-1 Environmental Effects Test Vessel

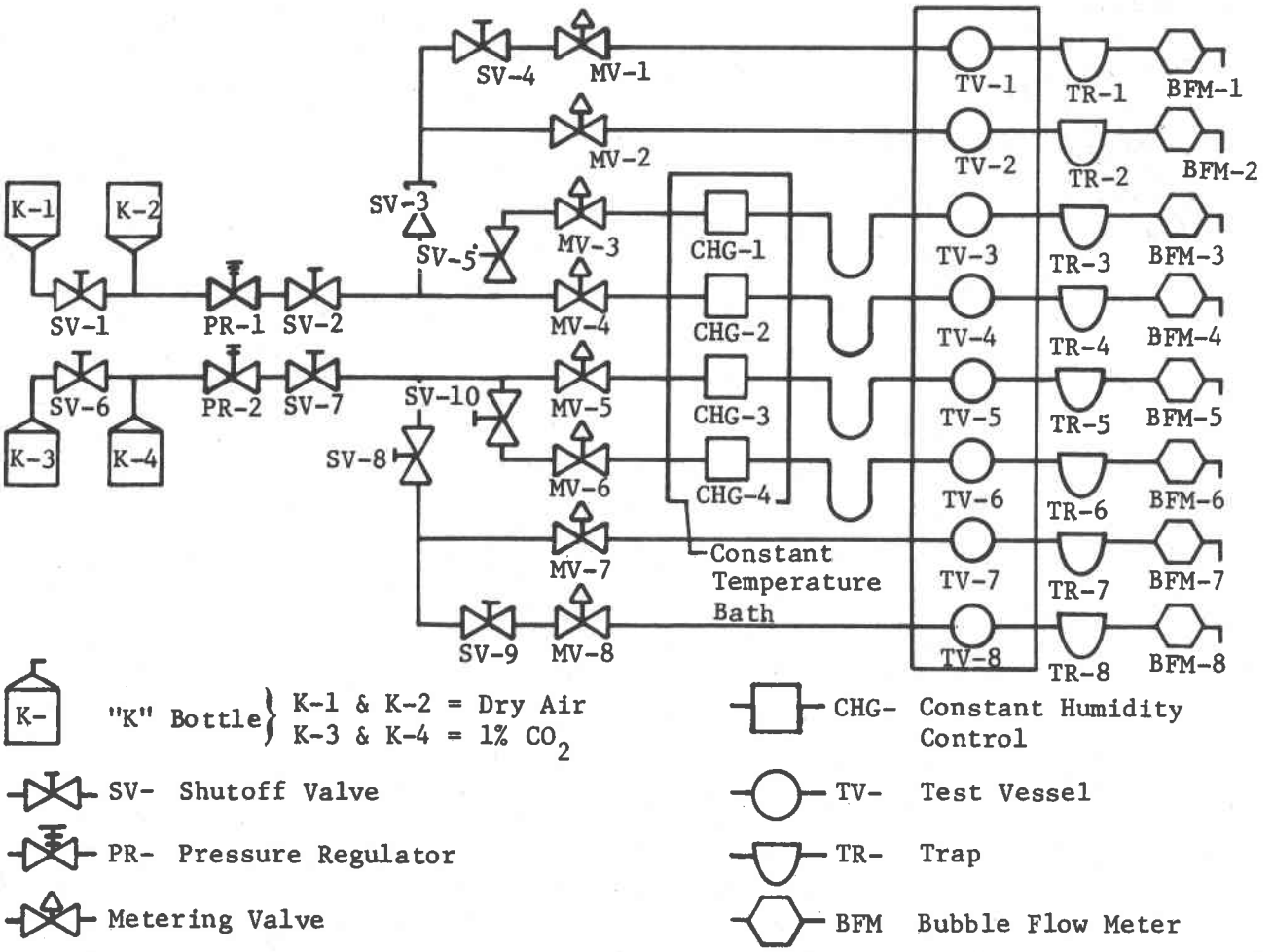

Figure II-2 Environmental Effects Test Flow Schematic

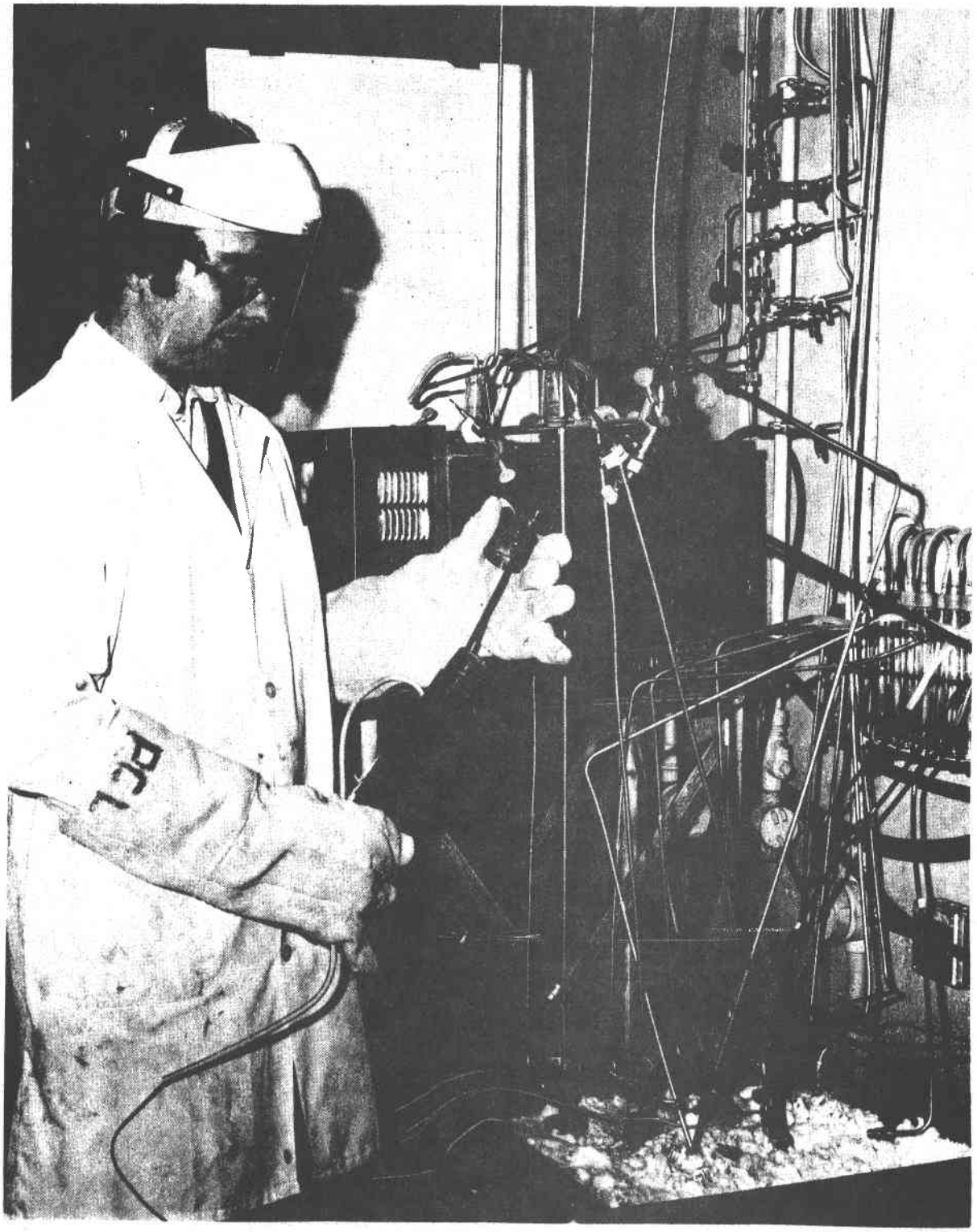

Figure II-3 Photograph of Environmental Effects Test Set-Up

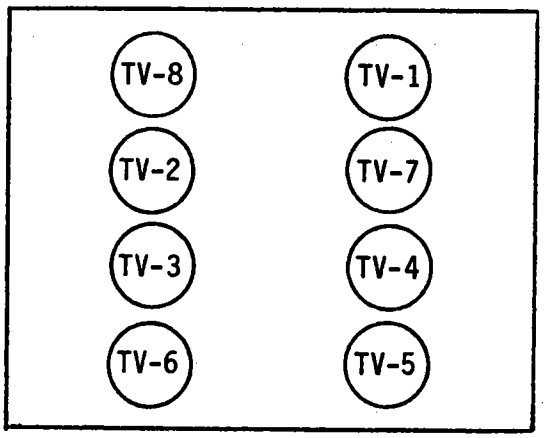

LOCATION	READOUT, °F
1	1090
2	1104
3	1105
4	1092
5	1093
6	1105
7	1098
8	1101

Figure II-4 Test Vessel Location and Temperature - Environmental Effects Test

Each of the eight passivated Incoloy 800 vessels (TV-1 thru TV-8) were filled with 200 grams of commercial-grade homogenized salt (Partherm 430, Park Chemical Company), and the vessels were placed in the test oven equilibrated at 593°C (1100°F). The center bubbler tube was removed prior to the salt loading. Once the salt had melted, flow was initiated through each center bubbler tube fitting, and the tube was lowered down into the salt to a setting of 1.3 cm (0.5 in.) above the vessel bottom. The fitting was tightened, and the flow rate through each vessel was adjusted to 2 ml/min at Denver barometric conditions (25°C, 613 torr) or 1.48 ml/min at STP (0°C, 760 torr). Oven temperatures, bubbler flow rates and humidity vessel water levels were checked daily during test operations, and adjustments were made as necessary. An Incoloy 800 test coupon of dimensions 1.9x1.9x0.16 cm (3/4x3/4x1/16 in.) was placed in each test vessel to determine I800 compatibility with molten nitrates containing high concentrations of carbonate and hydroxide, the reaction products of nitrate salt with carbon dioxide and water vapor.

At designated test intervals (i.e., 1-week, 5-week, 15-week, and 28-weeks), individual test vessels were removed from the test oven and their contents quenched and cooled rapidly by being poured into an Incoloy 800 tray inside a metal box that was purged with argon. The solidified salt samples were analyzed for carbonate, oxide/hydroxide, nitrate, nitrite, sodium, potassium, and chromium. At the end of the 28-week test, supernatant salt samples were withdrawn from their respective test vessels and analyzed for carbonate, oxide/hydroxide, and chromium.

2. Results

Results of the chemical analysis for the four test intervals are included in Table II-2. The analysis of untreated salt (Partherm 430) is included for comparison.

The supernatant analysis from the 28-week exposure test is included in Table II-3.

Table II-3 Supernatant Composition of Molten Salt After 28 Weeks

Analysis	Dry Air	100% R.H.	1% CO_2	100% R.H., 1% CO_2
Oxide (wt.%)	0.041	0.420	0.009	0.100
Carbonate (wt.%)	0.137	0.189	3.290	4.866
Chromium (ppm)	672	835	299	776

R.H. = relative humidity
ppm = parts per million

Table II-2 Results of Environmental Effects Test

ANALYSIS	HOMOGENIZED PARTHERM 430	ONE WEEK TEST				FIVE WEEK TEST			
		DRY AIR	100% R.H.	1% CO_2	100% R.H. 1% CO_2	DRY AIR	100% R.H.	1% CO_2	100% R.H. 1% CO_2
INSOLUBLE RESIDUES (Wt %)	0.060	0.127	0.073	0.573	0.072	0.061	0.087	0.047	0.058
OXIDE (Wt %)	0.018	0.029	0.080	0.009	0.012	0.050	0.450	0.017	0.037
CARBONATE (Wt %)	0.080	0.059	0.086	0.629	0.508	0.047	0.070	2.946	2.907
NITRITE (Wt %)	0.348	4.582	4.143	3.814	3.361	4.311	4.367	3.928	3.587
NITRATE (Wt %)	68.39	65.40	65.03	65.05	65.80	63.42	63.40	62.06	60.84
CHROMIUM (ppm)	1.5	123.9	84.2	60.7	43.2	176	224	70	48
WEIGHT CHANGE I-800 COUPON, Δ%	-	+.052	+.029	+.028	+.039	+.221	+.199	+.076	+.069

ANALYSIS	FIFTEEN WEEK TEST				TWENTY-EIGHT WEEK TEST			
	DRY AIR	100% R.H.	1% CO_2	100% R.H. 1% CO_2	DRY AIR	100% R.H.	1% CO_2	100% R.H. 1% CO_2
INSOLUBLE RESIDUES (Wt %)	0.068	0.071	0.155	0.115	0.191	0.074	0.004	0.008
OXIDE (Wt %)	0.018	0.112	0.013	0.016	0.045	0.372	0.019	0.105
CARBONATE (Wt %)	0.093	0.271	3.142	3.807	0.034	0.618	4.568	6.639
NITRITE (Wt %)	5.209	5.045	4.546	4.207	4.637	4.896	3.871	4.800
NITRATE (Wt %)	62.20	62.14	64.50	61.84	63.27	62.89	60.41	57.24
CHROMIUM (ppm)	425.5	340.8	132.2	136.4	644.6	866.0	338.0	840.0
MOLTEN SALT SAMPLE WEIGHT (GRAMS)	127.91	121.40	121.23	125.32	62.33	63.12	52.74	64.39
WEIGHT CHANGE I-800 COUPON, Δ%	+.176	+.119	+.132	+.114	-.140	+.340	+.145	-.237

R.H. = RELATIVE HUMIDITY
ppm = PARTS PER MILLION

An insignificant amount of oxide/hydroxide (0.05%) formed in the salt exposed to dry CO_2-free air, even at 593°C (1100°F). Decomposition of nitrate to form oxide is very slow under these specific test conditions.

An equilibrium constant for the conversion of nitrate to nitrite was calculated for the salts exposed to the various atmospheric constituents using the thermodynamic parameters calculated previously (Final Report, Conceptual Design of Advanced Central Receiver Power System, Phase 1, Contract EG-77-C-03-1724, September 1978). Calculations are shown in the following set of equations.

ΔH = 28100 cal/mole, enthalpy of reaction
ΔS = 26.0 cal/mole-K, entropy of reaction
ΔR = 1.987 cal/mole-K, ideal gas constant

For the reaction:

$$\underset{\text{Nitrate}}{NO_3^-} \longrightarrow \underset{\text{Nitrite}}{NO_2^-} + \underset{\text{Oxygen}}{1/2\ O_2}$$

the equiliblrium constant (Keq) is defined as:

$$Keq = \frac{[NO_2^-]\ (pO_2)^{1/2}}{[NO_3^-]}$$

where NO-2 = moles nitrite at equilibrium
$p\ O_2$ = partial pressure of oxygen at equilibrium
NO-3 = moles nitrate at equilibrium

Using the relationship

$$\ln Keq = -\frac{\Delta H}{R}\left(\frac{1}{T}\right) + \frac{\Delta S}{R}$$

and substituting the values of ΔH and ΔS for the nitrate-nitrite reaction obtained during the Phase I work, the predicted nitrate-nitrite equilibrium constant for molten salt at 593°C (1100°F) is 0.040 $atm^{1/2}$. Equilibrium constants for the four test conditions (dry air, 1% CO_2 in air, 100% relative humid air, and 1% CO_2 + 100% R.H. air) were determined from the chemical analysis of the bulk salt. The partial pressure of oxygen in air at Denver is 0.169 atm. An equilibrium constant for each atmospheric test condition (averaged over the four test intervals) is reported in Table II-4.

Table II-4 Effect of CO_2 and Water Vapor on Nitrite/Nitrate Equilibium

Gas Composition	$K_{eq}^{1/2}$ (atm)
Purified Air	0.041
1% CO_2	0.035
100% R.H.	0.041
1% CO_2 + 100% R.H.	0.036

The equilibrium constants for nitrate salt exposed to dry and humid air are in excellent agreement with the predicted value. The equilibrium constants for the molten salts exposed to CO_2 and CO_2 - H_2O are suppressed. Generally, nitrite concentrations were lower in those tests where carbon dioxide was present.

Further investigation is necessary to fully understand this result, but this could indicate that nitrite formation is the rate-limiting step in the formation of carbonates from nitrates.

The extent of reaction of carbon dioxide or water vapor with the molten nitrate mixture was determined by comparing the concentration of carbonate or hydroxide present in the salt at a given time to the amount that would be present if all of the carbon dioxide or water present had reacted with the salt. The relationship between the amount of carbon dioxide and water added to the system and the amounts which reacted to form carbonates or hydroxides is presented in Figure II-5. Supernatant carbonate (hydroxide) concentrations for the 28-week test are also included in this figure. The data indicates that the reaction between 1% carbon dioxide and molten salt was complete but the reaction between molten salt and water vapor was only 6-20% efficient within the experimental conditions. Results of the analysis of the supernatant liquors suggest that the solubility limit for X_2CO_3 (X = Na, K) was reached within 28 weeks of test. Hydroxide formed from the reaction of water vapor with molten nitrate salt apparently has not yet reached its solubility limit at 28 weeks of exposure time.

Analyses of the salt exposed to both water vapor and carbon dioxide indicate that carbonate was formed preferentially to hydroxide. It appears from the supernatant analysis that more soluble carbonate is present in this molten salt than was present in the salt exposed only to 1% CO_2.

The Incoloy 800 test coupons which were exposed either to dry air or to humid air containing 1% CO_2 deteriorated more rapidly (as evidenced by flaking effects) than the coupons exposed to either humid air or dry air containing 1% CO_2. A photograph of the coupons exposed to molten salt for 28 weeks under these four test conditions is included in Figure II-6.

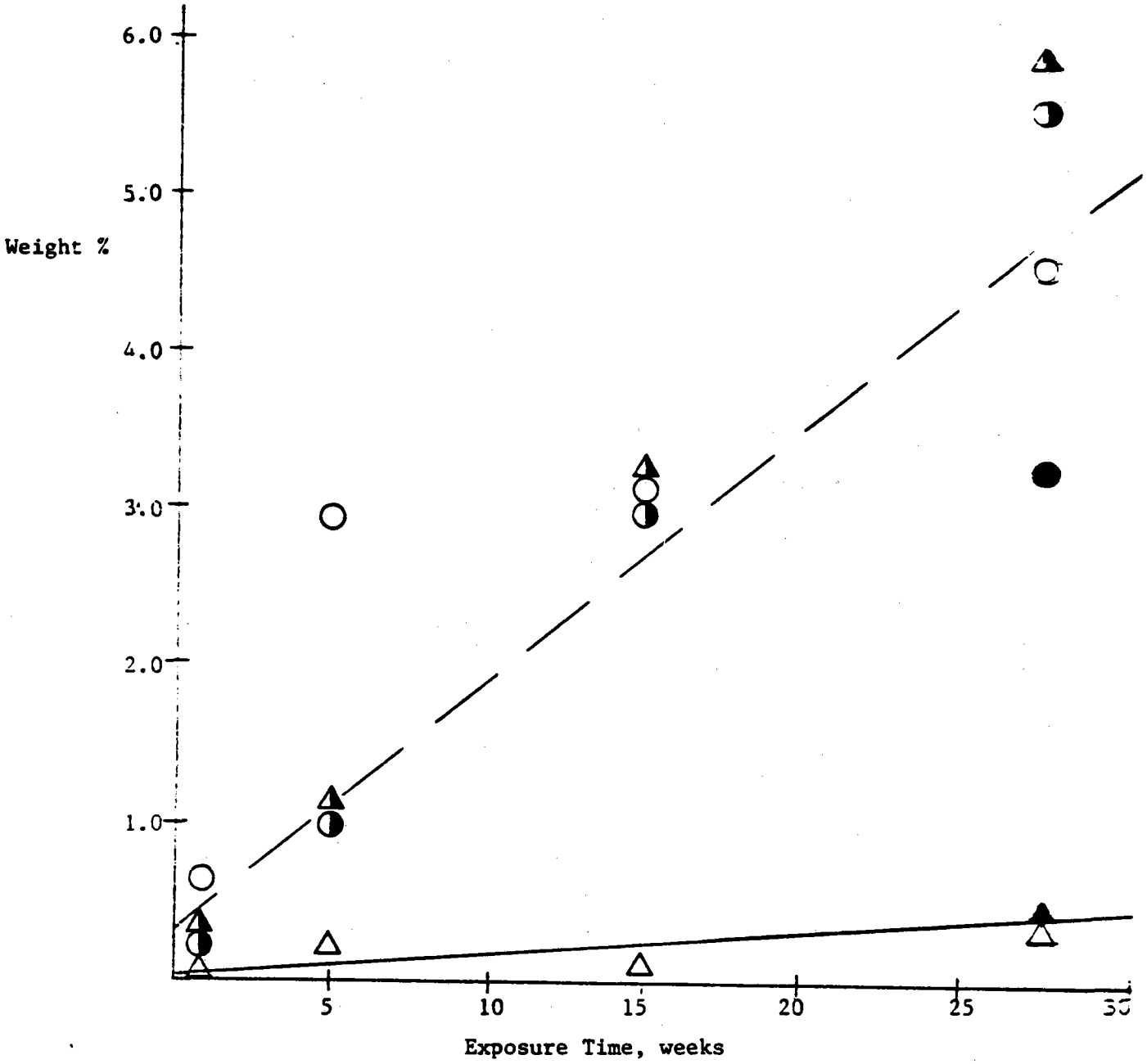

○ Carbonate formation, bulk salt (— — —) , weight %

◑ CO_2 added, grams CO_3^{-2}/100 grams salt

● Carbonate concentration, supernatant

△ Oxide concentration, bulk salt (_————), weight %

◭ H_2O added, grams O^{-2}/100 grams salt

▲ Oxide concentration, supernatant

○◑● Nitrate salt bubbled with 1% CO_2 in dry air

△◭▲ Nitrate salt bubbled with humid air without CO_2

Figure II-5 Efficiency of Conversion of CO_2 and Water to Carbonates and Oxides

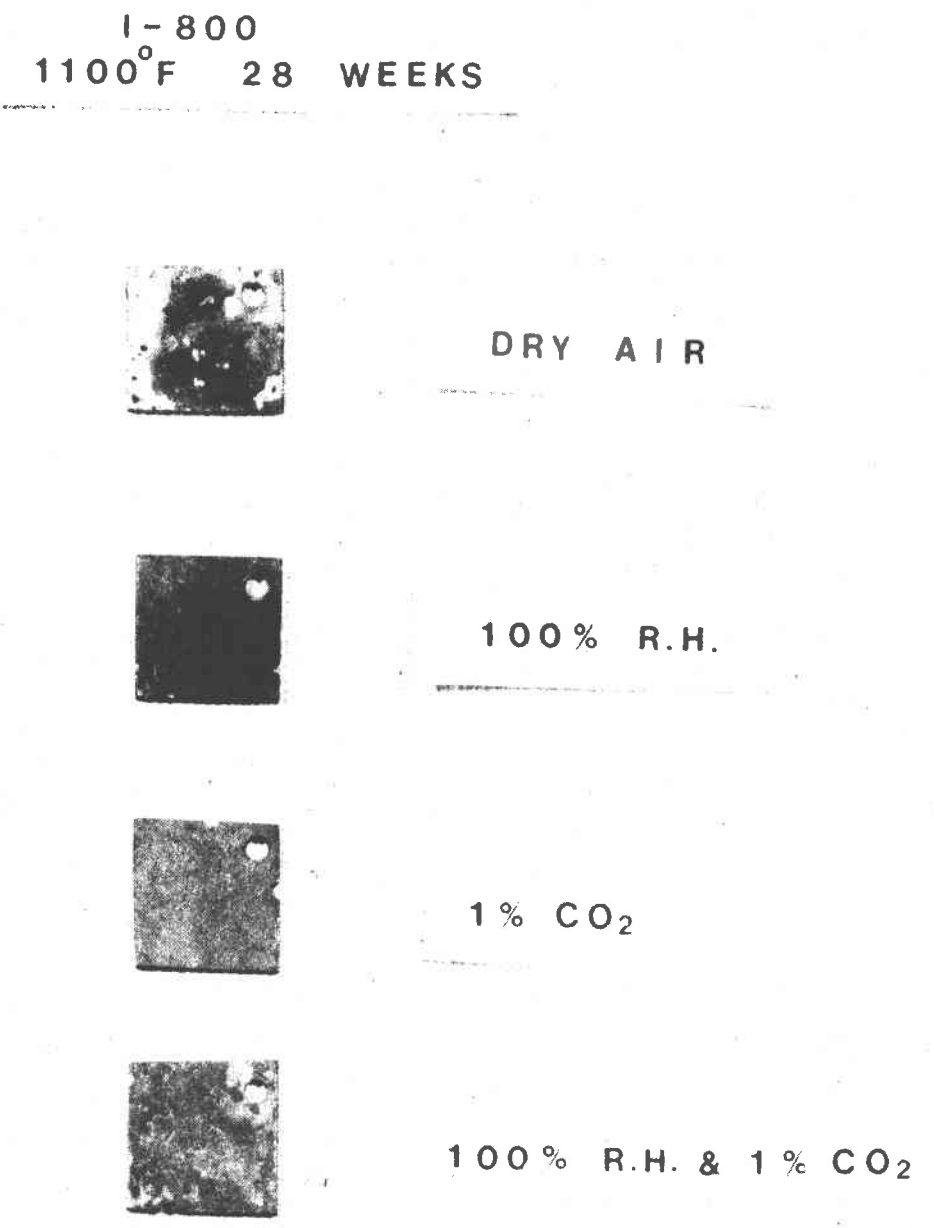

Figure II-6 Incoloy 800 Coupons from Environmental Effects Test

The following conclusions were made on the basis of the CO_2/H_2O tests:

- Negligible carbonate/oxide formation occurred in a molten salt mixture exposed to purified air for a period of 28 weeks (4700 hours) at 593°C (1100°F).

- Measured nitrate-nitrite equilibrium constants for salts exposed to purified air or humid air were in excellent agreement with the constants predicted from enthalpy and entropy data calculated from Phase I experiments. Measured equilibrium constants for salts exposed to carbon dioxide were lower than predicted.

- Absorption/reaction efficiencies for carbon dioxide with molten salt are near unity. The reaction of water vapor with molten salt to form hydroxide is 6-20% efficient under conditions employed in these tests.

- The apparent solubility of carbonate in molten salt exposed to dry 1% CO_2 is approximately 3.3% at 593°C (1100°F).

- Salts exposed to both water vapor and carbon dioxide react to form mainly carbonates with little hydroxide formation. The carbonate solubility in molten salts appears enhanced by the presence of water.

- Chromium levels are depressed by the addition of atmospheric carbon dioxide, paralleling the reduction of the nitrite concentration. This result suggests that the metallic corrosion phenomena in molten salt may be dependent on the nitrite concentration. This may explain why the coupon exposed to 1% CO_2 (low in nitrite) displayed a higher resistance to metallic corrosion than the coupon exposed to dry air (high in nitrite).

B. MOLTEN SALT REGENERATION TEST

The objective of these tests was to evaluate regeneration of molten salts containing carbonates and hydroxides/oxides by exposure to gaseous nitrogen dioxide.

1. Test Methods

A synthetic nitrate mixture of 60%/40% Na/KNO_3 was prepared by homogenizing reagent grade (chemically pure) sodium nitrate with the proper proportion of reagent grade potassium nitrate. Sodium nitrate and potassium nitrate reagent chemicals were obtained from the J. T. Baker Chemical Company, Glen Ellyn, Ill. This 60/40 mixture was subsequently doped with reagent grade sodium carbonate (Na_2CO_3) and/or reagent grade sodium hydroxide (NaOH) according to the test matrix shown in Table II-5. 250 grams of the doped salt mixture were added to each test vessel.

Table II-5 Molten Salt Regeneration Test Matrix

Test No.	Wt % Dopant	NO_2 Addition Rate	Bubble Duration
1	2.4% CO_3^{-2}	5 cc/min	132 hr
2	2.4% OH^-	5 cc/min	132 hr
3	2.3% CO_3^{-2}, 2.3% OH^-	5 cc/min	132 hr
4	Blank	5 cc/min	132 hr
5	2.3% CO_3^{-2}, 2.3% OH^-	No NO_2	132 hr

These chemically doped mixtures of reagent nitrate salts were exposed to a mixture of nitrogen dioxide in air (13.5% by chemical analysis) using the Incoloy 800 bubbler vessels used in the environmental effects test. An Incoloy 800 test coupon of 2.54x2.54x0.16 cm (1x1x1/16 in.) was placed in each reactor vessel to record weight change data and visual observations. A gas absorption tube containing calcium chloride and ascarite was attached to test vessel #5 to abosrb any water vapor/carbon dioxide from the ambient air, because no gas flowed through this control vessel. Figure II-7 depicts the flow schematic used in the molten salt regeneration test. The salt was maintained at 288oC (550oF) throughout the test period and flow rates were monitored twice daily and readjusted as needed. A gas bubbling tower containing 500 ml of a 5% NaOH, 18% Na_2SO_3 solution (sodium hydroxide/sodium sulfite scrubber liquor) was connected to the output of the bubble flow meter to absorb any unreacted NO_2 gas. At the end of the designated test period (132 hours), individual test vessels were removed from the oven and salt samples were quenched as described in subsection A.2 above. Test coupons were also removed, washed free of salt, dried under nitrogen and weighed. Salts were analyzed for carbonate, hydroxide, chromium and nitrite proportions, and changes in weight and visual appearances were recorded for the test coupons. Chemical conversion efficiences, calculated from the flow rate of the NO_2 gas mixture through each vessel, were based on the assumption that the carbonate ion and hydroxide ion react with gaseous nitrogen dioxide in the following manner:

$$CO_3^{-2} + 2NO_2 + O_2 \rightleftharpoons 2NO_3^- + CO_2 + 1/2\ O_2$$

$$2OH^- + 2NO_2 + 1/2\ O_2 \rightleftharpoons 2NO_3^- + H_2O$$

2. Results

Results of the nitrogen dioxide treated salts are in Table II-6.

Chemical conversion efficiencies calculated using the measured flow rates of the NO_2 mixture were unusually high, suggesting that gas leakage occurred during the test period. Visual leakage around the pipe vessel caps was observed during the first day of testing; this problem was resolved by wrapping the pipe threads with teflon tape. Due to this leakage, however, the actual flow rate through the test vessels was higher than that measured at the flowmeters.

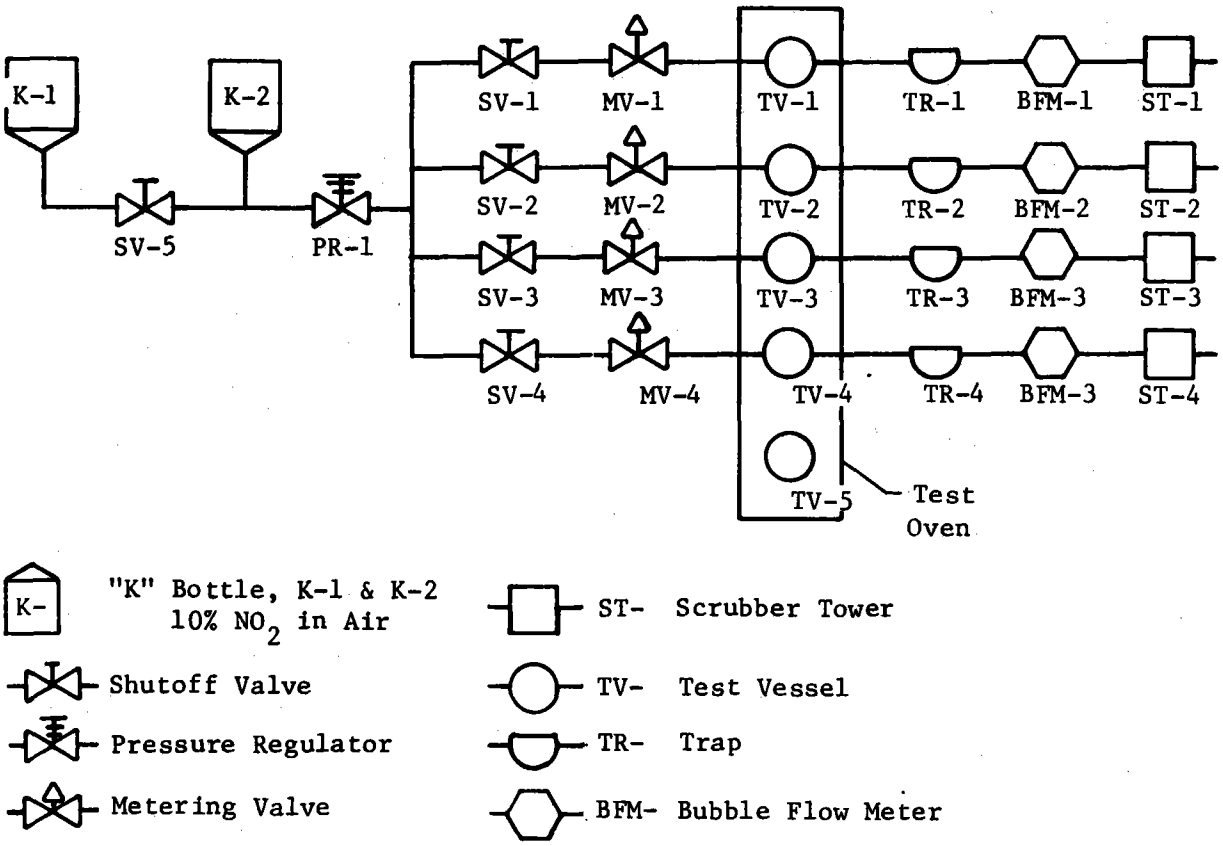

Figure II-7 Molton Salt Regeneration Test Flow Schematic

Table II-6 Salt Results, Molten Salt Regeneration Test

TEST NO.	INITIAL SALT COMP.	NO_2 ADD RATE	NO_2 ADDED (EQUIVALENT)	FINAL SALT COMPOSITION $\%CO_3^=$	$\%OH^-$	$\%NO_2^-$	CR PPM	% Reduction
1	2.4%CO_3^2	5cc/min	4.2	0.6	0.01	0.3	27	75%
2	2.4%OH^-	5cc/min	2.4	(0.04)	(0.01)	(0.04)	651	100%
3	2.3%CO_3^2 2.3%OH^-	5cc/min	1.6	0.7	0.01	0.5	346	70% 100%
4	BLANK	5cc/min	---	(0.04)	(0.01)	(0.04)	(0.5)	---
5	2.3%CO_3^2 2.3%OH^-	NO NO_2	---	2.0	2.1	(0.04)	363	15% 10%

The actual volume of gas that had passed through each test vessel was approximated from the initial loading (in m^3) and composition (volume % NO_2) of each gas cylinder supplied by the vendor and the final volume (in m^3) of each cylinder which was calculated from cylinder pressure data. On this basis it is estimated that 0.84 moles of pure nitrogen dioxide flowed through each of the four test vessels during the 132-hour test period. The number of equivalents of NO_2 added in each test was determined by dividing the total number of moles of NO_2 added in that test (0.84 moles) by the number of moles of NO_2 which would be required to convert all the doped carbonates and hydroxides. In all cases, an amount of NO_2 greater than stoichiometric was added.

Weight change data and visual observations for the Incoloy 800 coupons exposed to the molten salt/nitrogen dioxide environment are included in Table II-7. Photographs of these coupons are presented in Figure II-8.

Results indicate that the regeneration of carbonates are more difficult than the hydroxides. 4.2 equivalents of nitrogen dioxide are required to reduce the carbonate level by 75%. This corresponds to a reaction efficiency of about 18%. Efficiencies for the regeneration of hydroxides are closer to unity. The efficiencies of NO_2 regeneration may change drastically at higher temperatures either up or down - no test results are available for other temperatures.

The addition of dry nitrogen dioxide to molten salt mixtures containing carbonates and hydroxides does not cause any corrosion problems under the conditions tested.

Other regeneration techniques for nitrates are possible, such as nitric acid or metal nitrate reaction with carbonates and oxides. However, the NO_2 method was thought to be easiest to implement in a commercial system.

Table II-7 Coupon Results, Molten Salt Regeneration Test

TEST NO.	INITIAL SALT COMPOSITION	ATMOSPHERIC EXPOSURE	I-800 WT Δ mg/cm^2	PHYSICAL OBSERVATIONS
1	2.4% CO_3^{-2}	13.5% NO_2	+0.01	Shiny brass color, NVC
2	2.4% OH^-	13.5% NO_2	+0.00	Red, yellow, blue oxidative discoloration
3	2.3% CO_3^{-2} 2.3% OH^-	13.5% NO_2	+0.03	Blue oxidative discoloration
4	BLANK	13.5% NO_2	+0.01	Shiny brass color, NVC
5	2.3% CO_3^{-2} 2.3% OH^-	Dry Air	+0.06	Yellow, blue oxidative discoloration

NVC = No Visual Corrosion

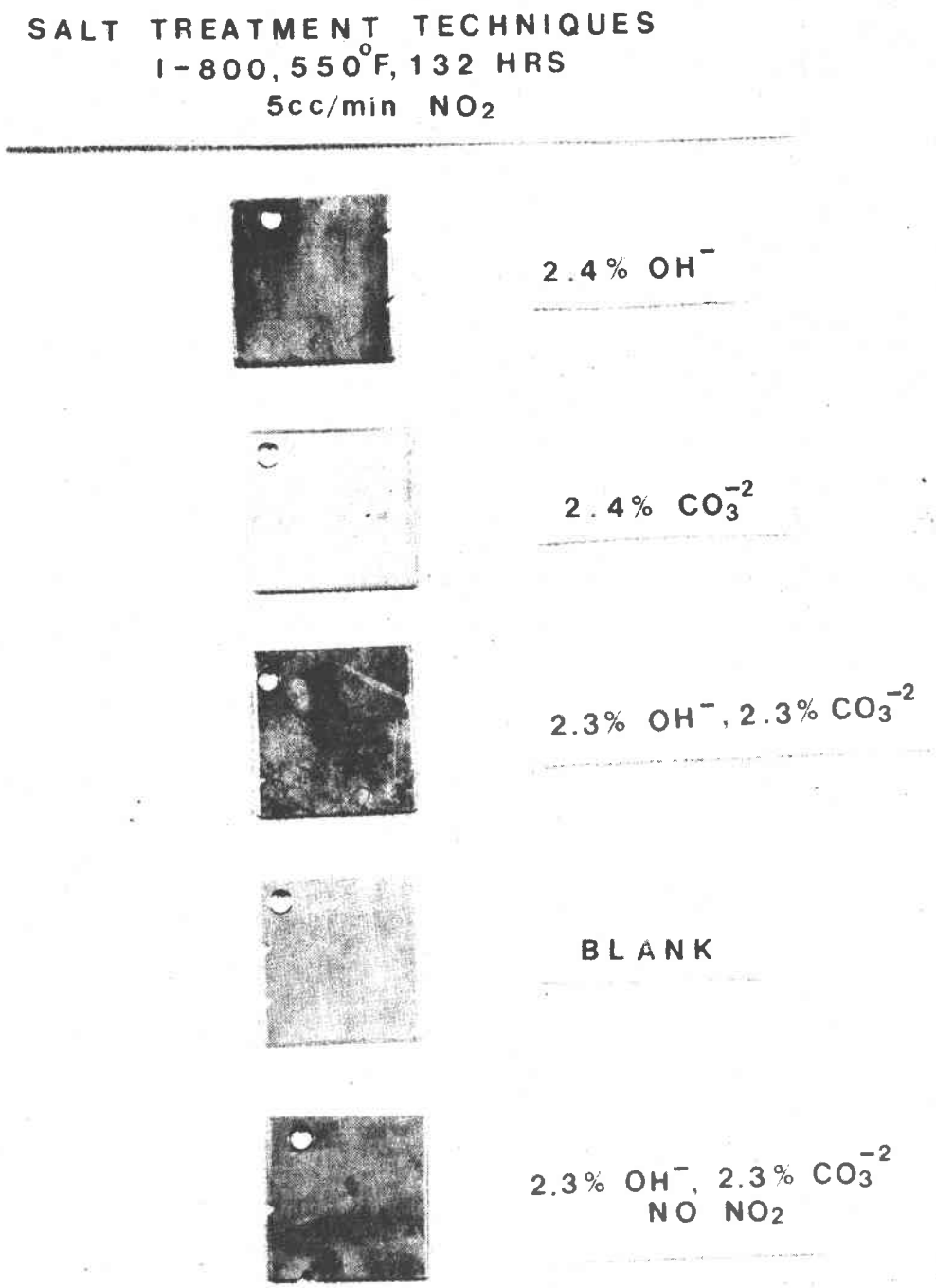

Figure II-8 Incoloy 800 Coupons from Salt Regeneration Test

III. DYNAMIC TESTING

A. LONG-TERM MOLTEN SALT FLOW LOOP

1. Objectives

The purpose of the molten salt flow loop was to simulate the thermal and fluid flow characteristics of a full-scale solar central receiver power system to permit the study of materials compatibility and salt stability in a dynamic system. These characteristics include:

1) Fluid velocity--3.5 m/s (11 ft/s) in the vicinity of the material samples,

2) Temperature profile--Gradients from 566°C (1050°F) at the hot end of the loop, 288°C (550°F) at the cold end, and

3) Materials--the loop is constructed of Incoloy 800 at the hot end and carbon steel at the cold end.

The loop was designed to permit the insertion and removal of sample coupons at various points in the flowing salt stream for analysis at 1000-hr intervals during the test. Dynamic testing will permit the investigation of:

1) Mass transport phenomena from the high to the low temperature part of the loop;

2) Materials compatibility and erosion in a flowing molten salt system;

3) Chemical stability of the molten salt in a flowing, thermally-cycled system; and

4) Electrolytic corrosion phenomena (if any) in a flowing molten salt system.

2. System Design

Figure III-1 shows a schematic of the molten salt flow loop. The sump contains molten salt maintained at 288°C (550°F). The salt is pumped through the inside tube of a counterflow heat exchanger by a cantilever pump where it is heated to 482°C (950°F). The salt is heated to 566°C (1050°F) in a three-stage electric resistance heater tube, then cooled to 371°C (700°F) as it passes through the outer tube of the counterflow heat exchanger. It then flows through a finned-tube forced convection air cooler and returns to the sump at 288°C (550°F). Seven sample ports are located at various points along the test loop to permit insertion and removal of metal coupons and salt sampling.

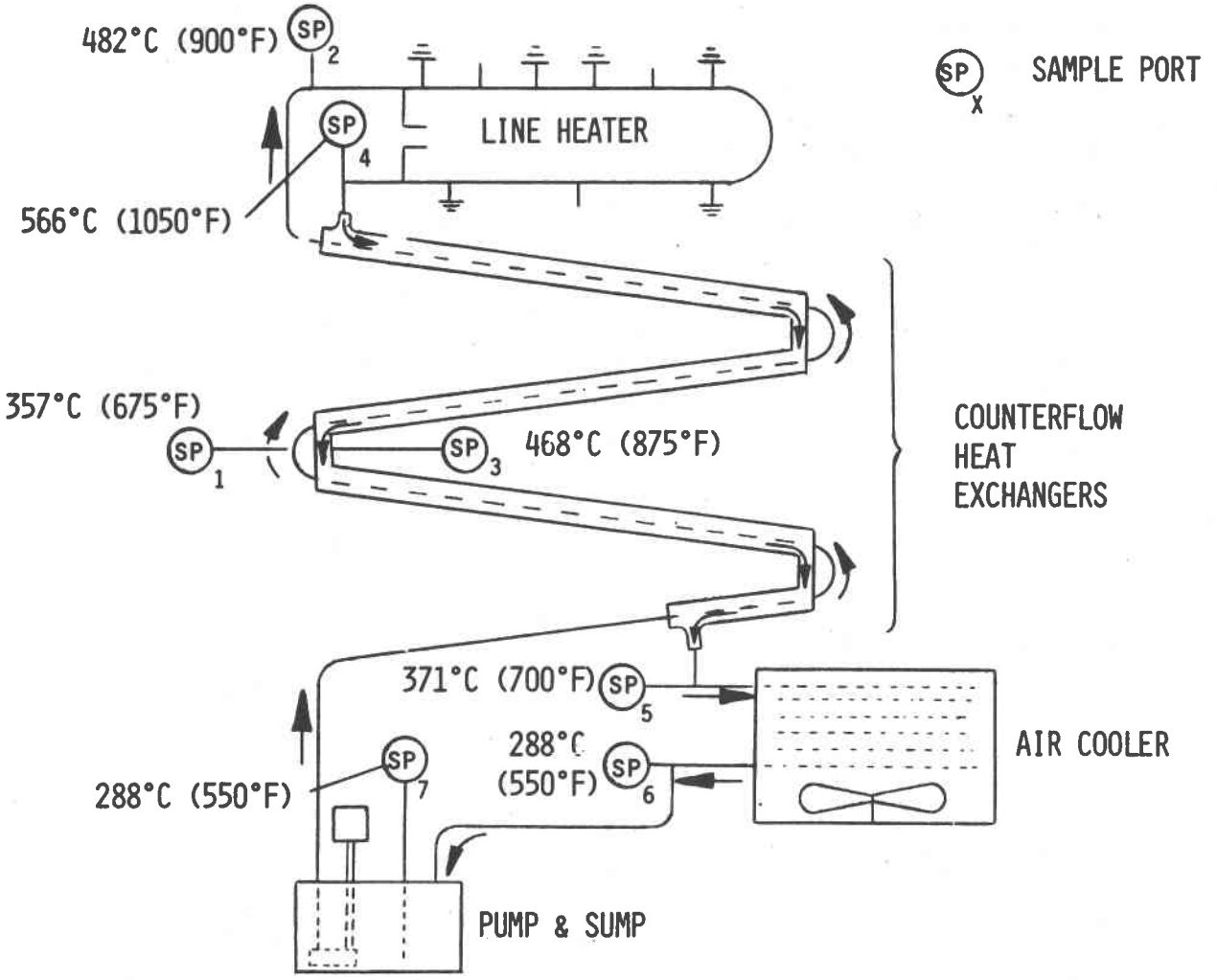

Figure III-1 Molten Salt Flow Loop Schematic

Figure III-2 shows the assembled flow loop. The pump and sump are located at the lower left. The three long legs of the counterflow heat exchanger can be seen at the left and the heater is at the top left. The air cooler is near the center of the photo and the control console is at the lower right.

Figure III-3 shows the cantilever pump on the molten salt sump. The sump is a stainless steel tank, 0.76 m (30 in.) in diameter and 0.76 m (30 in.) high, which holds the entire inventory of salt for the fluid loop, 0.34 m^3 (12 ft^3). To maintain the salt at 288°C (550°F), the sump was wrapped with temperature-controlled band heaters (which can be seen in the figure) and covered with fibrous insulation. The tank is vented to the atmosphere through a CO_2 and water vapor scrubber to prevent salt contamination.

The pump motor, rated at 5.6 kW (7.5 hp), drives a cantilevered 316 stainless steel impellor and shaft. There are no bearings or seals submerged in the salt.

The heat exchanger is a counterflow tube-in-tube type. The inner tube is 1.9-cm diameter x 1.7-mm wall (0.75-in. diameter x 0.065-in. wall) Incoloy 800 tube, and is concentric with the outer tube, a 3.2-cm (1.25-in.) schedule 40 pipe of Incoloy 800. Salt enters the inner tube at 288°C (550°F) and is heated to 482°C (900°F) by the counter-flowing salt in the outer tube that is cooled from 566°C (1050°F) to 371°C (700°F) at the inlet to the air cooler.

The total length for the four legs of the heat exchanger is 29.6 m (97.0 ft). The heat exchanger is constructed to allow complete drainage of salt when the pump is turned off to prevent salt from solidifying on the internal surfaces of the loop as it cools. The heat exchanger is also heat traced to allow tubes to be preheated to 260°C (500°F) prior to starting the system from ambient temperature. Figure III-4 shows the heat tracing being installed on one of the heat exchanger legs.

The line heater is a 1.9-cm diameter x 1.7-mm wall (0.75-in. diameter x 0.065-in. wall) Incoloy 800 tube resistively heated by passing high-amperage, low-voltage AC current through it. Salt enters at 482°C (900°F) and leaves at 566°C (1050°F). The line heater is 7.4-m (24.3-ft) long and consists of three independently-heated sections. Power for each section is supplied by a variable power source that feeds a transformer to step down the voltage and supply proper amperage. The power can be manually or automatically controlled in all three sections. Power is regulated by a power controller; each heater section is protected by an over-temperature kill to prevent the salt from exceeding 566°C (1050°F) during operation.

Power was supplied to the tubes by copper busbars that were brazed to the Incoloy tubes. These are shown in Figures III-5 and III-6 (the heater is shown uninsulated). The busbars were specially sized to permit proper current flow without overheating due to electrical resistance. Figure III-6 shows a closeup of the area around the braze joints. These sections were semienclosed and purged with dry nitrogen

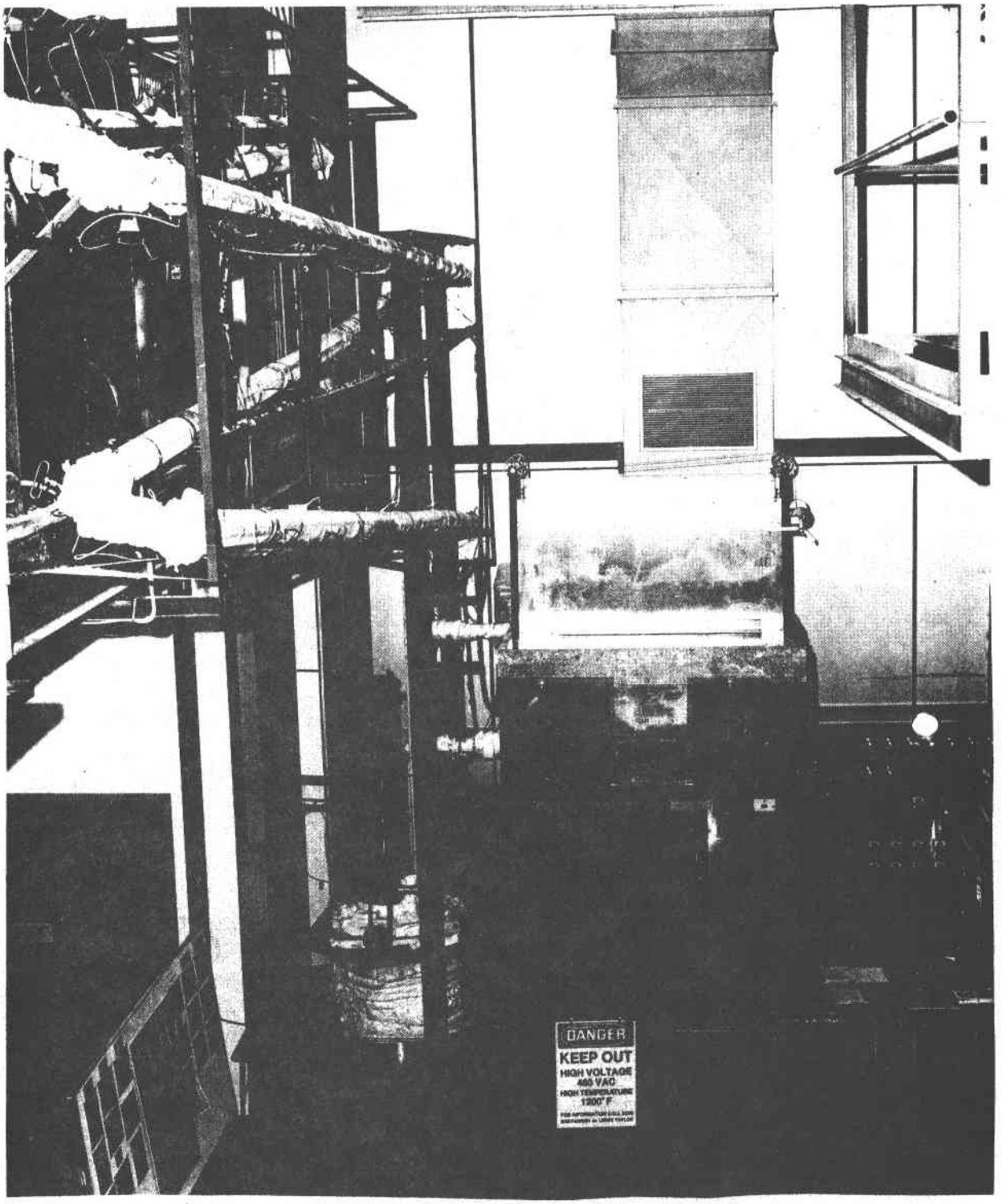

Figure III-2 Molten Salt Flow Loop

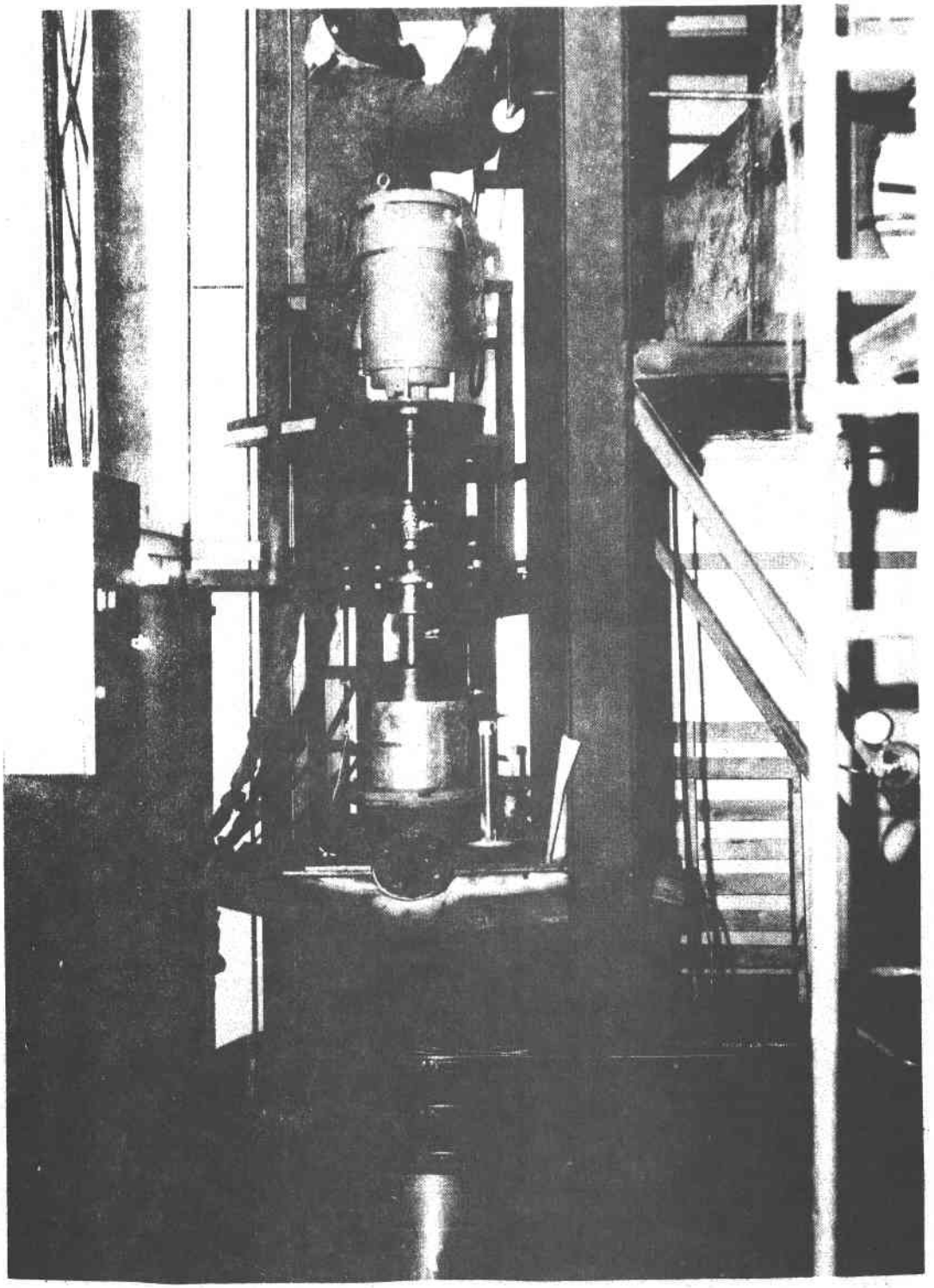

Figure III-3 Molten Salt Sump and Cantilever Pump

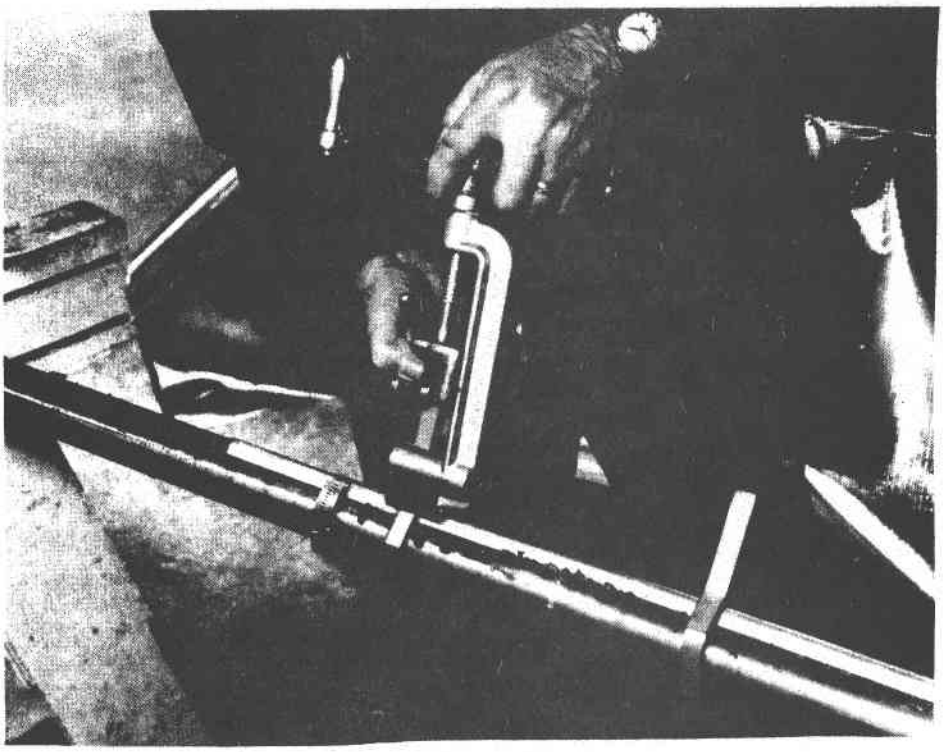

Figure III-4 Trace Heater Installation

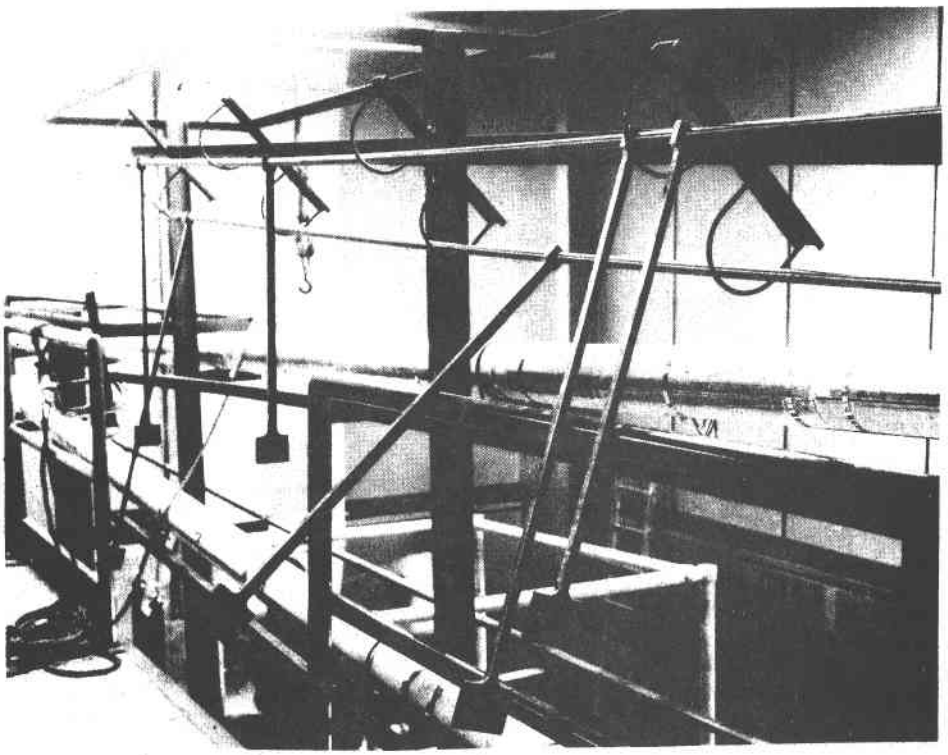

Figure III-5 Copper Busbars on Molten Salt Loop Line Heater

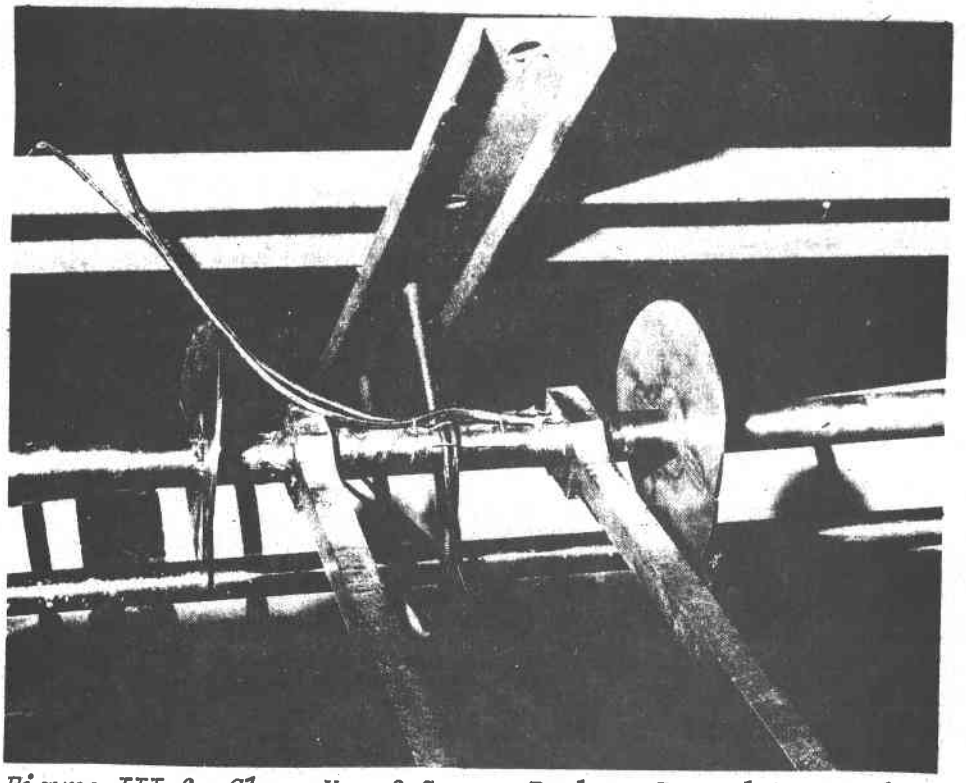

Figure III-6 Close-Up of Copper Busbars Brazed to Incoloy 800 Tube

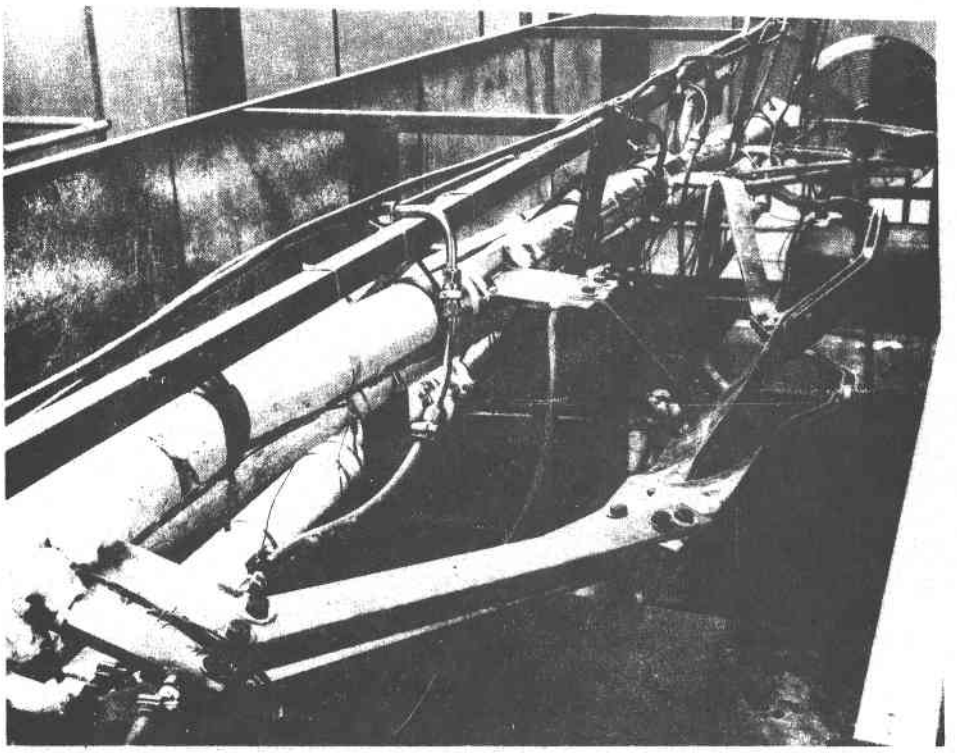

Figure III-7 Line Heater with Water-Cooled Incoloy 800 Tabs

to limit oxidation of the copper at high temperature. The opposite end of each busbar was water-cooled to prevent overheating due to the electrical resistance of the connection to the transformer cables.

After 1000 hours of testing it was discovered that the copper busbars were oxidizing around the braze joints at a greater rate than was expected. The busbars were removed and bolted outside of the insulation to 20-cm x 13-cm x 1.3-cm thick (8-in. x 5-in. x 0.5-in. thick) Incoloy 800 tabs that were welded to the line heater tubes. The water-cooled tabs, shown in Figure III-7, operated successfully and prevented the copper from oxidizing.

The air cooler at the outlet of the outer jacket of the heat exchanger was sized to reduce the salt temperature from 371°C (700°F) to 288°C (550°F) before returning the salt to the sump. The cooler consists of 11.0 m (36.0 ft) of 2.5-cm (1.0-in.) diameter carbon steel tubing with a fin density of 236 fins per meter (6 fins per inch). A closeup of these tubes is shown in Figure III-8. The tubes are sloped so that salt in the air cooler drains into the sump if the pump is turned off. A plenum chamber distributes the forced air from the dual fan system evenly over the finned tubes.

The cooler housing is insulated to prevent excessive cooling during operation. Insulated panels can also be lowered in front of the air inlet and outlet during startup. Trace heaters preheat the tubes prior to startup and are also used to melt salt in the finned tubes if the salt freezes during an emergency situation. Figure III-9 shows the air cooler and fans with the insulated panels in the raised (operating) position.

There are seven sample ports at various locations in the salt loop. Sample ports 1-5 (refer to the schematic, Figure III-1) had Incoloy 800 coupons inserted into the salt flow stream, ports 5 and 6 had carbon steel coupons inserted, and port 7 was used to sample the molten salt in the sump. Sample ports were designed so the fluid velocity across the coupons is approximately 3.5 m/s (11 ft/s), representative of the salt flow velocity in the full-scale molten salt central receiver system. The coupons were held in the salt stream on a removable sample holder, shown in FigureIII-10. The coupons were placed in slots in the holder, then inserted into the sample port, as shown in Figure III-11.

All lines in the loop are insulated and shielded with a thin sheet-metal shroud during operation as a safety precaution against possible leaks.

3. System Operation

Figure III-12 shows the control panel and instrumentation for the fluid loop. On the left are the main power input and the controls for the pump, cooler fans, line heaters, and sump heaters. At top center are the variacs used to control the trace heating during start-up. The temperature

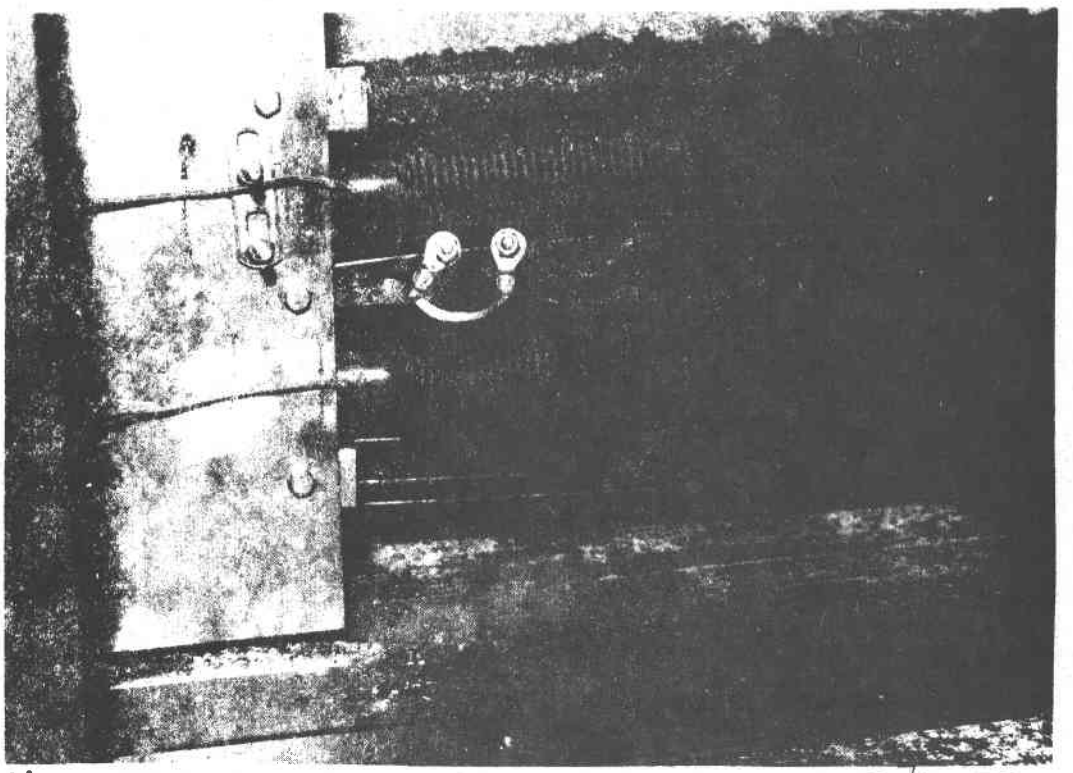

Figure III-8 Close-Up of Molten Salt Loop Finned Air Cooler Tubes

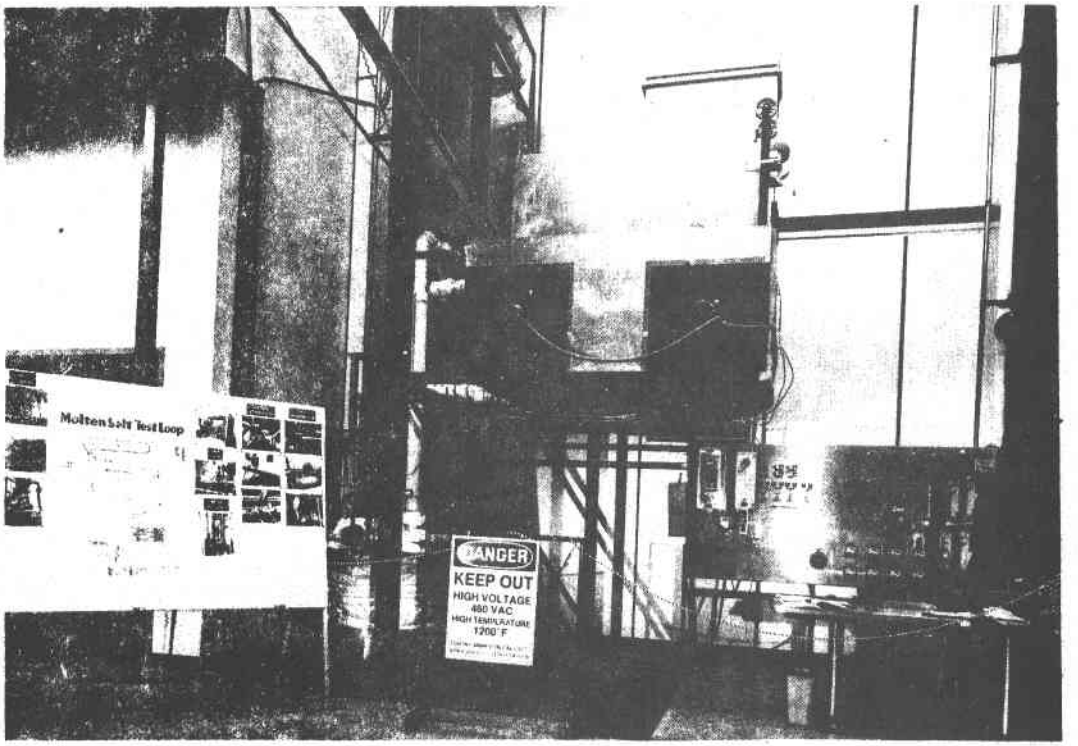

Figure III-9 Air Cooler and Fans Showing Insulated Panels

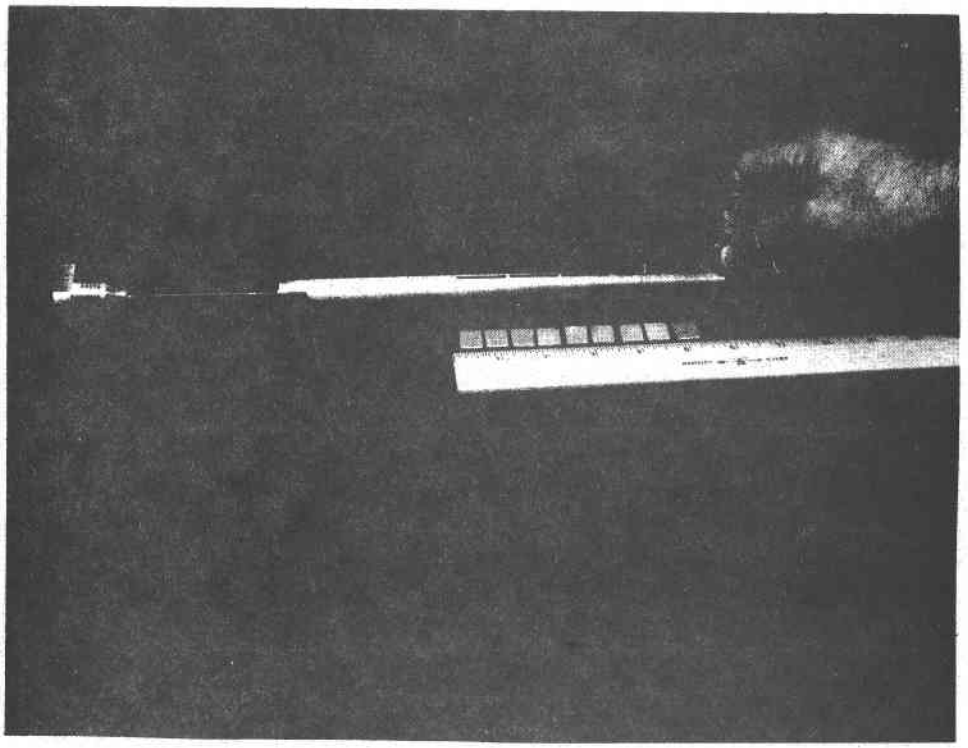

Figure III-10 Removable Materials Sample Holder, with Samples

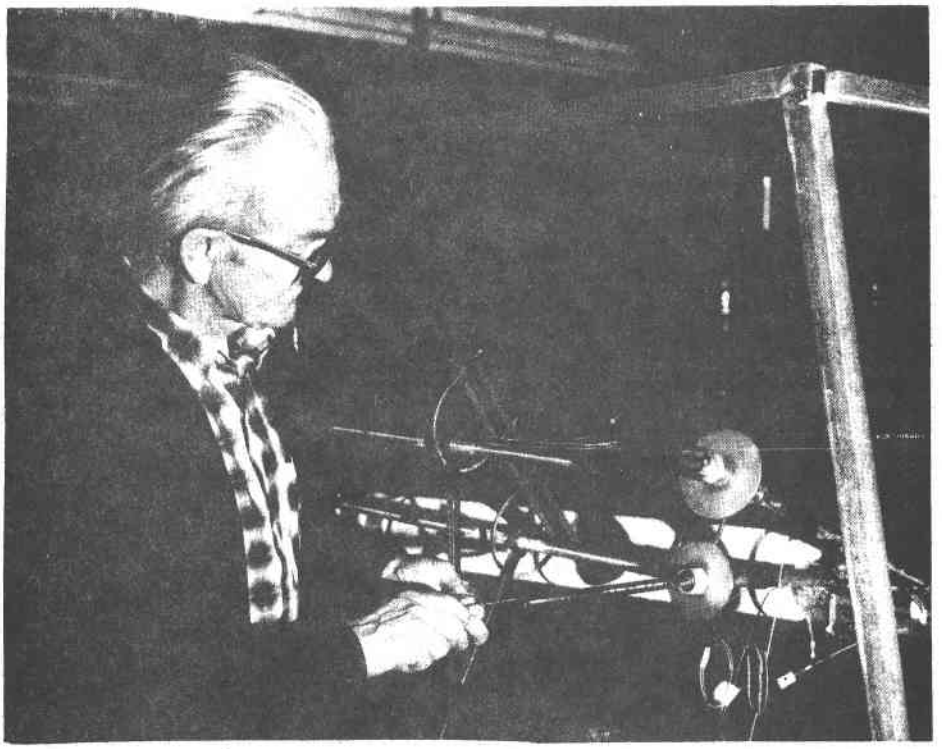

Figure III-11 Removal of Materials Sample Holder from Flow Loop

controllers for over- and under-temperature kills are at bottom center, and the four data loggers at right are used to monitor the over 120 thermocouples located at various points around the loop.

During start-up, the insulated panels on the air cooler are closed and the lines and cooler are preheated with the trace heating. When the lines reach the appropriate temperatures, the pump is turned on and salt flow through the system is verified. Power to the line heaters is then slowly increased while temperatures throughout the system are monitored until the temperature at the outlet of the line heaters stabilizes at about 566°C (1050°F). Heater power is then switched to automatic and the trace heaters are switched off.

The system was designed for continuous unattended operation over a period of at least 5000 hours. The material samples were checked every 1000 hours for weight change, and were metallurgically and chemically checked after the test is complete and at other times when weight change data indicated significant corrosion. Molten salt samples were taken every 1000 hours and analyzed chemically as required.

Figure III-12 Control Console for Molten Salt Flow Loop

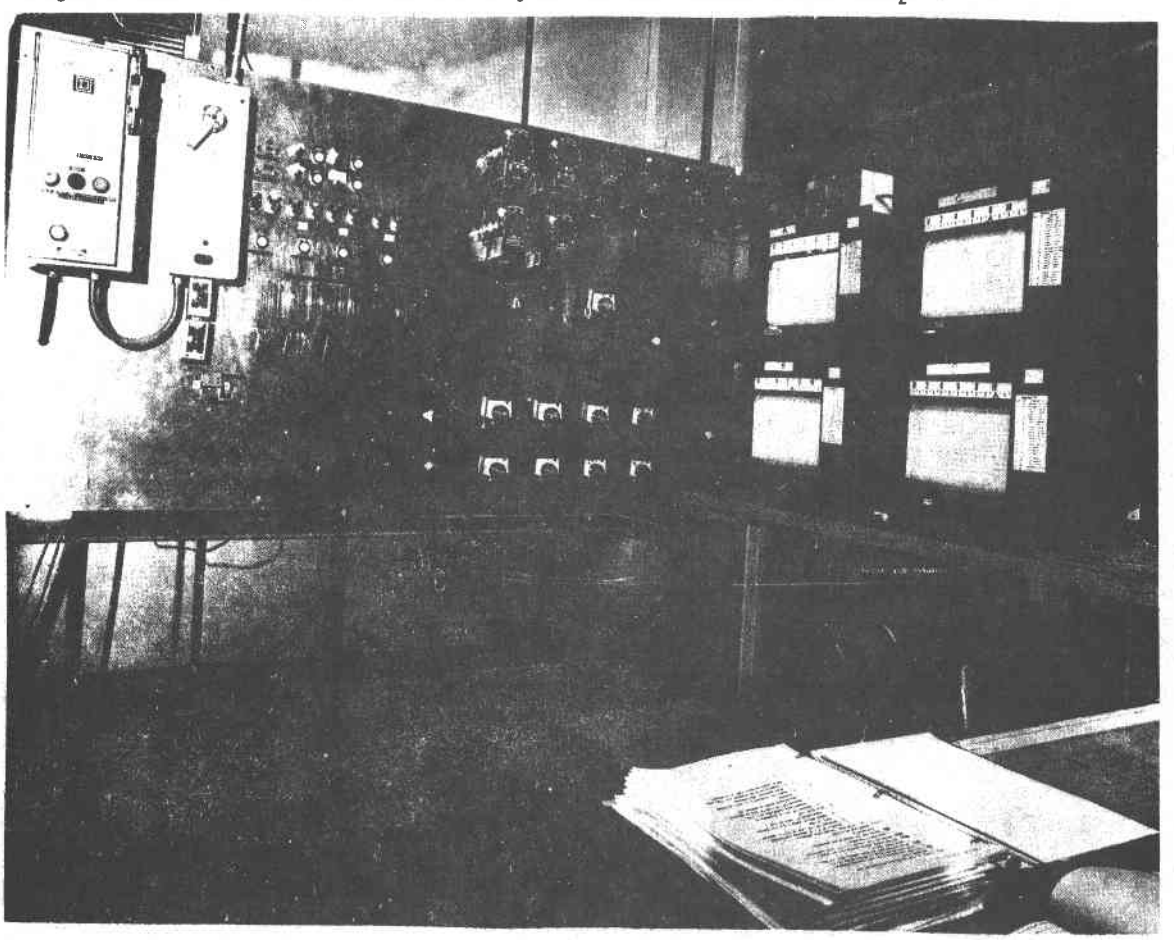

4. Results

b. Loop section chemical analyses - The objective of these analyses was to determine the kind and degree of metal degradation that occurred in the tubes in the pumped molten salt loop and to investigate localized phenomena including metallic corrosion, salt degradation, and precipitate formation. The internal surfaces of Incoloy 800 and carbon steel tubes were exposed to 5715 hours of flowing $NaNO_3$ - KNO_3 (60%, 40%) at various temperatures between 566°C (1050°F) and 288°C (550°F).

Tube specimens were selected from eight loop positions corresponding to temperatures between 288°C (550°F) and 566°C (1050°F) on both the feed side (sump to heater section) and the return side (heater to sump sections). These samples were sawed out of the loop, split longitudinally, and analyzed chemically and metallographically. A loop schematic showing sample section areas is given in Figure III-13. A table showing nominal and actual (thermocouple recorded) temperatures for these eight tube specimens is included in the figure.

Internal tube walls were examined for color, salt deposits, and type and distribution of particulate matter. These observations, both visual and microscopic, are recorded in Table III-1. Photographs of these tube sections are presented in Figures III-14 and III-15. Saw filings were brushed off of all the surfaces of each section and discarded. The interior walls were washed with hot water and brushed with a fiber brush to facilitate removal of water soluble salts. The wash water was saved and filtered to collect any water insoluble particulates that were present. External surfaces were treated in a similar manner. Tube walls were examined after washing; these observations are also tabulated in Table III-1. Visual observations of the insoluble particulates and washings from loop tube sections are presented in Table III-2. Photographs of washed tube sections are included in Figures III-16 and III-17. Photographs of the particulates collected on filter paper are included in Appendix A.

After filtration, wash water samples were evaporated to dryness, weighed, redissolved, and diluted to 100 ml with distilled water. Insoluble particulates were removed from the filter paper, weighed, and transferred to a small beaker. A mixture of 10 ml of concentrated hydrochloric acid (HCl), 10 ml of concentrated nitric acid (HNO_3), and 5 ml of distilled water was used to dissolve these particulates. Particulates which did not dissolve were heated gently in the acidified solution for 15 to 20 minutes and allowed to sit overnight. Filter papers containing trapped particulates were washed with warm 10% HCl and this wash was added to the appropriate HCl/HNO_3 mixture. Particulates which did not dissolve in the hydrochloric acid/nitric acid mixture were discarded.

Wash water samples (effluents) were analyzed for chromium, nickel, iron, calcium, and nitrite. Particulate solutions were analyzed for chromium, nickel, iron, and calcium. Analytical procedures for these determinations are documented in Appendix A. Calcium was included in the analysis because insoluble deposits containing high calcium were found on some areas of the loop coupons and tubing. Results of the chemical analysis for both the effluents and the particulates from sectioned tubes are included in Table III-3.

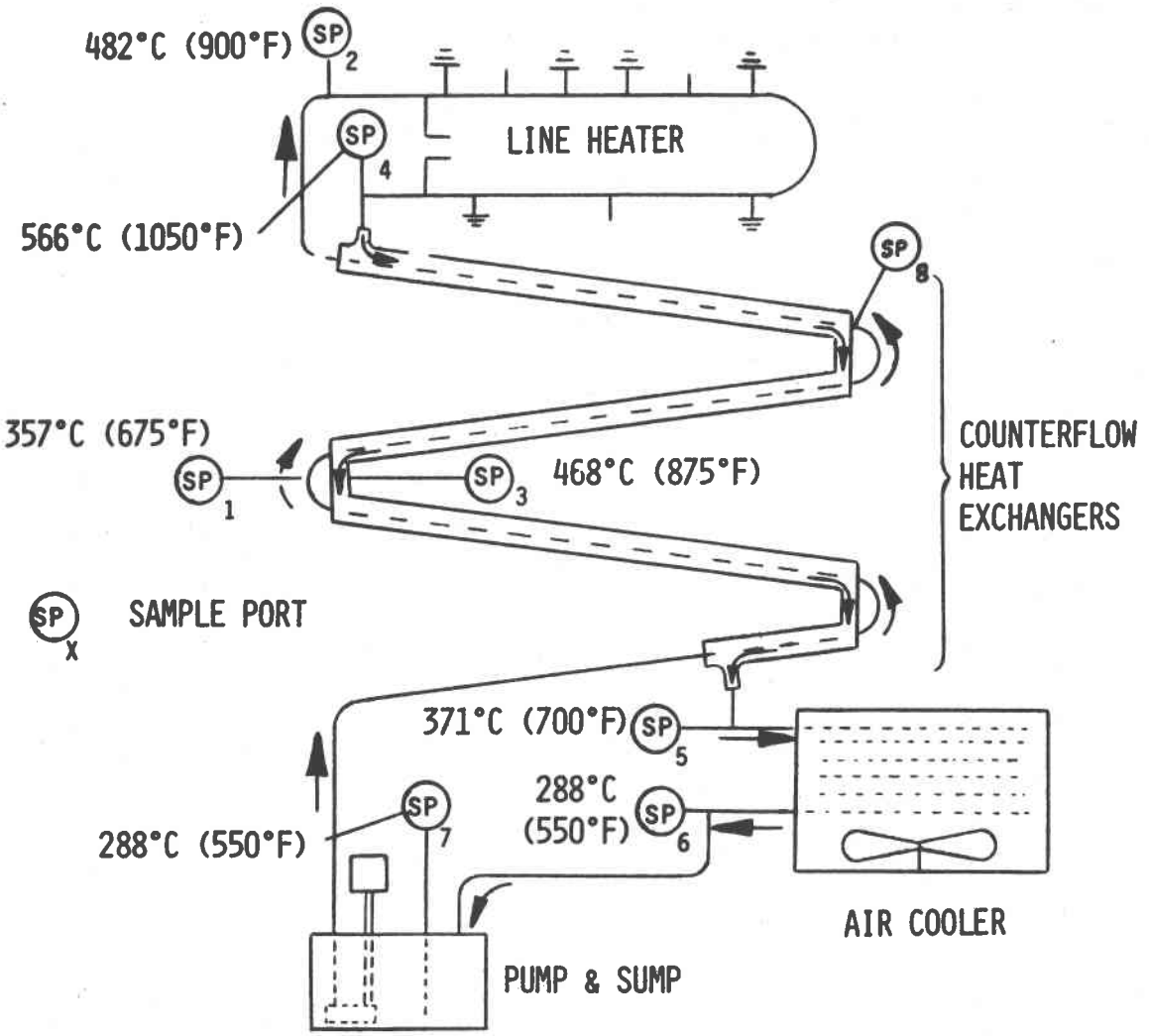

Position	Nominal Temperature °C (°F)	Actual Temperature °C (°F)
SP-1	357 (675)	371 (700)
SP-2	482 (900)	481 (896)
SP-4	566 (1050)	566 (1050)
SP8*	-	433 (811)
SP-3	440 (825)	448 (838)
SP-5	371 (700)	389 (732)
SP-6	288 (550)	302 (575)
SP7*	-	310 (590)

*SP7 and SP8 are not coupon-holding sample ports, but rather are locations from which tube sections were removed at the end of the test

Figure III-13 Molten Salt Loop Schematic Showing Sample Port Location and Temperatures

Table III-1 Observations of Internal Surfaces of Washed and Unwashed Loop Sections

Location and Length	Temp. °C (°F)	Unwashed Visual Observation	Unwashed Microscopic Observation X25	Washed Visual Observation
SP-1 (F) 20.96 cm (8¼")	371°C (700°F)	Brass temperature indicating a transparent oxide	Dark color appears as brittle coating. Surface gouging suggests tube was reamed prior to use	Shiny brass color with some darkening Ream marks and some scratches evident.
SP-2 (F) 22.86 cm (9")	482°C (900°F)	Coating scratched off. Green salt down center of tube. Beige and white salt collected at end of tube. Particulates evident.	Score marks look like scratches in tan paint.	Black in color except for brassy ream marks. Localized red discoloration. Most of the salt dissolved - some tan precipitate remained
SP-3 (F) 20.32 cm (8")	449°C (840°F)	Filings found imbedded in salt. Green salt has layers of metallic slivers and flakes.	Some of the green salt areas are due to very small "dots" of intense green coloration. Perhaps nucleated chromium rich crystals.	Brass colored with a small area of shiny blue-black discoloration on one side. Ream marks very evident.
SP-4 (R) 21.27 cm (8 3/8")	566°C (1050°F)	"River bed" drainage path of white salt seen. Brown salt seems to be insoluble in white salt.	Orange crystals condensed on nucleating white crystals. Red, orange, and black particles.	Uniform black coloration. Some red discoloration at one end of tube. Tan precipitate did not wash out.
SP-5 (R) 19.37 cm (7 5/8")	388°C (730°F)	Carbon steel tube is blistered (possibly flakes) and contains metal shavings. Salt is white in color.	Slight spalding effect on tube surface. "Snowflake" effect of salt. Flakes of black, red and orange.	Fairly uniform dark grey color. Some flaking showing shiny bare metal beneath and a few reddish colored patches.
SP-6 (R) 26.04 cm (10¼")	299°C (570°F)	Orange-pink salt collected. Obvious particulates.	Loose orange and black flakes. Similar to crystalline precipitate found on low temp. loop coupons. Mixed crystal-white and red.	Tan coating throughout heaviest at one end. Areas of green discoloration flaked off in some areas.
SP-7 (F) 5.96 cm (2 7/8")	310°C (590°F)	Surface is relatively smooth with very fine needles of white salt.	"Snowflake" crystals of salt on surface. Flaky salt Dendrites.	Tan coating throughout. Did not wash out with hot water.
SP-8 (F) Counter flow heat exchanger 14.61 cm (5 3/4")	443°C (811°F)	Surface has uniform black coloring - no evidence of reaming. Localized discoloration around welds. Rust discoloration around right-angle bend.	"Snowflake" crystals of salt on surface.	Very smooth uniform dark grey-blue color with small amount of brown discoloration in large portion of tube.

F - Feed Line (from pump up to 566°C (1050°F) heating section)

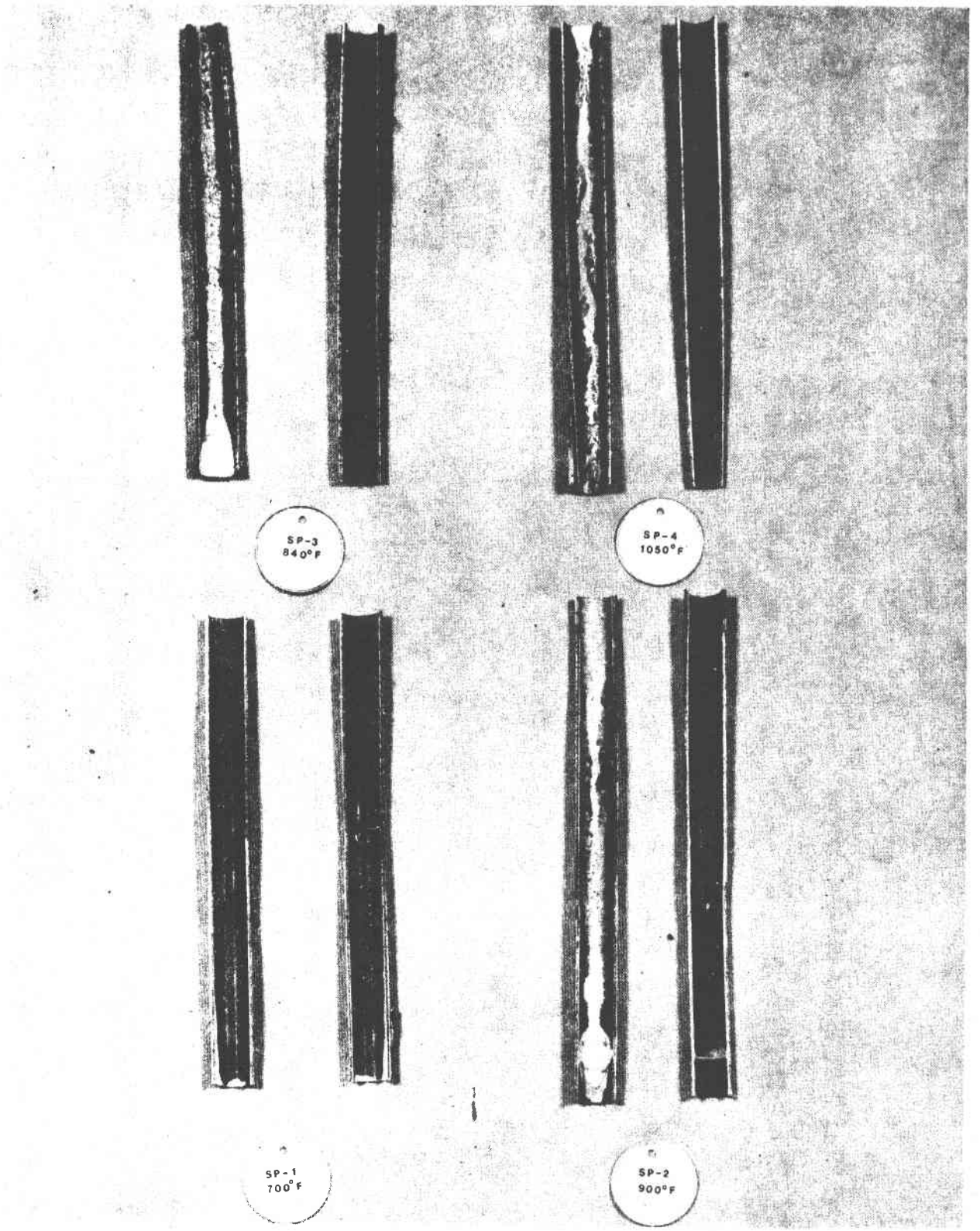

Figure III-14 Unwashed Tube Sections from Molten Salt Loop, SP1 through SP4

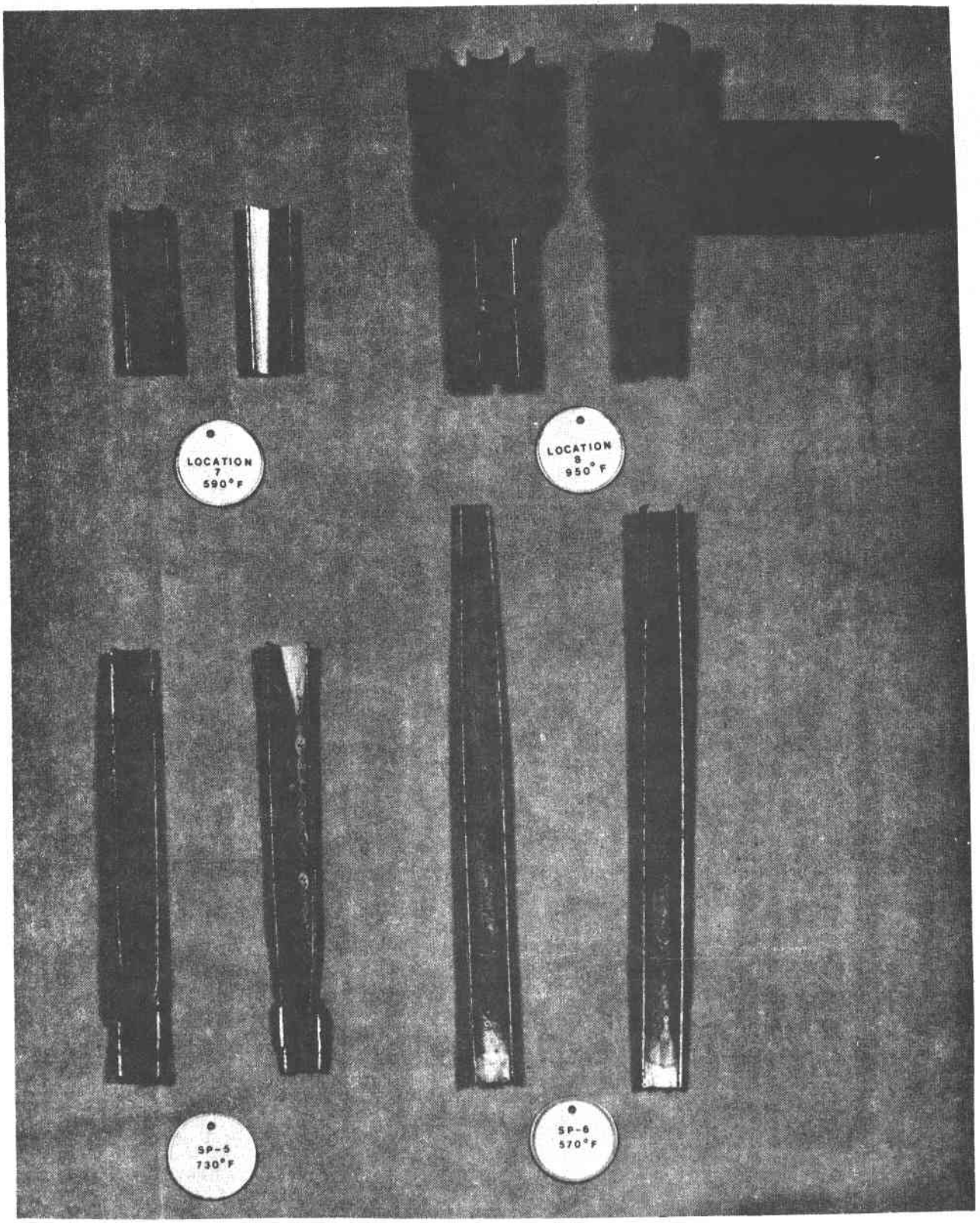

Figure III-15 Unwashed Tube Sections from Molten Salt Loop, SP5 through SP8

Table III-2 Observations of Collected Insoluble Particulates and Effluents from Loop Sections

Location	Temp.	Visual Observation of Particulates	Weight of Particulates	Visual Observations of Effluents
SP-1 (F)	371°F (700°F)	Minute amount of tan precipitate with a few black flakes and a few metallic flakes.	0.0141 g	Beige color
SP-2 (F)	482°C (900°F)	Tan precipitate with many small black flakes.	0.0940 g	Light yellow color
SP-3 (F)	449°C (840°F)	Tan to dark-grey precipitate with large amount of reddish-black flakes and a few metallic flakes.	0.2434 g	Clear yellow color
SP-4 (R)	566°C (1050°F)	Light tan precipitate with many black and fine red particulates.	0.4491 g	Yellow-green color
SP-5 (R)	388°C (730°F)	Tan precipitate with large black flakes and a few red flakes.	0.2192 g	Beige color
SP-6 (R)	299°C (570°F)	Reddish-brown precipitate with many small black flakes.	0.1478 g	Nearly colorless
SP-7 (F)	310°C (590°F)	Minute amount tan precipitate with a few metallic and a few black flakes.	0.0013g	Nearly colorless
SP-8 (F)	433°C (811°F)	Rust colored precipitate with metallic flakes and a few red flakes.	0.0279 g	Nearly colorless

F - Feed Line

R - Return Line

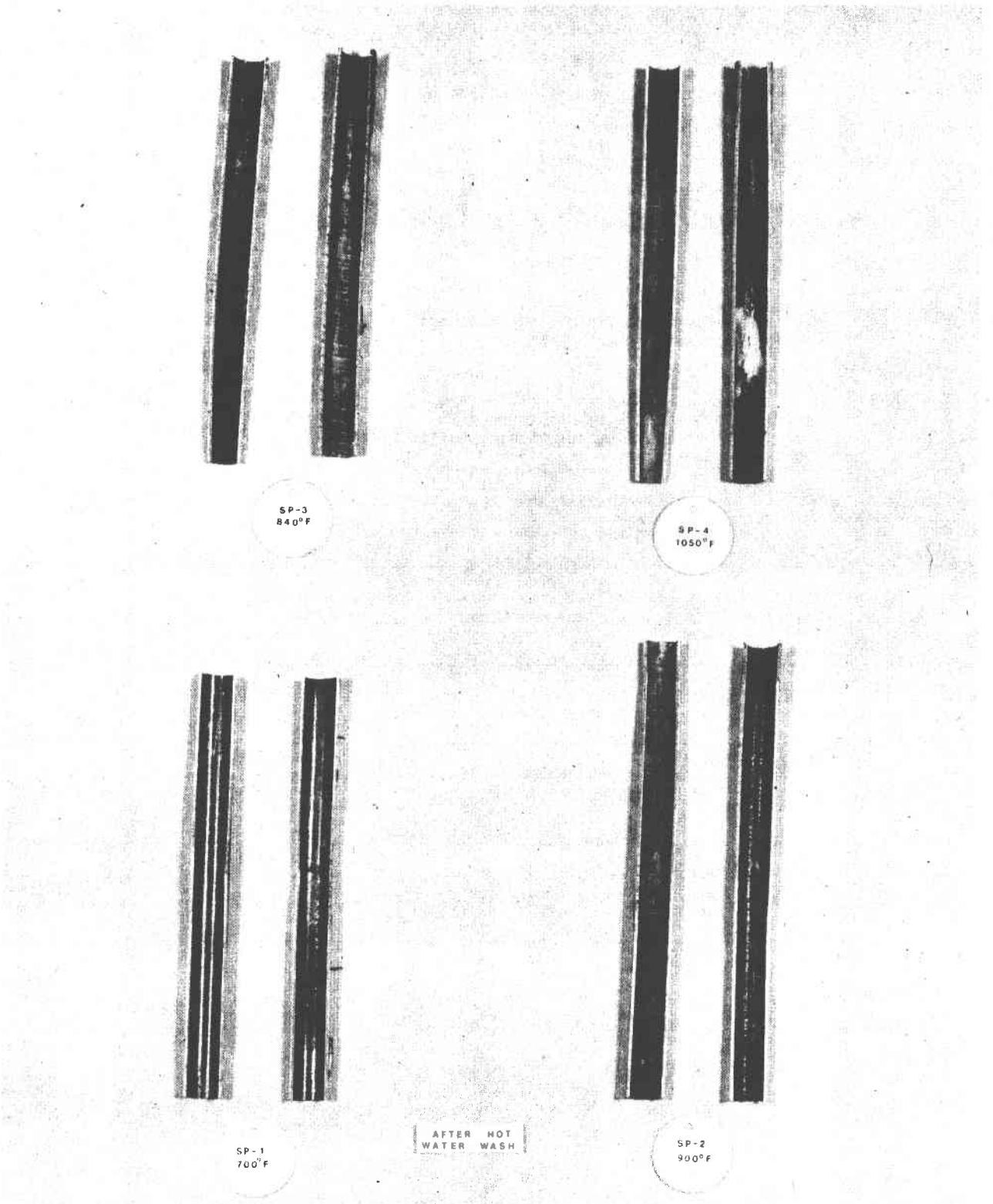

Figure III-16 Washed Tube Sections from Molten Salt Loop, SP1 through SP4

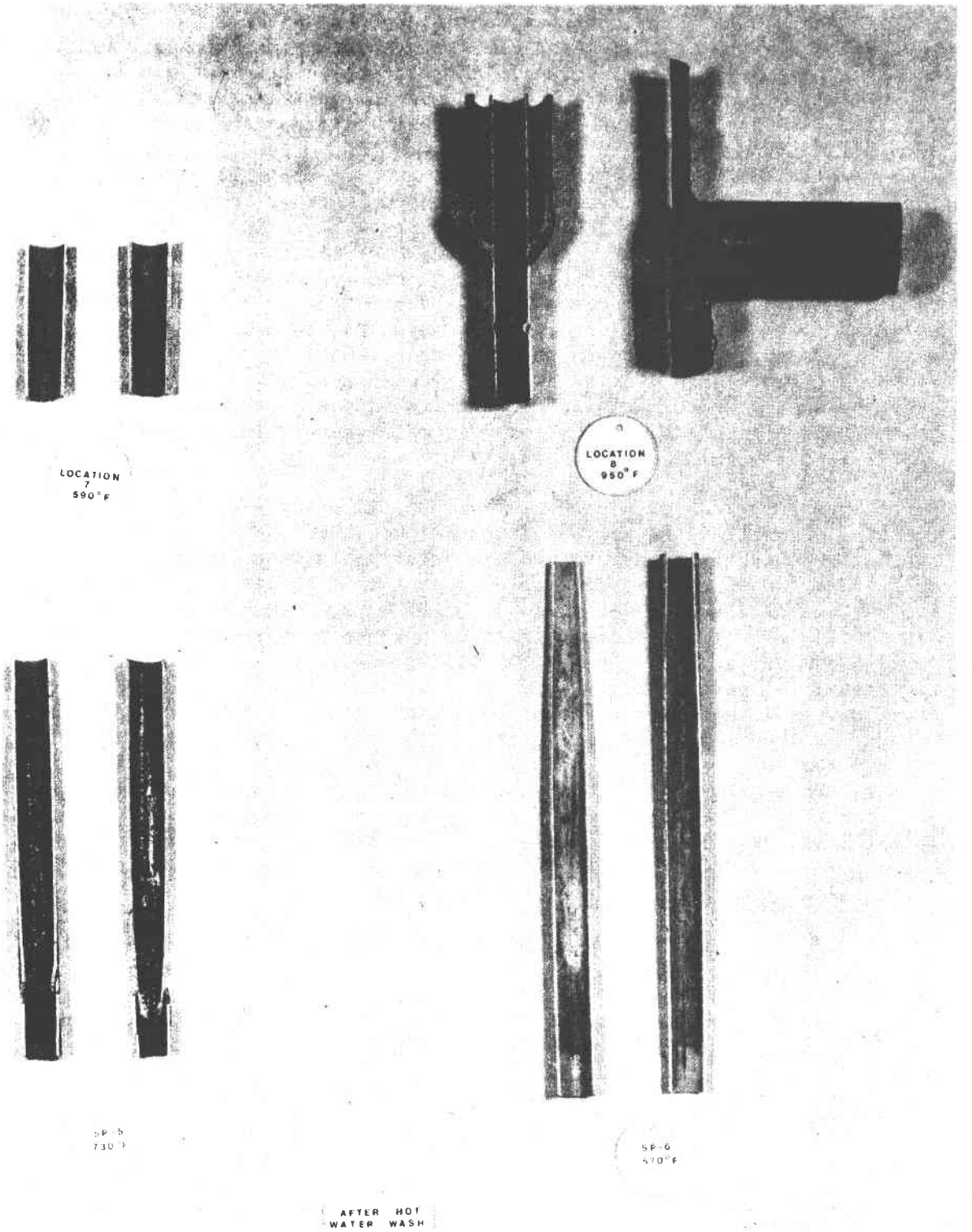

Figure III-17 Washed Tube Sections from Molten Salt Loop, SP5 through SP8

The graph in Figure III-18 gives the results from the chromium and nitrite analysis of the loop section residue wash water. The trends in the table show that chromium and nitrite concentrations of salts washed from the tube walls correlate well (correlation coefficient 0.89). Iron and nickel concentrations are low, and calcium only appears in section 7 (310°C (590°F)). The expected increase in nitrite concentration with sample location temperature only correlates in the feed side from the sump area at 299°C (570°F) to the heater area at 566°C (1050°F). The localized nitrite concentrations continue to increase in the loop in the return side after the heater section and reach a maximum of 17% midway down the heat exchanger at sample port 3. The nitrite value of 17% and the corresponding chromium value of 1.15% at sample port 3 are difficult to understand. The maximum equilibrium value for nitrite in the loop, assuming 1 atmosphere of air and 593°C (1100°F), is about 3 to 4%. The partial pressure of oxygen in the loop is probably greater than one atmosphere which should give lower nitrite (higher nitrate) values. The other parameter which could affect nitrite values is temperature. A calculation of the equilibrium temperature necessary for a nitrite value of 17% is 675°C (1250°F) to 700°C (1290°F).

Several explanations or hypotheses for exceptionally high nitrite and chromium concentrations are possible. Although no particular explanation can be proven, several hypotheses are briefly discussed below: A very definite trend or progression was evident for both nitrate and chromium in the wash residues as one follows the flow path around the loop. (See Figure III-13) If the decomposition of nitrate to nitrite were purely equilibrium controlled, the maximum nitrate would be at the highest temperatures (heater exit). However, the kinetics may be and probably are somewhat less than instantaneous. Therefore, at least several seconds may be required before nitrate/nitrite equilibrium can be established at a given temperature. This could locate the maximum thermal decomposition in the heat exchanger sections, and possibly around sample port 3 (this is the same area where loop coupons were found to show maximum corrosion, or weight loss). This discussion may explain relative concentration trends, but does not by itself explain the extreme nitrite and chromium concentrations referred to above.

A second possibility may be the formation of a nitrite-chromium complex, which precipitates from the salt at the metal surfaces but is soluble in wash water. This may represent an auto-catalytic mechanism whereby nitrite may increase the rate of chromium concentration by complexing (and removing from reaction equilibrium) the chromium ions as they are leached from the metal oxide layers. However the nitrite/chromium molar ratios (calculated from the chemical analyses) varied throughout the loop, and were much higher than the 6:1 expected for such a complex.

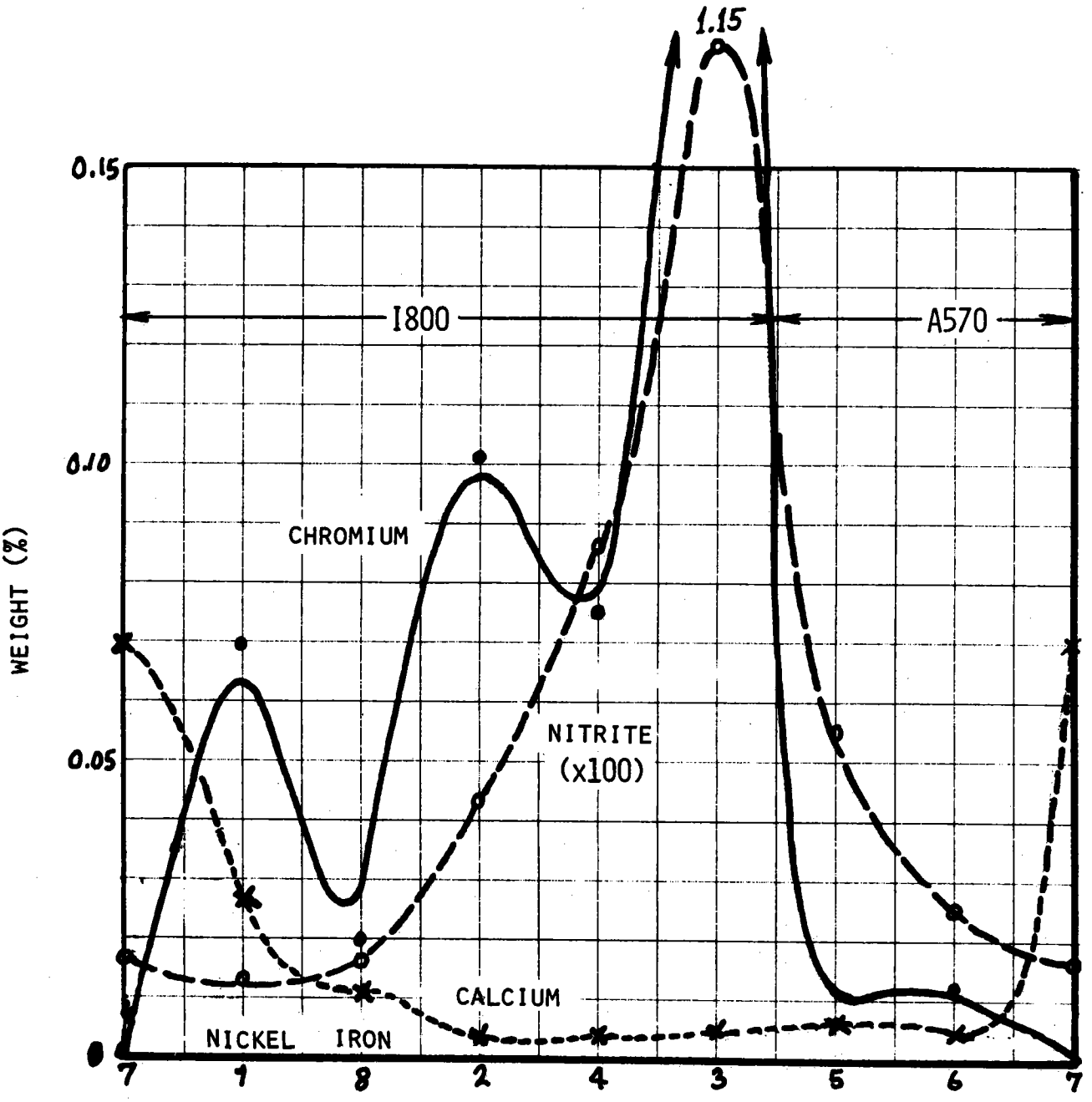

Figure III-13 Concentrations of Cr and NO_2 in Water Soluble Residues Washed From Fluid Loop Tube Walls

Another explanation for the inordinately high nitrite concentrations is the possible presence of localized areas of wall temperatures higher than the bulk temperatures of 566°C (1050°F). Boundary layers of non-turbulent liquid salt undoubtedly do experience higher temperatures (in the heater section) and less mixing than the bulk salt. As was stated earlier, temperature increases of 100°C (180°F) over the maximum operating temperature is sufficient to cause a nitrite concentration of 19%. The increased nitrite concentration combined with locally high temperature, could result in increased solubility of chromium.

Table III-3 Chemical Analysis of Internal Effluents and Particulates

Sample	Calcium	Chromium	Iron	Nickel	Nitrite
SP-1 Effluent	0.0282%	0.0696%	0.0003%	0.0043%	1.304%
Particulates	1.54%	2.24%	13.87%	2.74%	
SP-2 Effluent	0.0027%	0.1119%	0.0004%	0.0010%	4.327%
Particulates	0.26%	10.67%	41.60%	7.63%	
SP-3 Effluent	0.0045%	1.1522%	0.0004%	0.0010%	17.20%
Particulates	0.32%	3.98%	24.98%	5.57%	
SP-4 Effluent	0.0026%	0.0753%	0.0002%	0.0007%	8.833%
Particulates	0.037%	2.49%	27.79%	4.08%	
SP-5 Effluent	0.0061%	0.0062%	0.0002%	0.0011%	5.478%
Particulates	0.29%	3.88%	34.12%	4.81%	
SP-6 Effluent	0.0043%	0.0122%	0.0001%	0.0011%	2.479%
Particulates	9.48%	2.00%	24.36%	2.34%	
SP-7 Effluent	0.0710%	0.0004%	0.0002%	0.0001%	1.208%
Particulates	95.69%	3.85%	28.92%	6.36%	
SP-8 Effluent*	0.0111%	0.0101%	0.0021%	0.0036%	1.75%
Particulates	0.49%	3.55%	14.80%	6.24%	

* Unusually high concentrations possibly due to inaccurate particulate weight.

b. Bulk Salt Loop Chemistry - The objective of investigating the chemistry of the molten salt fluid loop was to determine the stability of molten salt in a dynamic thermal cycling system and to gain additional information relating to chemical corrosion phenomena in a dynamic system.

The nitrate salt was sampled prior to test initiation. At approximately every 1000-hour test interval, a molten salt plug was removed from the sump [288°C (550°F)] reservoir of the fluid loop. These salt plugs were analyzed for sodium, potassium, nitrate, nitrite, carbonate oxide/hydroxide, chromium, and calcium as detailed in Appendix A.

The results of the chemical analysis of the fluid loop salt are in Table III-4. The results delineated here indicate that carbonate and hydroxide decomposition products did not appreciably form in the loop after 5000 hours of operation (the sump was vented thru a CO_2/H_2O scrubber system). Chromium levels, representative of the degree of metallic (Incoloy 800) corrosion, did increase after every 1000 hours of loop operation. A graph of the salt chromium concentration as a function of the hours of salt exposure is presented in Figure III-19. Chromium levels appear to asymptotically approach a constant value with respect to time.

As chromium levels were observed to increase with time, the amount of nitrite in the salt mixture increased and also approached a constant level. Similar correlations have been observed in the loop section analysis and in static tests. The chromium concentration (wt%) in the loop salt samples plotted as a function of the nitrite composition of the same sample is shown in Figure III-20.

After 1002 hours of loop operation, a water-insoluble tan precipitate had collected on the surfaces of the carbon steel coupons removed from sample port 6, [(288°C) (550°F)] of the fluid loop (see Figure III-36), at which time the entire loop system was recharged with fresh salt. The used recharged salt was found to contain 4 ppm chromium and 66 ppm calcium by analysis. A 100X micrograph of the surface of one of the 550°F coupons (coupon "L") revealing the crystalline nature of the tan residue is shown in Figure III-21. A 100X scanning electron micrograph (SEM) is shown in Figure III-22. The corresponding SEM Kevex analysis of the residue on coupon "L" (Figure III-23) indicates that calcium was a major component in the residue, and iron a minor component. The broad carbon peak was due to sample preparation for the Kevex analysis.

The tan residue was scraped from the coupon surfaces and a semi-quantitative emission spectrum of the residue was performed at the Quality Control Laboratory at Martin Marietta. The resulting spectrum indicated that calcium was a major component (10%), boron a minor component (1-10%), and copper, magnesium, manganese, and silicon were trace components.

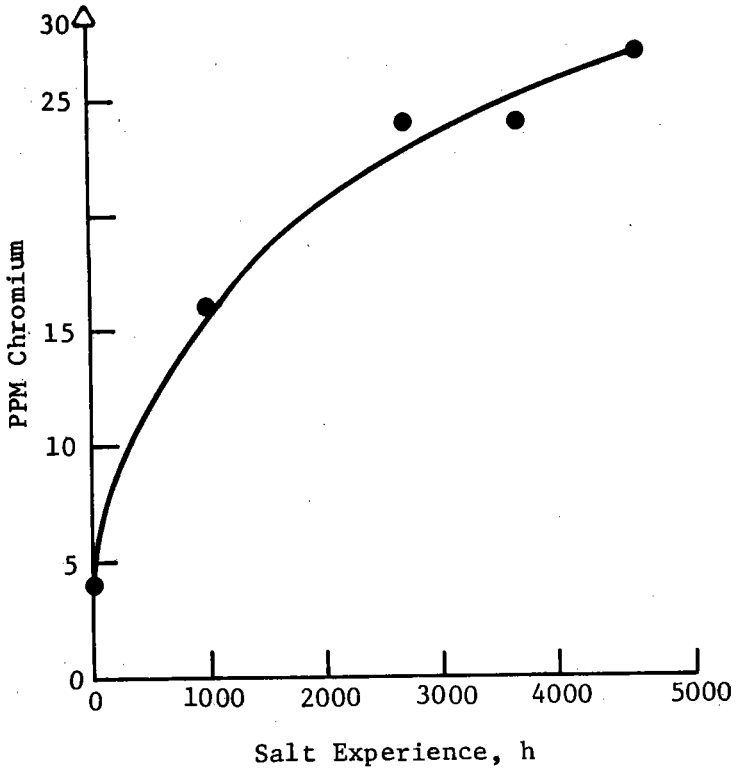

Figure III-19 Chromium Concentration vs Salt Exposure Time

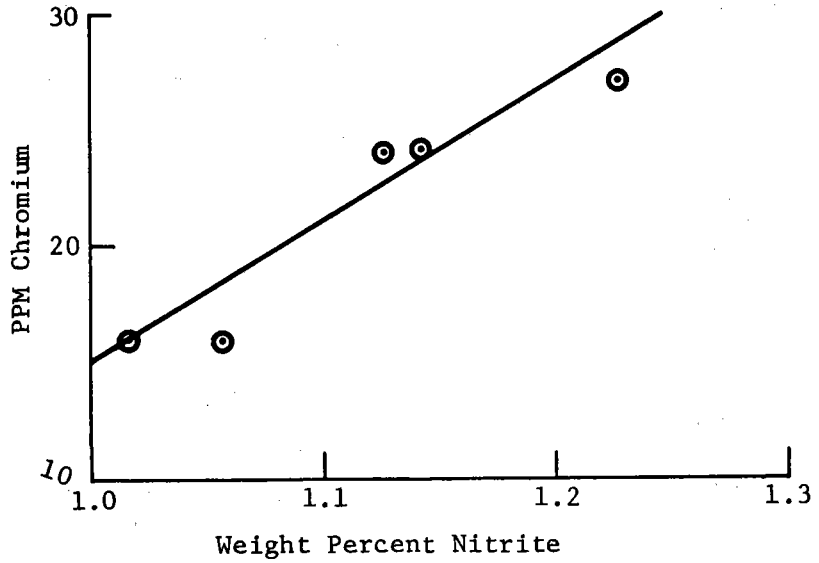

Figure III-20 Chromium-Nitrite Correlation for Fluid Loop Salt

Table III-4 Chemical Analysis of Fluid Loop Salt

FLUID LOOP SALTS						
COMPONENT WT %	0 HOURS	1000 HRS*	2000 HRS[1] 1000 HRS[2]	3700 HRS[1] 2700 HRS[2]	4719 HRS[1] 3719 HRS[2]	5715 HRS[1] 4715 HRS[2]
SODIUM	15.6	15.0	16.49	15.30	16.97	17.36
POTASSIUM	17.0	16.6	15.76	14.67	13.94	14.98
NITRATE	68.06	67.00	68.17	67.128	65.429	67.577
NITRITE	0.387	1.016	1.057	1.126	1.142	1.228
CARBONATE	0.067	0.007	0.007	<0.025	<0.025	<0.025
OXIDE	0.013	0.005	0.007	<0.007	<0.007	<0.007
CHROMIUM	0.0004	0.0016	0.0016	0.0024	0.0024	0.0027
CALCIUM	0.0065	0.0069	0.0029	0.0035	0.0026	0.0015
TOTALS	101.13	99.64	101.49	98.26	97.52	101.18

[1]LOOP EXPERIENCE IN HOURS
[2]SALT EXPERIENCE IN HOURS

*LOOP SYSTEM WAS CHARGED WITH FRESH SALT AT THIS TIME

Figure III-21 100X Micrograph of Tan Precipitate on Loop Sample

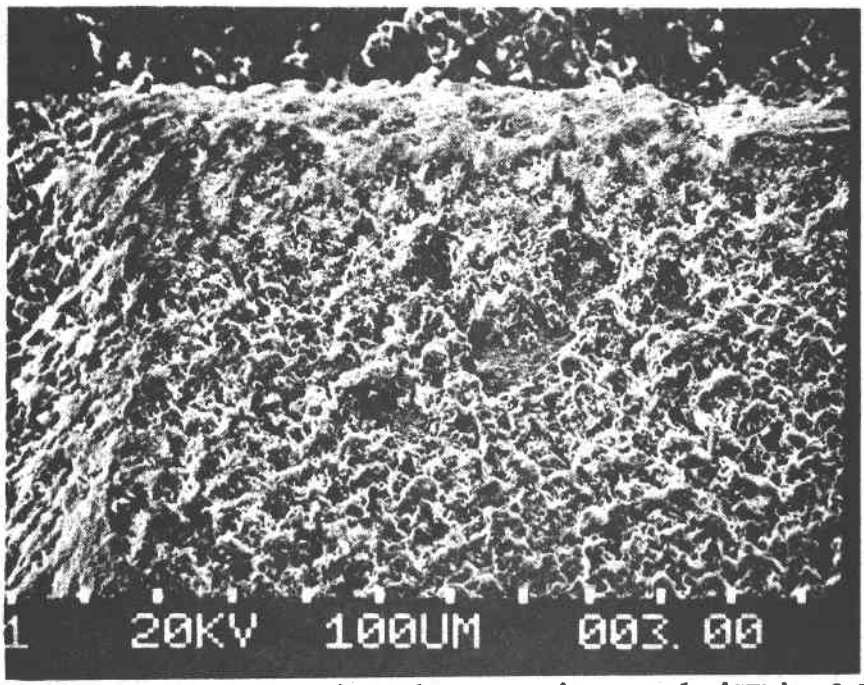

Figure III-22 100X Scanning Electron Micrograph (SEM) of Tan Precipitate on Loop Sample

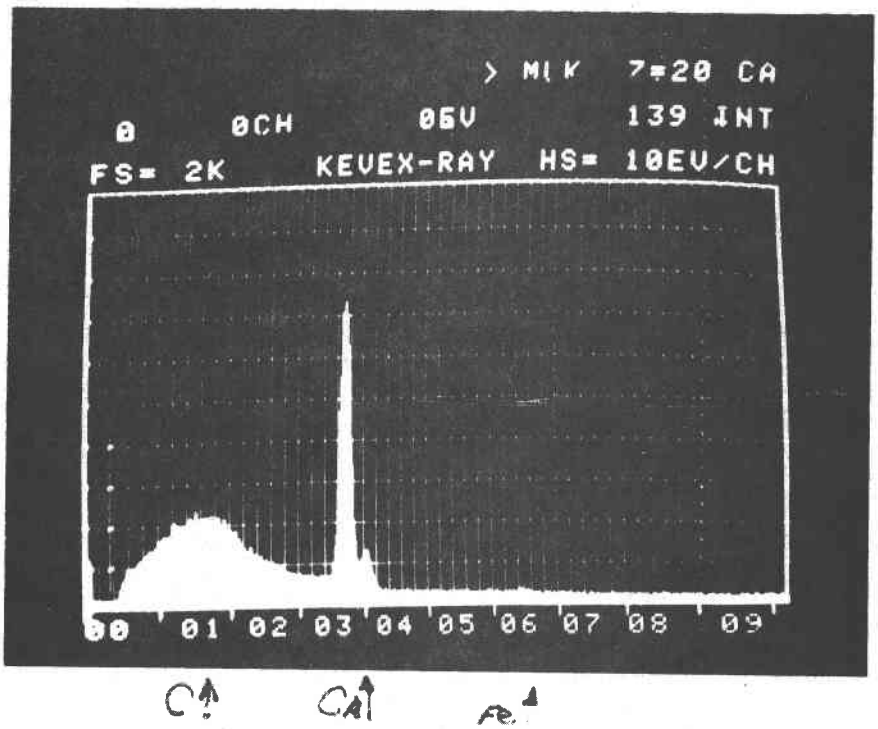

Figure III-23 SEM Kevex Analysis of Tan Precipitate

(1%). Atomic absorption analysis performed at the Chemical Technology Laboratory at Martin Marietta yielded the following additional data on the unknown residue:

Table III-4a Loop Deposit Removal from Carbon Steel Coupons (288°C, 550°F)

Component	Weight Percent
Calcium	34.63%
Sodium	0.0%
Potassium	0.0%
Iron	0.91%
Chromium	0.05%

Concurrent with the appearance of the calcium-rich deposit on the 288°C (550°F) carbon steel sample coupons, the calcium level of the recycling salt decreased from 69 ppm (0 hr) to 29 ppm (1000 hr, Figure III-24). This suggests that the low temperature carbon steel section of the loop acted to cold trap and/or nucleate calcium impurities from the technical grade nitrate salt. A specification sheet for Partherm 430 nitrate salt is included in Table III-5. A second possibility may be the inadvertent contamination of a loop section during sampling or repair which introduced ions into the salt that started nucleation (such as silicates from insulation).

After 5715 hours of loop operation, the calcium deposit did not reform on the carbon steel coupons. A large quantity (>400 mg) of a similar precipitate was, however, removed from two 1-m (3-ft) sections of collapsed counter-flow heat exchanger tubes (371-427°C, 700-800°F) that were removed from the loop after 1014 hours. In order to identify the unknown

Table III-5 Chemical Specification of Partherm 430 Salt (Park Chemical Company)

	Class 2
Sulfates (Max) (as SO_4)	0.18
Carbonates (Max) (as CO_3)	0.05
Total Chlorides (Max) (as Cl)	0.30
Alkaline Earths (Max) (Mg, Ca, Ba) (as oxides)	0.10
Fluorides	None
Moisture	0.50
Water Insoluble	0.10
Neutrality (pH 1% Sol)	6.0-8.5

NOTE: Partherm 430 will meet or be significantly below these max levels

Table III-7 Mass Spectral Analysis of Tan Precipitate (Camp Dresser and McKee, Inc.) Removed from Collapsed Tubing, 371-427°C (700-800°F)

Uranium	2	Terbium		Ruthenium		Vanadium	100
Thorium	4	Gadolinium		Molybdenum	60	Titanium	700
Bismuth	1	Europium		Niobium	30	Scandium	
Lead	700	Samarium		Zirconium	20	Calcium	≈8000
Thallium	1	Neodymium	2	Yttrium	1	Potassium	≈5000
Mercury	NR	Praseodymium	2	Strontium	40	Chlorine	70
Gold		Cerium	4	Rubidium	1	Sulfur	500
Platinum		Lanthanum	2	Bromine	4	Phosphorus	≈1000
Iridium		Barium	100	Selenium	6	Silicon	≈2%
Osmium		Cesium		Arsenic	100	Aluminum	≈2%
Rhenium	Internal Standard	Iodine	40	Germanium	1	Magnesium	≈30%
Tungsten	10	Tellurium		Gallium		Sodium	≈2000
Tantalum	1	Antimony	10	Zinc	≈1000	Fluorine	≈3000
Hafnium		Tin	9	Copper	500	Oxygen	≈4%
Lutetium		Indium	Internal Standard	Nickel	≈9000	Nitrogen	NR
Ytterbium		Cadmium	3	Cobalt	20	Carbon	NR
Thulium		Silver	1	Iron	≈2%	Boron	>1%
Erbium		Palladium		Manganese	≈3000	Beryllium	
Holmium		Rhodium		Chromium	≈9000	Lithium	20
Dysprosium							

NOTES: This sample is scheduled to be disposed of four months after the date of this report.
All elements for which values are not entered <1 ppm wt.
NR - Not reported.

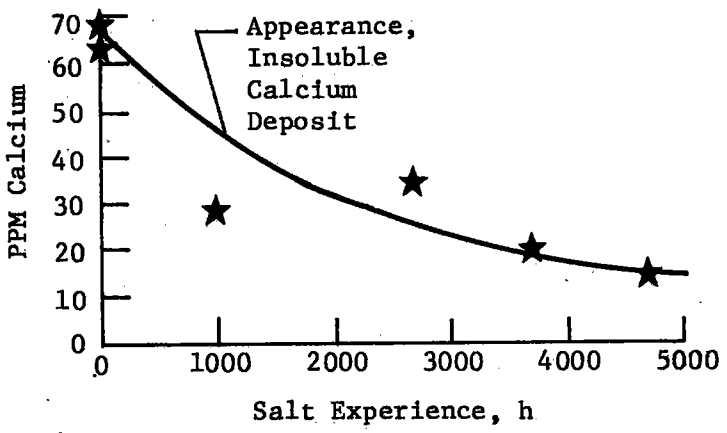

Figure III-24 Calcium Depletion in Fluid Loop Salt

residue, portions of the coating collected from the collapsed heat exchanger tubes (washed with hot distilled water to remove any occluded nitrate salts) were shipped to Huffman Laboratories, Wheat Ridge, Colorado, for oxygen, silicon, and calcium analysis and to Camp Dresser & McKee, Inc., Wheat Ridge, Colorado, for a spark source mass spectral analysis (geomascan). The elemental and semi-quantitative mass spectral analysis are included in Tables III-6 and III-7, respectively.

Table III-6 Elemental Analysis of Tan Precipitate (Huffman Laboratories)

Component	Weight Percent
Calcium	1.6
Oxygen	22.4
Silicon	1.5, 19.2*

*1.5 ppm determined by dissolving residue in nitric acid (probable silicates)
19.2 ppm determined by dissolving residue in hydrofluoric acid (probably SiO_2).

The low calcium and high magnesium concentrations were surprising because calcium was the major component of the precipitate which formed on the coupons at 288°C (550 F), while magnesium was seen to be the major component of the residue collected from the collapsed tube sections. To resolve this Ca/Mg anomaly, some of the coating in the tube area was analyzed by atomic absorption for calcium and magnesium at the Chemical Technology Laboratory, Martin Marietta. Our results indicate that the precipitate removed from the collapsed Incoloy 800 tubing contained 17.2% Ca and 16.7% Mg. The appearance of magnesium in the tan precipitate suggests: (1) the composition of the residue may be homogeneous throughout the loop (i.e., the residue may be calcium and magnesium double salts), or (2) different chemical species may precipitate from flowing salt at different temperature points in the loop. An infrared spectra of the precipitate from the collapsed tubing (KBr pellet, Figure III-25) is similar to the spectra for calcium or magnesium oxide (Figure III-26). However, subtle differences between the two spectra prevents us from positively identifying the residue as an oxide mixture. An x-ray powder diffraction was performed, yielding the following D-spacing with relative intensities:

D	I/I_o
2.14	100%
1.55	78%
1.94	60%
2.94	39%
2.70	32%
2.53	29%

This diffraction pattern did not yield a clearly identifiable pattern, and a computer search (NIH-EPA-JCPDS Powder Diffraction Search Match) suggested the compound might be a mixed oxide, silicate, or carbonate (Figure III-27).

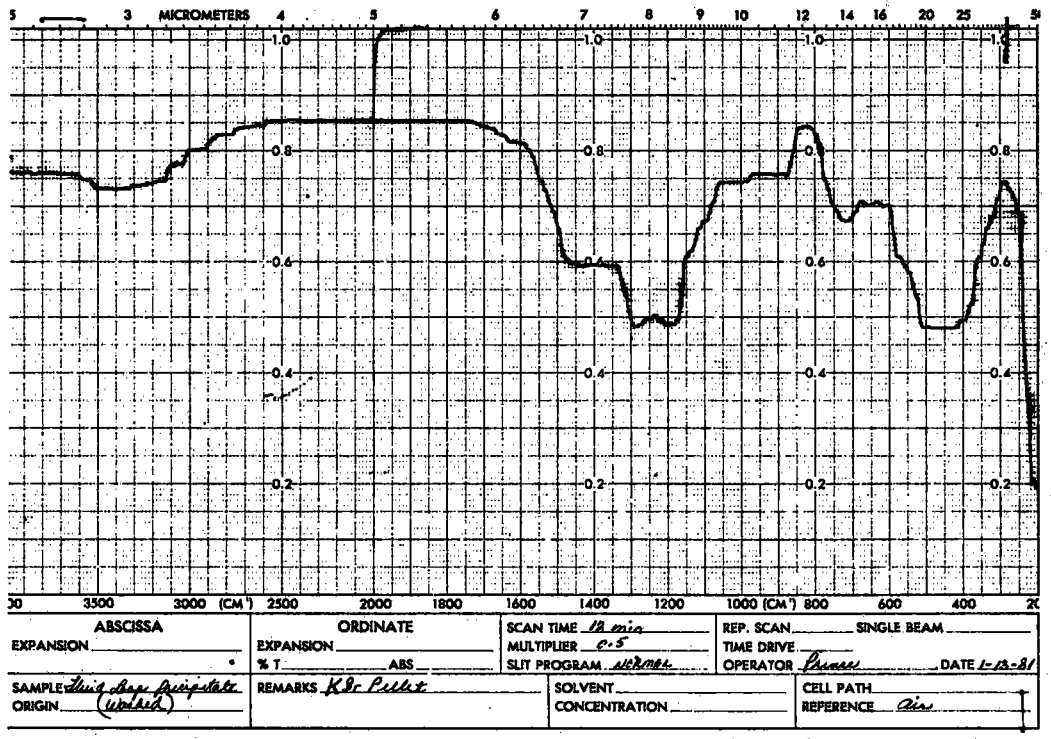

Figure III-25 Infrared Spectra of Tan Precipitate (Martin Marietta Chemistry technology Laboratory)

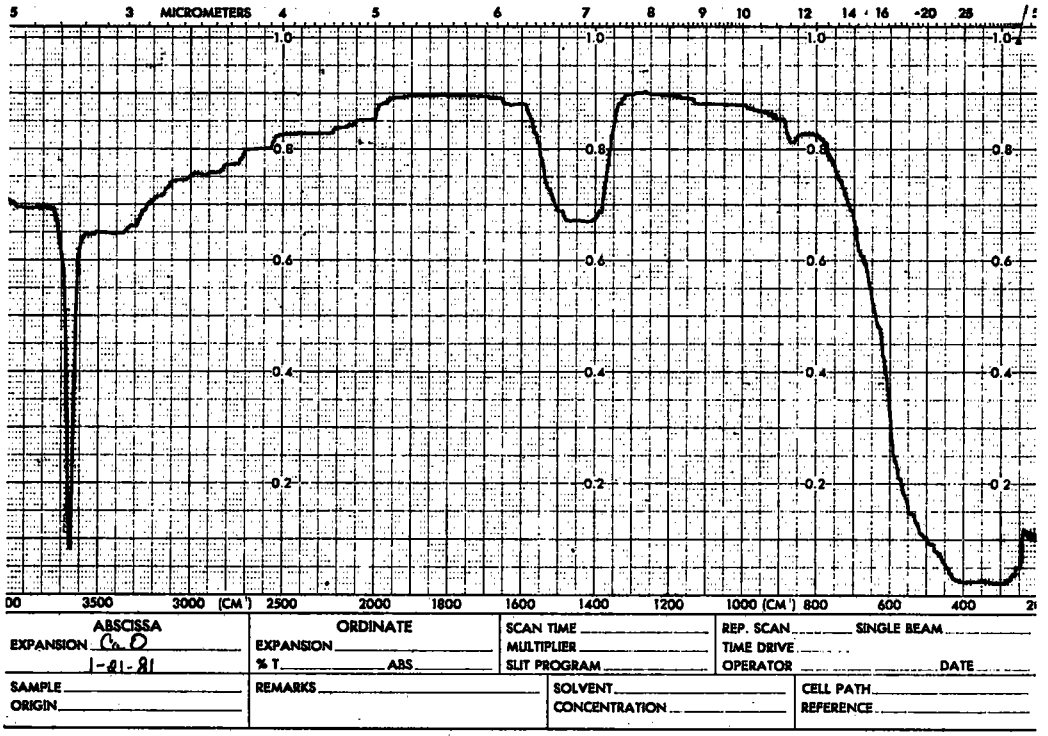

Figure III-26 Infrared Spectra of Calcium Oxide (Martin Marietta Chemistry Technology Laboratory)

Although identification of this deposit has not been made, the removal of calcium and or magnesium from the salt may eliminate the problem. The removal of these ions from molten salt could be accomplished by controlling the nitrate specifications, or 2, chemically, by adding an appropriate anion to cause precipitation of calcium and magnesium at a convenient location, or by using a cooled side stream to cause controlled precipitation of calcium and magnesium.

JCPDS#	USES%	SI	ML/X	AT(%)	IDENTITY
27-0082C	26	56.9	3/2	50	Calcium Magnesium Fluoride Silicate = Ca2Mg5(Si4O11)2F2
22-0434	32	43.8	2/1	79	Magnesium Germanium Oxide Hydroxide; Germanium magnesium hydroxide oxide (Ge2Mg4(OH)2O7) (9CI) = Mg4Ge2O7(OH)2 [12395-53-8]
18-0689	21	43.6	2/	36	Lead-Boron Sulfide; Thioboric acid (H4B2S5), lead(2+) salt (1:2) (8CI9CI) = Pb2B2S5 [20642-15-3]
11-0307*	20	43.5	2/	40	Gold cyanide (Au(CN)) (8CI9CI) = AuCN [506-65-0]
25-0808C	20	42.6	2/	37	Sodium Calcium Magnesium Silicate Hydroxide / Richterite [syn] (VAN8CI9CI) = Na2CaMg5Si8O22(OH)2 [33247-50-6]
24-0072C	18	42.6	2/	36	Iron Oxide / Hematite (Fe2O3) (9CI) = (Fe2O3)10R [1317-60-8]
25-0231O	21	42.3	2/	48	Cesium Rhodium Chloride Hydrate; Akatoreite (8CI9CI) = Cs2(RhCl5H2O) [12601-01-3]
19-0259	23	42.2	2/	49	Calcium Vanadium Oxide; Vanadic acid (H3VO4), calcium salt (2:3) (8CI9CI) = Ca3V2O8 [13550-42-0]
20-1390I	19	42.2	2/	32	Sodium Calcium Magnesium Iron Silicate Hydrox / Winchite (8CI9CI) = NaCa(Mg,Fe,Mn)5Si8O(OH) [12425-92-2]
1-0911	20	42.0	2/2	31	Sodium Zinc Phosphate; Phosphoric acid, sodium zinc salt (1:1:1) (9CI) = NaZnPO4 [20539-12-2]
25-0675*	20	41.6	2/1	31	Potassium Sodium Calcium Magnesium Silicate Hydroxide / Richterite (CaMg5KNaH4(Si4O12)2) [syn] (9CI) = KNaCaMg5Si8O22(OH)2 [66732-60-3]
1-0920I	20	41.3	2/1	41	Thorium (8CI9CI) = (Th)4F [7440-29-1]
28-1419	22	41.2	5/	42	Uranyl Sulfate Hydrate = UO2SO4.5UO3.18H2O
17-0750D	19	41.0	2/	43	Sodium Calcium Magnesium Iron Aluminum Silicate Hydrox / Richterite; ferrian; Richterite (VAN8CI9CI) = NaCaMgFeMnSiAlOH [17068-76-7]
16-0836O	21	40.8	2/4	38	Silver Sulfonyl Nitride; Sulfimide, silver(1+) salt (9CI) = Ag(NSO2)3 [66924-27-4]
24-1075*	18	40.2	2/	42	Cerium boride (CeB4) (8CI9CI) = (CeB4)20T [12007-52-2]
25-1008D	20	39.9	3/1	29	Ytterbium Silicate Chloride; Ytterbium chloride silicate (Yb3Cl(SiO4)2) (9CI) = (Yb3(SiO4)2Cl) [37341-95-0]
21-0490	20	39.7	2/1	27	Lithium Beryllium Hydride; Beryllate(1-), trihydro-, lithium (8CI9CI) = LiBeH3 [25282-11-5]
24-1458*	18	39.6	2/	44	Neodymium boride (NdB4) (9CI) = (NdB4)20T [12007-77-1]
24-1327*	18	39.5	2/1	43	Praseodymium boride (PrB4) (9CI) = (PrB4)20T [12007-78-2]
26-0509I	20	39.4	2/	46	Copper Chromium Oxide; Chromium copper oxide (Cr2CuO4) (8CI9CI) = CuCr2O4 [12018-10-9]
18-0513I	16	39.2	2/1	32	Europium Thallium; Europium, compd. with thallium (1:2) (9CI) = (Tl2Eu)6H [60883-26-3]
20-0794*	18	38.6	2/1	25	Nickel Tellurate; Telluric acid (H6TeO6), nickel(2+) salt (1:3) (8CI9CI) = Ni3TeO6 [16872-64-3]
23-0473	18	38.2	2/6	38	Potassium Boron Hydride; Borate(1-), octahydropenta-, potassium (8CI) = KB5H8 [12447-53-9]
20-1101	15	38.1	2/1	32	Sodium Copper Sulfate; Sulfuric acid, copper(2+) sodium salt (2:1:2) (8CI9CI) = Na2Cu(SO4)2 [15079-03-5]

Figure III-27 Powder Diffraction Search Match of Tan Precipitate

The buildup of this tan coating did not interfere appreciably with the loop operation. However, the potential for this type of problem in a full scale receiver system is very serious. If the precipitate is coming from the calcium and magnesium impurities in the commercial nitrate salts, then even at 50 ppm of Ca and Mg salts the potential of hundreds of pounds of coating or precipitate exists from the millions of pounds of molten salt. This precipitate may well nucleate at critical heat exchanger surfaces which has the potential of clogging tubes or altering heat flow characteristics.

c. Coupon analysis - Weight change data (reported in mg/cm^2) for coupons removed from the six loop sample ports were recorded for the 5715 hours of loop operation and are presented in Appendix A. The data is tabulated in 1000 hour exposure increments and a mean value ($\bar{X}$) and standard deviation (σ) were calculated for each interval. Some of the sample coupons (SP-3, SP-5, SP-6) were ground down after the initial weighing but prior to insertion, therefore, no weight change data is available for the first 1000 hour exposure for these coupons. Weight change data was also not available for the A-570 carbon steel coupons removed from sample port 5 (371°C (700°F)) after 4719 hours of loop opertion.

A graph of the average weight change, obtained from the data in Appendix A, versus time for the Incoloy 800 coupons exposed to flowing molten salt, is shown in Figure III-28. The direction of salt flow and attitude of the Incoloy-800 specimen sample holders are included in figures III-29 and III-30, respectively.

Incoloy test specimens located at sample port 4 (566°C (1050°F)) gained weight that paralleled the weight gain experienced by trace contaminant test coupons exposed to a reagent grade nitrate salt (579°C) doped with a maximum level of anionic impurities. Table III-8 compares the weight change results for these two material tests.

Table III-8 Comparison of Incoloy 800 Weight Gains in the Trace Contaminants Effects Test and in the Pumped Fluid Loop Test

Chemical Environment	Temp	1000 Hrs	2000 Hrs	3000 Hrs	4000 Hrs
Flowing Molten Salt	566°C	0.60	0.73	0.66	0.66
Static Max. Spec. Salt	579°C	0.54	0.56	0.72	0.80

A photograph of a 566°C (1050°F) loop coupon after 5715 hours of loop operation (Figure III- 31) shows a dull dark colored surface with some color lightening where the coupon was placed in the holder slots. The I-800 coupons removed from sample port 4 were the only test specimens which exhibited a weight gain under the conditions tested.

Incoloy-800 test specimens removed from sample port 1 (357°C (675°F)) displayed minute but consistent weight decreases with time, even though small weight gains were anticipated at this low temperature. The appearance of these coupons (see Figure III-31) exhibits a gold tinted oxide.

Specimens located at sample port 2 (482°C (900°F)) experienced greater weight losses than the coupons mentioned above. However, these weight losses, with respect to time, are small and probably not significant.

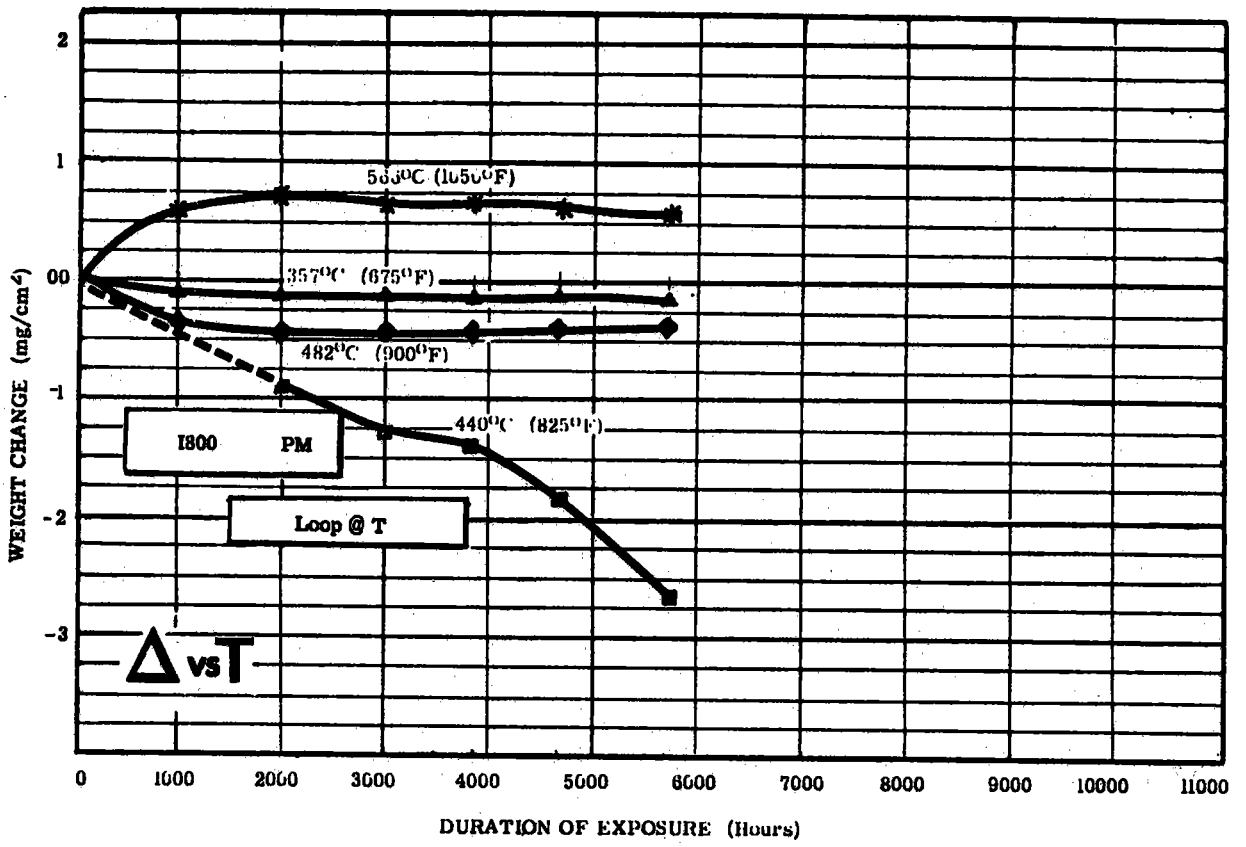

Figure III-28 Weight Change of I800 as a Function of Sample Port Temperature

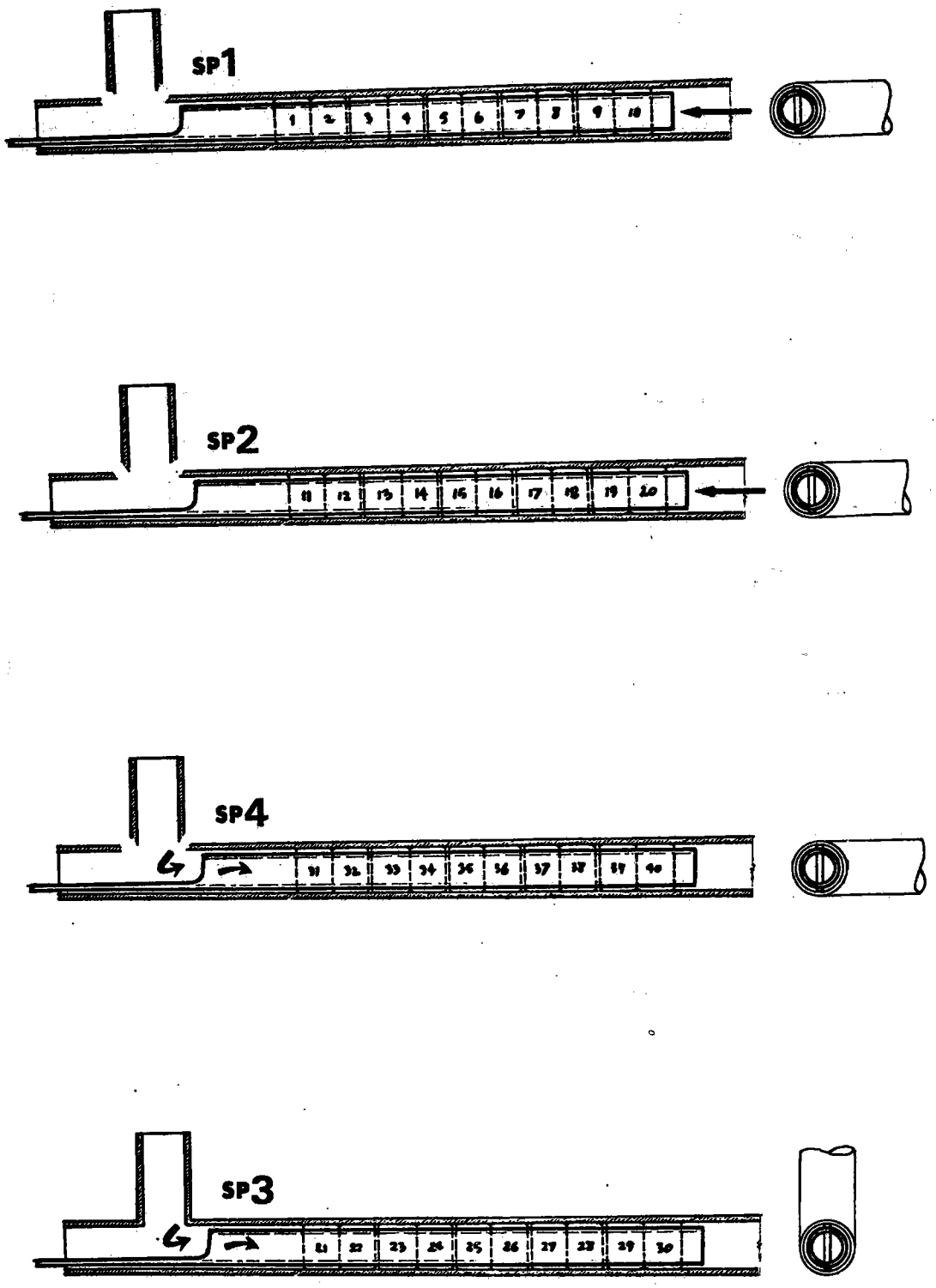

Figure III-29 Flow Direction of Molten Salt for I800 Sample Holders

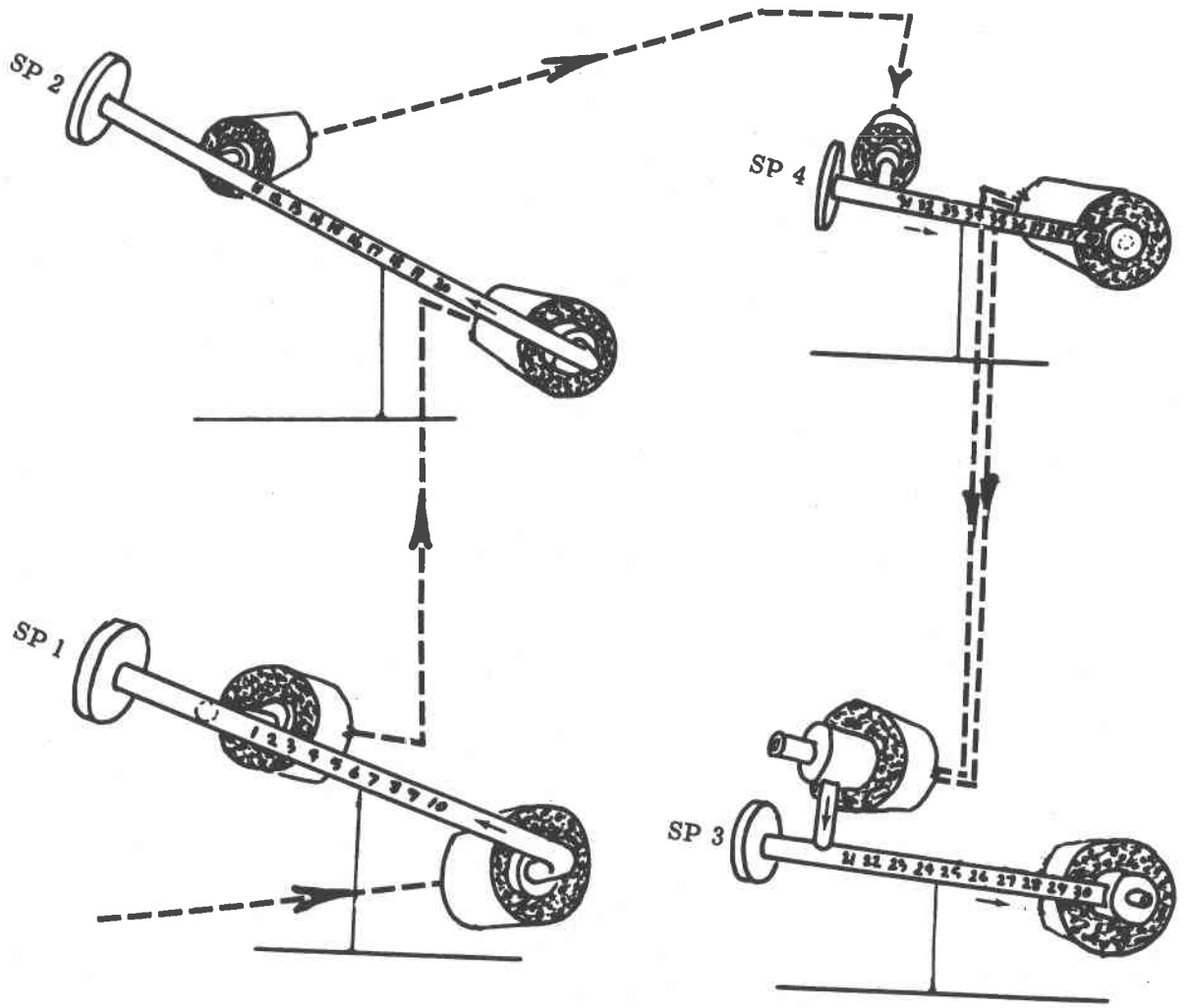

Figure III-30 Attitude of I800 Sample Holders in Molten Salt Loop

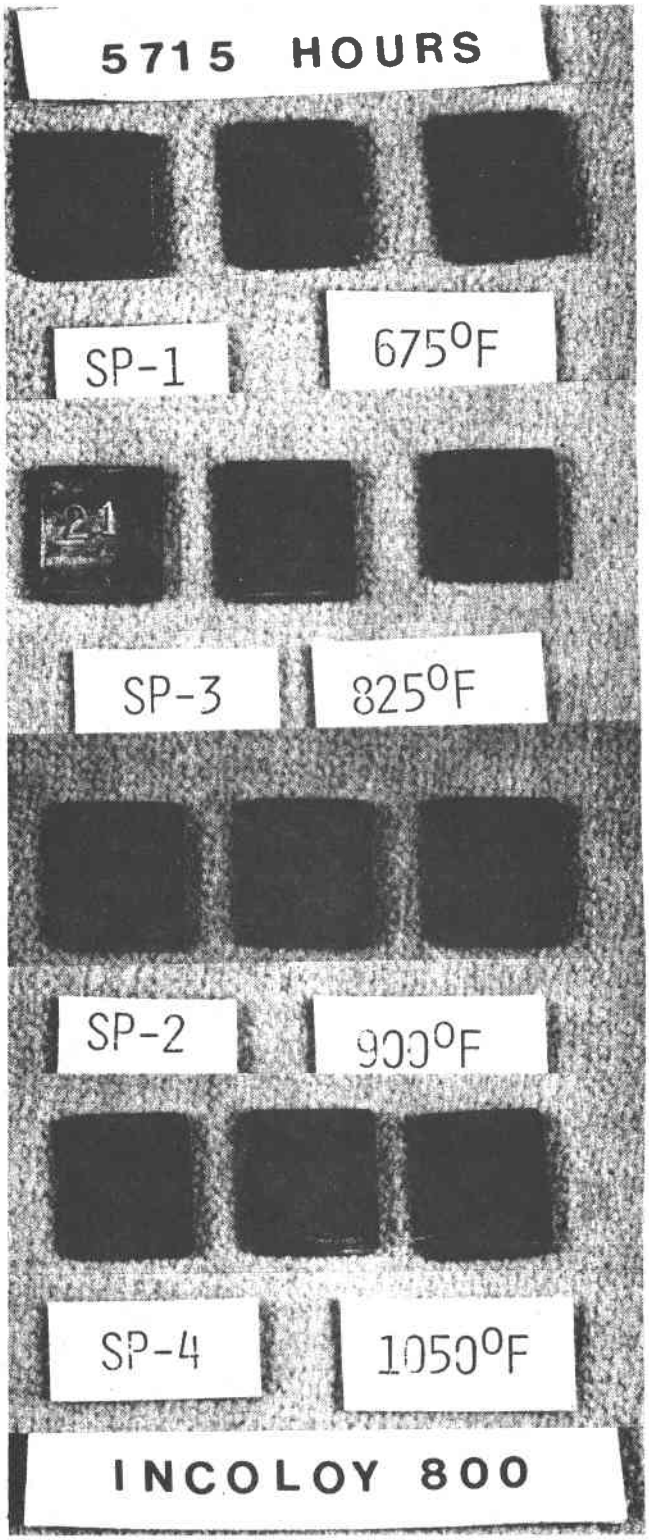

Figure III-31 Macrographs of I800 Coupons as a Function of Sample Port Temperature After Molten Salt Loop Exposure

The weight loss experienced by coupons removed from sample port 3 (440°C (825°F)) is the largest observed for the temperatures studied. Because weight changes were not available for these samples after 1000 hours of loop operation, the 440°C (825°F) weight change curve was extrapolated to zero time (dotted line on Figure III-28).

From the weight change - time results shown in Figure III-28, it appears that the oxidation behavior of I800 at 566°C (1050°F) and 482°C (900°F) is controlled by the competitive processes of oxide growth and flaking. This assumption is made by observing the trends shown in Figure III- 28, namely a slightly decreasing weight gain for the 566°C (1050°F) coupon (corresponding to a gradual oxide flaking process) after an inital weight gain (attributable to oxide growth). The 482°C (900°F) I800 coupon behavior appears similar, but with the order of controlling reactions reversed. The large, immediate weight loss for the 440°C (825°F) I800 coupon indicates a deviation from the expected oxide growth - flaking process. The absence of a weight gain section suggests that the controlling mechanism is either an oxide micro-flaking process or a metal dissolution process. Previous visual examination (see Figure III- 31) of these coupons after 5715 hours of molten salt exposure showed no evidence of drastic oxide flaking or spalling. Table III-9 lists the temperature dependence of the oxidation behavior of I800 and A570 (discussed later). A rough estimate of 30-year extrapolated metal loss values was made by adopting a model which assumes that (a) weight gains are due to surface oxides, (b) weight losses are due to flaking of surface oxides rather than metal dissolution, and (3) a worst-case scenario for long-term metal loss would consist of repeated cycles of oxidation weight gain followed by oxide spalling or flaking. Metal weight losses in a single oxidation/spalling cycle are estimated by assuming that all metal which is incorporated in an oxide is subsequently lost when that surface oxide flakes off. Metal penetration values are calculated from metal weight loss values by using conversion factors based on metal densities. Details of this extrapolation method are included in Appendix B.

Scanning Electron Microscopy (SEM) and light metallogrophy was performed on the I800 coupons. Figure III-32 shows micrographs of representative oxide layers for the four temperatures of salt exposure. Column 1 shows a 250X photomicrograph of a section ground and polished at an angle of 20 degrees, (which multiplies the layer thickness by 3.24) resulting in a total magnification of 810X. Column 2 shows the same surface as Column 1 at a total magnification of 3236X.

The 357°C (675°F) specimen displayed little oxidative surface growth, but did show an unexplained intrusion into the surface, as pictures in the 1000X SEM view of this section show.

The 440°C (825°F) specimen exhibited three distinct oxidation zones under the scanning electron microscope: the outermost zone was the least dense, exhibiting a coarse, dark structure; the center zone displayed a much finer structure; and the inner zone seemed to be a transition area between the alloy and the center oxidized zone. In general, the superstrate at 440°C is porous, channeled and fragile.

Table III-9 Extrapolated 30 Year Weight Change - Metal Reduction Values for I800 and A570 as a Function of Sample Port Temperature in Molten Salt Loop (See Appendix B)

MATERIAL	TEMPERATURE °C (°F)	WEIGHT CHANGE* (30 Years) mg/cm^2	METAL LOSS (30 Years) mm (X10^2)	MILS
I-800	357 (675)	- 5.8	.76	0.3
Parent Metal	440 (825)	- 191.7	23.9	9.4
	482 (900)	- 32.9	4.1	1.6
	566 (1050)	+ 105.2	35.2	13.9
A570	288 (550)	- 138.9	17.5	6.9
Parent Metal	371 (700)	- 230.1	29.2	11.5

* Method of weight change extrapolation:
  - Weight loss, Method c, Appendix B
  - Weight gain, Method b, Appendix B

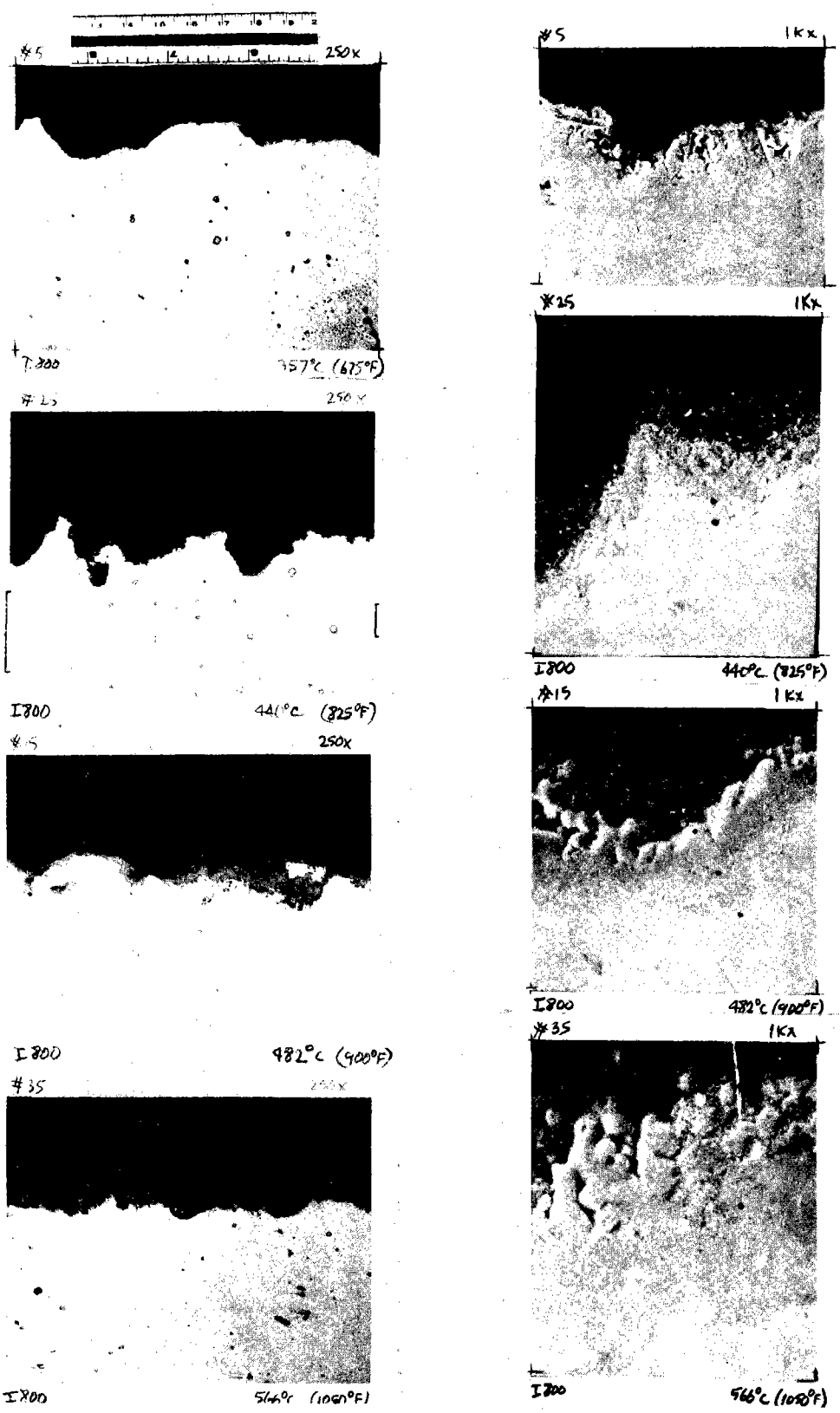

Figure III-32 SEM Micrographs of I800 Coupons as a Function of Sample Port Temperature After Molten Salt Loop Exposure

The 482°C (900°F) specimen displays a thin adherent oxide layer that is rooted in the metal substrate. This superstrate would not be likely to spall. Therefore, weight losses may result from metal etching by the salt.

The 566°C (1050°F) specimen displays less activity at the outer surface, although a number of coarse pores can be seen. The surface appearance of this specimen suggests that oxidation growth may occur at the metal substrate and oxidation products may be lost in micro quantities at the oxide/salt interface. Surface etching or metal leaching is not thought to play a role in the observed weight loss in this sample.

SEM Energy Dispersive X-Ray (EDX) was utilized to determine elemental trends across the oxide films. The 440°C (825°F) I800 coupon elemental profile across the substrate-oxide interface is shown in Figure III-33. Note the depletion of chromium into local substrate and outer oxide layers. These results support the observation of a local increase in the chromium concentration of the salt at sample port 3, 440°C (825°F). In addition, there was a notable increase in the local nitrite concentration in the salt at this location. The reason for the common occurances of these two effects at this temperature is not known at this time. The depletion of chromium noted above at the substrate-oxide interface and virtual absence of chromium in outer oxide layers was observed in Reference 1 as a part of thermal convection loop results of 316 stainless steel coupons exposed to 630°C (1166°F) molten salt[1]. It appears that the chromium depletion mechanism is highly alloy- and temperature-dependent.

The weight loss recorded for the 440°C (825°F) Incoloy 800 specimens appears to be the result of a removal of chromium, as opposed to the growth and spalling of oxide, postulated for the other three sets of I800 coupons.

The concern attributed to this behavior can be realized if one notes that continual removal of chromium from the matrix, in effect, locally changes the alloy composition, rendering it less corrosion resistant and possibly lowering its mechanical strength.

The suitability of this alloy to a 440°C salt exposure may depend on the mechanism(s) of material loss, which may be determinated by one of several materials studies, including:

a. a test designed to characterize the coupon oxidation product, both chemically and metallographically;

b. an extended exposure study of the 440°C Incoloy coupons in the loop environment, noting particularly any accelerated weight losses;

c. a study designed to test the feasibility of preoxidizing the samples in the loop to prevent further corrosion.

d. an investigation of local salt chemistry (especially NO_2/NO_3 concentration); and

1 R.W. Carling, et al "Molten Nitrate Salt Technology Development Status Report' SAND 80-8052 March 81.

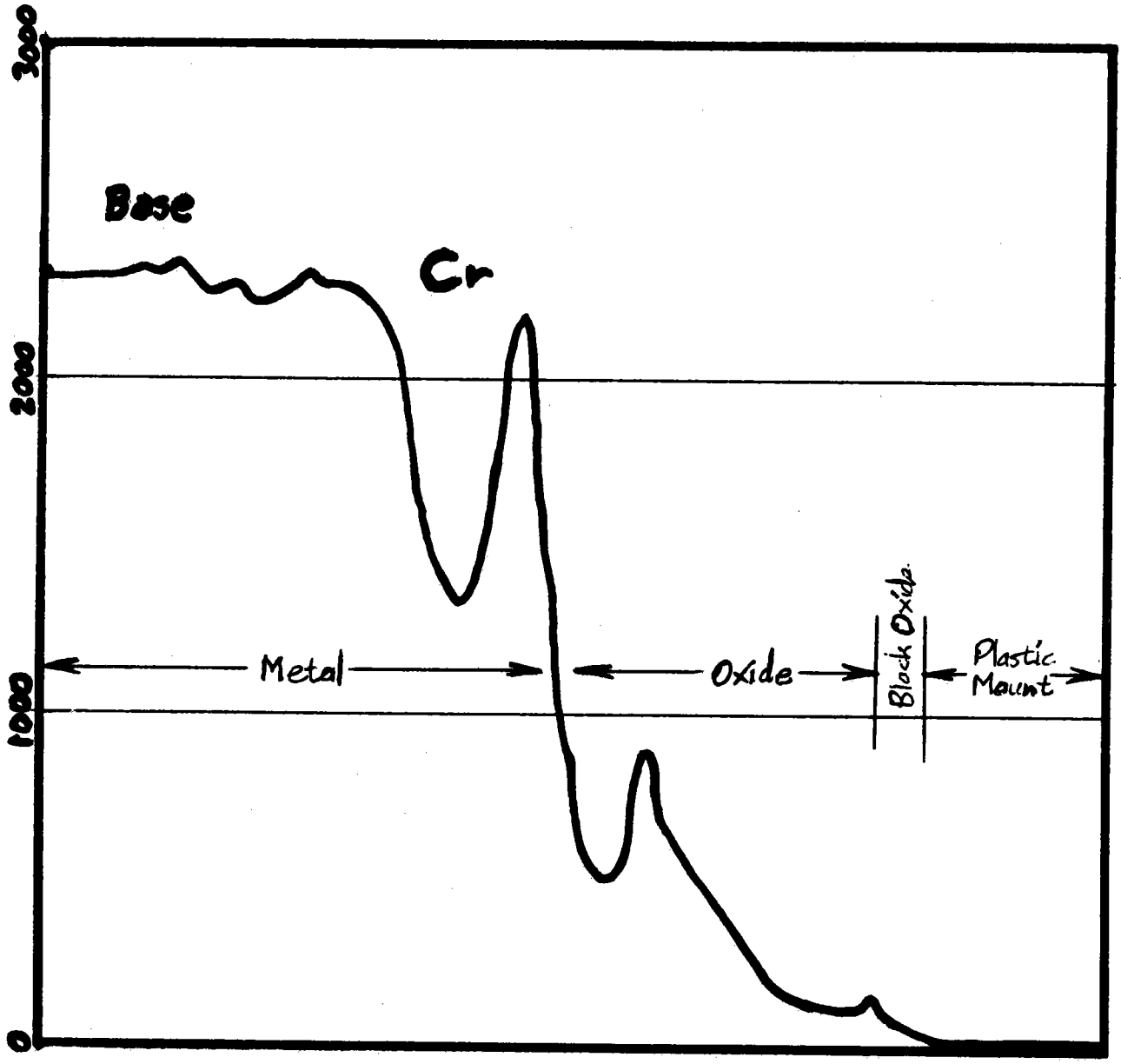

Figure III-33 SEM Energy Dispersive X-Ray (EDX) Elemental Profiles Across Oxide - Substrate Interface for I800 Coupon Exposed to 440°C (825°F) Salt in Flow Loop

e. studies designed to determine if weight losses may be minimized by doping the nitrate salt with a chemical corrosion inhibitor.

It was also observed that coupons contained in the SP-3 (440°C(825°F)) holder first exposed to flowing salt lost more weight than the last specimens in the coupon holder. This observation was consistent for each 1000 hour exposure interval. A graphical representation relating relative coupon position with weight change (mg/cm^2) is shown in Figure III-34. A three dimensional graphical representation relating coupon position, weight change, and exposure time is included in Appendix A. Coupons positioned upstream of flowing molten salt experienced a higher weight loss than those placed downstream. The observation that the last 1000 hour exposure produced a much greater weight loss at sample port 3 than the first 1000 hour exposure suggests (but does not confirm) an accelerated material loss. Evidence from the other sample ports also substantiate that material loss is greatest when the coupon is located upstream. This "skewing" of coupon weight change in an individual sample port due to coupon location may be due to several factors:

a. Material loss may be caused by particulate erosion, and may be higher in the early section of the sample port.

b. Diffusion of chromium through the metal oxidaton layer into the salt may be more rapid at one end of a sample port. Since diffusion processes are presumed to be slow with respect to fluid velocity, this rationale is not likely. The salt chromium concentration, however, is expected to be somewhat higher at the tailing end of the sample holder than at the leading end, where the coupons experience "fresh" salt, and diffusion processes are governed by concentration gradients.

c. Turbulent fluid flow into the sample holder (caused by the change in direction of salt flow in going from the tube elbow into the sample holder) may increase specimen fretting in the slot holders, excessive particulate erosion, or an increase in chromium solution.

Weight changes of A570 carbon steel specimens with respect to the duration of exposure to flowing molten salt at 288°C (550°F, sample port 6) and 371°C (700°F, sample port 5) are presented in Figure III-35. Because the first 1000 hour weight change data was not available, individual weight-loss curves were extrapolated to zero time and zero weight change as indicated by the dashed line. After 4000 hours of salt exposure, both sets of coupons appeared to attain a constant weight which may be representative of a balance between weight gain and weight loss.

Extrapolated 30 year weight loss and thickness reduction were presented previously in Table III-9. These values were calculated assuming a worst case linear weight loss. In actuality, the competitive oxide growth-flaking mechanism would prevent continual metal loss, thus the values shown in Table III-9 are conservative.

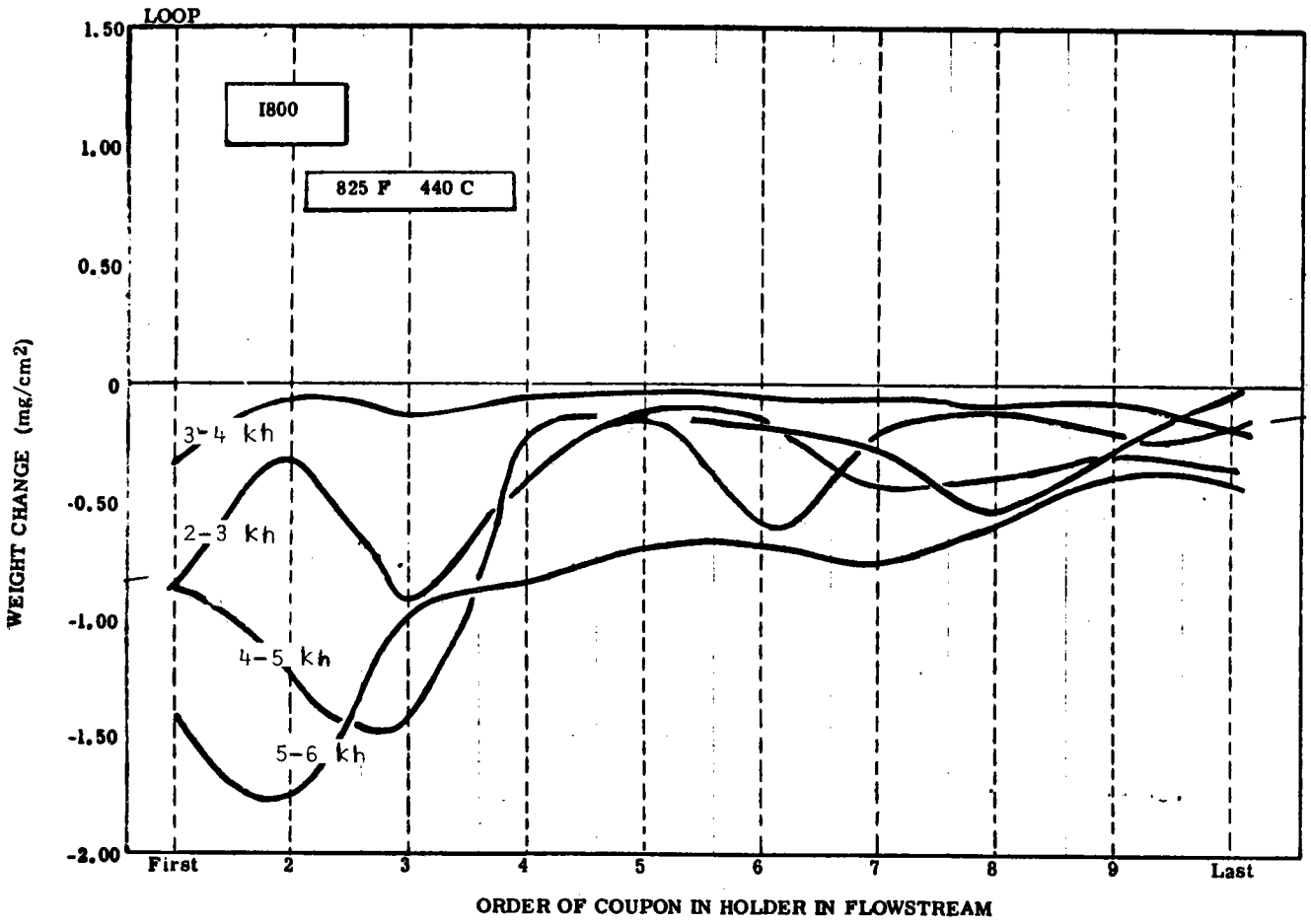

Figure III-34 Weight Change as a Function of Coupon Location in Specimen Holder for I800 at 440°C (825°F)

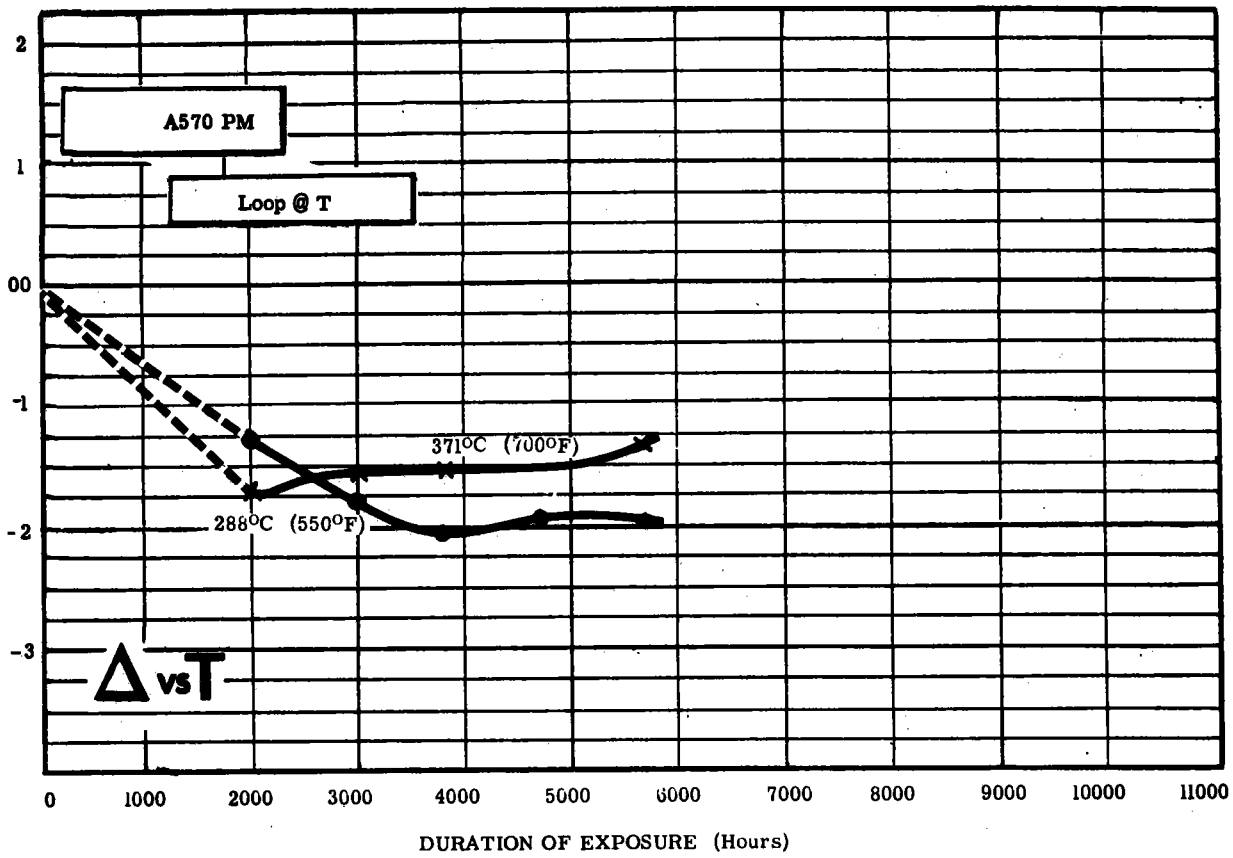

Figure III-35 Weight Change of A570 as a Function of Sample Port Temperature

Photographs of A570 carbon steel coupons removed from sample ports 5 (371°C) and 6 (288°C) after 5715 hours of loop operation are shown in Figure III-37. After 2000 hours, the low temperature, 288°C (550°F) specimens were covered with a hard brown precipitate that was insoluble in hot water but soluble in 10% hydrochloric acid (HCl). Analyses of this tan residue are documented in the following sections. The tan coat may have interferred with weight change determinations (coupons were washed with 10% HCl prior to weighing) and may have protected the metal surface from further salt oxidation or erosion. The tan residue was absent from the 288°C coupons removed after 5715 hours, and the metal had a rust-colored appearance (more of the 371°C (700°F) carbon steel specimens exhibited surface flaking after 5715 hours of molten slt exposure).

SEM photographs of A570 specimens removed from sample port 5 371°C (coupon "E") and sample port 6 288°C (coupon "0") are shown in Figures III-38 and III-39, respectively. The surfaces, as seen in the SEM, may be especially susceptible to particulate erosion.

The first five coupons in sample port 6 (288°C (550°F)) were found to lose about 8% more weight than the last five in the salt fluid stream. This dependence of A570 alloy weight loss on coupon position was also observed for the Incoloy specimens at higher temperatures. Figure III-40 shows the flow direction for the low temperature carbon steel specimens.

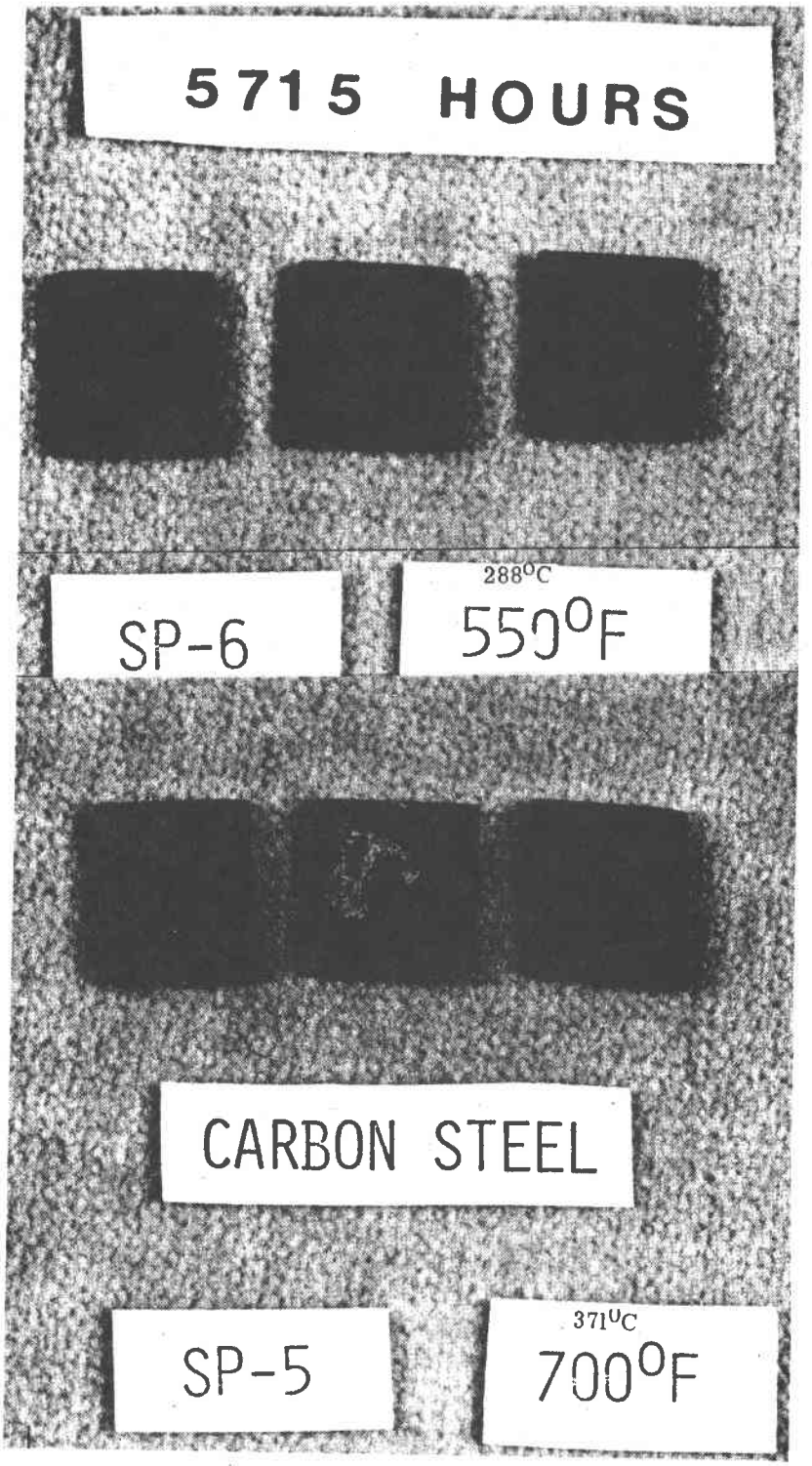

Figure III-37 Macrographs of A570 Carbon Steel Coupons as a Function of Temperature After 5715 Hours Loop Exposure

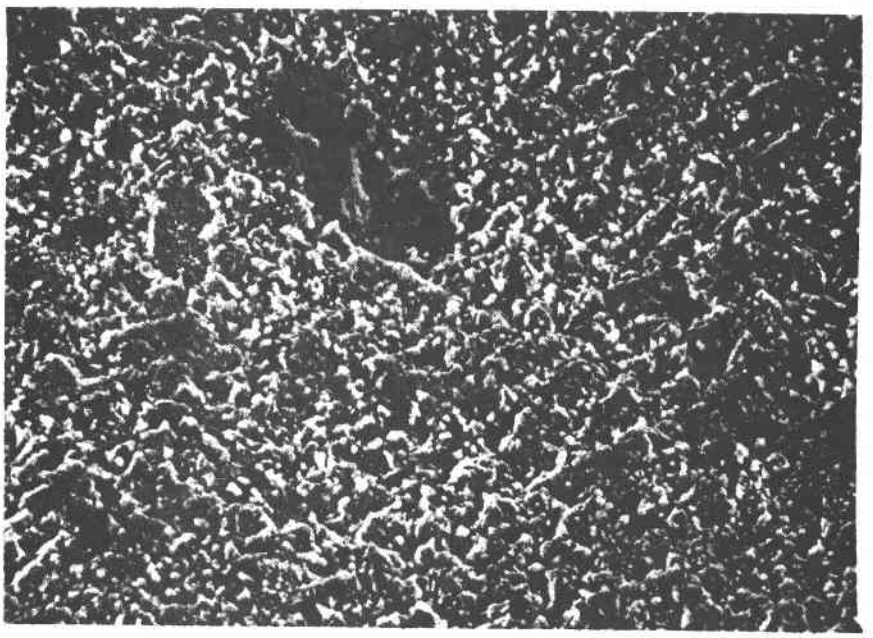

Figure III-38 SEM Micrographs of Surface of A570 Coupon Exposed to 288°C (550°F) Salt in Flow Loop (1000x)

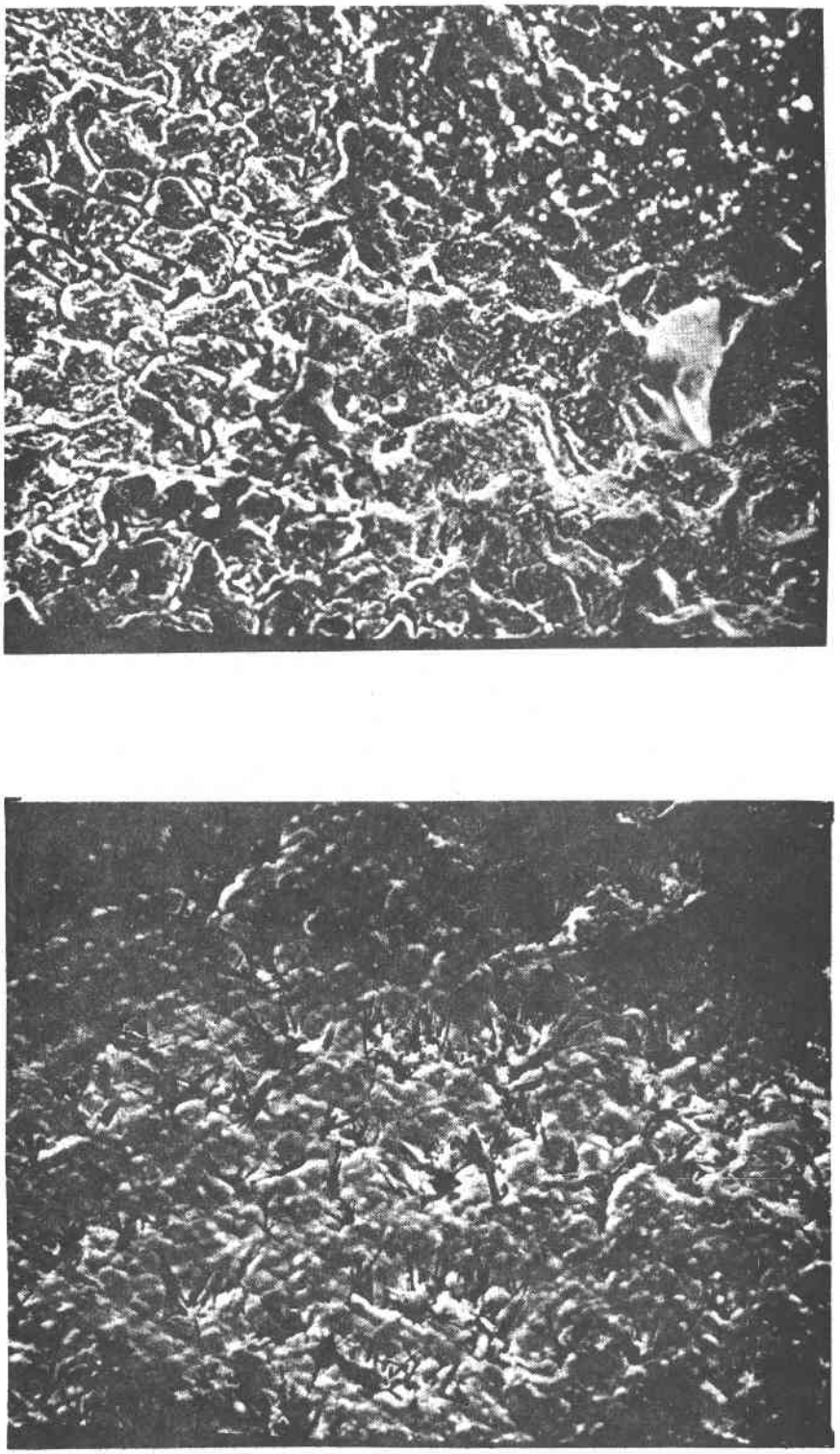

Figure III-39 SEM Micrographs of Surface of A570 Coupon Exposed to 371°C (700°F) Salt in Flow Loop (1000x)

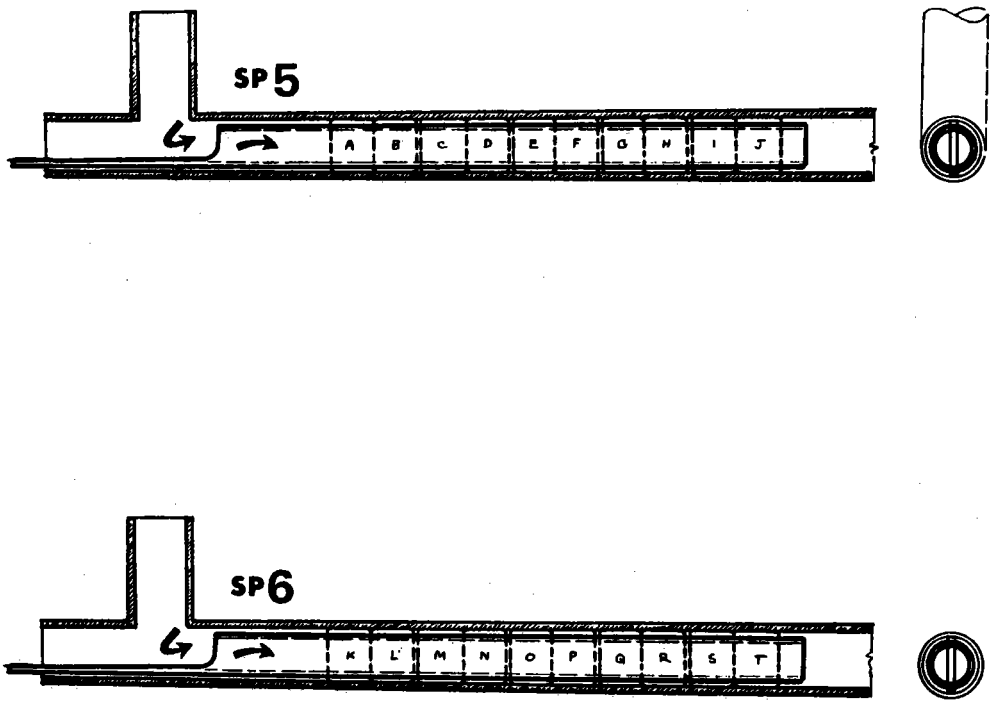

Figure III-40 Flow Direction of Molten Salt for Carbon Steel Sample Holders

B. ANALYSIS OF THE RECEIVER SRE SALT SAMPLES

Salt samples were taken from the 288°C (550°F) molten salt sump of the receiver SRE at CRTF in Albuquerque, New Mexico, during various conditions of solar radiative tests. These samples were transported to Martin Marietta Aerospace, Denver, and analyzed as described in Appendix A. In addition, a salt sample was removed from the receiver outlet [566°C (1050°F)] and compared with a sump sample taken on the same day. The outlet sample was collected in a 1.27cm (0.5 in.) diameter section of 304 SS tubing. The two salt samples were analyzed for nitrite composition to ascertain whether a higher nitrite concentration was formed in the tubes of the receiver panel. A higher nitrite composition would affect the determination of an apparent heat capacity (Cp) for molten salt and calculations of receiver efficiencies.

The results of the analysis of four receiver salt samples (R-1 through R-4) removed from the sump area of the receiver is included in Table III-10. The data indicate that no appreciable oxide or carbonate decomposition products were formed, although nitrite and chromium levels increased with time.

The results of the nitrite analysis for salts taken from the sump area and receiver outlet are as follows:

288°C (550°F) Sump Sample	1.12% Nitrite
566°C (1050°F) Outlet Sample	1.14% Nitrite

These results indicate that nitrite concentration may be expected to be homogenous in the salt flowing in the receiver SRE.

Note that the salt from the receiver sump, which was vented to the atmosphere for approximately six months, shows carbonate and oxide percentages much lower than those from the static laboratory tests. The reason for this is probably two-fold. First, and most importantly, the sump salt was kept at 288-316°C (550-600°F) during most of the SRE testing, which is lower than the static tests. Second, the surface area of salt exposed to the air compared to the salt volume is much lower for the sump than for the static tests.

Table III-10 Chemical Analysis of Receiver SRE Sump Salt Samples

Component WT %	R-1 7-29-80	R-2 9-18-80	R-3 10-17-80	R-4 12-1-80
Sodium	17.85	17.12	15.34	16.45
Potassium	14.96	16.10	15.77	16.21
Nitrate	68.246	67.804	67.281	66.660
Nitrite	0.078	0.604	1.060	1.263
Carbonate	(0.024)	(0.024)	(0.024)	(0.024)
Oxide	(0.006)	(0.006)	(0.006)	(0.006)
Chromium	0.0004	0.0005	0.0005	0.0007
TOTALS	101.16	101.66	99.48	100.61

IV. STRUCTURAL ALLOY IMMERSION TESTS

A. TRACE CONTAMINANTS EFFECTS TESTS

The objective of these tests was to evaluate the corrosion effects of anionic contaminants on selected candidate materials of construction for molten salt receivers and auxiliary equipment. The results should be useful both from a standpoint of material selection for molten salt handling equipment, and in determining if there is a need to control any of the impurities in the commercial salts. The test approach, including method of data presentation and analysis, is outlined in Subsection 1; this is followed by a presentation and discussion of results in Subsection 2 and 3 for the high-nickel; chromium and carbon steel alloys respectively. Supplementing the corrosion data, were chemical analyses performed on the doped nitrate salt baths used during the tests, as discussed in Subsection 4. Concluding remarks are presented in Subsection 5.

1. Test Method

A synthetic mixture of chemically pure reagent-grade nitrate salt (60% $NaNO_3$, 40% KNO_3) was prepared and subsequently doped with maximum amounts of chloride ion (Cl^-), sulfate ion (SO_4^{-2}), hydroxide ion (OH^-), and carbonate ion (CO_3^{-2}), as specified for commercial grade salt. The maximum specification of impurities in commercial grade sodium nitrate and potassium nitrate were obtained during Phase I by Badger Corp. The "Max Spec" used in the Trace Contaminants Test was determined from the maximum weight percent of each trace contaminant of interest allowed in either sodium nitrate or potassium nitrate (whichever was greatest). The maximum allowable concentrations of sodium sulfate and sodium chloride in sodium nitrate were a 0.35% and 0.25%, respectively. Therefore, these values were used as "Max Spec" in the trace contaminants test. The maximum allowable concentration of

sodium carbonate in sodium nitrate was 0.20 wt%. It was decided to use potassium carbonate in the Trace Contaminate Test. The "Max Spec" value of 0.26% potassium carbonate, contains the same concentration of carbonate in as 0.20% sodium carbonate.

Commercially available potassium nitrate contains 0.45% potassium oxide (by analysis). In addition, the specification allows for 0.1% sodium hydroxide. This amount of potassium oxide is equivalent to 0.38% sodium hydroxide; the total oxide/hydroxide is therefore equivalent to 0.48% sodium hydroxide, the "Max spec" used in the Trace Contaminants Test.

Immersion coupons of the candidate containment materials (Incoloy-800, RA 330, 316L, 347, ASTM A570 and ASTM A387) were prepared and exposed to the doped nitrate salts as shown in Table IV-1.

Table IV-1 Test Matrix for Trace Contaminants Tests

Chemical Dopant	WT%	579°C (1075°F) Incoloy 800	579°C (1075°F) RA330	579°C (1075°F) 316L	579°C (1075°F) 347	399°C (750°F) A570	288°C (550°F) A570	288°C (550°F) A387
NaOH	0.50	XXX	XXX	XXX	XXX	XXX	XXX	XXX
		XXX	XXX	XXX	XXX	XXX	XXX	XXX
K_2CO_3	0.26	XXX	XXX	XXX	XXX	XXX	XXX	XXX
		XXX	XXX	XXX	XXX	XXX	XXX	XXX
Na_2SO_4	0.35	XXX	XXX	XXX	XXX	XXX	XXX	XXX
		XXX	XXX	XXX	XXX	XXX	XXX	XXX
NaCl	0.25	XXX	XXX	XXX	XXX	XXX	XXX	XXX
		XXX	XXX	XXX	XXX	XXX	XXX	XXX
*NaCl	0.50	XXX				XXX	XXX	XXX
		XXX				XXX	XXX	XXX
Blank		XXX	XXX	XXX	XXX	XXX	XXX	XXX
		XXX	XXX	XXX	XXX	XXX	XXX	XXX
Max. Spec. of All.		XXX	XXX	XXX	XXX	XXX	XXX	XXX
		XXX	XXX	XXX	XXX	XXX	XXX	XXX

*Double the Max. Spec. Level.

The containers used in the trace contaminants tests were each constructed from the same material as the immersion coupons. Each end of the pipe containers [38.1 mm (1.5 in) diameter by 381 mm (15 in) long] was closed off with a pipe cap made of the same material. The matching of container materials to test specimen materials was performed to eliminate any dissimilar metal effects. A typical trace contaminant specimen container is shown in Figure IV-1.

Prior to the initiation of a test exposure, all specimen containers were passivated by exposure to molten salt for 48 hours. The Incoloy 800 (I800), RA 330, 316L,and 347 containers were exposed to 570°C (1075°F) molten salt while the A387 and A570 containers were exposed to 399°C (750°F) molten salt.

The high-nickel (I800, RA330) and stainless steel (316L, 347) alloy test specimens were vapor degreased and passivated in a nitric acid - sodium dichromate solution prior to immersion. The carbon steel coupons were vapor degreased prior to exposure.

Each container was filled with 250 grams of the appropriate salt mixture, as shown previously in Table IV-1. Test coupons were placed in the containers in such a manner as to prevent physical contact between specimens and container surfaces. Nichrome wire was used to suspend the coupons in the salt mixture. Three types of specimens were used to analyze the effects of trace contaminants in the salt; parent metal (PM), welded (W) and crevice geometry (W_c). Parent metal and welded specimens were of the same geometry, 19.05 mm (0.75 in) square by 1.60 mm (0.063 in) thick. The crevice coupons, which had limited use, were made by welding together two square [19.05 mm (0.75 in)] coupons in a lapped configuration. This geometry produced a 12.7 mm (0.5 in) long by 19.05 mm (0.75 in) wide crevice between the welded coupons.

Two stainless steel test ovens, chamber size, 51x51x15cm (20x20x6"), were used in the trace contaminants effects test. Test temperatures were controlled with a 30-amp Love Controller. Outlet purge tubes of individual vessels were manifolded together so that containers of common dopant ions were interconnected and lead to an ascarite/calcium chloride absorption tube (designed to remove atmospheric water vapor and carbon dioxide). Oven temperature(s) were maintained and recorded daily and adjusted as needed.

After every 1000 hour exposure interval the sample coupons were removed from the container, washed free of nitrate salt, dried in a nitrogen stream and weighed. At the end of 2000 hours, the salt was removed from each container (by pouring into a cold Incoloy tray) and each container recharged with fresh doped nitrate salt. At the end of 4000 hours the test was terminated. Weight change values for the exposed specimens were recorded for each of the four-1000 hour intervals. Salts removed after 2000 and 4000 hours of testing were analyzed for doped anions according to the analytical procedures described in Appendix B. Metallographic examination on each of the alloys exposed was performed to determine the nature and degree of chemical (salt) attack.

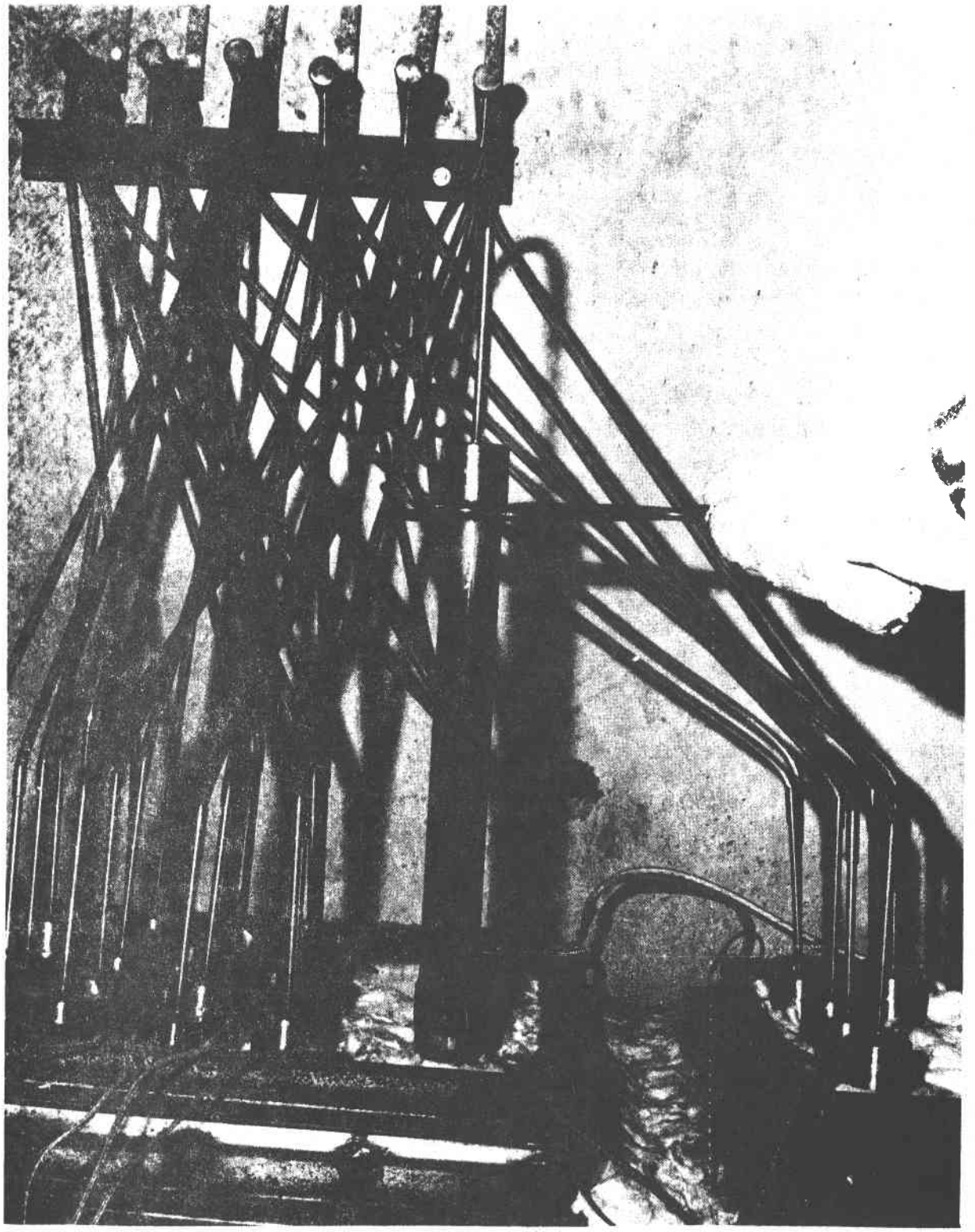

Figure IV-1 Trace Contaminant Specimen Container

Pages IV-5 through IV-8 and

Figures IV-2 and IV-3

have been deleted.

2. Results

a. High-nickel alloys, 300-series stainless steels - Average coupon weight change data (in mg/cm^2) for the high-nickel alloys and 300-series stainless steels (I800, RA330, 316L, 347), recorded at 1000 hour intervals are presented in Appendix B. The weight change vs time (t) plots obtained from Appendix B are shown on Figures IV-4 and IV-5. These figures show weight change behavior for unwelded (parent metal) coupons exposed to 580°C (1075°F) molten salt with different trace contaminant additions.

A diffusion limited, diminishing oxide growth behavior is seen for I800, RA300 and 316L. This limiting oxide film behavior suggests the removal of small shallow oxide flakes or particles compensated by oxide formation. The short duration of molten salt exposure does not allow confirmation of the true period of weight gain - weight loss behavior. The extended immersion tests, presented in the next section, should provide an insight into the long duration oxide behavior. By contrast, a linear oxidation rate for the given test duration is observed for 347 stainless steel coupons exposed to carbonate ($CO_3^=$), sulfate ($SO_4^=$) and chloride (Cl^-) additions to the salt. This linear oxidation behavior may be the result of rapid oxide, flake removal from the oxide, continually exposing fresh metal to the salt environment.

The hydroxide (OH^-) contaminant for the 347 results indicate a large flaking cycle behavior. This would most likely translate itself into a steadily decreasing sawtooth weight gain - weight loss curve with increasing exposure time.

The log Δ- log t graphical representation of the previous weight gain data is presented in Figure IV-6 and IV-7. Figure IV-8 presents a comparative log Δ - log t plot for all of the parent metal alloys subjected to blank salt and sum of all contaminant exposures. Examination of the log Δ - log t graphs (Figure IV-8) does not show a break in linearity for the blank salt (B) exposure for all of the parent metal alloys. The sum of all contaminant log Δ - log t graphs show a break in linearity for 347 and 316L which corresponds nicely to an oxide flaking process shown on the weight gain (Δ) - time (t) graphs for these conditions (see Appendix B.) In general, most of the alloys exposed to the trace contaminants experienced a break in oxidation weight gain kinetics during the test interval of 2000-4000 hours. As previously discussed, this breaks in linearity is associated with a change in the controlling mechanism, namely the onset of an oxide flaking process.

Appendix B contains weight change-time and log Δ - log t graphical representation of all the trace contaminant results not presented here. Table IV-2 and IV-3 lists comparative extrapolated weight loss and metal reduction values all of the trace contaminant additions.

In general, the extrapolated 30-year metal reduction appears to be greatest for the welded coupons exposed to all of the trace contaminant additions for the high nickel (I800, RA330) and 300-series stainless steel (347, 316L) alloys. The larger results attributed to the welded coupons may be the result of local compositional changes due to weld pool dilution,

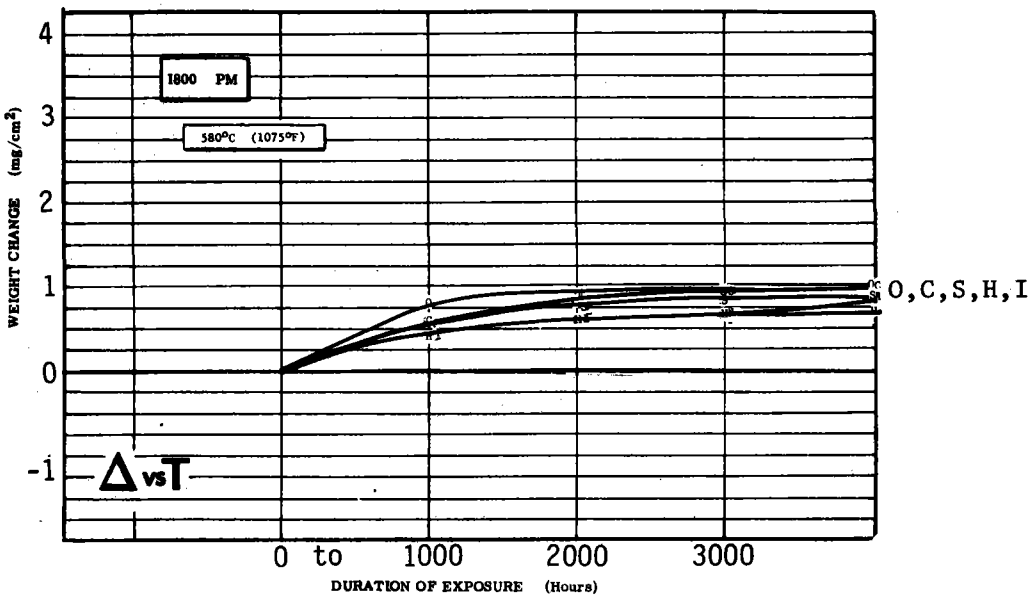

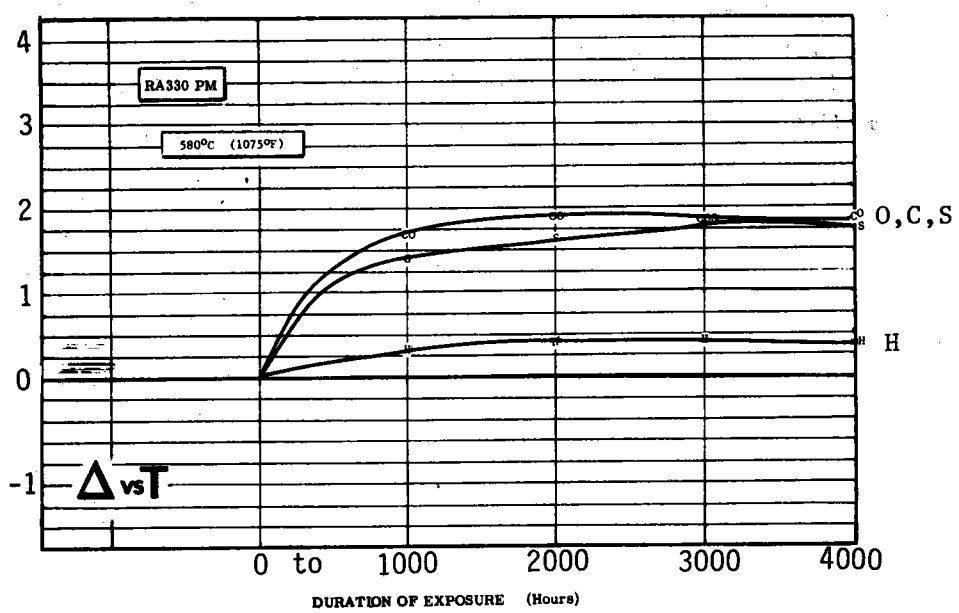

KEY:
- O 0.50 Wt % OH^-
- C 0.26 Wt % $CO_3^=$
- S 0.35 Wt % $SO_4^=$
- H 0.25 Wt % $C\ell^-$
- I 0.50 Wt % $C\ell^-$

Figure IV-4 Weight Change vs Time for I800 and RA330 Parent Metal Coupons in 580°C (1075 F) Molten Salt with Different Trace Contaminants

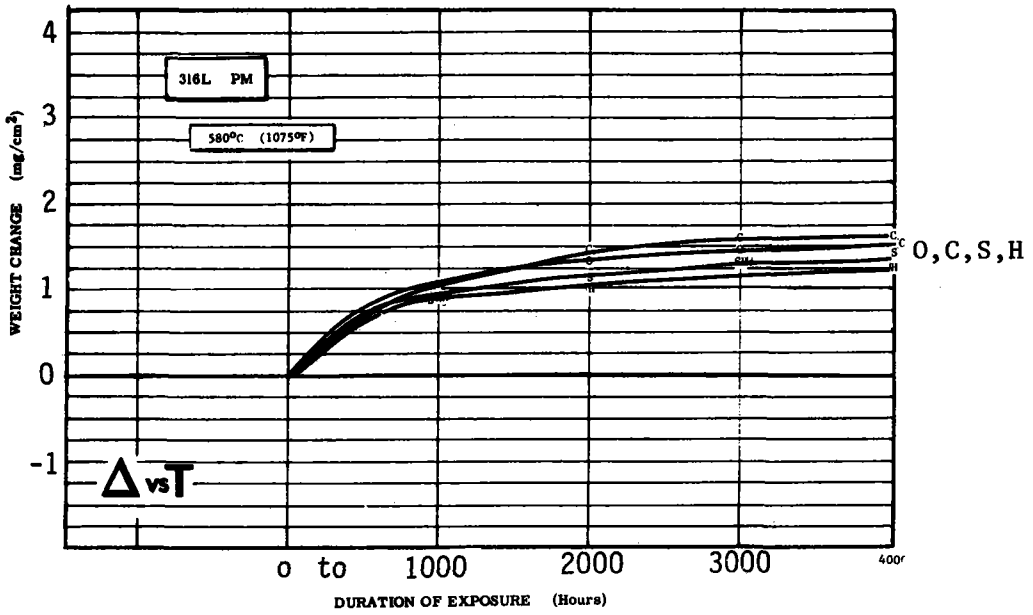

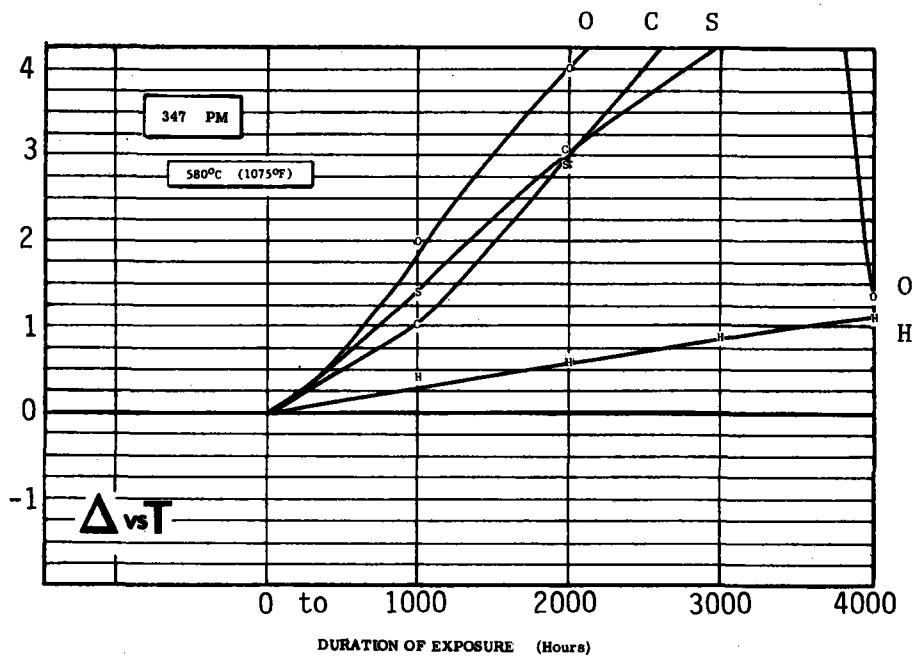

KEY:
- O 0.50 Wt % OH^-
- C 0.26 Wt % $CO_3^=$
- S 0.35 Wt % $SO_4^=$
- H 0.25 Wt % $C\ell^-$
- I 0.50 Wt % $C\ell^-$

Figure IV-5 Weight Change vs Time for 316L and 347 Parent Metal Coupons in 580°C (1075°F) Molten Salt with Different Trace Contaminants

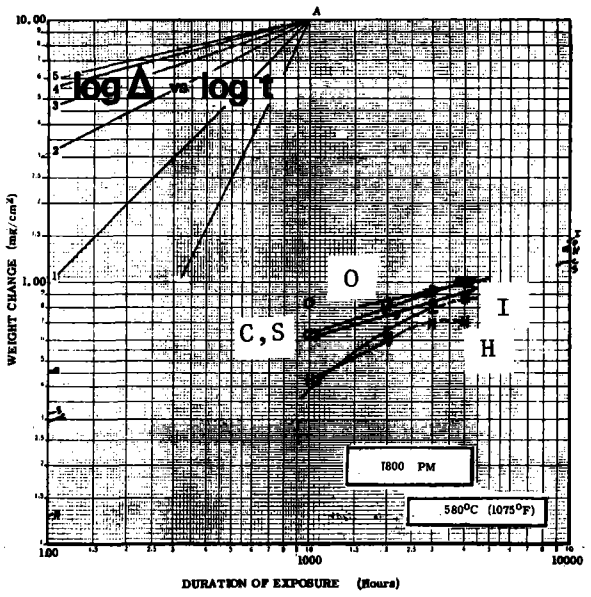

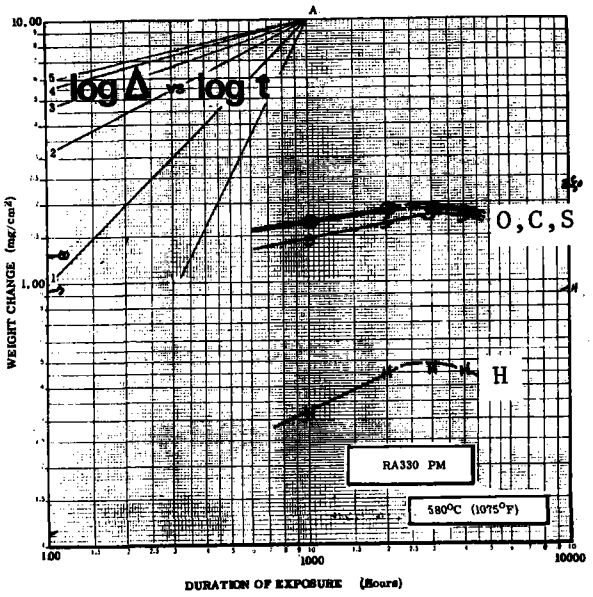

KEY:
- O 0.50 Wt % OH^-
- C 0.26 Wt % $CO_3^=$
- S 0.35 Wt % $SO_4^=$
- H 0.25 Wt % $C\ell^-$
- I 0.50 Wt % $C\ell^-$

Figure IV-6 Log Weight Gain vs Log Time for I800 and RA330 Parent Metal Coupons (Derived from Figure IV-4)

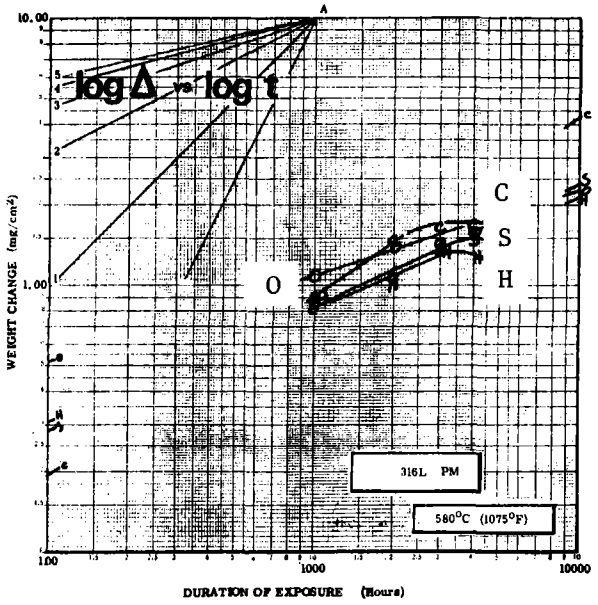

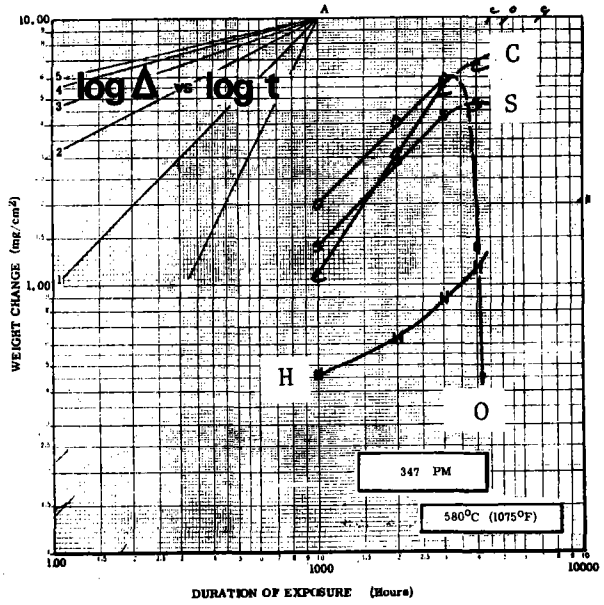

KEY:
- O 0.50 Wt % OH^-
- C 0.26 Wt % $CO_3^=$
- S 0.35 Wt % $SO_4^=$
- H 0.25 Wt % $C\ell^-$
- I 0.50 Wt % $C\ell^-$

Figure IV-7 Log Weight Gain vs Log Time for 316L and 347 Parent Metal Coupons (Derived from Figure IV-5)

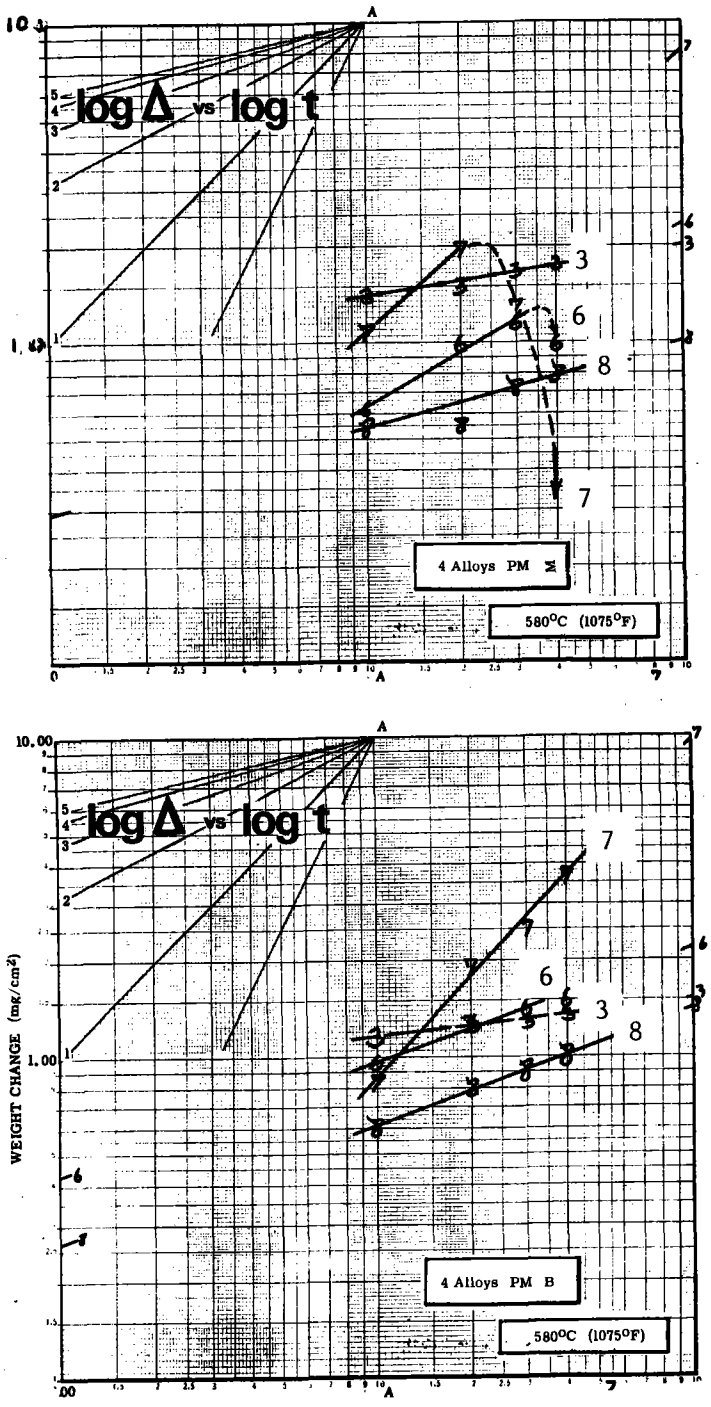

KEY: 3 - RA330
6 - SS316L
7 - SS347
8 - I800

Figure IV-8 Comparison of Log Weight Gain (Δ) vs Log Time (t) for High-Nickel and High-Chromium Alloys Exposed to Molten Salt at 580°C (1075 F)

Table IV-2 Extrapolated 30-Year Weight Gain and Metal Reduction for I800 and RA330 Exposed to 580°C (1075°F) Molten Salt

MATERIAL	TEST	WEIGHT GAIN (30 YEARS)[1] mg/cm^2	METAL LOSS[2] (30 YEARS) mm (x10^2)	mils
I800 @ 580°C (1075°F)	PM in B	66	22.1	8.7
	PM in SUM	52	17.4	6.9
	PM in $SO_4^=$	61	20.4	8.0
	PM in $CO_3^=$	66	22.1	8.7
	PM in OH^-	65	21.8	8.6
	PM in $C\ell^-$	74	24.8	9.8
	PM in 2x$C\ell^-$	95	31.8	12.5
	W in B	76	25.5	10.0
	W in SUM	82	27.5	10.8
	W in $SO_4^=$	69	23.1	9.1
	W in $CO_3^=$	76	25.5	10.0
	W in OH^-	85	28.5	11.2
	W in $C\ell^-$	116	38.9	15.3
	W in 2x$C\ell^-$	158	52.9	20.8
RA330 @ 580°C (1075°F)	PM in B	89	29.8	11.7
	PM in SUM	115	38.9	15.3
	PM in $SO_4^=$	158	52.9	20.8
	PM in $CO_3^=$	210	70.4	27.7
	PM in OH^-	210	70.4	27.7
	PM in $C\ell^-$	53	17.8	7.0
	PM in 2x$C\ell^-$	NT		
	W in B	229	76.7	30.2
	W in SUM	448	150.1	59.1
	W in $SO_4^=$	171	57.3	22.6
	W in $CO_3^=$	66	22.1	8.7
	W in OH^-	569	190.6	75.0
	W in $C\ell^-$	77	25.8	10.2
	W in 2x$C\ell^-$	NT		

LEGEND: B = Blank Salt; PM = Parent Metal, W = Welded Sample; SUM = Sum of All Contaminants; NT = Not Tested

NOTE: 1 - 30 year weight gain extrapolation, method b (Appendix B).
2 - Weight gain-to-metal reduction conversion factor 0.00335 $\frac{mm}{mg/cm^2}$ based on assuming Fe_3O_4 major oxide phase (see Appendix B).

Table IV-3 Extrapolated 30-Year Weight Gain and Metal Reduction for 316L and 347 Exposed to 580°C (1075°F) Molten Salt

MATERIAL	TEST	WEIGHT GAIN (30 YEARS) mg/cm^2	METAL LOSS (30 YEARS)[3] mm (x10^2)	mils
316L @ 580°C[1] (1075°F)	PM in B	112	37.5	14.8
	PM in SUM	94	31.5	12.4
	PM in $SO_4^=$	113	37.9	14.9
	PM in $CO_3^=$	208	69.7	27.4
	PM in OH^-	113	37.9	14.9
	PM in $C\ell^-$	113	37.9	]4.9
	PM in 2x$C\ell^-$	NT		
	W in B	203	68.0	26.8
	W in SUM	144	48.2	19.0
	W in $SO_4^=$	217	72.7	28.6
	W in $CO_3^=$	250	83.8	33.0
	W in OH^-	224	75.0	29.5
	W in $C\ell^-$	105	35.2	13.8
	W in 2x$C\ell^-$	NT		
347 @ 580°C[2] (1075°F)	PM in B	255	85.4	33.6
	PM in SUM	255	85.4	33.6
	PM in $SO_4^=$	430	144.1	56.7
	PM in $CO_3^=$	704	235.8	92.9
	PM in OH^-	505	169.2	66.6
	PM in $C\ell^-$	75	25.1	9.9
	PM in 2x$C\ell^-$	NT		
	W in B	468	156.8	61.7
	W in SUM	387	129.7	51.0
	W in $SO_4^=$	408	136.7	53.8
	W in $CO_3^=$	660	221.1	87.0
	W in OH^-	568	190.3	74.9
	W in $C\ell^-$	77	25.8	10.2
	W in 2x$C\ell^-$	NT		

LEGEND: B = Blank Salt; PM = Parent Metal, W = Welded Sample; SUM = Sum of All Contaminants; NT = Not Tested

NOTE: 1 - 30 year weight gain extrapolation, method b (Appendix B)
2 - 30 year weight gain extrapolation, method a (Appendix B)
3 - Weight gain to metal reduction conversion factor 0.00335 $\frac{mm}{mg/cm^2}$ based on assuming Fe_3O_4 major oxide phase (Appendix B)

oxide formation during the welding operation (even though protected by an inert gas) and local thermal effects within the weld heat affected zone. Specifically, for the high Nickel alloys, twice the maximum specificaton for chloride ($2Cl^-$) and OH^- additions lower the oxidition resistance in molten salt for I800 and RA330 respectively. For the 300-series stainless steel alloys, carbonate ($CO_3^=$) trace additons appear to be the most detrimental to oxidation resistance in molten salt. It is most important to recognize that the Cl^- and $SO_4^=$ can be kept out of the molten salt by specifications. The $CO_3^=$ and OH^- content depend on the molten salt exposure to H_2O and CO_2 bearing air. Thus it appears likely that the intrusion of Cl^-, OH^-, and CO_3 may be controllable by atmospheric control and impurity specification management.

It is interesting to note certain trends evident from the extrapolated 30-year thickness reduction and weight loss values. The blank salt (B) exposures were often observed to have larger extropalated values than some of the single contaminant tests. In addition, the extrapolated chloride (Cl^-) results were generally low, except for I800. These observations, along with metallographic observations (to be discussed later) suggest that the chloride contaminated salts may have selectively etched the coupon surfaces early in the weight gain cycle. This etching, plus the gradual parabolic - cubic oxidation kinetics observed for chloride contaminated salts, suggests a microscopic flaking process. This behavior would manifest itself as a continual oxide removal process, resulting in small weight gain (Δ_p) values used in the data extrapolation analysis. This microscopic oxide behavior magnitude also accounts for the observation that the sum-of-all-contaminant extrapolated results were equal to or slightly lower than the blank salt values. Calculated time rate exponents from $\log\Delta$ - log t plots (Figure IV-8) for the high nickel and chromium alloys are shown in Table IV-4. It is evident from the magnitudes of the logarithmic slopes that the 300-series stainless steel alloys (especially 347SS) exhibit greater metal loss for a given trace contaminant condition. This is confirmed by noting the results of Tables IV-2 and IV-3. The linear oxidation behavior of 347 is confirmed by the values shown in Table IV-4. The time rate kinetics for 316L and I800 are comparable, the difference in extrapolated metal reduction is due to the larger magnitude of the peak weight gain Δp (and intercept on $\log\Delta$- log t plot) for 316L. The oxidation behavior of RA330 predicts fairly large metal reductions based on the method of data analysis (described in the experimental section). However, the observation of the small logarithmic slope (or large A) suggest that the oxidation behavior of RA330 would be minimal.

Visual examination of the coupons confirms the prediction of minimal oxidation for RA330. The scale after 4000 hour molten salt exposure was hard and non-smearable, thus rejecting the previous hypothesis of equal microscopic rates of oxide growth and flaking. Therefore, it appears the formation of a tightly adherent, protective oxide is characteristic for RA330 during a 579C (1075°F) molten salt exposure.

Table IV-4 Time Rate Exponents Determined from Slope of logΔ -log t Graphs in Figure IV-8 for High-Nickel and 300-Series Stainless Steel

Material	Trace Additions	Slope of LogΔ - log t plot (1/A) Before Break In Linearity[1]	A
I800	Parent Metal (PM)		
	-Blanks Salt (B)	0.357	2.8
	-Sum[2] (S)	0.254	3.9
RA330	PM-B	0.116	8.6
	-S	0.169	5.9
347	PM-B	1.050	1.0
	-S	0.895	1.1
316L	PM-B	0.357	2.8
	-S	0.555	1.8

1 Determined from Figure IV-8
2 Sum of all trace contaminants

Pages IV-19, -20, -21, and

Figures IV-9, -10, -11

have been deleted.

These visual observations suggest that the extrapolated metal reduction values for RA330 are very conservative. The flaking observed for 347 stainless steel support the large metal reduction extrapolations in Table IV-2 and the oxide growth-flaking behavior shown on the weight gain (Δ) - time (t) graph between 2000-4000 hours in Figure IV-5. The high-Nickel alloy, I800 does not show oxide flaking or a frangible scale up to 4000 hours of molten salt exposure. However, it was observed that the I800 scale was smearable, suggesting that the maximum exposure period of 4000 hour may represent the onset of an oxide flaking weight loss cycle. The low carbon stainless steel 316L did show indications of oxide flaking and a frangible scale before the maximum 4000 hour of molten salt exposure. Examination of the welded coupons indicate the weld bead itself may be affecting the extrapolated results, leading to larger welded vs. parent metal extrapolations, as previously noted. Caution should be exercised in the analysis of molten salt oxidation behavior of welds, since accelerated scaling may occur in the weld heat affected zones. Evidence from metallographic analysis, to be presented next, indicates heat affected zone effects are minimal with respect to molten salt oxidation behavior. The micrographs shown in Appendix B of the high-Nickel and 300-series stainless steel alloys exposed to trace contaminated salt reveal some interesting trends about the metallurgy of the alloy near the surface, the texture of the metal/oxide interface, and the character of the oxide forming over it. In some cases these appearances support or explain the weight gain data.

The surface structure of 316L generally shows a dense thin oxide. In most pictures grain boundary oxidation is clear but shallow, amounting to less than one quarter of a typical grain diameter. Only slight effects show in the transition and heat affected zones of the weld specimens.

Grain boundary oxidation is more outstanding in the 347 specimens. In the large grains of the welded coupons it stands out clearly in all but the Cl^- specimen. Yet it hardly ever proceeds further than one grain diameter, even in the weld/base metal transition region. In the Parent metal specimens the oxidation appears diffuse, seeming to originate at surface grain boundaries, then consuming the grains themselves. The Cl^- contaminated specimens for 347 appear to have their oxides and substrate etched. This is supported by the distinctly lower weight gain-time curve, seen for Cl^- in Figure IV-5. The fragileness of the OH^- and $SO_3^=$ contaminated coupons suggested by the weight loss in Figure IV-5 is supported by the dark discrete bands under their oxides (Appendix B) which appear to be voids.

A thin and smooth oxide is observed for salt exposed I800, even in the weld/base metal transition region for welded coupons. In the parent metal and welded exposures to sum of all contaminants and chloride (Cl^-) additions, surface pits are evident for I800. These pits appear to be associated with voids near the interface of the weld metal. The voids seen for I800 Cl^- coupons suggest etching may be occurring at the metal/oxide interface. RA330 seems to be least affected by pits, or selected etching. The oxides on the chloride (Cl^-) contaminated coupons seems to be so thin as to suggest

a low rate of oxide formation. The parent metal, sulfate exposed coupon for RA330 shows a ragged oxide on a diffuse interface. This is peculiar because the higher population of precipitates near the oxide layer is more prominent here than under other contaminant conditions. Furthermore, the oxide appears to penetrate grains on a front that resembles grass root penetration into a soil substrate. Outside of this unknown case region below the oxide, there appears to be no metallurgical alterations to RA330.

b. Carbon steel and Cr-Mo alloys - Average coupon weight change data (in mg/cm^2) for A570 carbon steel and A387 Cr-Mo low alloy steel (grade 11), recorded at 1000 hour intervals, is presented in Appendix B. The weight change (Δ) vs time (t) plots for A570 at 288°C (550°F) and 400°C (750°F) is shown in Figure IV-12. These figures present trace contaminant addition effects on the oxidation behavior of unwelded, parent metal coupons in molten salt. These graphs suggest early oxide exfoliation behavior for A570, typically within 2000 hours of exposure. Actual weight loss after an initial weight gain cycle can be seen for the A387 (Figure IV-13) carbonate ($CO_3^=$) exposure and A570 sulfate ($SO_3^=$) exposure (Figure IV-12). A lack of oxide flaking behavior is observed for A387 and A570 chloride (Cl^-) and hydroxide (OH^-) contaminants during the test exposure of 4000 hours. Additional weight change time behavior for welded coupons is included in Appendix B for reference.

Extrapolated 30 year weight gain and metal reduction was determined with the technique described in Appendix B. Table IV-5 lists representative results including the worst case extrapolations for the carbon steel and Cr-Mo alloys. In general, the oxidation resistance for the unwelded, parent metal coupons was greater than for their welded counterparts for both carbon steel alloys.

The A570 coupons after 3000 hours of exposure to 400°C contaminated molten salt are shown on Figure IV-15 . These photographs indicate a conspicuous loss of oxide "plate" in the specimens from the $SO_4^=$ and $CO_3^=$ exposures and a little from the Cl^- exposure. The photomicrographs shown in Appendix B show no detrimental metallurgical effects, except a variation in oxide thickness between coupons.

The porous nature of the chloride (Cl^-) contaminated parent metal coupon is very evident. This suggests that the diminishing rate of oxide growth represents an oxide metal process that is controlling.

The appearances of the A570 coupons after 4000 hrs (at 288°C, 550°F) (Fig IV-16) show a bright dense looking oxide on specimens from the blank salt tray, and amorphous black colored films from the sum of contaminants tray.

The carbonate ($CO_3^=$) and sulfate ($SO_4^=$) contaminated coupons were similar in appearance, i.e. with bright and dense films. The rusty color at the weld fusion lines in all of the welded coupons, except for the blank salt coupon, indicates a different oxide from the rest of the specimen surface, one that was either formed or converted during

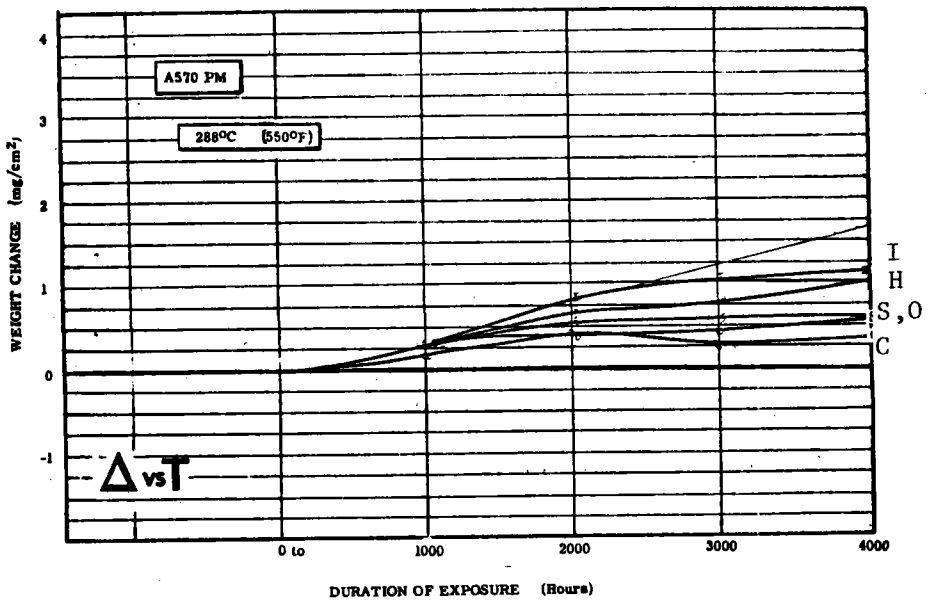

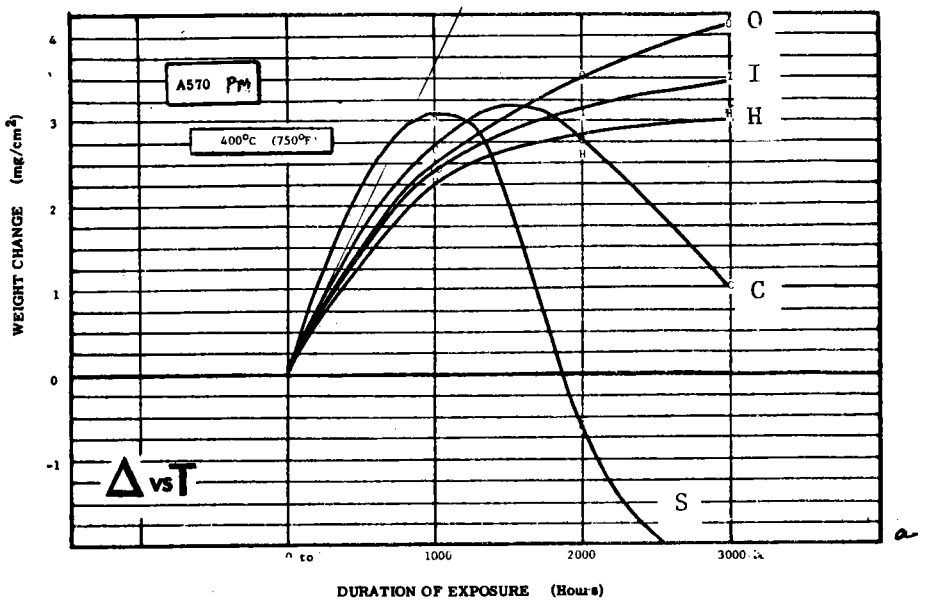

KEY:
- O 0.50 Wt % OH^-
- C 0.26 Wt % $CO_3^=$
- S 0.35 Wt % $SO_4^=$
- H 0.25 Wt % $C\ell^-$
- I 0.50 Wt % $C\ell^-$

Figure IV-12 Weight Change vs Time for A570 as a Function of Temperature During Trace Contaminant Tests

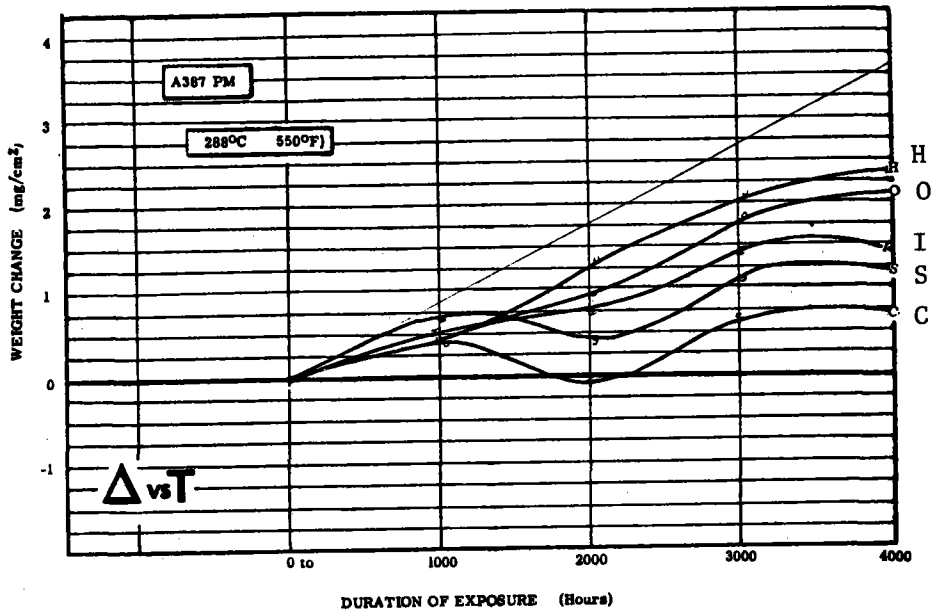

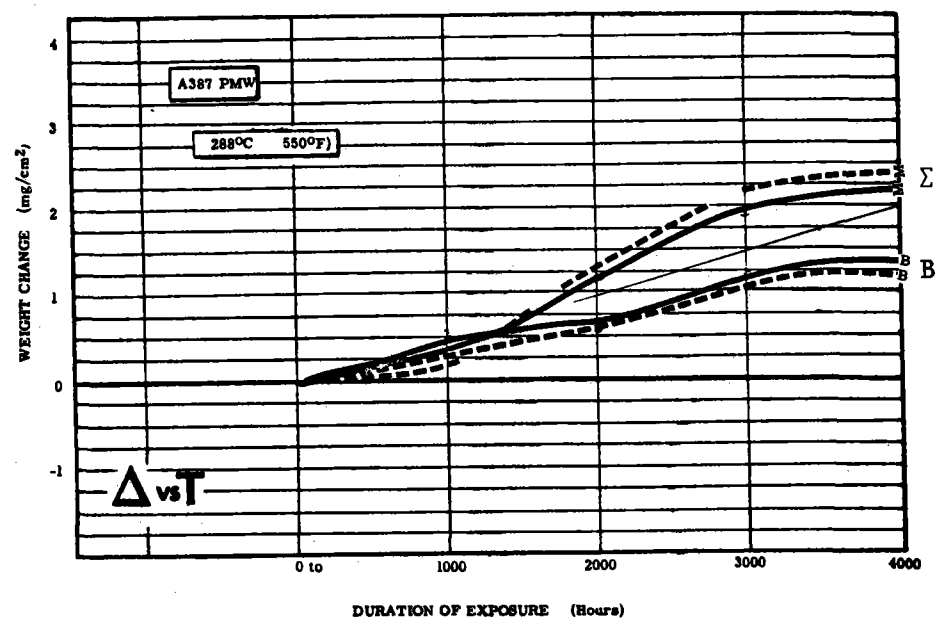

KEY:
- O 0.50 Wt % OH^-
- C 0.26 Wt % $CO_3^=$
- S 0.35 Wt % $SO_4^=$
- H 0.25 Wt % Cl^-
- I 0.50 Wt % Cl^-

Figure IV-13 Weight Change vs Time for A387 from Trace Contaminants Tests at 288°C (550 F)

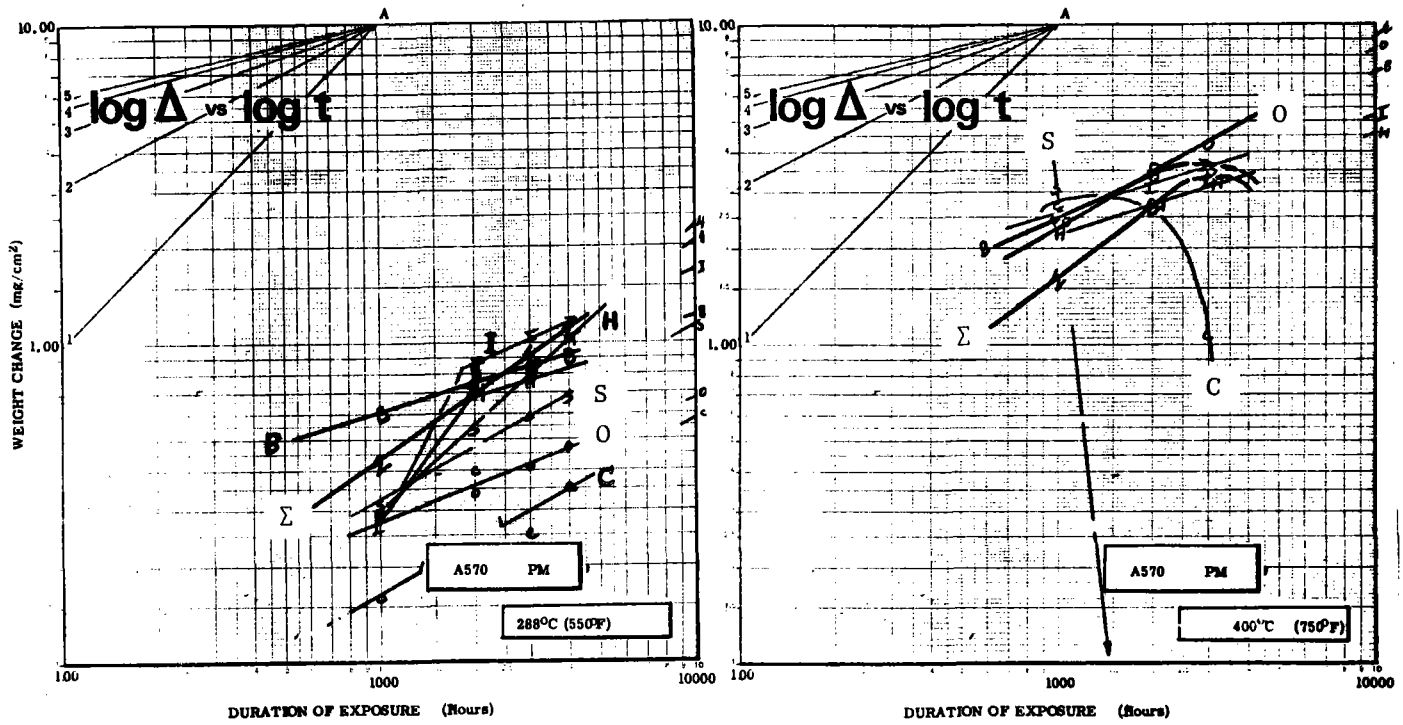

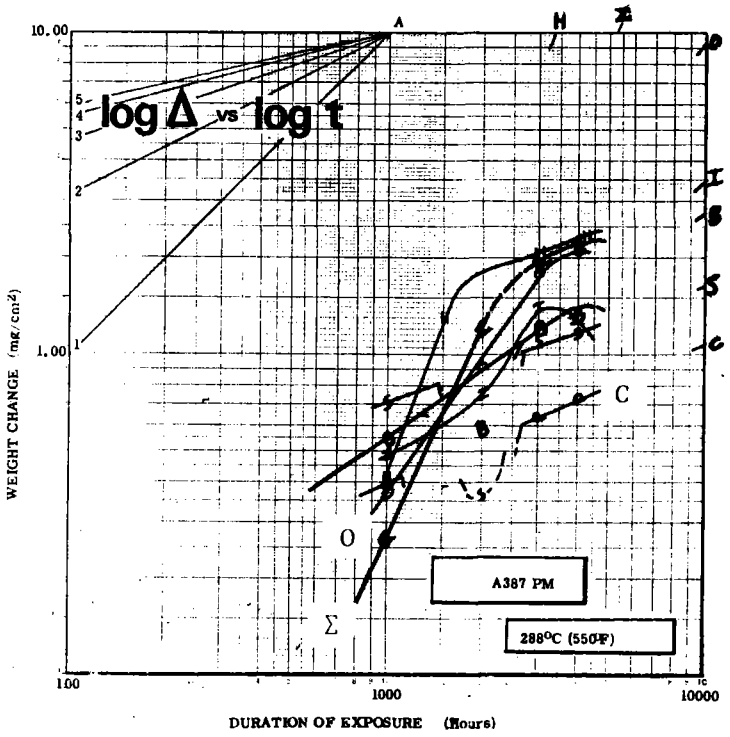

KEY:

O	0.50 Wt % OH^-
C	0.26 Wt % $CO_3^=$
S	0.35 Wt % $SO_4^=$
H	0.25 Wt % Cl^-
I	0.50 Wt % Cl^-
B	Blank Salt
Σ	Sum of all Contaminants

Figure IV-14 Log Δ -Log t Plots for A570 and A387 (Derived from Figures IV-12 and IV-13)

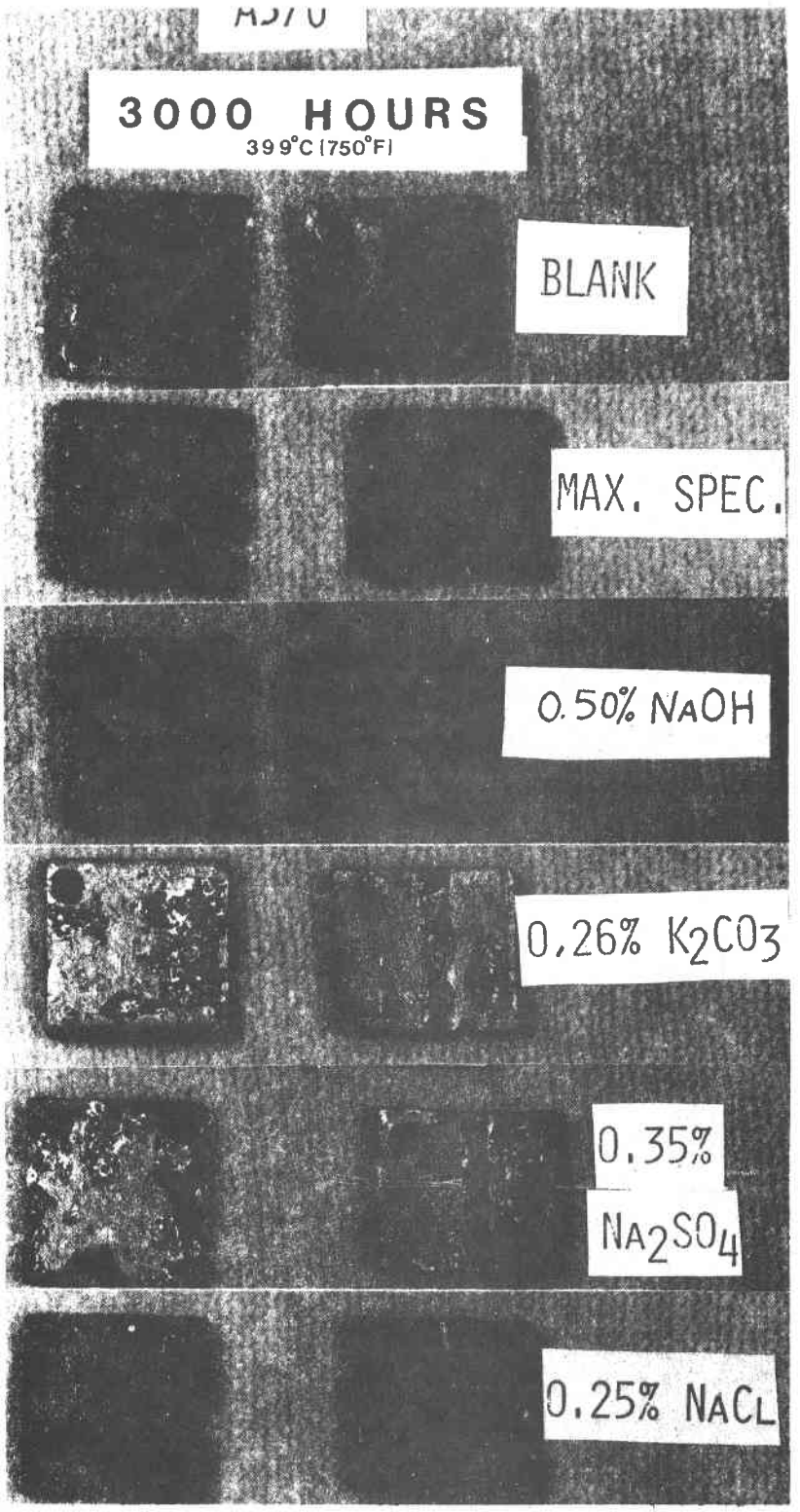

Figure IV-15 Photographs of A570 After 3000 Hours Exposure to 400°C (750 F) Molten Salt

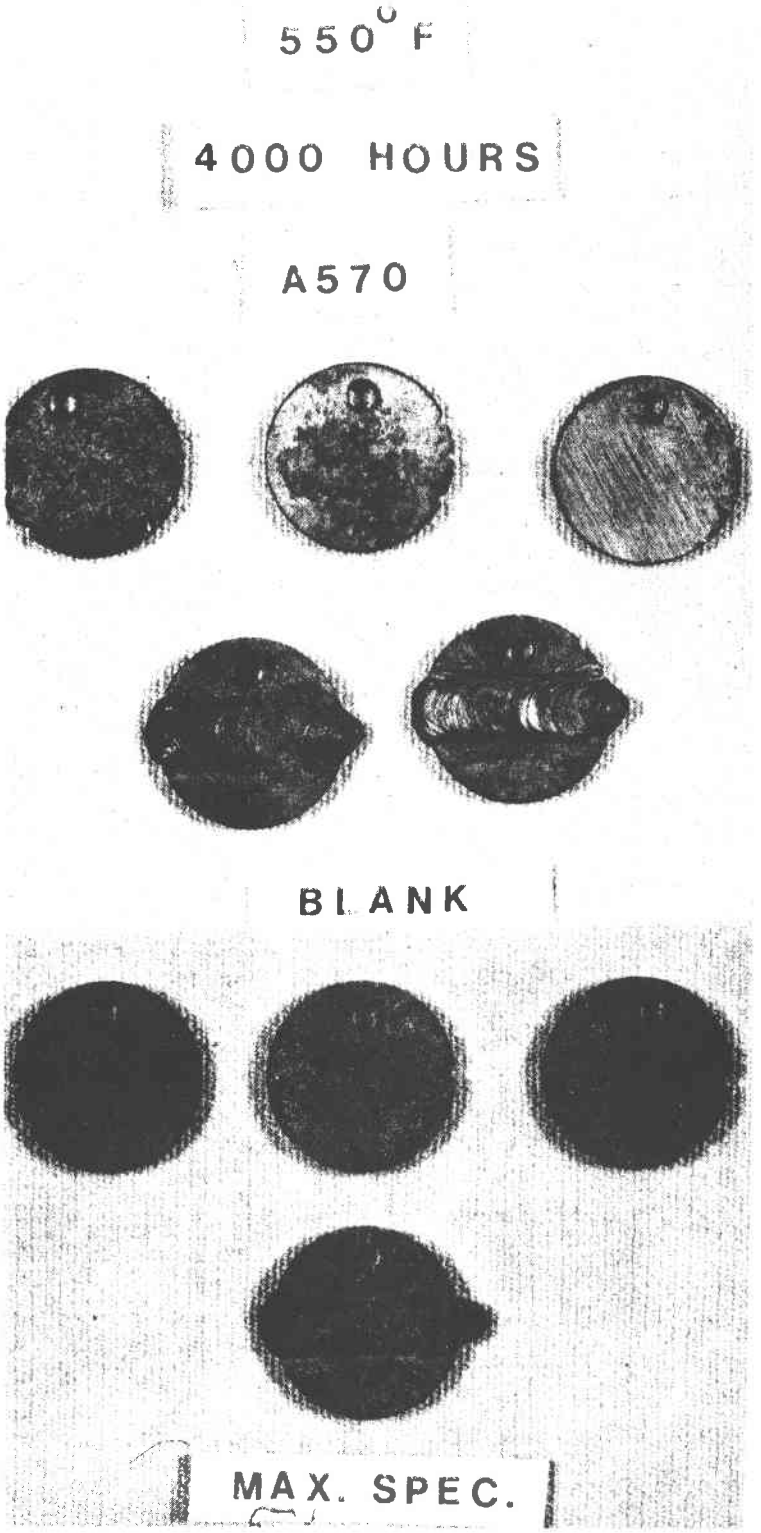

Figure IV-16 Photographs of A570 After 4000 Hours Exposure to 288°C (550 F) Molten Salt

welding. This would make weight gain readings unusual for welded specimens in the first cycle of growth-and-spalling. The photomicrographs of the A570 (288°C) coupons (Appendix B) show nothing unusual in the metal up to the oxide interface except for larger grains closer to the surface, which cannot be attributed to the salt. Even the transition zones by welds seem to have been equally oblivious to the presence of an attacking medium. There is one curious picture where a large pore lies in the metal under the oxide skin for an A570 parent metal coupon exposed to the OH^- contaminant.

In contrast, the appearance of the A387 specimens (Figure IV-17) all show an advanced state of oxidation in the form of "shingles" or scales and very small blisters. The Cl^- and the $SO_4^=$ group seem most advanced. The reason for the greater deterioration of the A387 surface is not clear. The blister formation may be the result of (a) local advanced etching, (b) a gas formation, or (c) compressive stresses in the oxide skin. The rapid weight gain and weight loss of these coupons can be related to this morphology. The sum of contaminants welded specimens show discrete areas where the oxidation and blistering is advanced.

The microstructure of A387 (Appendix B) reveals no unusual events or processes either near the surface or at the weld transitions. It is interesting to note, however that the oxide on A387 seems more ready to spall from the metal substrate than for A570.

Examination of the extrapolated weight gain-metal reduction results in Table IV-5 indicates that A570 carbon steel appears more resistant to oxidation in contaminated molten salt at 288°C (550°F) than A387 Cr-Mo steel (grade 11). The nominal compositions of A570 and A387 differ in chromium, molybdenum, and silicon content, with A387 having larger percentages of these alloys (see Appendix B). This minor variation in composition may indeed affect the relative degrees of oxidation experienced by these alloy. Increasing the molten salt temperature to 399°C (750°F) drastically increases the oxidation rate of A570. A570 at this temperature and A387 at 288°C molten salt exposure demonstrated the classical weight gain-weight loss behavior, as observed from the weight change-time graphs. This process was confirmed by visual observations: the A387 coupons experienced blister formation, while the A570 coupons showed loss of surface oxide layers by flaking.

The increase in the oxidation behavior for A570 as a function of temperature is clearly shown on the weight gain-time plots (Figure IV-12) as well as the $\log \Delta$ -log t plots in Figure IV-14. The critical parameter that dictates the accelerated attack for A570 as the temperature is increased is the peak weight gain, Δp. From both types of graphical representation (linear and log-log) of the data, the 399°C results show a much larger magnitude of weight gain than the 288°C results ($> 3 mg/cm^2$ vs 0.5 mg/cm^2 at 1500 hrs). A comparison of the oxidation kinetics is given in Table IV-6, indicating little difference between the cases, i.e., that the same mechanism is controlling the oxidation of A570 at both temperatures.

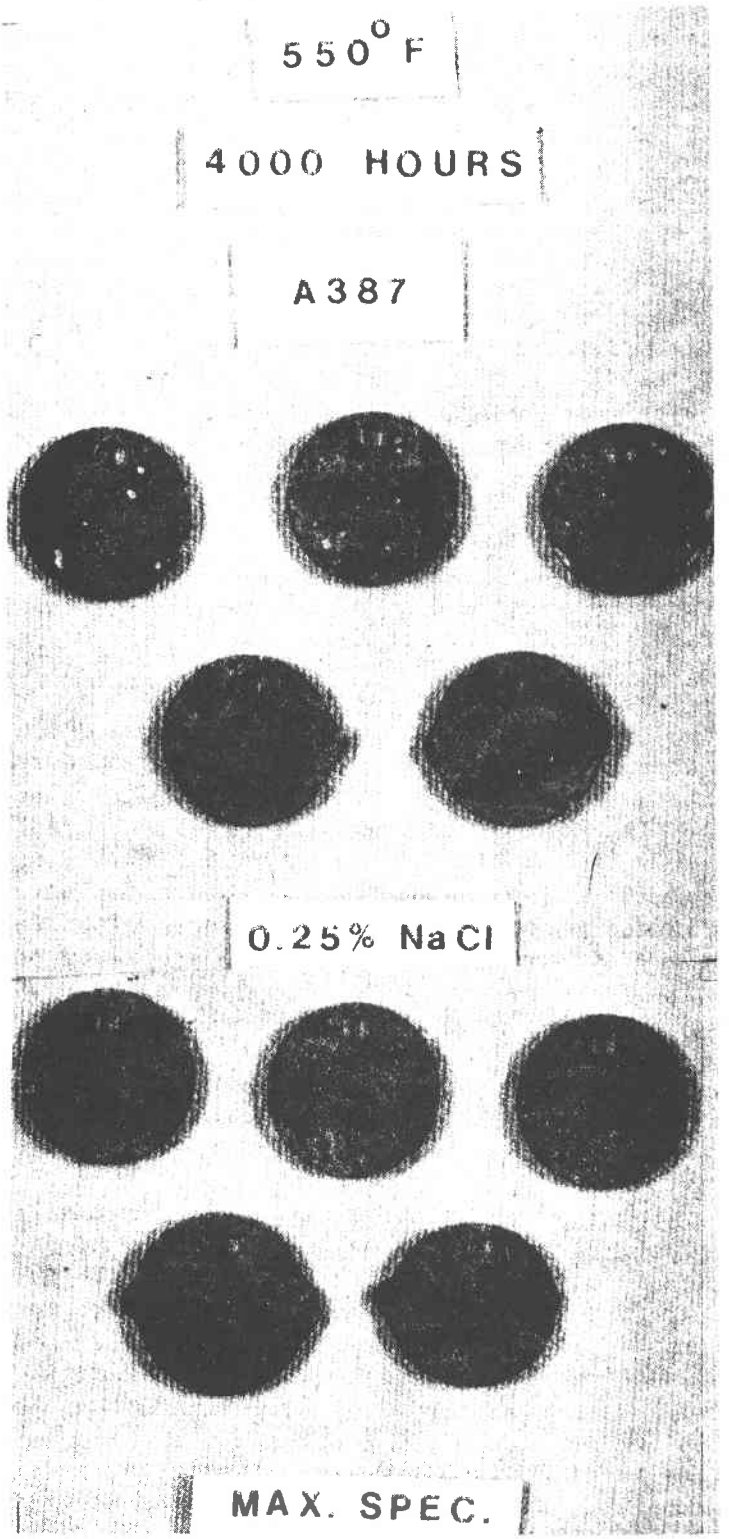

Figure IV-17 Photographs of A387 After 4000 Hours Exposure to 288°C (550 F) Molten Salt

Table IV-5 Extrapolated 30-Year Weight Gain and Metal Reduction for A570 and A387 Exposed to 288°C (550 F) Molten Salt

MATERIAL	TEST	WEIGHT GAIN (30 YEARS)[1] mg/cm²	METAL LOSS[2] (30 YEARS) mm (x10²)	mils
A387 @ 288°C (550°F)	PM in B	92	30.8	12.1
	PM in SUM	148	49.6	19.5
	PM in $SO_4^=$	158	52.9	20.8
	PM in $CO_3^=$	149	49.9	19.7
	PM in OH^-	167	55.9	22.0
	PM in $C\ell^-$	391	131.0	51.6
	PM in $2xC\ell^-$	140	46.9	18.5
	W in B	82	27.5	10.8
	W in SUM	207	69.3	27.3
	W in $SO_4^=$	116	38.9	15.3
	W in $CO_3^=$	173	58.0	22.8
	W in OH^-	167	55.9	22.0
	W in $C\ell^-$	267	89.4	35.2
	W in $2xC\ell^-$	82	27.5	10.8
A570 @ 288°C (550°F)	PM in B	61	20.4	8.0
	PM in SUM	72	24.1	9.5
	PM in $SO_4^=$	45	15.1	5.9
	PM in $CO_3^=$	47	15.7	6.2
	PM in OH^-	31	10.4	4.1
	PM in $C\ell^-$	92	30.8	12.1
	PM in $2xC\ell^-$	119	39.9	15.7
	W in B	21	7.0	2.8
	W in SUM	28	9.4	3.7
	W in $SO_4^=$	16	5.4	2.1
	W in $CO_3^=$	16	5.4	2.1
	W in OH^-	11	3.7	1.5
	W in $C\ell^-$	11	3.7	1.5
	W in $2xC\ell^-$	11	3.7	1.5
A570 @ 399°C (750°F)	PM in B	389	130.3	51.3
	PM in SUM	347	116.2	54.8
	PM in $SO_4^=$	823	275.8	108.5
	PM in $CO_3^=$	559	187.3	73.7
	PM in OH^-	377	126.3	49.7
	PM in $C\ell^-$	272	91.1	35.9
	PM in $2xC\ell^-$	316	105.9	41.7
	W in B	324	108.5	42.7
	W in SUM	326	109.2	43.0
	W in $SO_4^=$	461	154.4	60.8
	W in $CO_3^=$	438	146.7	57.8
	W in OH^-	386	129.3	50.9
	W in $C\ell^-$	1118	374.5	147.5
	W in $2xC\ell^-$	NT		

LEGEND:

B = Blank Salt
PM = Parent Metal
W = Welded Sample
SUM = Sum of All Contaminants
NT = Not Tested

NOTES: 1 - 30 year weight gain extrapolation method b (Appendix B)

2 - Weight gain to metal reduction conversion factor = 0.00335 $\frac{mm}{mg/cm^2}$ based on assuming Fe_3O_4 major oxide phase (Appendix B)

In summary, since there was no microstructural evidence of catastrophic impairment for A570 carbon steel and A387 Cr-Mo steel (grade 11) studied, their use appears possible in a molten salt application with consideration of one or more of the following: (1) compensation for wall loss in design, (2) using fillers to take out solids which will be produced abundantly (3) by planning on certain replacement schedules, and (4) (affecting all of the above) keeping contaminants low.

Alternatives also include the restriction of low alloy steels to lower temperature service and using alloys with modest amounts of the elements that increase corrosion resistance for intermediate temperatures.

Table IV-6 Comparison of Time Rate Exponents from log Δ -log t Plots for A570 and A387

Material	Salt Temperature °C (°F)	Trace Contaminant	Slope $\left(\frac{1}{A}\right)$ Log Δ – Log t Plot	A
A387 Parent Metal	288 (550)	Blank Salt	0.710	1.4
		Sum	2.20	0.5
A570 Parent Metal	288 (550)	Blank Salt	0.317	3.2
		Sum	0.686	1.5
A570 Parent Metal	399 (750)	Blank Salt	0.444	2.3
		Sum	0.733	1.4

NOTE: Sum = Sum of all contaminants

B. EXTENDED IMMERSION TESTS

These tests consisted of extending the exposure time for samples tested during our Phase I program. The purpose of these long term exposures was to observe the oxidation behavior of the alloys tested in the trace contaminant effects tests described in Section IV.A.

1. Test Method

The salt used for these tests was technical grade, blank salt without any trace additions. The coupons were suspended in trays exposed to an open air atmosphere, as shown in Figure IV-18. Thus the level of contaminants present in the salt is not known.* The alloys tested were I800, RA330, 316, 321, 347 and A286 at 580-621°C (1075-1150°F) for exposures up to 18,000 hours. One carbon steel alloy, A516, was exposed to 400°C (750°F) molten salt for up to 16,000 hours. Weight change data were determined at predetermined test intervals, and visual observations were recorded.

2. Results

Table IV-7 lists extrapolated weight gain-metal reduction values for the alloys tested. Good agreement for I800 can be inferred by a comparison of the extrapolated values of Table IV-7 with those from the trace contaminant tests (Table IV-2). It should be noted that for the materials that showed almost immediate weight loss, i.e., the 300 series austenitic stainless steels, the extrapolated values were determined using the worst slope of the weight change-time curves. For the alloys that exhibited initial weight gain (I800, RA330), the technique described in the experimental section of the trace contaminant section was used. Figures IV-19 to IV-22 show the weight change-time graphical behavior for the extended immersion tests. Comparing the extrapolated values with the results of Section IV.A, it appears that the level of metal reduction values predicted previously is low. For example, the oxidation behavior of RA330 may need further study since these results suggest it does not obey the assumed cyclic oxide growth flaking behavior. It appears, from visual examinations of RA330 (Appendix C) that the oxide found after the molten salt exposure is hard and non-smearable. This confirms the weight gain behavior exhibited from the tests, i.e., a highly protective adherent oxide which does not allow oxide flake removal.

The oxide behavior of 347 also shows deviation from the Section IV.A predictions: its cycle time for initiation of oxide loss appears to be much larger than predicted. Therefore the values reported in Section IV.A for 347 appear to be highly conservative. Visual examinations showed I800 to have developed a tightly adherent oxide showing no evidence of flaking. Areas of oxide flaking on coupon surfaces were observed for 321, 316, A286 and 347. The ambiguous behavior or oxide growth-loss interactions is observed with A516 carbon steel. Its weight loss values appear reasonable, although visual examination showed a badly flaked and pitted coupon surface.

---

*This means that carbonate and hydroxide content of the salt was probably higher than during the trace contaminants tests. In similar tests, we have measured carbonate and hydroxide levels significantly above specification values. Since we have shown that carbonate and hydroxide level can significantly affect corrosion rates the results of these tests should not be used to determine weight loss for design purposes.

Table IV-7 Extrapolated 30-Year Weight Change and Metal Reduction for Alloys Tested in Extended Immersion Test

MATERIAL	WEIGHT CHANGE IN 30 YEARS (mg/cm^2)		METAL REDUCTION IN 30 YEARS mm x 10^2	mils
I800	-263	(a)	32.9	12.9
	+175	(b)	58.6	23.1
	-56	(c)	6.9	2.7
RA330	-56.4	(a)	7.1	2.8
	+56.4	(b)	18.9	7.4
	-30.3	(c)	3.8	1.5
321	-986	(a)	121.3	47.8
	-751	(c)	92.4	36.4
316	-822	(a)	102.7	40.4
	-488	(c)	61.1	24.0
347	-658	(a)	80.9	31.8
	-164.4	(c)	20.3	8.0
A286	-329	(a)	41.4	16.3
	-135.4	(c)	17.0	6.7
A516 399°C (750°F)	+47.0	(b)	15.7	6.2

(a) Worst slope of Δ-t weight loss.
(b) Weight gain - weight loss cyclic method.
(c) Average weight loss or gain from Δ-t plots at maximum test duration.

(See Appendix B for explanation of weight-change calculations.)

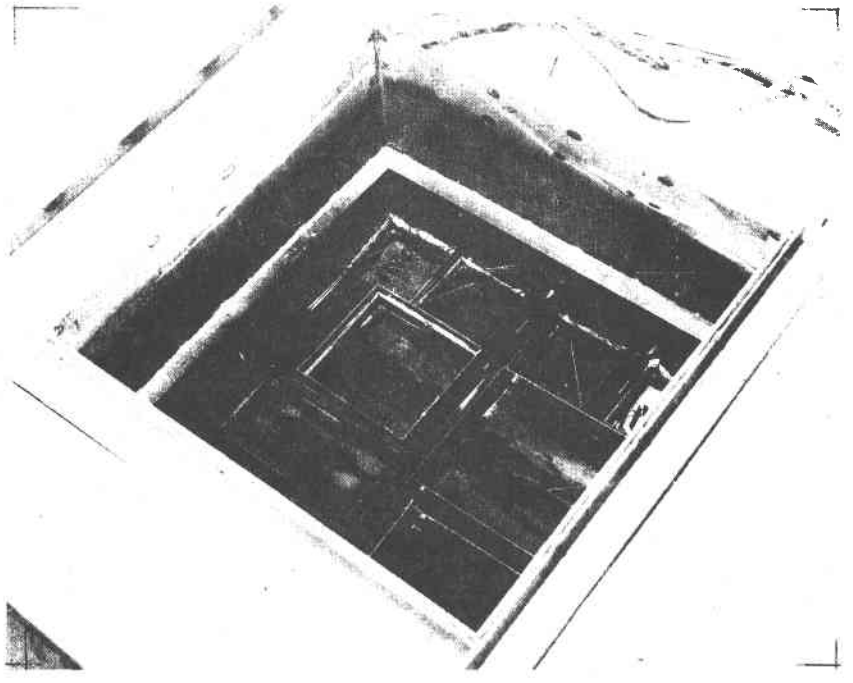

Figure IV-18 Experimental Set-up for Extended Immersion Tests

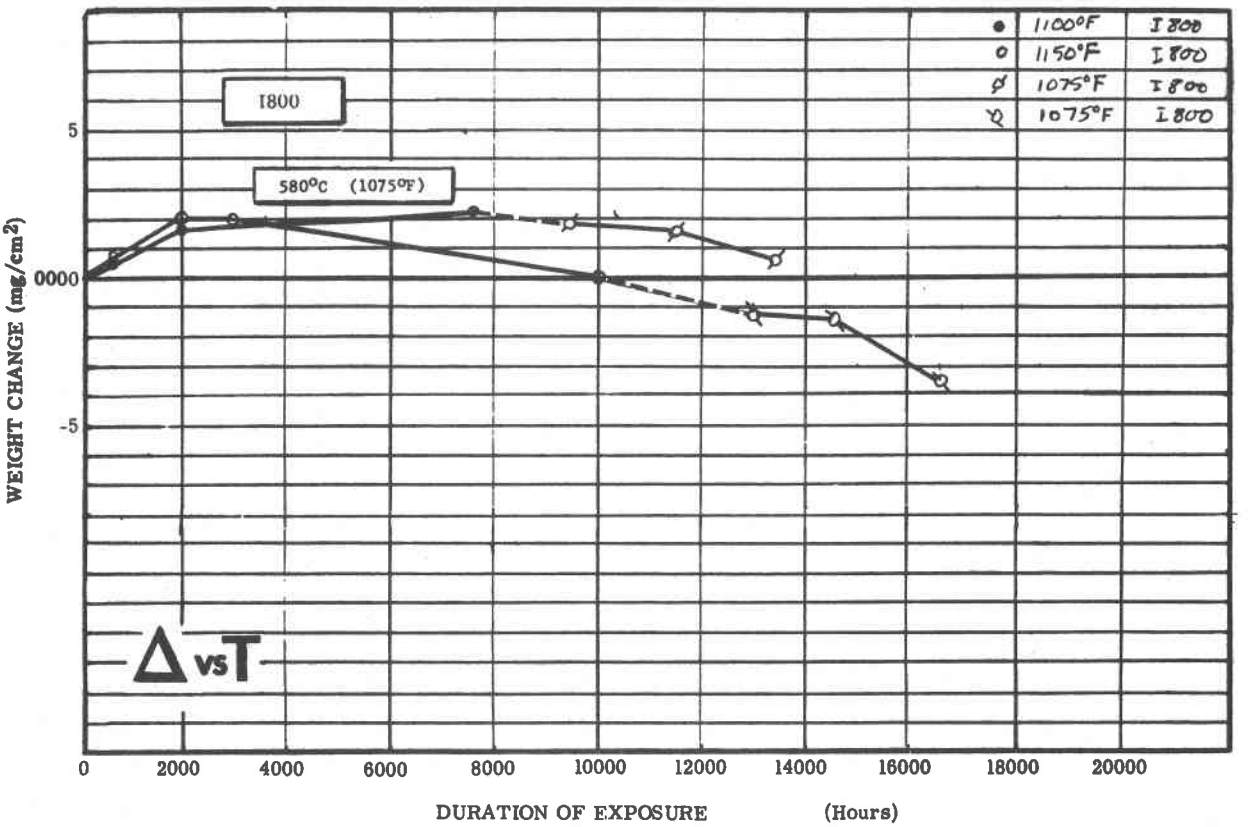

Figure IV-19 Weight Change vs Time for I800 After Extended Molten Salt Immersion

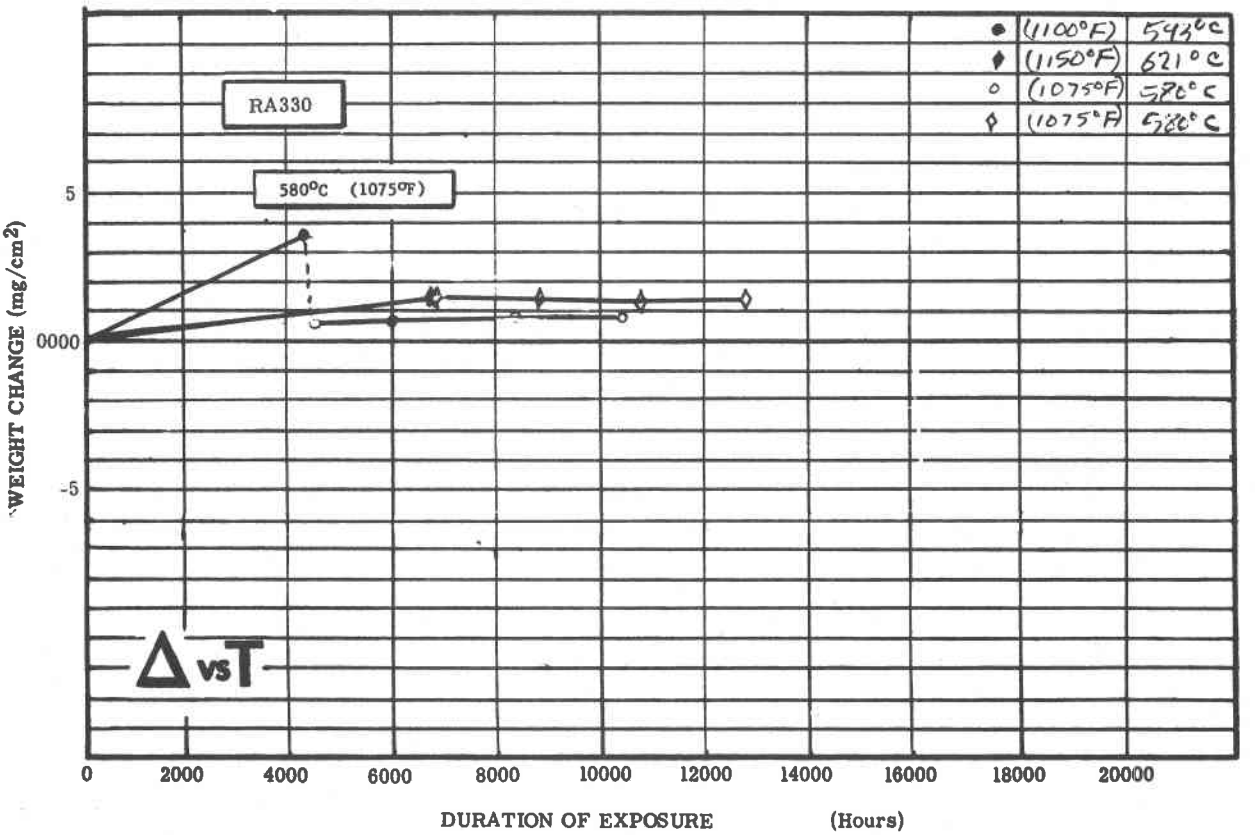

Figure IV-20 Weight Change vs Time Results for RA330 After Extended Molten Salt Immersion

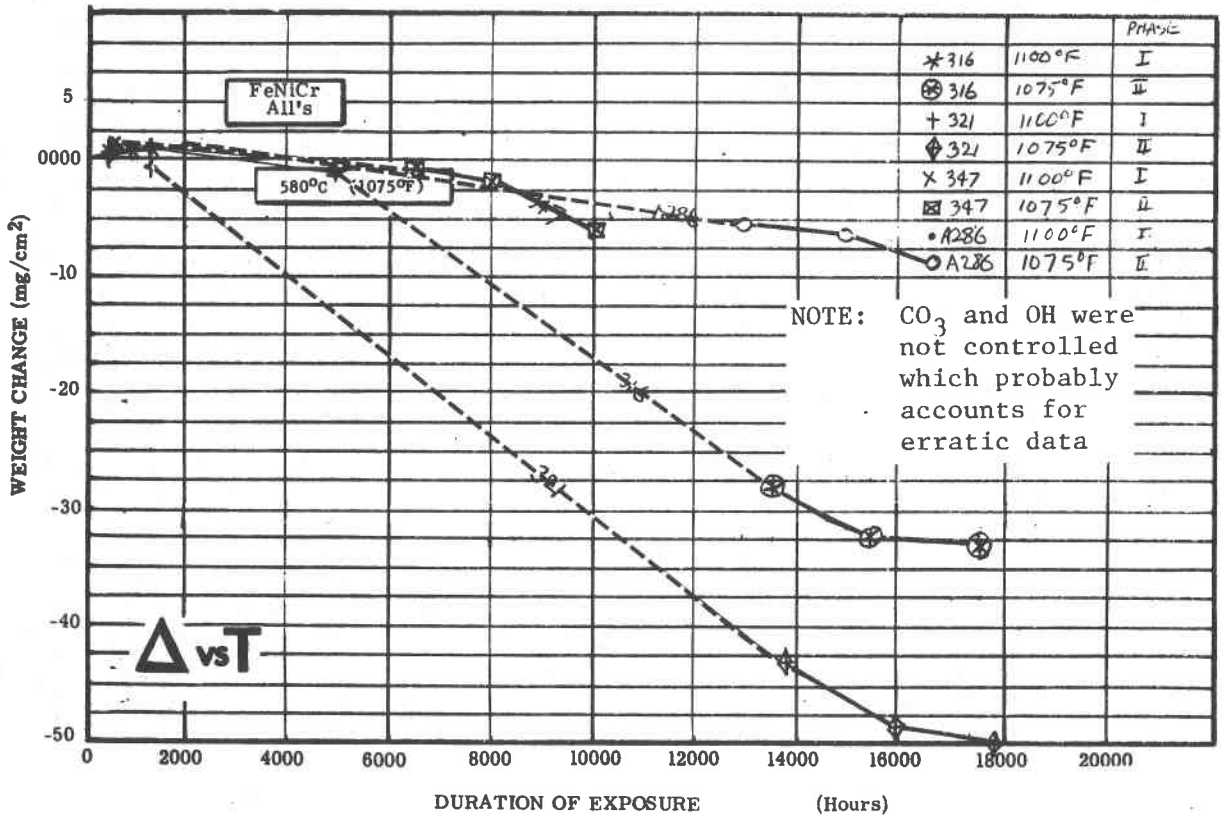

Figure IV-21 Weight Change vs Time for 300 Series Stainless Steel Alloys and A286 After Extended Molten Salt Immersion

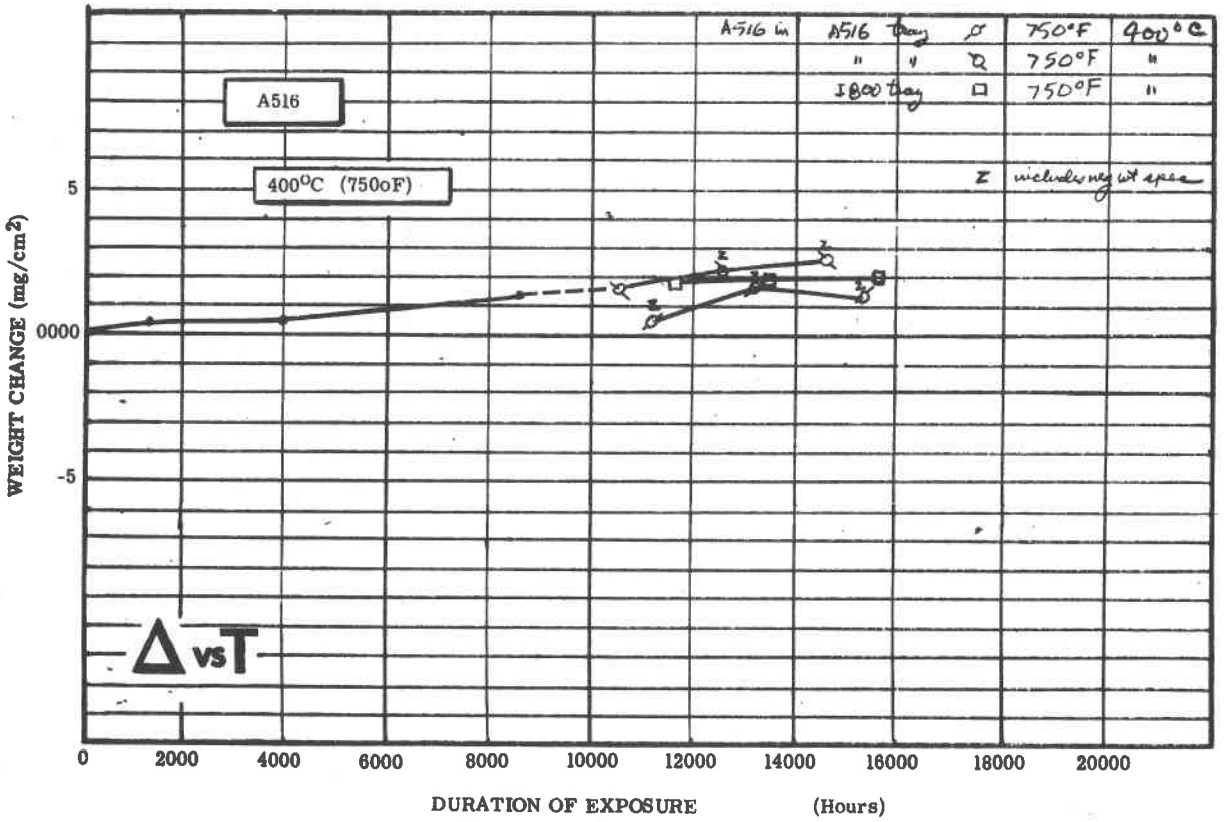

Figure IV-22 Weight Change vs Time for A516 Carbon Steel After Extended Molten Salt Immersion

C. SURFACE PREPARATION EFFECTS TEST

The purpose of this test was to characterize the nature and degree of molten salt [399°C (750°F)] oxidation on low temperature alloy specimens with machined surfaces vs as-rolled surfaces.

This particular test was designed primarily to resolve conflicting low temperature alloy material data derived from the Phase I materials immersion tests and the Phase II trace contaminant tests. Results of Phase I immersion testing indicated that A516 carbon steel specimens with machined surfaces were quite compatible with molten salt at 399°C (750°F), gaining only an average of 0.40 mg/cm^2 in 1000 hours. A570 carbon steel specimens with as-received (rolled) surfaces, however, gained 1.61 mg/cm^2 in 1000 hours at 399°C (740°F) when exposed to reagent grade salt doped with the maximum specification of contaminants during the Phase II testing program. This rate of growth indicated that A570 was unacceptable for use at these service temperatures. This discrepancy in the reported weight change data for the two test programs was suspected to derive from one of three possible causes:

1) Compositional differences between A516 carbon steel and A570 carbon steel (see Appendix D);

2) Compositional differences in the salt; and

3) Surface preparation effects on weight change.

1. Test Method

Two round A570 test coupons of 2.16 cm (0.85 in.) diameter and 0.32 cm (0.125 in.) thick were used in this test. One coupon face was surface machined, leaving the opposite face in the as-received (rolled) condition. Two test coupons of A516 alloy carbon steel were prepared in the identical manner. Six A387 alloy test coupons 2.16 cm (0.85 in.) diameter, 0.635 cm (0.250 in.) thick were machined on both faces. Alloy coupons were suspended from nichrome wire into molten salt at 399°C (750°F) and exposed for 1000 hours. After removal, these specimens were washed in water and dried under a nitrogen stream. Coupons were weighed, and surfaces were examined, with particular attention paid to the coating condition and thickness.

2. Results

The effect of surface preparation on oxidation behavior was determined by visual microscopic observations.

The machined surfaces of the A387 Cr-Mo Alloy (grade 11) specimen contained small blisters widely spaced (see Fig. IV-23). The A516 carbon steel as-rolled surface was inappropriate for this test, in as much as it appeared to contain mill scale (see Fig. IV-24), i.e., an oxide growth from a thermomechanical treatment, which may accelerate upon exposure to the molten salt environment. The A570 carbon steel as-rolled surface was initially a grit-blasted specimen with bare metal exposed. After 1000 hours of exposure to

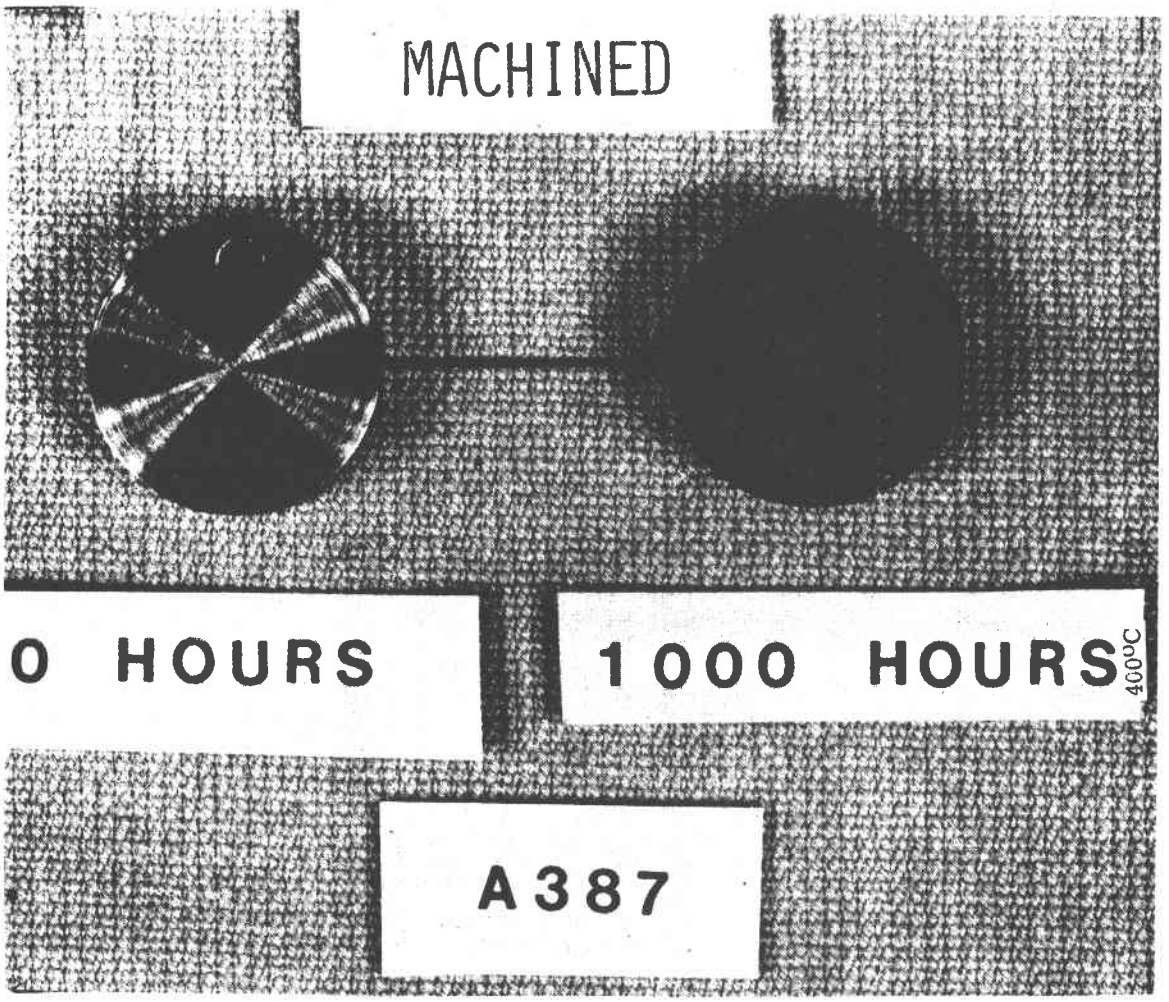

Figure IV-23 Macrographs of A387 Coupons After Exposure to 399°C (750 F) Molten Salt for 1000 Hours

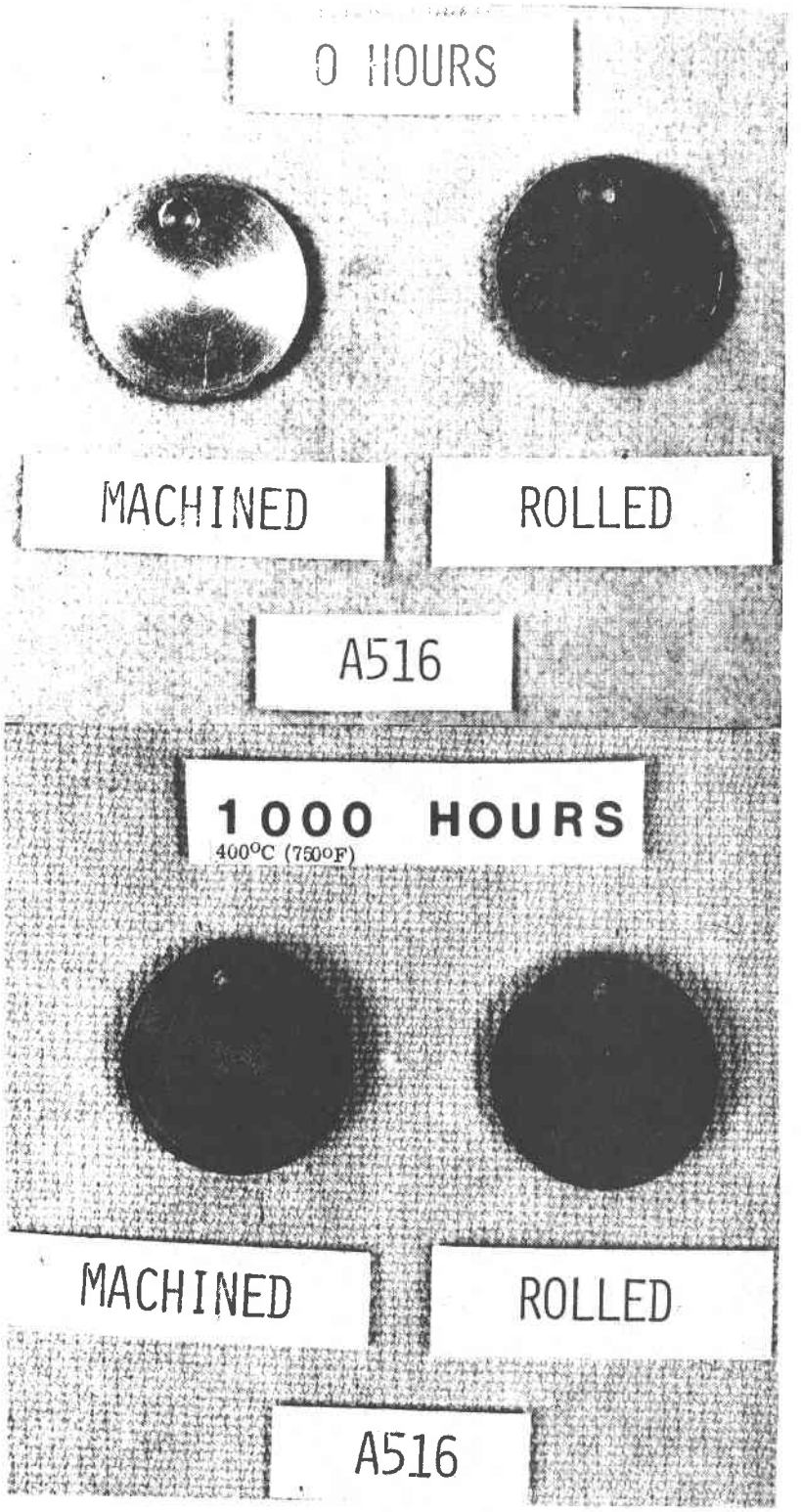

Figure IV-24 Macrographs of A516 Coupons After Exposure to 399°C (750 F) Molten Salt for 1000 Hours

molten salt at 399°C (750°F) the rolled face of the A570 specimen appeared to be less oxidized than the machined face (see Fig. IV-25). The rolled A570 face also appeared more resistant to chemical oxidation than the machined face of the A387 specimen. A quality judgement between A516 and 570 is hard to make. The former looks hard and adherent but has begun a severe breakdown in isolated locations with obviously more to follow. The A570 was breaking down gradually and more uniformly in very small blisters. Concluding, it appears from visual examinations that there were no surface preparation effects on the oxidation behavior of A570 and A516 carbon steels and A387 Cr-Mo low alloy steel after a 399°C (750°F) molten salt exposure.

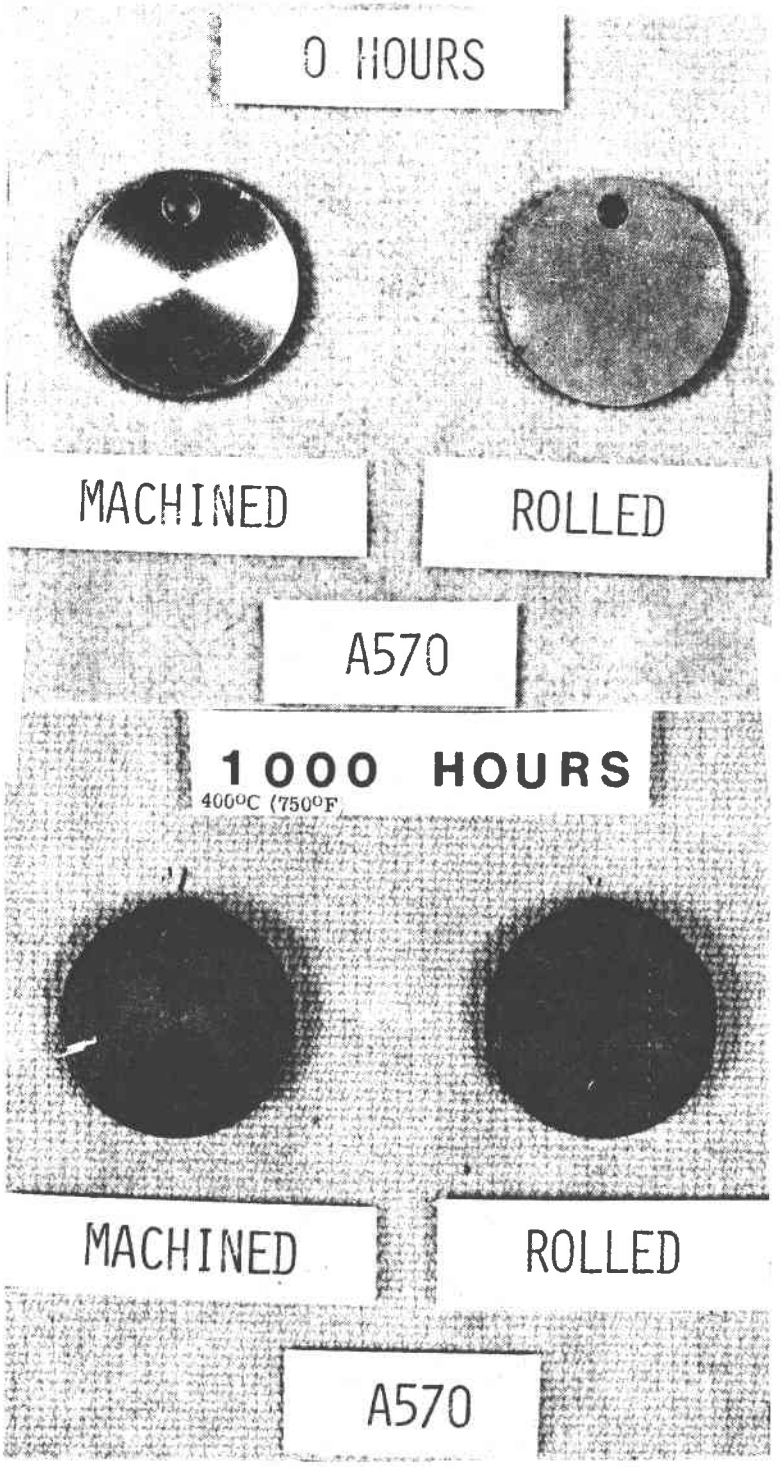

Figure IV-25 Macrographs of A570 Coupons After Exposure to 399°C (750°F) Molten Salt for 1000 Hours

D. SPECIAL PURPOSE MATERIALS IMMERSION TESTS

The objective of these immersion tests was to determine the compatibility of limited-use material like seals, gaskets, packings, and valve trim with molten nitrate salts.

1. Test Methods

Selected seal, gasket, and packing materials were suspended from nichrome wire into Incoloy 800 trays containing commercial-grade molten salt. The Incoloy trays were passivated using a nitric acid-dichromate solution prior to use. The temperature of the test oven was maintained at 399°C (750°F). Materials were weighed periodically for weight change, where the porosity of the materials allowed, and were examined visually every 1000 hours of test time. Materials were exposed to the molten salt environment for a total test time of 5000 hours unless a prior material failure occurred, at which point it was removed from the test. Certain materials (Crane IX187 and Stellite #6) were tested for an extended period of time (6000 hours).

Upon removal for measurements or observations, each specimen was washed with running tap water to remove residual nitrate salt, brushed gently with a stiff fiber brush, and dried under a nitrogen stream. After all measurements had been completed, the material was returned to the molten salt bath. Each type of material was tested in a separate Incoloy 800 tray to exclude possible interactions between dissimilar materials.

2. Test Results

Visual observations as well as weight change data for the eleven special purpose materials tested are in Table IV-8. In general, the Stellite #6 material (both parent metal and weld specimens were tested) displayed excellent corrosion resistance. Only localized areas of blue and brassy oxidative discolorations were observed. Materials of graphite composition, such as the Crane IX187 gasket and the Crane GF graphite packing, reacted readily with molten salt, dissolving the graphite. Tungsten carbide formulations containing cobalt or nickel binders dissolved completely in molten salt, although silicon carbide displayed sustained corrosion resistance.

Metallic-foil packing material predictably reacted with the oxidizing molten nitrate salt. Copper foil blackened after only 1000 hours of exposure, and then dissolved completely after 5000 hours. Aluminum Crane 100 Al remained intact after 5000 hours of exposure to molten salt, although the metallic luster of the foil was lost. Similarly, the nickel Crane 100 Ni displayed excellent corrosion resistance to molten salt at 399°C (750°F).

Photographs of unexposed materials and materials exposed to molten draw salt are presented in Figures IV-26 through IV-28.

Table IV-8 Visual Observation of Special Purpose Materials Exposed to Molten Salt

MATERIALS	OBSERVATIONS	# HRS IN TEST	WEIGHT CHANGE
GASKET MATERIAL			
- Crane IX 187	Graphite - Outer layer gone, core swollen, brittle	6,000	---
VALVE TRIM AND SEALS			
- Stellite #6	NVC (blue)	6,000	-.008%
- Tungsten Carbide, Co Binder	Dissolved	140	---
- Tungsten Carbide, Ni Binder	Dissolved	3,000	---
- Silicon Carbide	NVC (red)	5,000	-.415%
- Mica Asbestos Valve Stem	Fragmented	4,000	---
- Asbestos with Rubber Binder	Fragmented	4,000	---
PACKINGS			
- Aluminum, Crane 100 Al	NVC	5,000	
- Copper, Crane 100 Cu	Foil dissolved	5,000	---
- Graphite, Crane GF	Dissolved	816	---
- Nickel, Crane 100 Ni	NVC	5,000	---

NVC = No Visual Corrosion

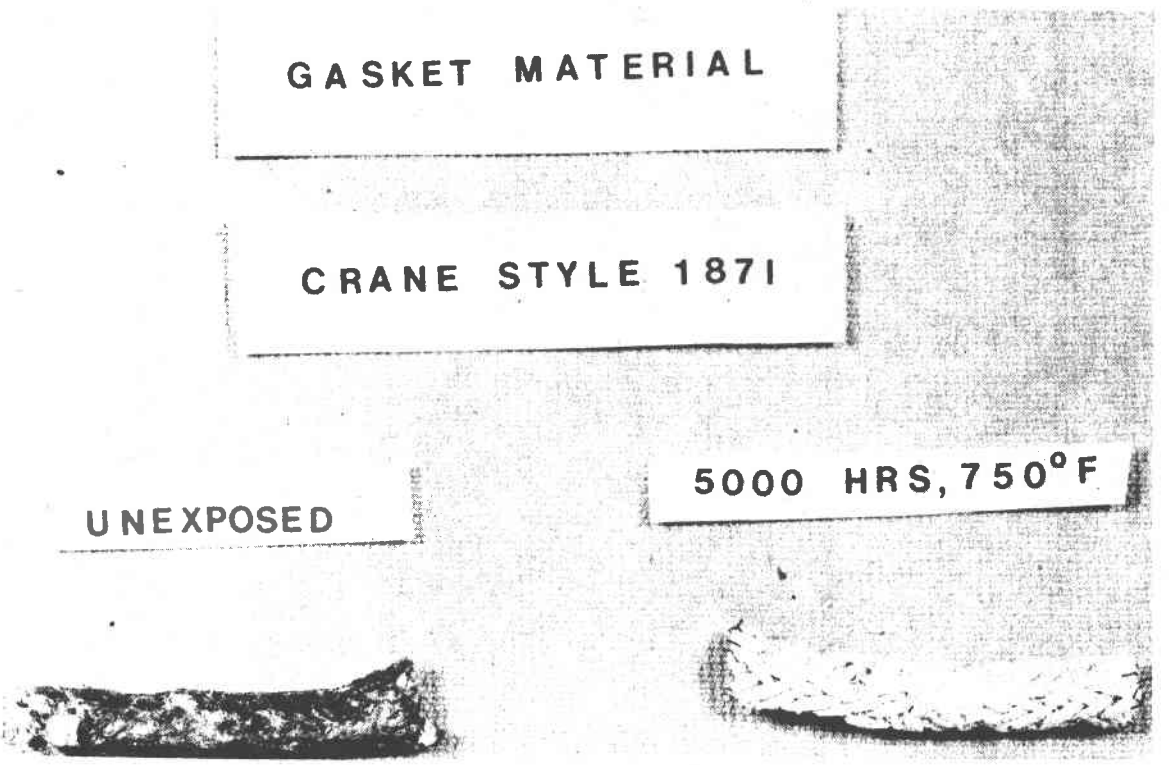

Figure IV-26 Macrographs of Candidate Gasket Material After 399°C (750 F) Molten Salt Exposure

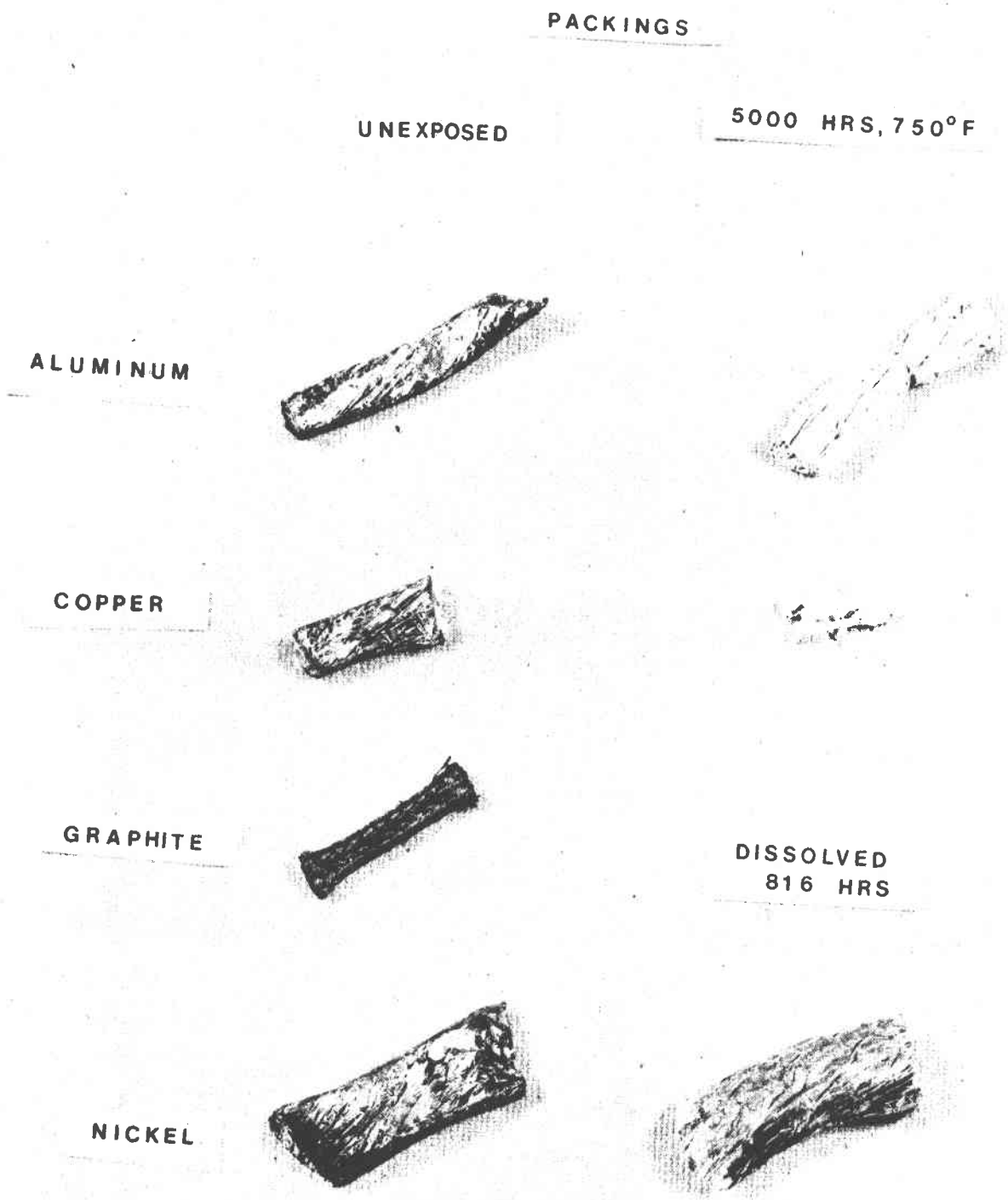

Figure IV-27 Macrographs of Candidate Packing Materials After 399°C (750 F) Molten Salt Exposure

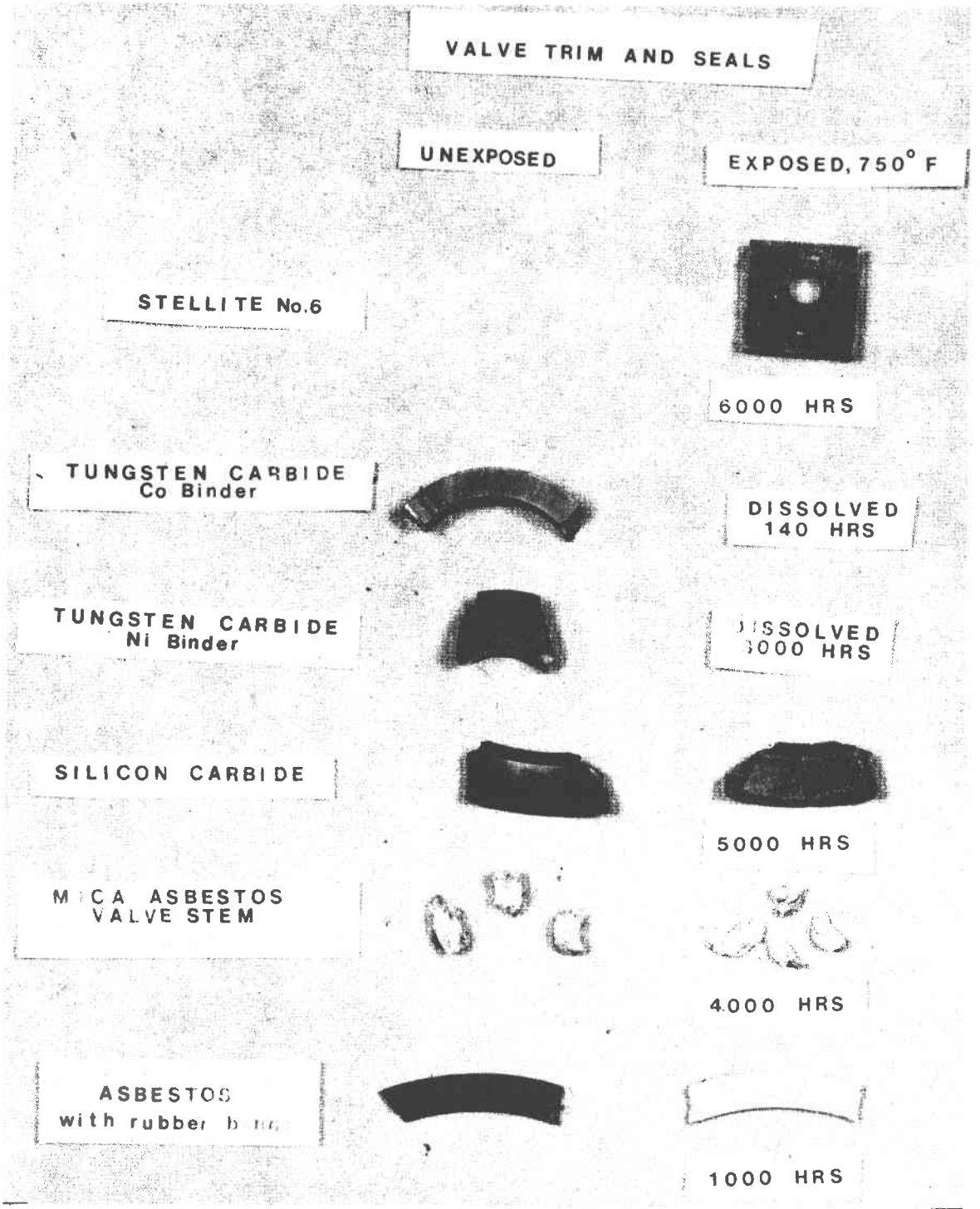

Figure IV-28 Macrographs of Candidate Valve Trim and Sealing Materials After 399°C (750 F) Molten Salt Exposure

V. MATERIAL MECHANICAL PROPERTIES IMMERSION TESTS

A. INTERGRANULAR CORROSION/TENSILE TEST

The purpose of these tests was to assess the susceptibility of the candidate materials to intergranular corrosion after a previous molten salt exposure. The candidate materials tested were 316, 316L and 347 stainless steels, Incoloy 800 and RA330.

1. Test Method

Parent metal and weld samples of each alloy were fabricated into test specimens as shown in Figure V-1. After an initial passivation treatment in nitric dichromate solution, parent metal samples of each alloy were placed in the following environments:

1) Air at 580°C (1075°F) for 8 months (5760 hours);

2) Salt at 580°C (1075°F) for 6 months (4300 hours);

3) Salt at 580°C (1075°F) for 9 months (6480 hours).

Welded specimens were placed in the molten salt bath for a 9 month exposure. Test specimens were separated from each other using nichrome wire, and were placed in a passivated Incoloy 800 container with technical grade sodium/potassium nitrate salt. After the environmental exposures were complete, the samples were washed in running water and dried. One specimen each of parent metal and welded preparation was given a room temperature tensile test after the environmental exposures given above. In order to determine the degree of sensitization experienced by the test materials after the thermal salt exposure at 580°C, individual specimens of all alloys (parent metal and welded) were given a four-hour exposure to a 10% nitric -3% hydrofluoric acid solution at 70°C (158 °F) prior to tensile testing. Weld bend tests were also performed on salt exposed specimens with and without prior acid treatment. Ultimate tensile strength (UTS), yield strength (YS) and total elongation were determined from the room temperature tensile tests. Subsequent metallography was performed.

2. Results

A summary of the room temperature mechanical properties after the elevated temperature air and salt exposures is presented in Table V-1. It is apparent from the results that all of the alloys tested experienced some degree of strengthening after the 580°C (1075°F) air and salt exposures. This behavior is linked to a precipitation (chromium carbides) hardening effect for the austenitic stainless steels, since the exposure temperature is within the lower bound for chromium carbide nucleation. The strengthening observed for the I800 is the result of a two-fold effect, namely precipitation of a face centered cubic precipitate (γ'', Ni_3 (Al, Ti)) and the previously mentioned chromium carbide precipitation.

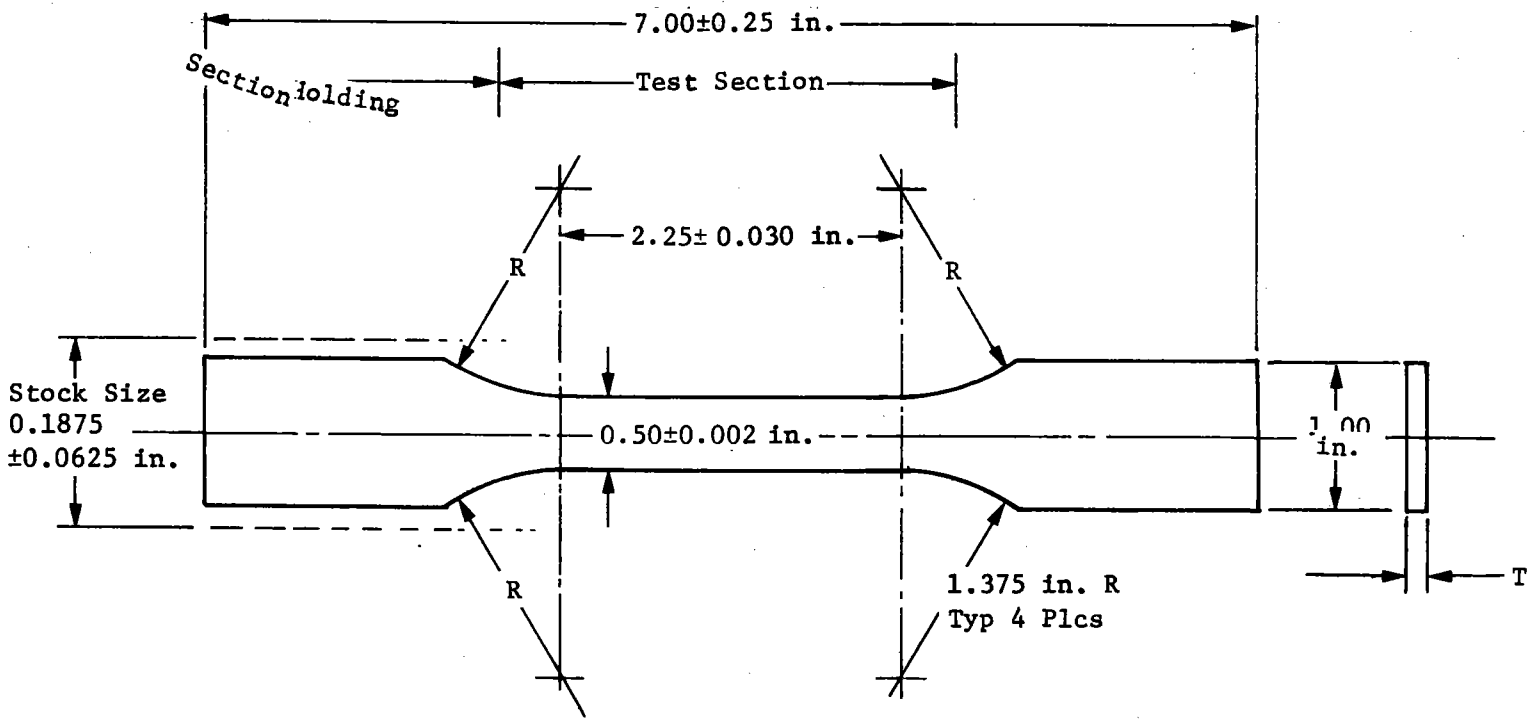

Figure V-1 Intergranular Corrosion/Tensile Test Specimen Geometry

Table V-1 Room Temperature Mechanical Properties of High-Nickel and 300 Series Stainless Steel Alloys After Extended 580°C Air and Molten Salt Exposure

MATERIAL	ENVIRONMENT	TENSILE STRENGTH MPa	YIELD STRENGTH MPa	ELONGATION %
I800	UNEXPOSED	668	427	40
PARENT METAL	AIR, 580°C (8 MONTHS)	706	412	*
	SALT	716	426	34
WELDED	SALT	727	430	*
316L	Air, 580°C			
PARENT METAL	(8 MONTHS)	643	304	63
	SALT	640	302	60
WELDED	SALT	631	333	34
347	AIR, 580°C			
PARENT METAL	(8 MONTHS)	761	457	46
	SALT	749	449	37
WELDED	SALT	717	415	23
316	AIR, 580°C			
PARENT METAL	(8 MONTHS)	663	292	54
	SALT	668	306	45
WELDED	SALT	651	333	34
RA330	UNEXPOSED	599	289	45
PARENT METAL	AIR, 580°C (8 MONTHS)	658	350	*
	SALT	636	335	42
WELDED	SALT	636	339	*

*FRACTURE OUTSIDE SPECIMEN GAGE LENGTH, INVALID ELONGATION VALUES

Figures V-2 through V-3 show micrographs of parent metal tensile specimens after the 8 month air and 9 months salt exposures. Figure V-2 compares the high Ni alloys, I800 and RA330. There appears to be minimal structural damage to either alloy. The RA330 exhibits a fairly continuous precipitate network at grain boundaries and slight surface pitting (much less than one grain deep) after the air and salt exposures. The Incoloy 800 structure is characterized by large titanium carbonitride precipitate particles throughout the matrix. The 300 series stainless steels, 347 and 316L microstructures after the air and salt exposures are shown in Figure V-3. The 347 exhibits a very fine grain structure with many discontinuous grain boundary precipitates. These are most likely columbium and tantalum carbides. Also note the surface pits in the air exposed and the oxide ingress from the salt exposed specimen. The microstructure of 316L shows grain boundary penetration, up to one grain in depth for both previous exposure conditions, and what appears to be fairly continuous grain boundary carbides.

The microstructure of 316 (see Appendix E) appeared similar to 316L except for a very well ordered array of carbides located on the grain boundaries. Examination of the room temperature mechanical properties of Table V-1 and the microstructural analysis show that there is no drastic structural or microstructural degradation of any of the test materials due to the molten salt exposure.

An additional study was performed to determine the degree of chromium carbide sensitization of the candidate alloys after the high temperature thermal exposure at 580°C. The interest of these tests was to observe conpositional variation (i.e., carbon level) effects on the propensity for sensitization. Parent metal samples exposed to air and salt at 580°C (1075°F) and weld specimens exposed to salt at 580°C (1075°F) were given at 10% nitric -3% hydrofluoric acid etch at 70°C (158°F) for four hours. Room temperature tensile tests were performed on these specimens. A summary of the tensile test results after acid exposure is presented in Table V-2. From these results, the high carbon alloys (see Table V-3) 316 and I800 were shown to have a sensitized microstructure. The low carbon alloys 316L, RA330 and the stabilized stainless steel 347 were not observed to have a heavily sensitized microstructure. Selected metallography is included in Appendix E for reference.

The results of the room temperature weld bend tests supported the previous results, namely surface cracking and deformation for the austenitic stainless steels (347, 316, 316L). RA330 exhibited minor surface deformation. The Incoloy weld specimens, given the acid treatment, exhibited complete fracture.

In summary, it appears the exposure of the candidate alloys to molten nitrate salts at 580°C for up to 9 months has no deleterious effects on alloy structural integrity or microstructural stability. From these results it appears I800, RA330, 347, 316L and 316 appear acceptable for molten salt containment at 580°C.

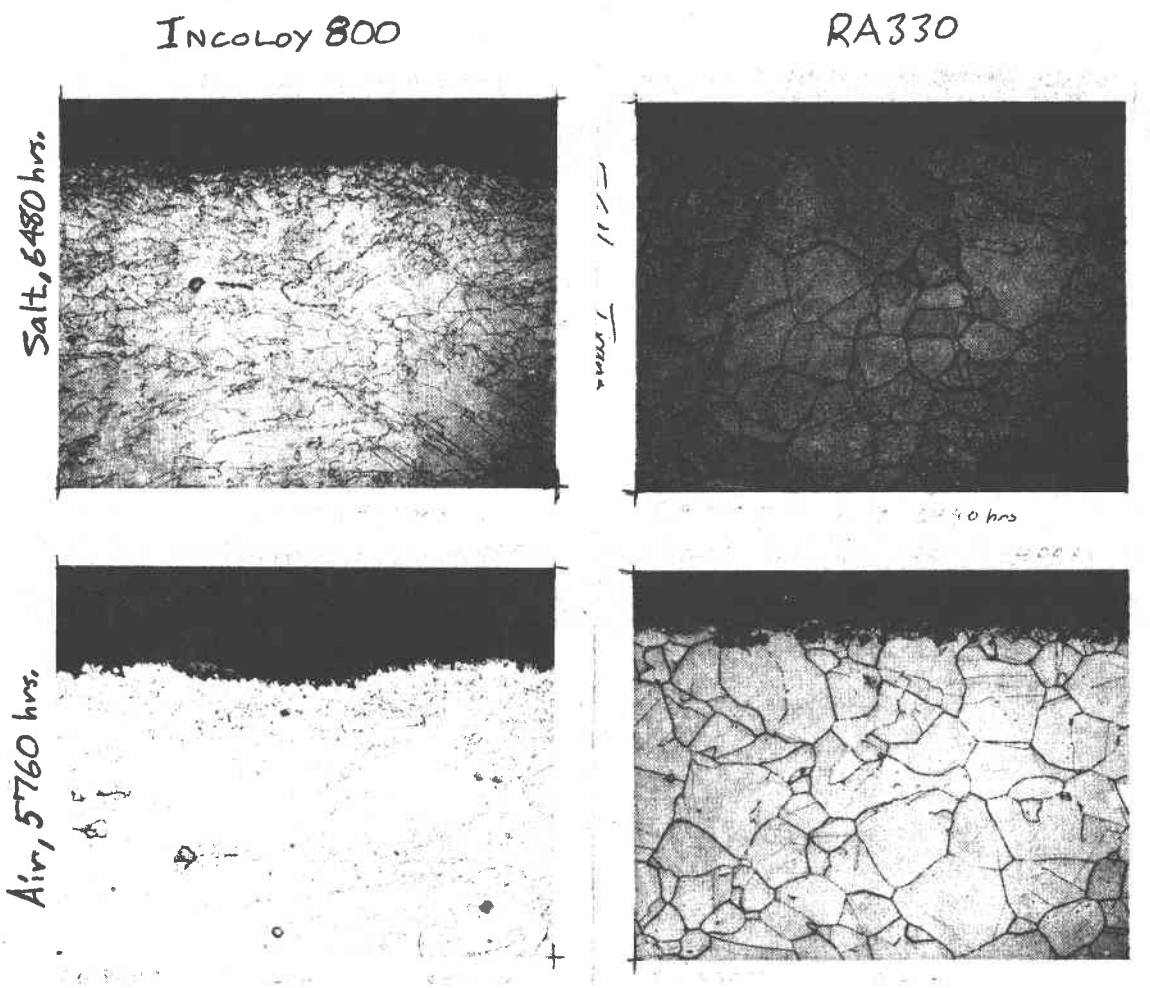

Figure V-2 Micrographs of I800 and RA330 Parent Metal Tensile Specimens After 8 Months Air and 9 Months Molten Salt Exposure at 580°C (1075 F)

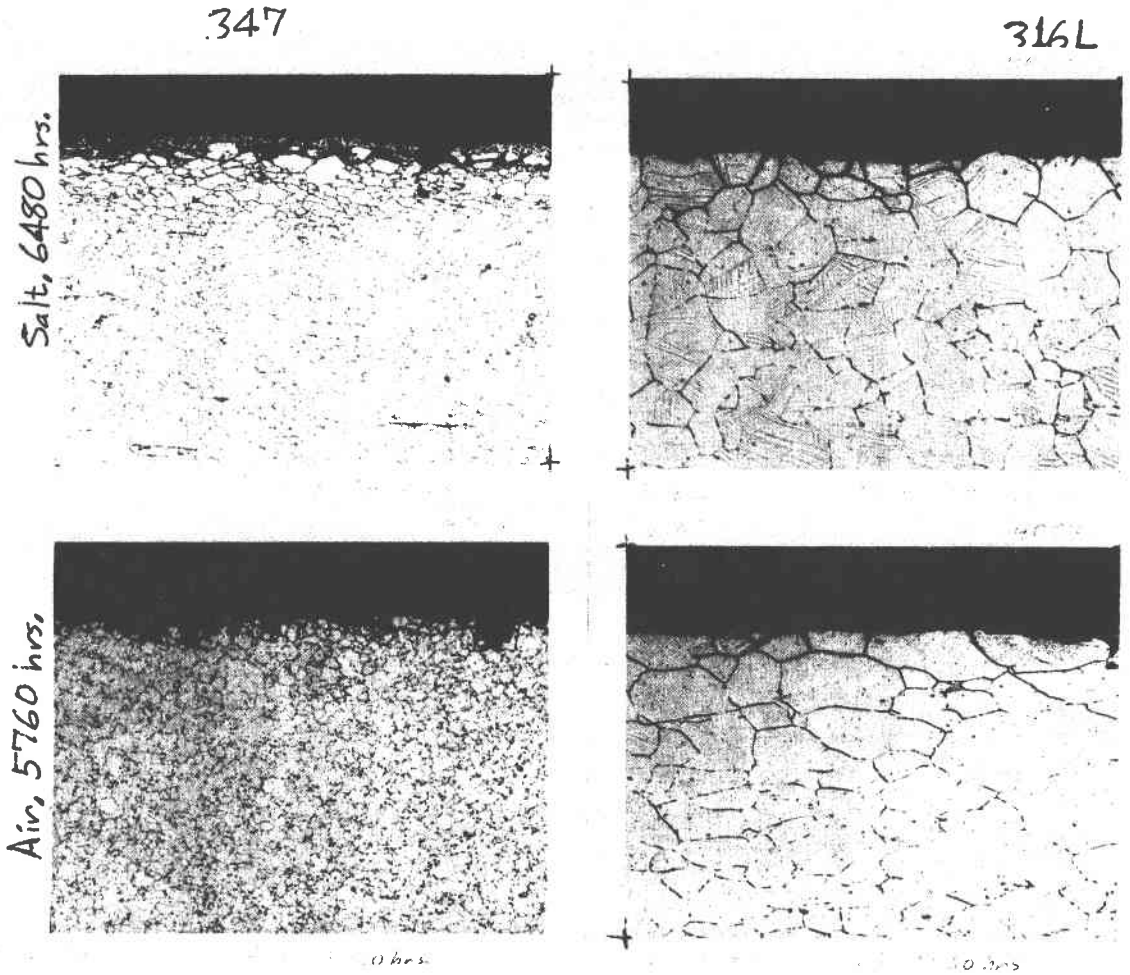

Figure V-3 Micrographs of 347 and 316L Parent Metal Tensile Specimens After 8 Months Air and 9 Months Molten Salt Exposure at 580°C (1075 F)

Table V-2 Room Temperature Mechanical Properties of High-Nickel and High-Chromium Alloys After Extended 580°C Air and Molten Salt Exposure with Previous Acid Treatment before Tensile Testing

MATERIAL	ENVIRONMENT	TENSILE STRENGTH (MPa)	YIELD STRENGTH (MPa)	ELONGATION %
I-800 Parent Metal	Air, 580 °C (8 months)	710	434	NR
	Salt, 580 °C	725	427	NR
Welded	Salt, 580 °C	505	347	5
316L Parent Metal	Air, 580 °C (8 months)	650	299	61
	Salt, 580 °C	597	290	41
Welded	Salt, 580 °C	577	296	28
347 Parent Metal	Air, 580 °C (8 months)	758	454	47
	Salt, 580 °C	770	451	43
Welded	Salt, 580 °C	703	428	23
RA330 Parent Metal	Air, 580 °C (8 months)	637	355	43
	Salt, 580 °C	645	344	44
Welded	Salt, 580 °C	644	330	NR

*316 Samples consumed during acid treatment, no mechanical properties determined

NR - Not Reported

The austenitic stainless steel 316 and high-nickel I800 were shown to be susceptible to sensitization, due to their high carbon contents.

The effects of high carbon compositions (and, therefore, a sensitized microstructure) on the electro-chemical corrosion behavior after long-term molten salt exposures is not known at this time.

Table V-3 Nominal Compositions of Alloys Used in the Intergranular Corrosion/Tensile Tests

Comp. %	RA330	I800	316L	347	316
Ni	35	32.5	12	11	12
Cr	19	21	17	18	17
Fe	43	46	68	68	68
Si	1.25	0.50	1.00	1.00	1.00
Mn	1.50	0.80	2.00	2.00	2.00
C	.05-.08(2)	.05(1)	.03	.08	.08
Mo			2-3		2-3
Others				Co + Ta = $(10_x C)$	

NOTE: (1) Actual wt. % carbon for I800 - 0.08

(2) Actual wt. % carbon for RA330 - 0.02

B. STRESS CORROSION TESTS/CREEP LOADING

Stress corrosion tests were performed to determine the susceptibility of candidate salt container materials, Incoloy 800 (I800) and RA330, to stress-assisted corrosion.

1. Test Method

Constant load creep tests in 580°C (1075°F) 60 wt% $NaNO_3$ - 40 wt% KNO_3 molten salt were conducted with the creep frames shown in Figure V-4. A typical dogbone specimen configuration (Figure V-5) was selected for the creep loading in molten salt. The test parameters of total creep time and average creep rate were selected to achieve a condition of 1% total creep strain. Data from the Aerospace Materials Handbook for RA330 and Huntington Alloys literature for I800 was utilized to determine the initial stress level for a given creep rate at the desired temperatures. It should be noted that these values of stress were taken from curves for steady state creep rates, since there is limited creep data available for these alloys. Table V-4 shows the test matrix along with the measured creep strains and calculated average creep rates during the molten salt exposure. At the end of the molten salt creep exposures, the set of 3 pre-passivated dogbone specimens were washed with water, quickly blown dry, and the change in their one-inch gage length measured. This measurement gave an indication of total creep strain and, therefore, creep rate experienced by the pre-machined dogbone specimens. After the molten salt creep exposure, individual dogbone specimens were cut from the series of specimens shown in Figure V-5.

Parent metal (unwelded) and welded specimens of the two alloys were tensile tested in room temperature air after the creep loading. Ultimate tensile strength (UTS), 0.2% offset yield strength (YS), and % elongation over the one inch gage section were determined as a function of time and initial stress level in the molten salt. In addition, weld specimens were also tested by a standard 180° bend test after their creep loading exposure in the molten salt.

Selected metallography was performed on the samples to examine the synergistic affects of creep loading in molten salt on the structural integrity of the high nickel alloys, I800 and RA330.

2. Results

The comparison of the total creep rate in molten salt with literature values for creep rates of high temperature air exposures would give limited usefulness. The range of strain during the salt exposures indicates the major portion of the test is within the primary portion of the total creep curve, where typical literature values are for secondary, steady state creep.

Metallographic analysis of I800 (Figure V-6) specimens after the molten salt creep exposure show no drastic surface effects. As the creep loading time was increased, the oxide film increased in thickness. Note the apparent tearing along large titanium carbonitride precipitates after 10 hours of creep loading. A curious 'void' formation appear after 118 hours and is very evident at 1000 hours of creep loading in the molten salt. The occurrence of these 'voids' or etch pits is localized to precipitates on grain boundaries. Since

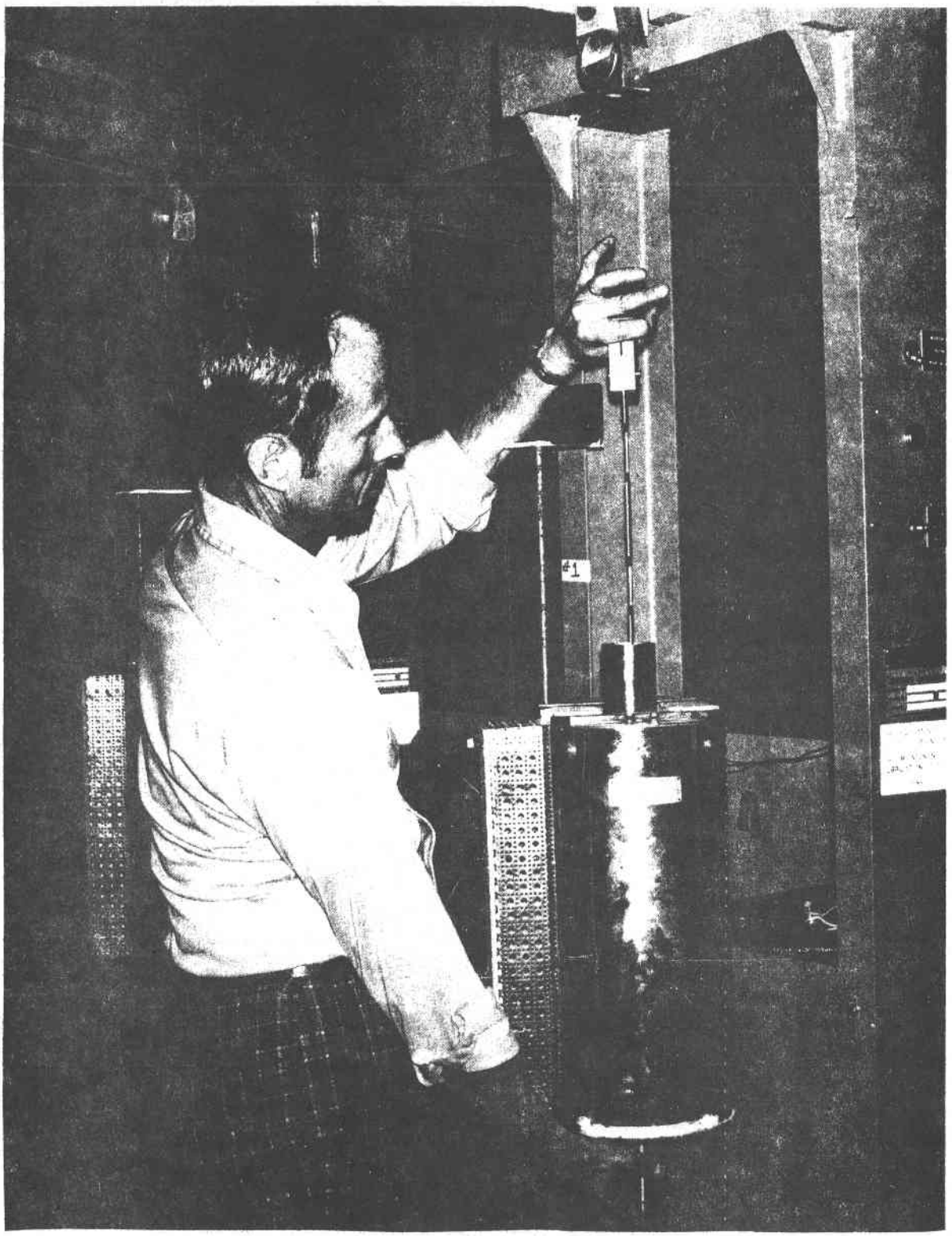

Figure V-4 Photograph of Creep Test Fixture

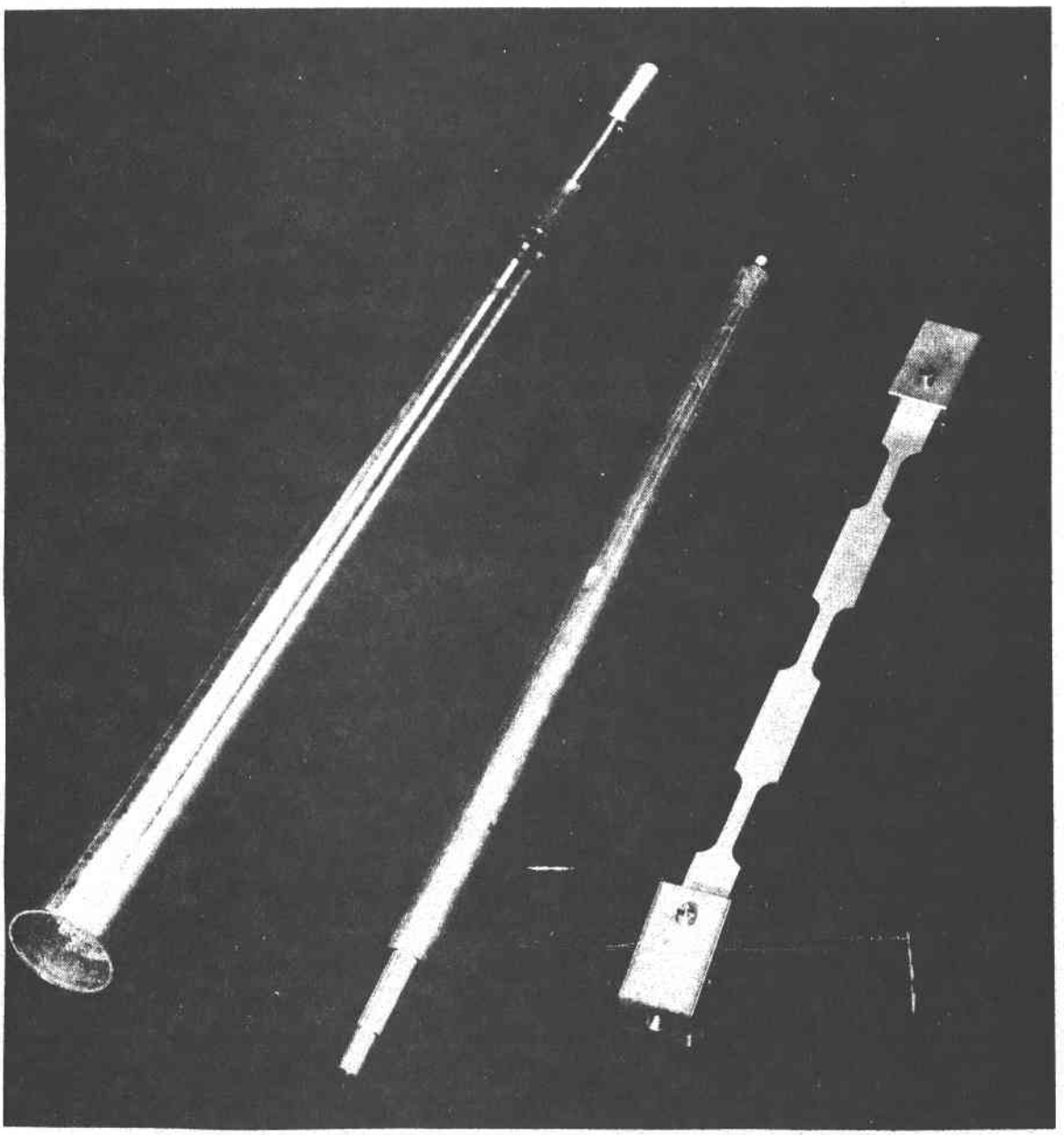

Figure V-5 Dogbone Specimen Configuration Used in Creep Loading/Stress Corrosion Investigation

Table V-4 Initial Stress Levels and Test Times Required to Produce 1% Creep Strain for High-Nickel Alloys in Molten Salt

MATERIAL	TEST TIME (hrs)	INITIAL STRESS LEVEL[1] MPa	(ksi)	INTENDED CREEP RATE (%/hr)	MEASURED CREEP STRAIN (%)	ACTUAL AVERAGE CREEP (%/hr)
I800	10	244	(34.8)	0.1	0.36	.036
	100	210	(30.0)	0.01	0.9	.009
	1000	142	(20.3)	0.001	0.8	.0008
RA330	10	211	(30.2)	0.1	2.7	0.27
	100	175	(25.0)	0.01	1.6	0.16
	1000	141	(20.2)	0.001	1.3	0.0013

NOTE: (1) Under constant load creep tests, the stress level increases with time as the sample elongates.

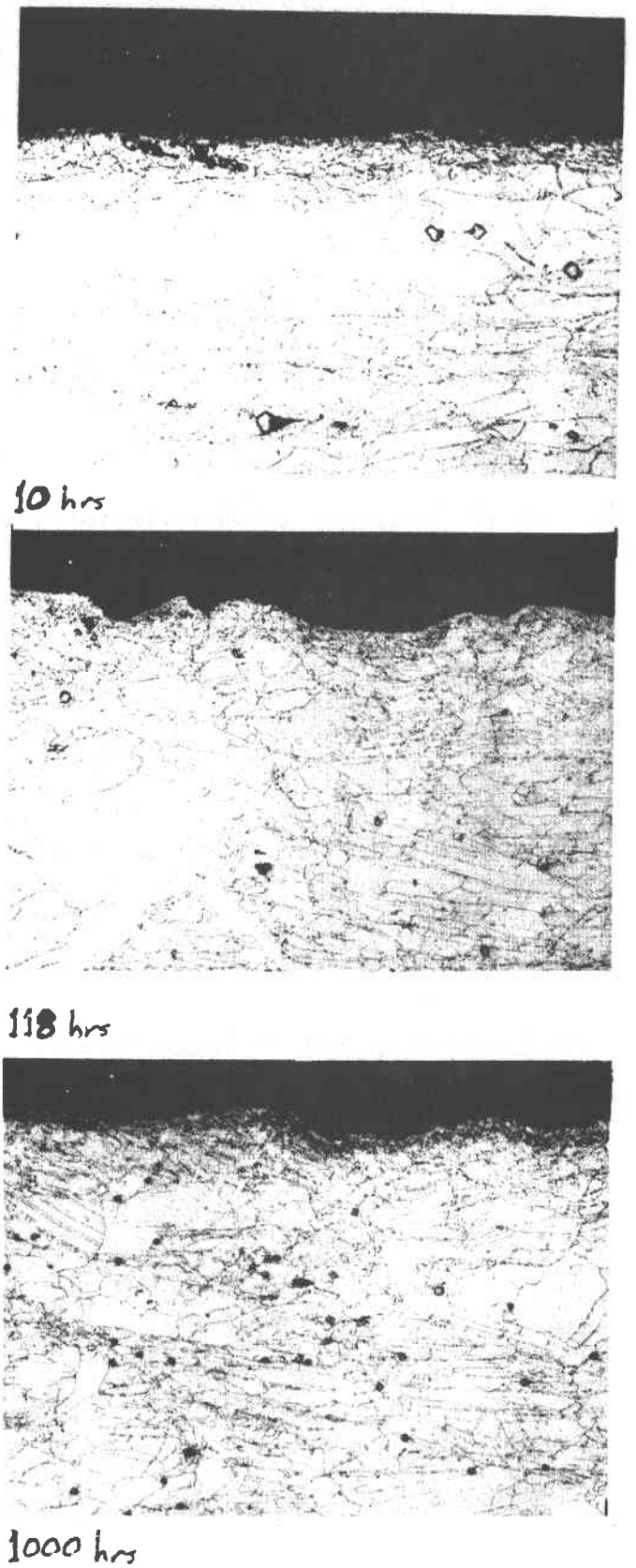

Figure V-6 Micrographs of I800 Parent Metal Creep Specimen After Room Temperature Tensile Testing

baseline creep tests in high temperature air were not performed, it is not known at this time whether these grain boundary anomalies represent a high temperature deformation effect for this high carbon (~0.08 wt%) heat or an artifact of specimen preparation. The low density of these 'voids' at grain boundary triple points does not correspond with observed grain boundary creep effects usually associated at grain boundary junctions. It is suggested that since the occurrence of the grain boundary 'voids' is strictly confined to internal regions of the I800 microstructure, that the salt exposure is not responsible for this effect. Fractographic examinations of fracture surfaces as well as baseline creep information would be necessary to determine the exact nature of these observed grain boundary voids.

The microstructure of RA330 as a function of creep time exposure in the salt is shown in Figure V-7. There appears to be no metallurgical problems associated with the creep loading in salt for RA330. Note, however, the increased distribution of grain boundary precipitates with time.

With respect to the welded samples, Figures V-8 and V-9, both materials show no evidence of corrosive attack in the weld heat affected zone except forthe presence of an external oxide. Additional micrographs of welded specimens for both alloys subjected to short time creep loading in molten salt are included in Appendix F. The 1000 hour samples both show broad, shallow pits entering 0.008 mm (0.3 mils) into the metal. This pitting, while not overly harmful at 1000 hours, may be serious when longer time periods are considered. This would be particularly valid in a high stress cycle environment. If the pits sharpen or deepen, they would provide initiation sites for fatigue damage.

Graphical representation of the room temperature tensile properties of I800 and RA330 parent metal and welded creep specimens, as a function of prior creep loading time in the molten salt environment, is shown in Figures V-10 and V-11. The baseline mechanical properties of I800 (zero creep load - salt exposure time) indicate the material was in the hot rolled condition when received. Note the mechanical property variation for I800. The initial decrease in strength parameters with time of creep loading is attributable to a stress relief treatment, whereas the sudden increase in strength and decrease in elongation after 10 hours of creep loading represents a precipitation strengthening behavior. Note the comparable welded and parent metal strength values of Figure V-10. These variations in the mechanical properties are atributable to the high carbon content (~0.08 at %) of the heat of I800 tested.

The low carbon RA330 exhibits relative insensitivity to mechanical property variation with creep-salt exposure (see Figure V-11). In general, the welded mechanical properties are slightly lower than parent metal values for RA330. After 1000 hours of creep-salt exposure, the strength parameters converge. This effect can be

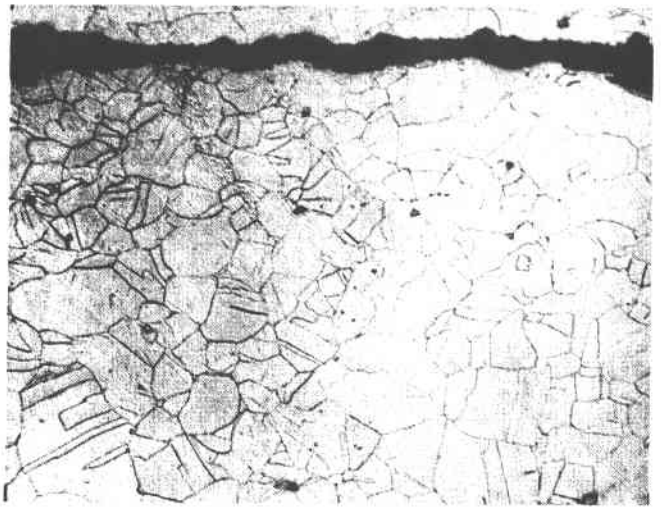

10 hrs

100 hrs

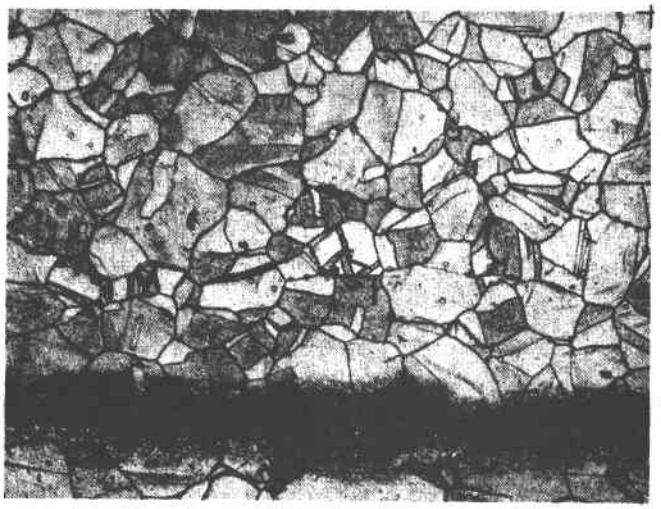

Figure V-7 Micrographs of RA330 Parent Metal Creep Specimen After Room Temperature Tensile Testing

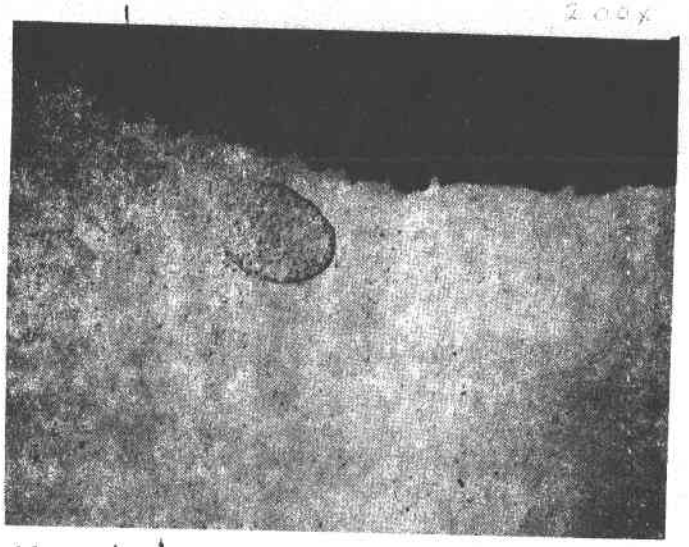

Unetched

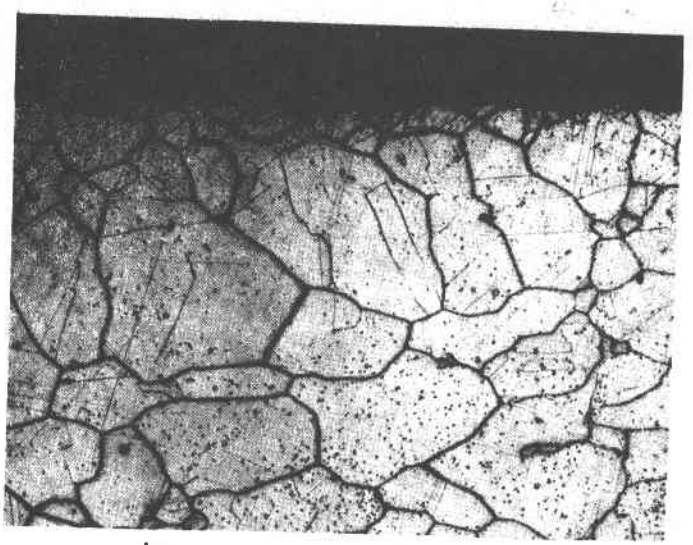

Etched

Figure V-8 Micrographs of I800 Welded Creep Specimen After Room Temperature Tensile Testing

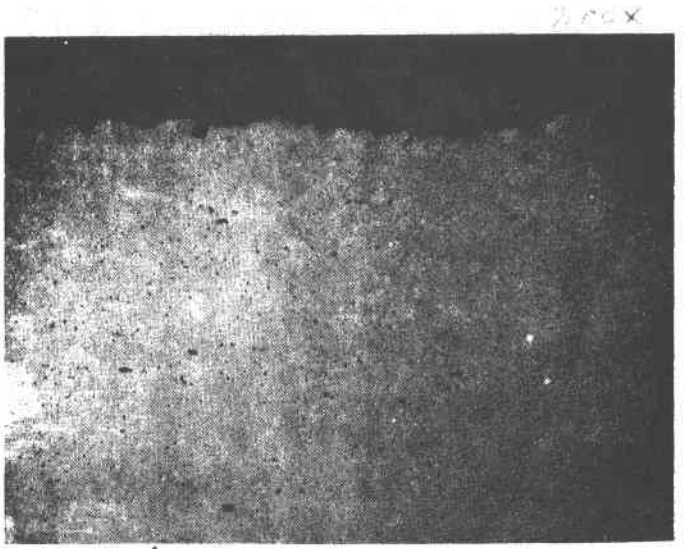

Unetched

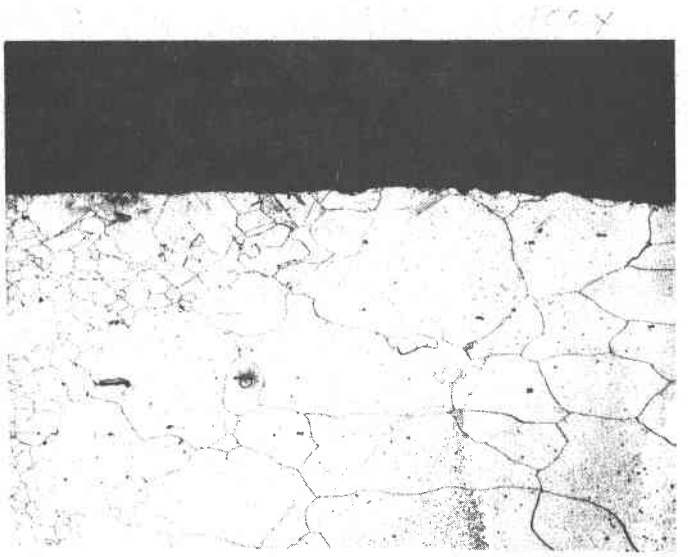

Etched

Figure V-9 Micrographs of RA330 Welded Creep Specimens After Room Temperature Tensile Testing

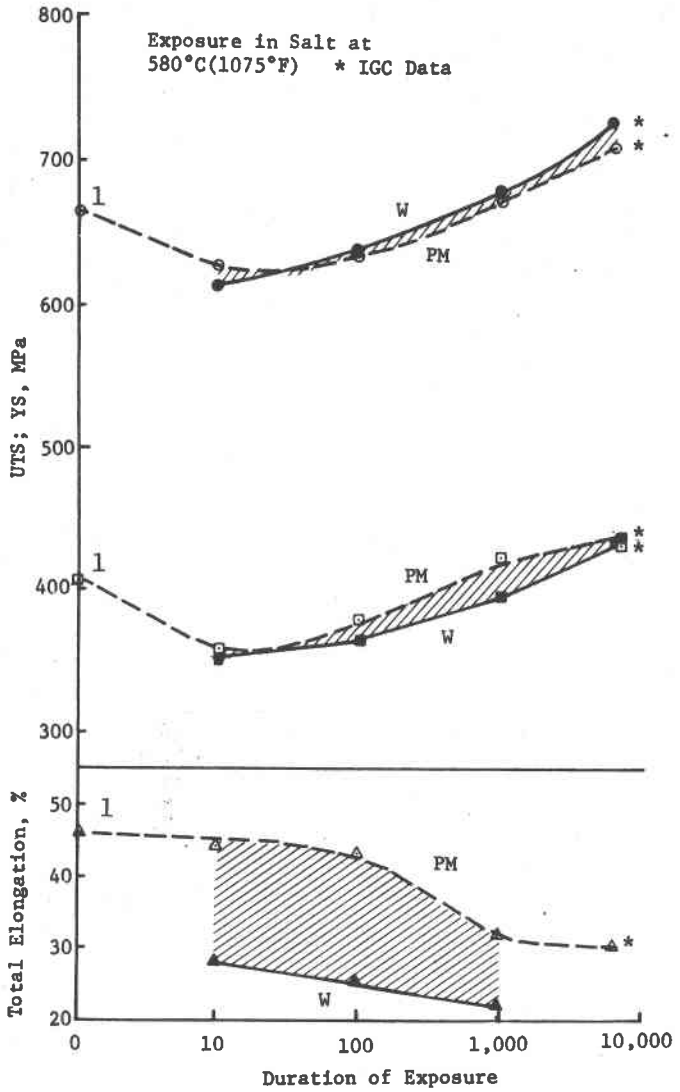

NOTE: 1 - Tensile properties of specimens not previously exposed to molten salt creep loading

Figure V-10 Room Temperature Mechanical Properties of I800 as a Function of Creep Loading Time in 580°C (1075°F) Molten Salt

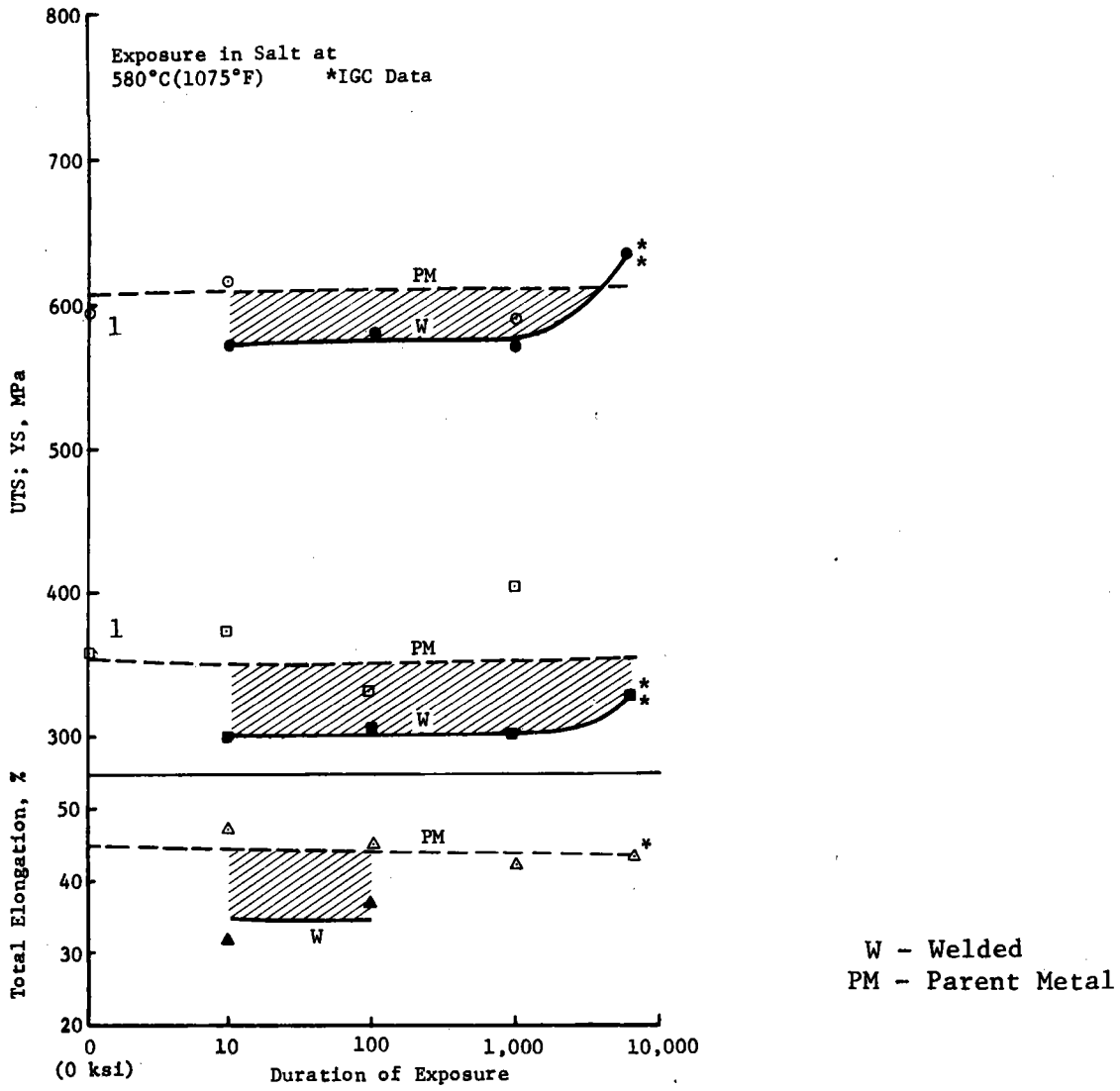

NOTE: 1 = Tensile properties of specimens not previously exposed to molten salt creep loading.

Figure V-11 Room Temperature Mechancial Properties of RA330 as a Function of Creep Loading Time in 580°C (1075°F) Molten Salt

attributed to a precipitate strengthening mechanism supported by the microstructural observation of grain boundary carbide precipitation of RA330 after 1000 hours of creep-salt exposure (See Figure V-7).

In the weld bend test neither the RA330 or Incoloy 800 suffered any complete failures as seen in Figure V-12. Both materials displayed only surface cracking of less than 0.01mm or surface deformation in the HAZ for the 10 and 100 hour exposure periods. After 1000 hours exposure the RA330 still showed surface cracking, while the Incoloy 800 had one sample which had a crack of 0.03mm or 1 grain deep. This agrees with the decrease in ductility of the Incoloy 800 samples seen in the tensile results at 1000 hours.

In summary, creep loading of the high-nickel alloys I800 and RA330 in molten salt at 580°C showed minimal degradation in terms of structural integrity or microstructural alterations. The variation in room temperature mechanical properties for I800 is the result of the combined effects of a thermal treatment on a high carbon material.

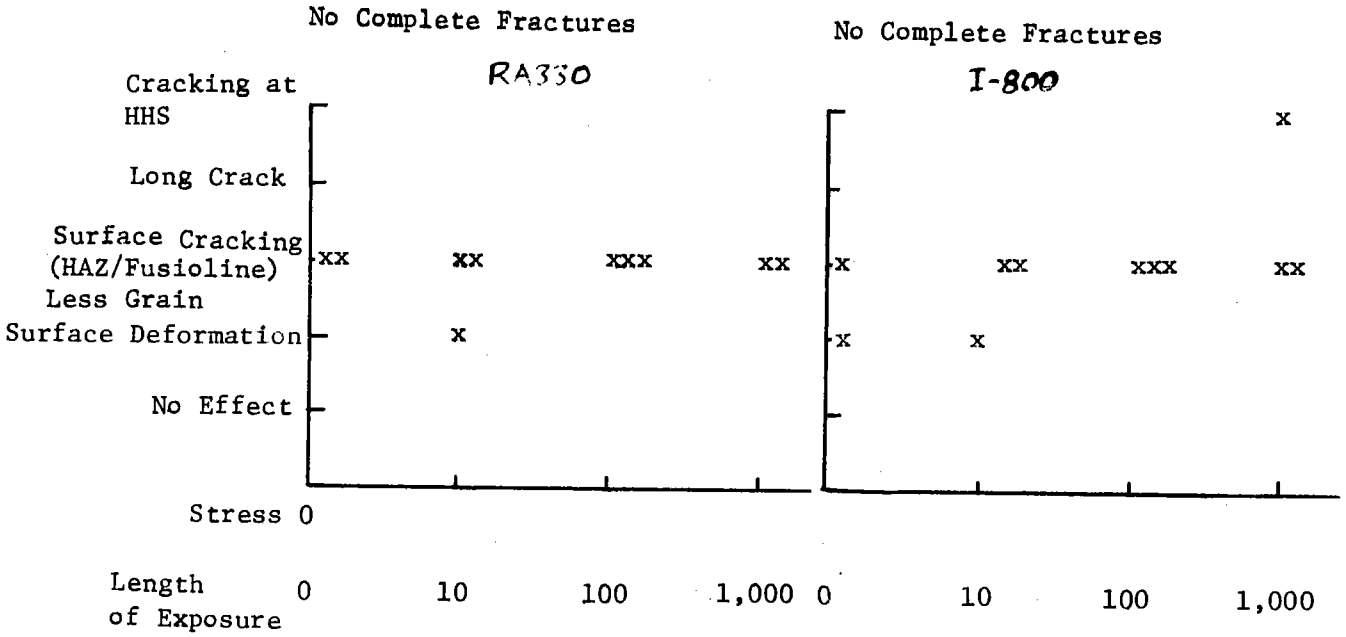

Figure V-12 Room Temperature Weld Bend Test Results for I800 and RA330 After Creep Loading in 580°C (1075 F) Molten Salt

C. CORROSION FATIGUE TEST

The intent of this test was to provide fatigue data for candidate receiver meterials immersed in hot molten salt. The test is similar to the conventional tension fatigue test except that the sample is immersed in 593°C (1100°F) molten salt.

Corrosion fatigue S-N curves derived from this test would be compared to typical S-N curves for the metals in 593°C (1100°F) air. Any tendency of the passivation layer to flake off would be evaluated by visual examination and by comparing post-test with pre-test specimen weights.

No testing was performed for this test section due to a mechanical failure in the gripping device for the tensile fatigue specimens. Determination of the cause of the failure is being performed.

D. THERMAL CYCLING TESTS

The objective of these tests was to demonstrate the tenacity of the oxide passivation layer on metal test specimens during severe thermal shock from 593°C (1100°F) to 27°C (80°F).

1. Test Method

Three coupons each of Incoloy 800, RA330, 316L, 347 and A570 were passivated in molten salt for 2000 hours. The high nickel (I800, RA330) and high-chromium stainless steel (316L, 347) coupons were then heated in an air furnace to 593°C (1100°F), while the A570 carbon steel coupons were annealed at 399°C (750°F).

After a five minute equilibration period, the alloy specimens were removed from the furnace and cooled in a -10°C (14°F) helium jet (Fig. V-14). This cycle was repeated 25 times. The specimens were subsequently reheated in the air furnace, quenched in ambient 25 ± 5°C (77 ± 9°F) distilled water, dried under a nitrogen stream and reheated for a total of 25 cycles. The sample coupons were weighed and inspected visually every ten cycles.

2. Results

Visual examinations of the alloys indicated that they all retained their structural integrity with no evidence of flaking. It is important to note that thermal cycling conditions are far more severe than those expected in a solar thermal storage system.

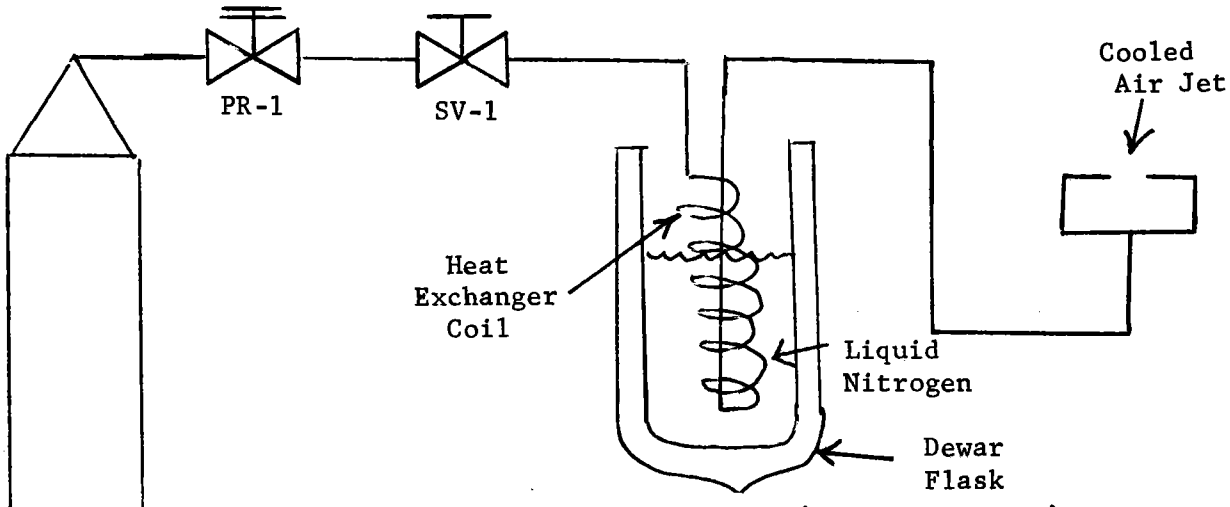

Legend: K-1 "K" Bottle Purified Helium (Low in CO_2, H_2O)
PR-1 Pressure Regulator
SV-1 Shutoff Valve

Figure V-14 Quenching Apparatus Used for Thermal Cycling Tests

VI. TECHNICAL DISCUSSION OF RESULTS

A. SALT CHEMISTRY

The chemistry of molten nitrate salts is important in the development, design and operation of a power system which uses a mixture of sodium nitrate and potassium nitrate as the heat storage and transfer medium, because these salts undergo chemical reactions at the proposed operating temperatures. These reactions may affect properties of the salt such as heat transfer coefficients, heat capacities, melting temperatures, or compatibility with construction materials. In addition, if the reaction product has limited solubility in the salt, precipitates might form at some region in the system where the solubility limit has been exceeded. In this section, salt chemistry (as determined from the static test programs) and its effect on molten salt central receiver power systems are discussed.

1. Nitrite Formation

When mixtures of sodium and potassium nitrates are heated to the power system upper operating temperature, nitrate ion (NO_3^-) is converted to nitrite ion (NO_2^-) with the concurrent evolution of oxygen gas:

$$NO_3^- \longrightarrow NO_2^- + 1/2\ O_2$$

During Phase I of the Advanced Central Receiver Power System program, a series of tests was conducted to determine the equilibrium of this reaction in molten salt (60% sodium nitrate - 40% potassium nitrate) at temperatures near 566°C (1050°F). The relationship between the concentrations of nitrite and nitrate ions in molten salt and oxygen pressure above the salt was found to be defined by:

$$Keq = \frac{[NO_2^-]}{[NO_3^-]}\ [pO_2]^{1/2}$$

At 562°C (1044°F), the value of the equilibrium constant (Keq) was determined to be 0.022 atm $^{1/2}$. In an open system where venting of oxygen can occur, the extent of conversion of nitrate to nitrite is dependent only on the pressure and temperature of oxygen above the molten salt. If the pressure of oxygen is changed, the change in extent of conversion to nitrite will be inversely proportional to the square root of the ratio of the initial and final oxygen pressures. If the system is open to the air (Denver oxygen pressure in air equals 0.16 atm) at 562°C (1044°F) the salt at equilibrium will contain 2.6% nitrite; if the air is replaced by oxygen at Denver ambient pressure (0.8 atm), the weight percent of nitrite ion will derease to 1.1%. If the atmosphere above the system were continuously purged with nitrogen, nitrite concentration would continue to increase because the oxygen pressure could not attain equilibrium values. This occurred during a Phase I test in which the ullage gases above a reactor were evacuated several times and replaced by nitrogen. At the end of the test, the

nitrite ion concentrations had risen to 13% (by weight). If the molten salt is heated in a closed system where the oxygen pressure is not kept constant, but increases as the nitrite is produced, the final oxygen pressure and extent of conversion to nitrite will depend on the amount of salt initially present in the system and the volume of the ullage space.

During Phase I, the relationship of the nitrite/nitrate equilibrium to salt temperature was determined from salt samples heated in air to several temperatures. The relationship of equilibrium constants to temperature is:

$$\ln K_{eq} = -\frac{\Delta H}{R}\left(\frac{1}{T}\right) + \frac{\Delta S}{R}$$

From a least squares fit of the equilibrium and temperature data, the thermodynamic parameters for conversion to nitrite were calculated to be

$H = 28{,}100$ cal/mole $S = 26.0$ cal/mole - ^{o}K

and the relationship between equilibrium and temperature for our molten salt is:

$$\ln K_{eq} = -14{,}000\left(\frac{1}{T}\right) + 13.1$$

In Table VI-1, the expected equilibrium constants and weight percents of nitrite ion expected, if the salt is heated in air (0.16 atm O_2), are listed for several temperatures. The expected weight percent of nitrite ion, negligible at 288°C (550°F), the lower system operating temperature, increases to 3.0% at 566°C (1050°F), the upper operating temperature.

The rates of the conversion of nitrate to nitrite have not been extensively studied. In one of the tests performed during Phase I, in which salt in a closed system was heated to approximately 560°C (1040°F), the reaction reached equilibrium (as determined by monitoring pressure of the evolved oxygen) within 30 hours and reached 80% of equilibrium pressure within ten hours. The rate of the formation of nitrite ion is dependent on the oxygen pressure and the nitrite concentration and temperature; it is not dependent on the surface area of the salt or any agitation of the salt. However, the rate of the reverse reaction:

$$1/2\ O_2 + NO_2^- \longrightarrow NO_3^-$$

in which oxygen must be transported from the surface to the inside of the salt, will be highly dependent on the salt surface area and any agitation of the salt as well as the nitrite ion concentration and oxygen pressure.

One of the consequences of the formation of nitrate ion when molten salt is heated is that heat will be required not only to raise the temperature of the salt, but also to produce the equilibrium concentration of nitrite ion. The equation for the total heat required when one mole of salt is heated to temperature T is given by:

$$Q = Cp \cdot T + \Delta H \, (Keq / (pO_2)^{1/2} + Keq)$$

where Cp = heat capacity of salt, 33.8 cal/mole - °K
ΔH = heat of nitrite formation, 28,100 cal/mole NO_2^-
Keq = equilibrium constant at maximum temperature

Table VI-1 Effect of Temperature on Conversion of Nitrate to Nitrite

Temperature, °C (°F)	Keq	NO_2^- (Weight%)
288 (550)	7.0×10^{-6}	0.001
344 (650)	6.2×10^{-5}	0.008
399 (750)	4.1×10^{-4}	0.052
455 (850)	2.0×10^{-3}	0.25
510 (950)	7.9×10^{-3}	0.98
538 (1000)	1.5×10^{-2}	0.19
566 (1050)	2.6×10^{-2}	3.0
593 (1100)	4.4×10^{-2}	5.0
621 (1150)	7.4×10^{-2}	7.9

When molten salt is heated from 288°C to 566°C in air, the molar heat required is

= 33.8 [(278) + (28,100)(0.026/) (0.4 + 0.026)]

= 9396 cal/mole + 1715 cal/mole = 11,110 cal/mole

This relationship must also be considered whenever heat capacities are being calculated. If conversion to nitrite is not taken into account, erroneous heat capacities can be calculated.

Nitrite formation does not adversely affect (raise) the melting point of molten salt; addition of nitrite ion lowers the melting point of nitrate salts. The lowest temperature eutectic molten salt contains about 40% sodium nitrite. Nitrite ions are also highly soluble in nitrate salts; therefore, precipitate formation will not occur in molten nitrate salts whose only impurity is nitrite ion.

During the environmental effects test, definite correlation was observed between nitrite and chromium concentrations in molten salt. Corrolation coefficients of 0.98, 0.95, 0.95 and 0.97 were obtained for Cr and NO_2 at 1-wk, 5-wk, 15-wk and 28-wk CO_2/H_2O tests, respectively, for example, after 28 weeks in the supernatant of the salt which had been exposed to dry, CO_2-free air, the chromium concentration was 670 ppm and the nitrite concentration was 4.8%. In the supernatant of the salt which had been exposed to dry air containing 1% CO_2, the chromium concentration was 270 ppm and the nitrite composition was 3%. Chemical analysis of all of the salt indicated that this discrepancy in chromium concentrations could not be accounted for by the precipitation of insoluble chromium species. Another example of the correlation between chromium and nitrite was found during the Phase I test in which the nitrite concentration reached 13%. After 6000 test hours the chromium concentration was 4000 ppm, the highest observed in any static test in either Phase I or Phase II.

A reasonable explanation for this correlation is that chromium or chromium oxides are being leached from the alloy surfaces by nitrite ions. One possible mechanism for this phenomenon is that chromium, initially oxidized by nitrate ions, complex with nitrite ions to form soluble nitrite chromium complexes. This type of reaction is analogous to the dissolution of gold by aqua regia (3:1 hydrochloric acid/nitric acid). Oxidation of gold by nitric acid, which normally proceeds only to a slight degree, occurs rapidly and completely because oxidized gold reacts with chloride ions to form the stable tetrachlorogold (III) complex. Similarly, the extent of oxidation of chromium by nitrate ion:

$$Cr + NO_3^- \longrightarrow Cr^{+3} + NO_2^-$$

could be increased by the reaction of oxidized chromium with nitrite ions:

$$Cr^{+3} + x\ NO_2^- \longrightarrow [Cr\ (NO_2^-)_x]^{+3-x}$$

Evidence suggestive of the formation of nitrite chromium complexes is the green color of the molten salts after they have cooled and are dissolved in water prior to chemical analysis. This color is probably due to the presence of a chromium species since very low Ni and Fe were found by atomic adsorption.

If the species were chromium III oxide, it would not be soluble in water. Therefore, it is reasonable to believe that the green color of aqueous solutions of the salt may result from a nitrite chromium (III) complex. As a result of the strong coordination abilities of the nitrite ion, this complex is likely to persist in water. However, chromates may and probably do exist in the molten salt solution also. The atomic adsorption method of analysis used does not differentiate between Cr VI and Cr III.

2. Carbonate/Hydroxide Formation

Another reaction which occurs slowly in molten salt is the formation of oxides through decomposition of nitrites with concurrent evolution of nitrogen gas, nitric oxide (NO), or nitrogen dioxide (NO_2). Decomposition of nitrites to oxides becomes significant in sodium and potassium nitrates at temperatures above 700°C (about 1300°F). In all molten salt tests performed in the absence of atmospheric contaminants at temperatures up to 593°C (1100°F), oxide concentrations remained less than 0.05% even when high nitrite concentrations were present. However, in the presence of water or carbon dioxide, oxides undergo further reactions to hydroxides or carbonates. (Although the discussion given here refers only to oxides being coverted to hydroxides or carbonates, it is generally valid for any possible direct conversions of nitrates without proceeding through oxide intermediates.) Carbonates and hydroxides can build up to significant concentrations in molten salts.

The reaction of molten salt with water vapor at 593°C (1100°F) appeared to reach equilibrium between one and five weeks. After that time, additional water did not react with the oxide, and hydroxide/oxide concentrations at equilibrium remained relatively low. The equilibrium for the reaction:

$$O^{-2} + H_2O \rightleftharpoons 2OH^-$$

is apparently in the direction of water rather than hydroxide formation.

The chromium concentration in the salt, exposed to humid in air (840 ppm), was greater than the chromium concentration in the salt exposed to dry air (670 ppm), although nitrite concentrations were comparable. This increase in chromium concentration is reasonable, because chromium (III), unlike iron (III) and nickel (II), forms soluble hydroxy-chromium complexes. Therefore, it is possible that oxidation of chromium becomes favored by the presence of hydroxide ions for the same reasons it is enhanced by the presence of nitrite ions.

Hydroxides are extremely soluble in molten nitrates (20% at 288°C (550°F)). Oxides are much less soluble. However, it is unlikely that oxide concentrations would ever reach their solubility limits [(0.23% at 288°C (550°F) and 2.3% at 566°C (1050°F)]. However, there is a possibility that trace quantities of alkaline

earths (calcium or magnesium) which may be present in commercial grade nitrates, and whose salts are less soluble than those of sodium or potassium, could form precipitates with oxides or hydroxides.

The reaction of molten salt with carbonate is a serious concern. In the reaction:

$$O^{-2} + CO_2 \rightleftharpoons CO_3^{-2}$$

the equilibrium is in the direction of carbonate rather than carbon dioxide. Virtually all of the carbon dioxide added (with dry air) to the molten salt in the 28-week test was converted to carbonate. In this test, the supernatant carbonate concentration (3.3%) was less than the carbonate concentration in the entire salt (4.6%), indicating that the solubility limit of carbonate was exceeded before the reaction reached equilibrium. Therefore, reaction of molten salt with carbon dioxide will never reach equilibrium; carbonate formation will continue until all of the salt is converted to carbonate. It is interesting to note that the addition of water vapor, along with carbon dioxide, increased the solubility of carbonate, although carbonate precipitation still occurred. When molten salts are exposed to both carbon dioxide and water, carbonate formation dominates.

Formation of high concentrations of carbonate at high system operating temperatures creates a solubility problem. However, even if carbonate concentrations do not approach 1%, solubility problems can still occur if the salt is cooled. The solubility of carbonate at 566°C (1050°F) decreases to 0.5% at 288°C (550°F). Therefore, even if carbonate concentrations are kept below the solubility limit at upper operating temperatures, precipitation of carbonates can occur when the salt is cooled. Carbonate ion may also react with trace quantities of alkaline earth elements to form species which are even less soluble than those formed with potassium or sodium.

3. Salt Regeneration vs Atmosphere Control

In the preceding section, the severe impact of carbon dioxide on molten salt chemistry and the less severe effects of water vapor were discussed. In this section, a technique for removal of carbonates and hydroxides is compared with a technique for preventing contact of the salt with carbon dioxide or water vapor.

During the salt regeneration test, molten salt samples at 288°C (550°F), contaminated with carbonates and hydroxides, were regenerated by treatment with a mixture of nitrogen dioxide (NO_2) in air. The regeneration of carbonates and hydroxide involves the following series of reactions:

$$CO_3^{2} \rightleftharpoons CO_2 + O^{-2} \quad \text{or}$$

$$2OH^- \rightleftharpoons H_2O + O^{-2}$$

$$O^{-2} + 2NO_2 \rightleftharpoons 2NO_2^- + 1/2\ O_2$$

$$2NO_2^- + O_2 \rightleftharpoons 2NO_3^-$$

or a more direct conversion of $CO_3 + OH^-$ to $NO_2^- + NO_3^-$ by NO_2, the results of which are:

$$CO_3^{2} + 2NO_2 \rightleftharpoons CO_2 + 2NO_3^- + 1/2\ O_2$$

$$2OH^- + 2NO_2 \rightleftharpoons H_2O + 2NO_3^- + 1/2\ O_2$$

These reactions are driven towards completion by the reaction of the nitrite ion with oxygen which, at 288°C (550°F) is virtually quantitative. During the salt regeneration test, each salt was exposed to four equivalents of nitrogen dioxide. Conversion of hydroxide to nitrate was 100% complete; conversion of carbonate to nitrate was 75% complete. The reduced efficiency of the carbonate conversion is a result of the equilibrium between carbonate/carbon dioxide equilibrium favoring carbonate to a greater degree than the equilibrium between hydroxide and water favoring hydroxide.

The costs of salt regeneration versus the cost of scrubbing carbon dioxide and water from the salt system atmosphere is based on the following:

1) Atmosphere Components 25°C (77°F)
   Water = 0.016% (50% relative humidity)
   Carbon Dioxide = 0.033%
2) Absorption Capacity 4Å Molecular Sieve
   22 lb H_2O/100 lb sieve
   10 lb CO_2/100 lb sieve
3) Efficiency of NO_2^-
   Hydroxide (100%)
   Carbonate (18%)
4) Price
   4Å Molecular Sieve 1.78/lb
   NO_2 (as N_2O_4) 0.36/lb

The cost of chemicals to regenerate 0.45 kg (1 lbm) each of hydroxide and carbonate with NO_2 is $5.14. The cost of enough 4Å Molecular sieve to absorb the water and carbon dioxide equivalents of 0.45 kg (1 lbm) each of hydroxide and carbonate is $58.25.

Although the above price indicates that molecular sieves require an eleven-fold higher initial cost in chemicals, molecular sieves can be regenerated by being heated and purged with dry nitrogen. Molecular sieves can be regenerated at least 100 times which reduces the cost of the sieves to $0.58 for each pound of hydroxide and carbonate equivalents. Although this estimate does not include equipment and labor costs, it is reasonable to believe that use and regeneration of sieves will be less costly. Although salt regeneration with nitrogen dioxide does appear feasible, it may still be used only sparingly to remove oxides formed during long term use of the salt or to remove hydroxides and carbonates formed due to low-level leakage of carbon dioxide and water vapor scrubber systems.

Other methods of scrubbing or removal of water vapor and carbon dioxide exist besides molecular sieves. These methods are almost all chemical adsorbants or reactants such as $CaCl_2$ for H_2O and NaOH for CO_2. These systems were not studied in any depth but they would probably be more expensive to implement due to more difficulty in the regeneration process.

Other methods of chemical conversion of oxides and carbonates to nitrates also exist. Nitric acid treatment would be effective but probably a more difficult and corrosive process to implement. Addition of nitrate salts such as $Ca(NO_3)$ or $Mg(NO_3)$ would probably precipitate the carbonates and oxides as insoluble salts and regenerate the sodium potassium nitrates. This, however, would most likely lead to precipitation problems which should be avoided in any flowing systems. Preliminary loop evidence shows that these problems may already exist to some degree from salt impurities.

B. DYNAMIC SYSTEM TESTING

1. Bulk Salt Chemistry

In a system in which molten salt undergoes thermal cycling, the extent of conversion of nitrate to nitrite and the rate at which equilibrium is established will depend on the residence time of salt at each temperature, oxygen pressures and ullage volumes in areas where salt is being heated, and oxygen pressures, surface areas and degree of salt agitation in areas where salt is being cooled. In a system where molten salt is recycled between 288°C and 566°C, nitrite concentrations would cycle between 0.001% and 3.0% if the salt were allowed time to equilibrate with air at both temperatures. The molten salt pumped fluid loop and the receiver SRE are not open to air at the high temperature end, but are vented at the sump (low temperature end). Residence time in the sump is much less than the time required for complete transport of oxygen throughout the salt. Therefore, in an operating thermal cycling system, bulk nitrite concentrations will be lower than 3.0% at 566°C and higher than 0.001% at 288°C.

In the salt pumped fluid loop, the nitrite ion concentration of the salts taken from the sump increased 1.23% after 4700 hours. The rate of increase was slow during most of the cycling. In the receiver SRE nitrite ion concentrations of salts taken from the sump increased from 0.08% to 1.26% during the time period from 7-29-80 to 12-1-80. Nitrite ion concentrations of salts, taken simultaneously from the 288°C and 566°C ends of the receiver SRE, were virtually identical (1.13 $\pm$ .01%). It is anticipated that nitrite ion concentrations in the high temperature end of the salt pumped fluid loop at the end of the test were also virtually identical to the 1.23% found in the sump. In both systems, a pseudo-equilibrium nitrite concentration is reached throughout the entire system. The whole magnitude and rate at which this equilibrium is attained are function of design and operating parameters of the system. In both the receiver SRE and in the loop, this pseudo-equilibrium nitrite concentration, although it may not have been reached during the test period, is not likely to be much greater than 1.2%. After nitrite concentrations reach equilibruium values in pumped systems in which thermal cycling occurs, all heat absorbed by the salt will be used only to increase its temperature.

The salts taken from the sump of the salt pumped fluid loop contained low concentrations of chromium. These increased from 4 ppm to 27 ppm as nitrite concentrations increased.

In both the salt pumped fluid loop and the receiver SRE, oxide and carbonate concentrations remained minimal (0.05% indicating that oxide and carbonate formation will remain minimal in operating systems if carbon dioxide and water vapor are excluded. The SRE, however, had no scrubber provisions to remove CO_2 and water vapor. This is probably because the SRE sump was kept at a lower temperature (below 316°C [600°F]) and the salt surface-to-volume ratio was low.

2. Nitrite/Chromium Correlation

The data from these chemistry tests as well as the loop salt analysis and other tests tend to point out a definite correlation between percent nitrite and percent chromium dissolved in the salt. For example, the loop tube residue wash showed a correlation coefficient of .089. For Cr + NO_2 and the environmental effects tests showed Cr/NO_2 correlation coefficients of 0.98, 0.95, 0.95 and 0.97 for the 1-wk, 5-wk, 15-wk and 28-wk tests respectively.

The reason for this correlation is not certain from these tests, but it possibly is due to the affinity nitrite has for complexing (thereby dissolving) chromium compounds. The higher nitrite concentrations may dissolve the chromium from the Incoloy 800 oxide layers yielding a chromium-depleted oxide layer, possibly more susceptable to corrosion.

Also, it is interesting to note the salt analysis from water washes of different loop tube section residues. However, these are tube residue analyses, not bulk salt analyses. Note in particular the very high (17%) nitrite at the 449°C (840°F) section (see Table VI-2). This is the sample area where high coupon weight loss was noted. This is particularly interesting since chromium concentration reached over 1 percent in this area (1.15%). This high nitrite and chromium might be dismissed as coincidence if it were not for a progressive increase in nitrite (and chromium) as one progresses from the loop sump at 288°C (550°F) to the 449°C (840°F) section of the heat exchanger. A possible reason that the chromium concentration at the 566°C (1050°F) heater section is not at maximum may be due to the kinetics of the reaction $NO_3 \rightarrow NO_2 + 1/2\ O_2$ being slow relative to loop flow rate, 3m/s (10 fps), thereby taking several seconds after flowing through the heater to reach full decomposition. Also, an explanation for the very high nitrite in several loop sections (8 to 17%) may be found in the steep rise the equilibrium nitrite values with relatively small increases in temperature after about 590°C (1095°F) or so. The equilibrium temperature in nitrite salts, at ambient pressures, for 17% nitrite is between 675°C (1240°F) and 700°C (1290°F). Therefore, relatively small over-temperature conditions or possibly just heat transfer deltas in salt boundary layers may produce local high nitrite concentrations in circulated salts. It is interesting to note that this hypothesis relating salt temperature to nitrite concentration, which in turn is related to leached chromium concentration, and, therefore, alloy corrosion fits with Sandia Lab's reported data which finds alloy steels are attacked rapidly in molten salt above 600°C. The correlation of chromium concentration in the salt versus nitrite concentration is evident from the majority of tests completed.

Table VI-2 Nitrite and Chromium Concentrations of Water-Soluble Residues from the Walls of the Molten Salt Loop

LOCATION	FLOW DIRECTION	TEMPERATURE, °C(°F)	% NITRITE	% CHROMIUM
Sump		288 (550)	1.2	0.0004
S P 1	Ascending	358 (675)	1.3	0.07
S P 8	Ascending	432 (811)	1.7	0.01
S P 2	Ascending	483 (900)	4.3	0.11
S P 4	Descending	566 (1050)	8.8	0.07
S P 3	Descending	449 (840)	17.2	1.15
S P 5	Descending	388 (730)	5.5	0.006
S P 6	Descending	310 (590)	2.5	0.01

A number of explanations are possible for the presence of a region of high nitrite and chromium concentrations at sample port 3 [449°C (840°F)].

- o The structure and tenacity of the oxide layer formed at that temperature is such that it is less resistant to corrosion.

- o The solubility limits of a nitrite-chromium complex could be exceeded at (840°F) and precipitation begun (as evidenced by the intensely green particles) which could further increase the rate and extent of chromium depletion.

- o Sample port 3 was placed at a bend in the heat exchanger, which could affect the size and velocity of the layer nearest the wall, resulting in buildup of nitrite and increased oxidation of chromium.

- o The nitrite and chromium concentrations just lag slightly behind a direct correlation with loop section temperatures. Since temperature is directly related to equilibrium nitrite formation, and since the kinetics are not instantaneous, the maximum decomposition of nitrite may be at some point downstream from the heater section and then may reverse to lower nitrite values corresponding to the lower temperatures downstream. This is exactly what is seen in the loop residue wash analysis. If one accepts the existence of a long-lived boundary layer of salt exposed to temperatures higher than bulk, then increased local concentrations of nitrite may be possible.

- o The extremely high nitrite values in the loop residue may be an anomaly caused at shutdown by slight overtemperature conditions during the shutdown sequence; and/or by preferential draining of the bulk salt, leaving boundary layer salt to adhere to tubes and remain behind.

3. Loop Precipitate

This material was first precipitated (or plated) as a dense coating of insoluble tan or light brown material in loop sections and coupons in the 454°C (850°F) return section of the loop. Various analyses have been performed on scrapings of this material and results indicate the composition to be somewhat variable in different loop sections. The major constituents are calcium, magnesium, and possibly silicon, carbon, boron and oxygen. This insoluble substance is probably a mixture of two or more salts or possibly a complex salt such as calcium magnesium hydroxy-silicate. Possible anions are: oxide, silicate, carbonate or boride. These materials may be formed from reactions of salt impurities, or they may have been externally introduced during salt charging or loop repair especially from asbestos gasket or silicate insulation materials.

The possibility that the constituents of this coating are being precipitated from commercial salt impurities leads to potentially serious consequences in multimillion pound commercial salt systems. Part per millions of salt impurities equal hundreds of pounds of potential system fouling precipitates in large receiver systems. This is especially disturbing if the cyclic solution/precipitation occurs at one particular temperature range as is possible from the loop data.

C. STRUCTURAL ALLOY IMMERSION AND MECHANICAL PROPERTY ANALYSES

The discussion of the oxidation behavior of the candidate containment materials in molten salt (60 wt% $NaNO_3$-40 wt% KNO_3) must include experimental results from the dynamic loop, trace contaminant and extended immersion tests. In general, the oxidation behavior of all the alloys (high-nickel and carbon steels) except RA330, exhibited an oxide growth-flaking behavior for all of the above experimental conditions. The hi-nickel RA330 demonstrated parabolic oxide growth kinetics with stable adherent scale formation from microstructural analysis. For the Incoloy 800 and alloys 347, 316L, 316 and 321 exposed to 579°C (1075°F) molten salt, microstructural analysis showed slight surface pitting, grain boundary attacks and oxide intrusion. The other steels (A570, A516, A387) exposed to molten salt exhibited a uniform, general corrosion attack. There was no microstructural evidence of a highly localized, catastrophic attack on the carbon steels.

The general trend of greater oxidation resistance for welded vs parent metal specimens of the carbon steel alloys was observed. This trend is reversed for the high-nickel alloys.

The experimental results indicate that carbon steel materials could be considered for salt containment, even at intermediate salt temperatures [399°C (750°F)], if compensation were allowed for metal removal during design. Control of the trace contaminants hydroxide (OH^-) and carbonate ($CO_3^=$) in the salt composition would remove the worst case oxidation for 347 and RA330. Based on the extended immersion tests, with the long term oxidation behavior used to complement the trace contaminant tests, it appears I800 and RA330 would be acceptable containment materials for 566°C (1075°F) molten salt. The stabilized stainless steel 347 did show an oxide intrusion into the surface grains; 316L showed slight grain boundary penetration. These effects may increase with time. Further oxidation behavioral study is needed on these alloys before their use can be confidently recommended for high temperature (566°C) salt containment. Controlling chloride (Cl^-) intrusions may be more difficult in the salt specifications. The lowering of Cl^- levels would increase the oxidation resistance of I800 and all of the carbon steels. An intermediate temperature oxidation anomaly for I800 exposed to flowing molten salt with no trace contaminants was observed. The depletion of chromium from outer oxide layers and at areas adjacent to the oxide/substrate interface at 440°C (824°F) was observed. This lower temperature behavior should be studied by static immersion since this depletion of chromium effectively lowers the corrosion resistance and mechanical integrity of the alloy. This chromium depletion behavior was also observed by other investigators for 316 stainless steel in a thermal convection loop with 630°C (1166°F) Partherm 430 (60 wt% $NaNO_3$ - 40 wt% KNO_3). It appears this behavior is highly alloy composition/salt temperature dependent. No reduction in metal substrate chromium levels was found in 566°C (1075°F) flowing salt, confirming static immersion results. A location-dependent effect was also observed for I800 and

A570 in flowing molten salt. Specimens closer to the undisturbed salt flow showed greater weight loss, suggesting a flow pattern effect on material oxidation behavior.

The analysis of the mechanical integrity tests after a previous molten salt exposure shows no large degradation in terms of mechanical property response or microstructural alterations for RA330, I800 or 347 stainless steel. Welded samples of the molybdenum-stabilized 316 was severely sensitized; 316L was also sensitized in the weld HAZ even with its low carbon content. In addition, the high carbon content (~0.08 wt%) of the I800 allowed for its sensitization after a welding treated and high temperature salt anneal. Room temperature mechanical property determination after creep loading in molten salt showed no abnormal effects due to the salt environment on I800 and RA330. The effects of carbon levels was again demonstrated, as strength parameters increased with time of previous creep-salt exposure with a corresponding decrease in elongation for I800. This effect was attributed to carbide strengthening as a function of temperature exposure. The effects of salt were seen only as a mild oxide scale; its thickness increased with salt exposure time. The observation of grain boundary voids or pits characteristic of the internal structure of creep-loaded I800 was noted, but its cause was not determined. It may very well be a temperature - time effect, characteristic of the high carbon Incoloy 800. This behavior was not attributed to the salt exposure during the creep loading. Previous investigations did not observe any deleterious effects on creep lifetime for I800 ($\sim$0.04 wt% carbon) exposed to salt under different initial stress levels. Microstructural observations showed oxide intrusion along carbide sensitized grain boundaries to a depth of 0.08 mm (0.003 in). It should be noted that the excessively high stress levels reported for this study were 3 times the yield strength at temperature for this metallurgical condition (solution treated) of I800. These observations, even under extremely severe conditions, suggests that the carbon content and metallurgical condition (i.e., solution treated, annealed, hot worked) of I800 may need to be controlled to insure adequate high temperature material integrity.

VII. CONCLUSIONS AND RECOMMENDATIONS††

A. SALT CHEMISTRY

a. The stability of molten salt is adequate for long-term solar use with carbonate and hydroxide control (by either scrubbing or salt regeneration).

*b. There is a need for further investigation of the deposits found in the intermediate temperature sections of the molten salt loop. This may be accomplished by laboratory-scale test-simulation of the conditions leading to such deposits. This is necessary due to the potential for heat exchanger fouling as systems requiring large amounts of salt are operated.

*c. Further investigation is required to determine the effect of nitrate/nitrite equilibrium on chromium leaching.

*d. Preliminary economic estimates of atmospheric scrubbing and salt regeneration favor the former method of carbonate and hydroxide control. The need for more complete economic studies in this area is indicated.

B. MATERIALS TESTS

a. I800 and RA 330 are acceptable materials for long-term high-temperature [up to 580°C (1076 F)] service. 316 and 316L may also be suitable, pending further investigations.

*b. Control of the carbon content of I800 and RA330 may be necessary to minimize possible long-term structural degradation of these alloys. (Particularly if sensitization is found to be detrimental to long-term service behavior).

c. There were no salt-related detrimental effects on either the oxidation behavior or the structural integrity of I800 and RA330.

d. It is recommended that this investigation be extended to other candidates for intermediate temperature (280-480°C) alloys - [possibly from the low-chromium ferritic steel (2-¼ Cr - 1 Mo) family.]

---

††An asterisk (*) ahead of an item indicates requirement for future development in that area.

*e. Additional mechanical testing in molten salt environments should include creep-fatigue interactions, and slow strain rate testing.

*f. Based on visual examination of a limited number of carbon steel test coupons, there were no indications of significant effects of surface preparations on material behavior. There is a need to investigate the possibility of passivating tube surfaces to prevent initial high corrosion or oxidation.

g. The carbon steels are suitable low-temperature molten salt containment materials, up to 288°C (550 F).

h. The low alloy steel A387 (1¼ Cr - ½ Mo) appears to be a suitable candidate for low-temperature service (up to 288°C) provided chloride (Cl^-) impurity levels in the molten salt are controlled.

j. Carbon steels appear to be a suitable intermediate-temperature containment material if proper design allowances can be made for material loss.

C. MOLTEN SALT FLOW LOOP

a. There is no evidence of material transport in the molten salt flow loop.

*b. The flow loop tests should be continued for the following reasons:

- Determine the long term weight loss of the specimens.
- Examine the effect of preoxidizing the surfaces in air on the weight loss.
- Investigate the cause of the tan colored deposit at the low temperature end of the loop.

*c. It is recommended that molten salt samples from both the high, and low temperature ends of the loop be analysed for nitrite to verify that a pseudo-equilibrium exists in the loop.

*d. Water-insoluble precipitates from coupons and loop sections should be subjected to elemental analyses, X-ray diffraction and infrared spectroscopy. Similar analyses should be conducted of residues from the sump. Also, sections of the SRE should be analyzed if possible.

e. I-800 coupons exposed to flowing salt in the loop exhibited similar weight gains at 565°C (1050 F) as those in the trace contaminants tests. Coupons at 329°C (625 F) and 482°C (900 F) exhibited minor weight changes. The largest changes occurred at the 440°C (825 F) sample port, and accelerated with time.

APPENDIX A

MOLTEN SALT CHEMISTRY ANALYSITICAL PROCEDURE AND OTHER SUPPORTING DATA FOR SECTIONS II AND III

APPENDIX A - TABLE OF CONTENTS

APPENDIX A - LIST OF FIGURES

APPENDIX A LIST OF TABLES

MOLTEN SALT CHEMISTRY
ANALYTICAL PROCEDURES

I. PREPARATION OF SAMPLE

The sample obtained is a solidified "melt" of a homogeneous salt mixture initially containing potassium nitrate and sodium nitrate in a fixed molar ratio. Carbonate, hydroxide and nitrite ions are absent in the original salt composition, but may be found in various proportions in the solidified melt, i.e., in the thermally reacted salt. It is thus imperative that all preparatory and analytical procedures are chosen so as to insure that contamination of the salt from these ions as well as from nitrate ions does not occur.

Remove the solidified melt from the metal tray and pulverize the entire sample using a mortar and pestle. Weigh a portion of the sample and transfer the weighed salts (120-140 grams) quantitatively to a one liter Erlenmeyer flask fitted with a rubber stopper with an associated ascarite tube. The weighings should be performed on an analytical balance to an accuracy of 0.01 gram and recorded accurately. Add approximately 700 ml of degassed, glass-distilled water to the flask and attach the stopper-ascarite tube assembly. Distilled water may be degassed by boiling and subsequent cooling to a temperature slightly below its boiling point.

When all the salt has gone into solution, filter the solution hot through a Whatman #1 filter paper into a one liter volumetric flask. Rinse the filter paper three times with gas-free distilled water and add the effluent to the same one liter volumetric flask. Stopper the flask with an ascarite tube and allow the contents to cool to room temperature. Dilute the solution to the mark with gas-free distilled water, attach the ascarite tube, label the solution and set it aside for chemical analysis.

II. DETERMINATION OF INSOLUBLE RESIDUES

To determine the quantity of insoluble material in the salt mixture, weigh a clean, dry Whatman #1 filter paper to 0.1 mg, filter the hot dissolved salt solution (performed under "preparation of sample"), dry the filter paper and

contents in a 50°C oven, and reweigh the filter paper and residue. It is convenient to fold the filter paper before drying to avoid loss of particulates.

The insoluble residue concentration in weight percent of the original sample is given by the following equation:

$$\frac{\text{(Weight of filter paper + residue) - (Weight of filter paper)}}{\text{sample weight}} \times 100$$

III. OXIDE (HYDROXIDE) ION DETERMINATION

The concentration of oxide ion, O^{-2}, in the original sample is determined as a weight percent of water soluble oxide in the prepared salt solution. To remove carbonate ion which is an interferent in this determination, an excess amount of neutral barium chloride solution is added to precipitate the carbonate ion as the barium salt.

IV. CARBONATE ION DETERMINATION

The concentration of carbonate ion in the original salt sample is determined by titrating an aliquot of the sample with 0.1N HCl, and subsequently titrating a second aliquot treated with an excess of barium chloride to the end-point with 0.1N HCl. The difference in acid titration volumes is a quantitative measure of the carbonate composition in the original sample.

Procedure

Pipet a 20.00 ml aliquot of the aqueous salt solution into a clean 100 ml beaker and add sufficient gas-free distilled water to immerse a combination hydrogen ion electrode and add 2 drops of phenolphthalein. Titrate the solution immediately with 0.100N HCl and record the end-point. A Sargent-Welch Recording Titrator was found to be convenient for this purpose.

Transfer a second 20.00 ml aliquot of the identical salt solution to a clean 100 ml beaker. Slowly add 10 ml of 10% (W/V) barium chloride solution

neutralized to pH 7.00 ± 0.05 to the beaker and bring the volume up with gas-free distilled water to immerse the combination hydrogen ion electrode. Titrate this solution and record the end-point as before.

The chemistry involved in the potentiometric titration of carbonate and hydroxide ions is as follows:

$O^{-2} + H_2O \rightleftharpoons 2OH^-$ hydroxide formation

$OH^- + H^+ \rightleftharpoons H_2O$ hydroxide neutralization

$CO_3^{-2} + H_2O \rightleftharpoons HCO_3^- + OH^-$ carbonate hydrolysis

$OH^- + H^+ \rightleftharpoons H_2O$ hydroxide neutralization

$CO_3^{-2} + Ba^{+2} \longrightarrow BaCO_3\downarrow$ carbonate precipitation

Calculations

The total concentration of carbonate ion in the original salt sample is expressed as follows:

$$\text{Weight \% } CO_3^{-2} = \frac{\left(\begin{array}{l}\text{Volume HCl required}\\ \text{to titrate sample}\end{array} - \begin{array}{l}\text{Volume HCl required to}\\ \text{titrate sample + } BaCl_2\end{array}\right) \times 0.1N\ HCl \times 60\ g\ mole^{-1}\ CO_3^{-2} \times \text{Original Solution Volume (l.)}}{.01 \times \text{sample volume (ml)} \times \text{original sample weight (in grams)}}$$

$$\text{Weight \% } O^{-2} = (\text{as } X_2O\text{: X = Na, K})$$

$$\frac{\left(\begin{array}{l}\text{Volume HCl required to}\\ \text{titrate sample + } BaCl_2\end{array}\right) \times 0.1N\ HCl \times 16\ g\ mole^{-1}\ O^{-2}\ (X_2O) \times \text{Original Solution Volume (l.)}}{0.01 \times \text{sample volume (ml)} \times \text{original sample weight} \times 2 \text{ moles XOH}}$$

NOTE: In the above calculations, the titration volumes and sample volumes are entered in milliliter (ml) quantities, while the original solution volume is expressed in liter (l) quantities.

V. NITRITE ION DETERMINATION

The concentration of nitrite ion (NO_2^-) in the original salt sample may be determined by reacting a specified volume of the salt solution with permanganate ion ($MnO4^-$). In a warm acidic medium the reaction between nitrite ion and permanganate ion is quantitative in which the oxidation product, nitrate ion (NO_3^-), is formed.

$$5NO_2^- + 2MnO_4^- + 6H^+ \rightleftharpoons 5NO_3^- + 2Mn^{+2} + 3H_2O$$

Poor results are obtained if an acidified solution of nitrite ion is slowly titrated with permanganate, resulting from the volatility and instability of nitrous acid and the air oxidation of nitrite to nitrate. The classical procedure of Lunge was, therefore, adopted. In this procedure an acidified permanganate solution of known volume and concentration is titrated against the prepared salt solution.

The permanganate solution is standardized by reaction with pure arsenious oxide, As_2O_3:

$$5As_2O_3 + 4MnO_4^- + 12H^+ \rightleftharpoons 5As_2O_5 + 4Mn^{+2} + 6H_2O$$

A trace of iodate (IO_3^-) is added to catalyze the reaction between arsenious oxide and permanganate.

Procedure

A. Preparation of a Potassium Permanganate Solution

Dissolve approximately 3.2 grams of pure $KMnO_4$ in one liter of distilled water. Heat the solution to boiling and keep hot for one hour. Filter the permanganate solution through a sintered glass crucible into a clean, dry glass-stoppered flask and store in the dark when not in use.

B. Standardization of the Potassium Permanganate Solution

Weigh out 0.20 to 0.25 g. of pure arsenious oxide, As_2O_3, to the nearest 0.1 mg in a tared vessel, dissolve in 10 ml of 3N NaOH, add 15 ml of 6N HCl, transfer quantitatively to a 125 ml erlenmeyer flask, add 50 ml of

water and one drop of 0.002 M potassium iodate, and titrate with the permanganate solution to the first rose color. Record the volume of permanganate used in the titration.

C. Volumetric Analysis of Nitrite Ion

For a solution which is approximately 1% (w/w) in nitrite ion transfer 10.00 ml of the potassium permanganate solution into a 500 ml erlenmeyer flask, add 10 ml of 3 M H_2SO_4 and 250 ml of glass-distilled water, heat to 40°C, and titrate with the nitrite solution. Towards the end of the titration when the solution has a pale violet color, add the nitrite solution very slowly until decolorization is complete.

Calculations

A. Standardization of Permanganate

The concentration of the potassium permanganate solution expressed in equivalents of $KMnO_4$ per liter of solution is determined by the following equation:

$$N_{KMnO_4} = \frac{\text{weight } As_2O_3 \text{ (g)}}{\text{Volume } KMnO_4 \text{ (ml)} \times \text{milliequivalent weight } As_2O_3}$$

$$N_{KMnO_4} = \frac{(\text{tare weight} + \text{weight } As_2O_3) - (\text{tare weight})}{\text{Volume } KMnO_4 \text{ (ml)} \times 0.04946}$$

B. Concentration of Nitrite Ion in the Original Salt Sample

The concentration, in weight percent, of nitrite ion in the initial salt sample is given by the following equation:

$$\text{Weight \% } NO_2^- = \frac{\text{Volume } KMnO_4 \text{ (ml)} \times NKMnO_4 \times \text{Original Solution Volume (l)} \times 46 \text{ g mole}^{-1} NO_2^-}{2 \times \text{Volume (ml) } NO_2^- \text{ titrant} \times \text{sample weight (in grams)} \times 0.01}$$

VI. NITRATE ION DETERMINATION

The concentration of nitrate ion in the original salt sample is determined by reacting the nitrate solution with an excess of ferrous ion and titrating the latter back with a standard potassium dichromate solution:

$$3Fe^{+2} + NO_3^- + 4H^+ \underset{\text{catalyst}}{\overset{\Delta}{\rightleftharpoons}} 3Fe^{+3} + NO + 2H_2O$$

$$6Fe^{+2} + 2\ Cr_2O_7^{-2} + 14H^+ \rightleftharpoons 6Fe^{+3} + 2\ Cr^{+3} + 7H_2O$$

In the reaction between ferrous ion and nitrate ion, ammonium molybdate is added to catalyze the forward reaction. Air is excluded from the flask to prevent air oxidation of ferrous ion.

It is imperative to exclude contaminants from nitrate ion, as nitrite will also oxidize the ferrous ion. This is accomplished quite simply by boiling the original solution with ammonium chloride:

$$NO_2^- + NH_4^+ \longrightarrow N_2\uparrow + 2H_2O$$

A solution of Barium diphenyl amine sulfonate was utilized as the redox indicator for the reaction between ferrous ion and dichromate ion. At the end point of the reaction, the solution develops a deep purple hue due to the formation of an oxidation product of diphenyl benzidine.

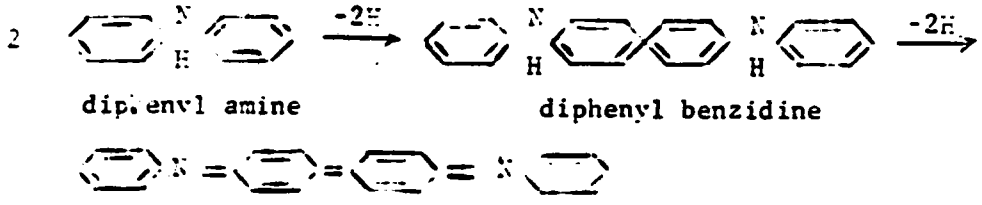

diphenyl amine — diphenyl benzidine

diphenyl benzidine blue

It was determined experimentally that barium diphenylamine sulfonate was a superior indicator than diphenyl amine and exhibited a sharper end point.

Procedure

A. Preparation of 1% Barium Diphenyl Amine Sulfonate

Add 1.0 gram of solid barium diphenyl amine sulfonate to a 100-ml volumetric flask, dilute with 50-75 ml of distilled water and heat on a heating plate to dissolve the sample. After the salt has dissolved, cool and dilute to the mark with distilled water.

B. Preparation of 0.18N Ferrous Sulfate

Weigh approximately 12.51 grams of pure $FeSO_4 \cdot 7H_2O$ to the nearest 0.1 mg and transfer to a 250 ml volumetric flask. Dilute to the mark with 1N H_2SO_4.

C. Preparation of 0.1N $K_2Cr_2O_7$

Dry approximately 6-7 grams of pure potassium dichromate for 2 hours at 175°C. Weigh 4.904 grams of the dried dichromate to the nearest 0.1 mg, and transfer quantitatively to a 1-l volumetric flask. Dilute to the mark and mix thoroughly.

D. Destruction of Nitrite Ion

Transfer 20.00 ml of the nitrate/nitrite solution to a flask containing a few micro-boiling chips. Add 20 ml of distilled water and 2 drops of phenopthalein. Neutralize the solution with 0.1N HCl and add 20 ml 4 M NH_4Cl. Gently heat the solution to boiling. When nitrite is consumed, microbubbles of nitrogen gas are formed. When only bubbles from the boiling solution are evolved and microbubble formation has ceased, heat the solution for five more minutes and remove from the hot plate. Cool to room temperature, transfer the contents of the flask to a 100 ml volumetric flask and dilute to the mark with distilled water.

E. Volumetric Analysis of Nitrate Ion

Transfer 3.00 ml of the diluted nitrate solution to a 250 ml erlenmeyer flask. Pipette 25.00 ml of 0.18N ferrous iron solution to the flask and add 70 ml of 12N hydrochloric acid. Add three to five grams of solid sodium bicarbonate, in small portion, to displace the air in the flask and close the flask with a stopper, from which a rubber tube leads to a suspension of 50 grams of sodium bicarbonate in 100 ml of water. The dropper fitted in the

stopper contains 3 ml of 1% ammonium molybdate solution. Heat the solution to boiling, and add the catalyst after two or three minutes. Continue boiling for 10 minutes or until the solution turns a bright orange. Replace the sodium bicarbonate suspension with a fresh saturated solution, remove the flask from the heat, and cool gradually by placing in a cold water bath.

After the flask and contents have cooled to room temperature, unstopper the flask, and add 35 ml of 6N ammonium acetate for every 50 ml of solution titrated (70 ml of 6N NH_4 Ac will usually suffice) and 3 to 5 ml of 85% phosphoric acid. The acetate reduces the concentration of the strong acid between 1 and 2N. Titrate the solution slowly with 0.1N $K_2Cr_2O_7$ using 10-12 drops of the diphenyl amine sulfonate indicator. The end point of the reaction should be a green to violet transition. The ferrous ion solution is standardized under the same condition as described above.

Calculations

A. Standardization of Ferrous Ion Solution

The concentration of ferrous sulfate solution expressed in equivalents of ferrous iron per liter of solution is given by the equation:

$$N_{Fe^{+2}} = \frac{(\text{volume } K_2Cr_2O_7 \text{ titrant (ml)}) \times (0.100N)}{25.00 \text{ ml } FeSO_4 \cdot 7\ H_2O}$$

B. Concentration of Nitrate Ion in the Original Salt Solution

The concentration in weight percent of nitrate ion found in the original salt solution is expressed by the following equations:

Volume (ml) ferrous sulfate solution to end point =

$$25.00 - \left(\frac{\text{volume } K_2Cr_2O_7 \text{ (ml)} \times 0.1N}{N_{Fe^{+2}}}\right)$$

Weight percent nitrate ion =

$$\frac{(\text{volume } Fe^{+2} \text{ solution to end point})(N_{Fe^{+2}}) \left(\frac{62.00g\ NO_3^-}{3 \times 1000}\right)\left(\frac{1000 \text{ ml}}{20 \text{ ml}}\right)\left(\frac{100 \text{ ml}}{3 \text{ ml}}\right) \times 100}{\text{sample weight in grams}}$$

$$= \frac{(\text{volume } Fe^{+2} \text{ solution to end point})\ (N_{Fe^{+2}}) \times 3444.44 \times \text{vol. of orig. sol (l.)}}{\text{sample weight in grams}}$$

VII. CHROMIUM DETERMINATION

Procedure

A. Preparation of Standards

Standards are prepared from the Varian 1000 ppm Chromium Stock Solution and diluted to 100 ml in a volumetric flask with distilled water to equal 1, 2, 5 and 10 ppm (0.1, 0.2, 0.5 and 1.0 ml of stock diluted to 100 ml).

B. Atomic Absorption Conditions

Wave length - 357.9 nm

Slit 0.2

Lamp - multi element with current setting of 8

Background correct - on

Integration time - 3 seconds

Use sample with ASD program

Flame ratio - 39/30 (oxidant/fuel)

C. Preparation of Samples

Samples must be diluted with distilled water to read between 1-10 ppm (1:10 dilution will usually suffice).

D. Read the standards and samples using a distilled water blank. Plot the calibration curve and read the conc. of the samples from this graph.

Calculations

Concentration of chromium in the original salt solution:

$$\text{ppm Cr} = \frac{\mu g\ Cr}{\text{sample weight (g)}} = \frac{\text{ppm analyzed x dilution x } \dfrac{\text{volume of}}{\text{orig dilution (ml)}}}{\text{sample weight in grams}}$$

VIII. SULFATE ION DETERMINATION

The concentration of sulfate ion in the original salt sample is determined by reacting a sample (acidified to pH 4 with concentrated HCl), with solid Barium chloranilate in a 50% ethyl alcohol buffered solution to liberate the highly colored acid-chloranilate ion.

Procedure

A. Preparation of Acetate Buffer, pH 4.63

Dissolve 12.6 g of sodium acetate in distilled water. Add 6.4 ml of acetic acid and dilute to 1 liter with distilled water. Stopper with an ascarite tube.

B. Preparation of Stock Standard Solution

Dissolve 1.4790 g of oven-dried (105°C) Na_2SO_4 in distilled water and dilute to 1 liter in a volumetric flask. 1.0 ml = 1.0 mg SO_4^{-2}

C. Preparation of Calibration Curve

Prepare a series of standards by diluting suitable volumes of stock solution plus 10 ml acetate buffer, 50 ml ethyl alcohol to 100 ml with distilled water. Add 0.3 g solid Barium chloranilate. Stopper and shake for 10 minutes. Centrifuge after 15 minutes and read clear supernantant on the Cary Spectrophotometer at 530 nm using a 5 cm cell. The following dilutions are suggested:

ml of Stock Solution	Sulfate Conc., mg/l
1.0	10
2.0	20
4.0	40
6.0	60
8.0	80
10.0	100
15.0	150
20.0	200
30.0	300
40.0	400

A calibration curve is generated by plotting the absorbances as a function of the standard concentrations.

D. Preparation of a Blank Salt Solution

20 ml of a solution of a 40/60 $KNO_3/NaNO_3$ Reagent grade mixture (concentration equivalent to that of the samples, i.e., 11.6 g diluted to 100 ml) is carried through the test procedure with the samples.

E. Test Procedure

Run a blank, blank salt solution and 20 ml of the sample solution (acidified to pH 4) through the procedure used in the generation of the calibration curve. Read the concentration in mg/l from the graph. Calculate the % SO_4^{-2} and subtract the % SO_4^{-2} of the blank salt from the sample.

F. Calculations

Concentration of Sulfate Ion in the original salt solution.

$$\% \ SO_4^{-2} = \frac{\text{mg/l x dilution x orig volume of solution (1)}}{\text{sample weight x 1000}} \times 100$$

IX. CHLORIDE ION DETERMINATION

The concentration of chloride ion in the original salt sample is determined by titrating potentiometrically an acidified aliquot of the sample with .02N $AgNO_3$ after standardization of the $AgNO_3$ using a stock NaCl standard (1.0 ml = 2.0 mg Cl^-)

Procedure

Standardization of $AgNO_3$: Pipet 1.0 ml of the chloride standard (2 mg Cl^-/ml) into a clean 100 ml beaker containing 40-60 ml distilled deionized water. Acidify to pH 2 with conc HNO_3. Titrate against 0.02N $AgNO_3$ using the Sargent-Welch Recording Titrator set at 200 mv and rate 4. Repeat 2 more times and calculate the average response (mg Cl^-/chart division).

Run the samples in the same manner as above using an aliquot size that approximates that of the standard (5 ml of a .25% (w/w) salt solution was adequate)

Calculation

Concentration of NaCl in the original salt solution.

$$\% \text{ NaCl} = \text{Number of Chart Divisions} \times \text{mg } Cl^-/\text{Div} \times \frac{\text{Dilution}}{1000} \times \frac{58.5}{35.5} \times \frac{100}{\text{original sample weight}}$$

X. POTASSIUM DETERMINATION

Procedure

A. Preparation of Standards

Standards are prepared from the Varian 1000 ppm Potassium Stock Solution and diluted to 100 ml in a volumetric flask with distilled water to equal 10, 20 and 30 ppm (1.0, 2.0, and 3.0 ml of stock diluted to 100 ml).

B. Atomic Absorption Conditions

Flame Emission Mode

NOTE

Light from the hollow cathode lamps and the background correction lamp must be excluded before attempting to measure flame emission.

Wave Length: 766.4

Slit: 0

Background Correct: Off

Integration Time: 3 Seconds

Multiple Setting: 3

Use sample with ASD program

Flame Ratio: 38/29 (Oxidant/Fuel)

Gain: Set at 70% on peak meter with the highest standard

C. Preparation of Samples

Samples must be diluted with distilled water to read between 10-30 ppm (1:1000 dilution will usually suffice).

D. Read the standards and sample using a distilled water blank. The printed readout result is already calculated to read ppm.

Calculations

Concentration of potassium in the original salt solution:

$$\text{ppm K} = \frac{\text{ppm analyzed x dilution x volume of orig. dilution (ml)}}{\text{sample weight in grams}}$$

XI. SODIUM DETERMINATION

Procedure

A. Preparation of Standards

Standards are prepared from the Varian 1000 ppm Sodium Stock Solution and diluted to 100 ml in a volumetric flask with distilled water to equal 10, 20 and 30 ppm (1.0, 2.0, and 3.0 ml of stock diluted to 100 ml).

B. Atomic Absorption Conditions

Flame Emission Mode

NOTE

Light from the hollow cathode lamps and the background correct lamp must be excluded before attempting to measure flame emission.

Wave Length: 589.0

Slit: 0

Background Correct: Off

Flame Ratio: 40/28 (Oxidant/Fuel)

Gain: Set at 70% on peak meter with the highest standard

Use sample with ASI program

Integration Time: 3 Seconds

Multiple Setting: 3

C. Preparation of Samples

Samples must be diluted with distilled water to read between 10-30 ppm. (1:1000 dilution will usually suffice).

D. Read the standards and samples using a distilled water blank. The printed readout result is already calculated to read ppm.

Calculations

Concentration of sodium in the original salt solution:

$$\text{ppm Na} = \frac{\text{ppm analyzed x dilution x volume of orig. dilution (ml)}}{\text{sample weight in grams}}$$

MOLTEN SALT CHEMISTRY

ANALYTICAL REFERENCES

1. I. M. Kolthoff and G. E. Noponen - Diphenylamine Sulfonic Acid as a Reagent for the Colorimetric Determination of Nitrates. Journal of the American Chemical Society, 55, 1448 (1933).

2. I. M. Kolthoff, E. B. Sandell, E. J. Meehan and Stanley Bruckenstein. Quantitative Chemical Analysis, Fourth Edition. The Macmillan Company, London, 1969.

3. I. M. Kolthoff, E. B. Sandell and B. Moskovitz - The Volumetric Determination of Nitrates with Ferrous Sulfate as Reducing Agent. Journal of the American Chemical Society, 55, 1454 (1933).

4. Douglas A. Skoog and Donald M. West - Fundamentals of Analytical Chemistry, Second Edition. Holt, Rinehard and Winston, Inc., New York, 1969.

5. Carl A. Streul and Philip R. Averell, editors - Analytical Chemistry of Nitrogen and its Compounds, Part II. Wiley-Interscience, New York, 1970.

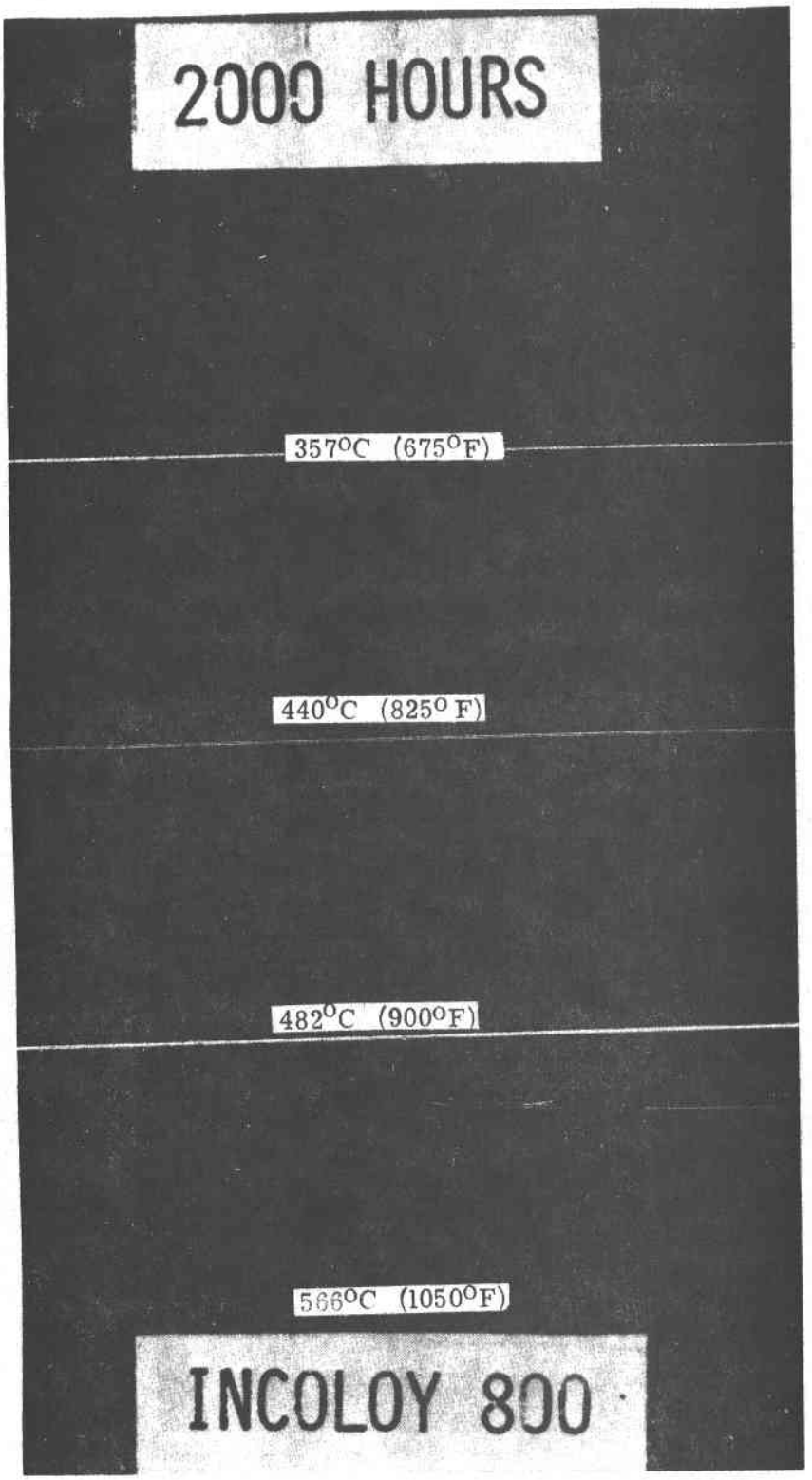

Figure A-1 *Photographs of I800 Parent Metal Coupons After 2000 Hours Flowing Molten Salt Exposure as a Function of Sample Port Temperature*

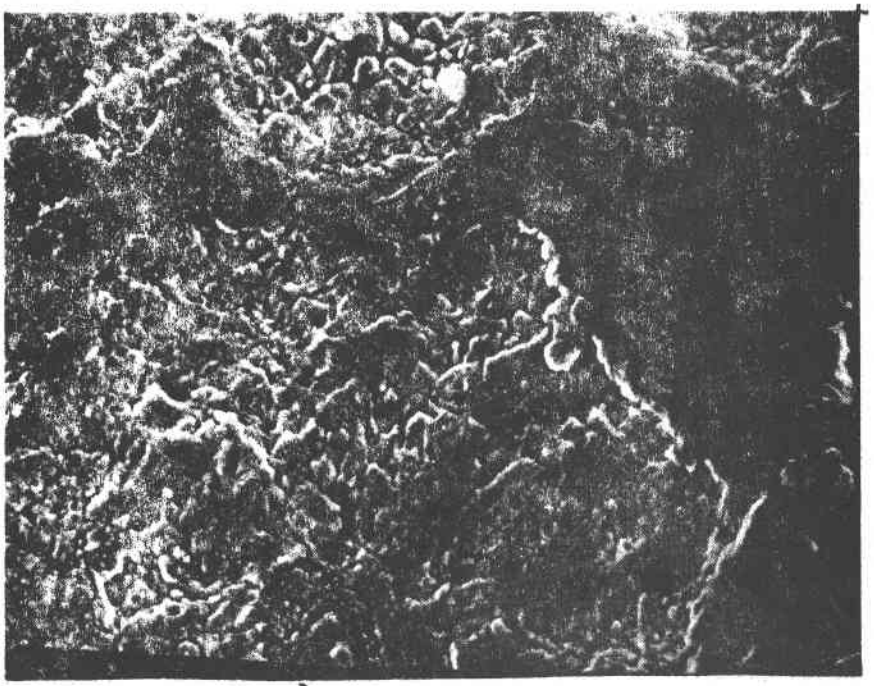

375°C (675°F)

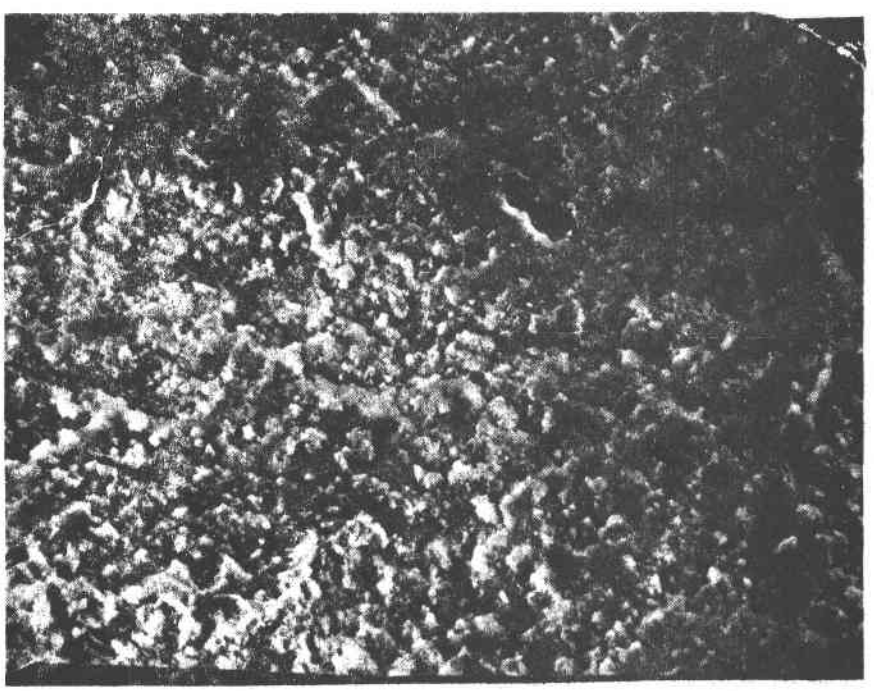

440°C (825°F)

Figure A-2 *SEM Surface Micrographs of I800 Parent Metal Coupons After Flowing Molten Salt Exposure at 357°C (675°F) and 440°C (825°F)*

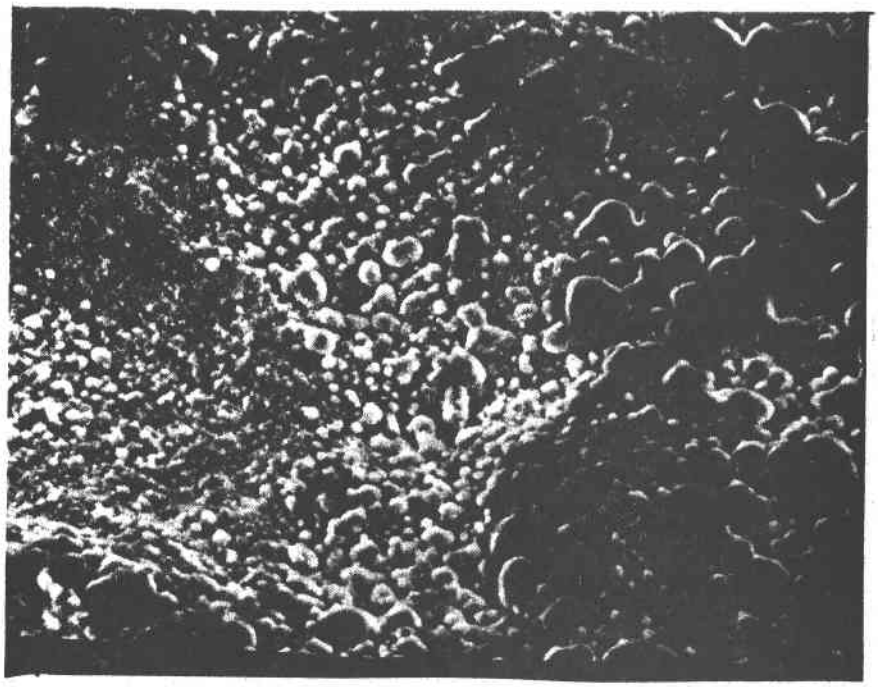

482°C (900°F)

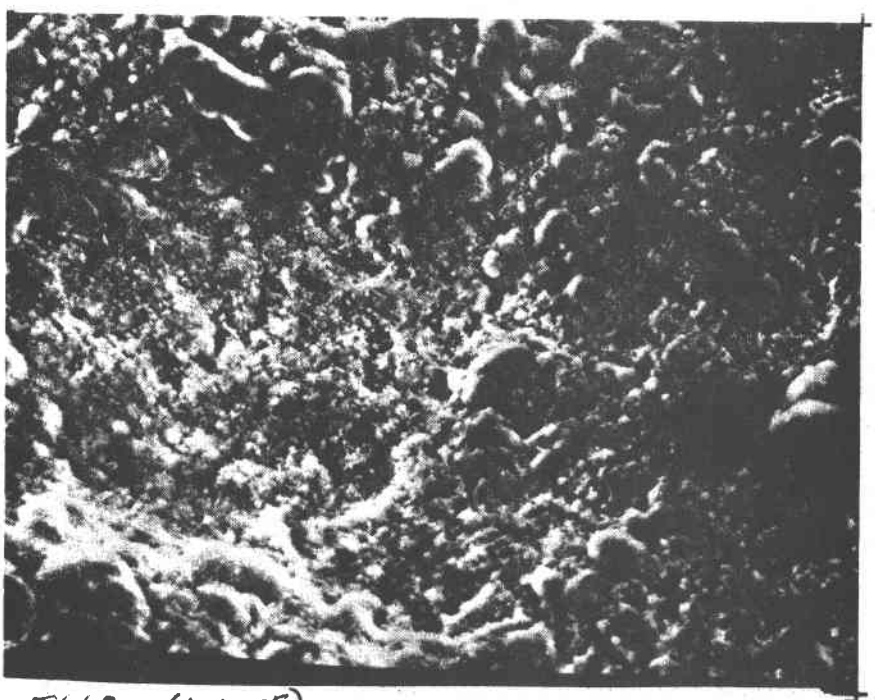

566°C (1050°F)

Figure A-3 *SEM Surface Micrographs of I800 Parent Metal Coupons After Flowing Molten Salt Exposure at 482°C (900°F) and 566°C (1050°F)*

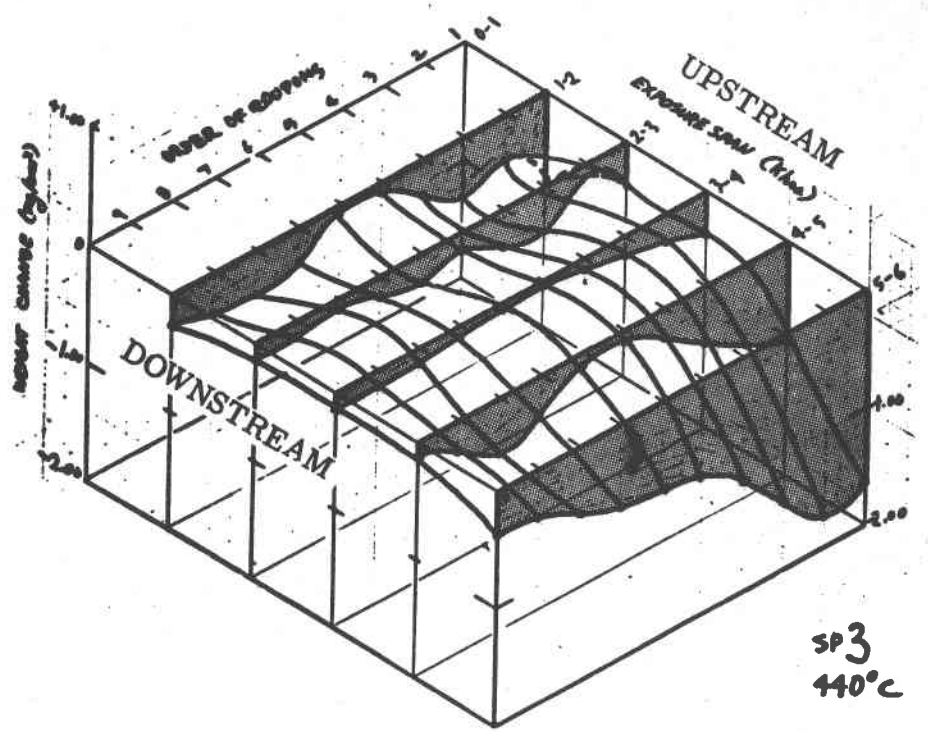

LOOP COUPON WEIGHT LOSS

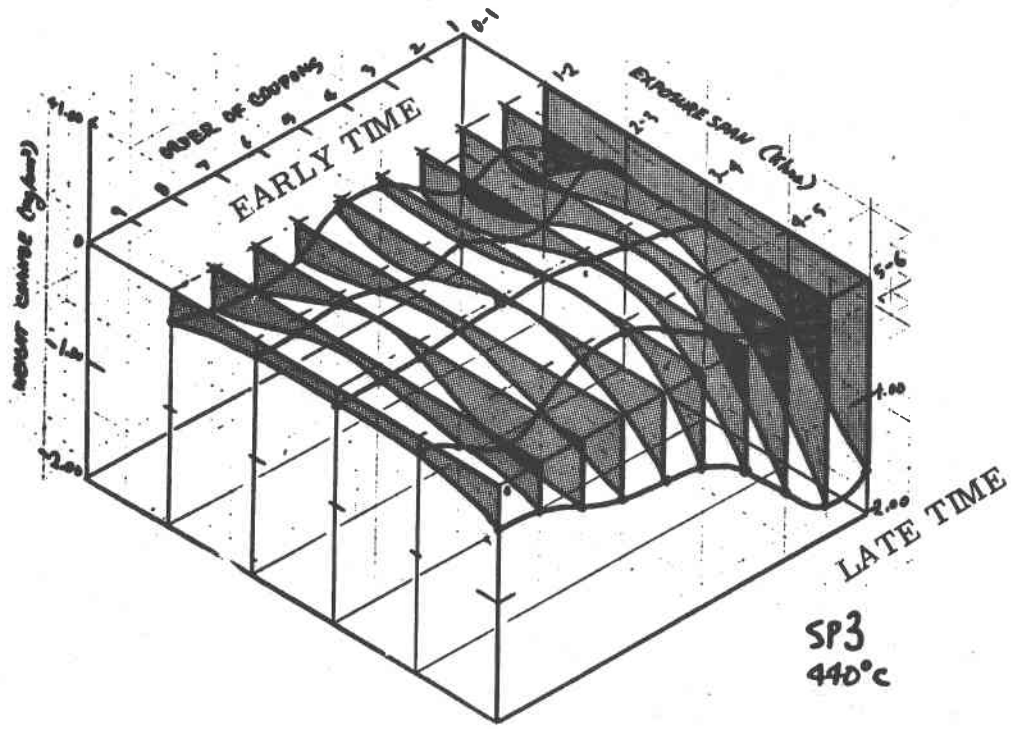

Figure A-4 Three Dimensional Graphical Representation of I800 Parent Metal Weight Change as a Function of Sample Position and Time of Exposure in 440°C (825°F) Flowing Salt

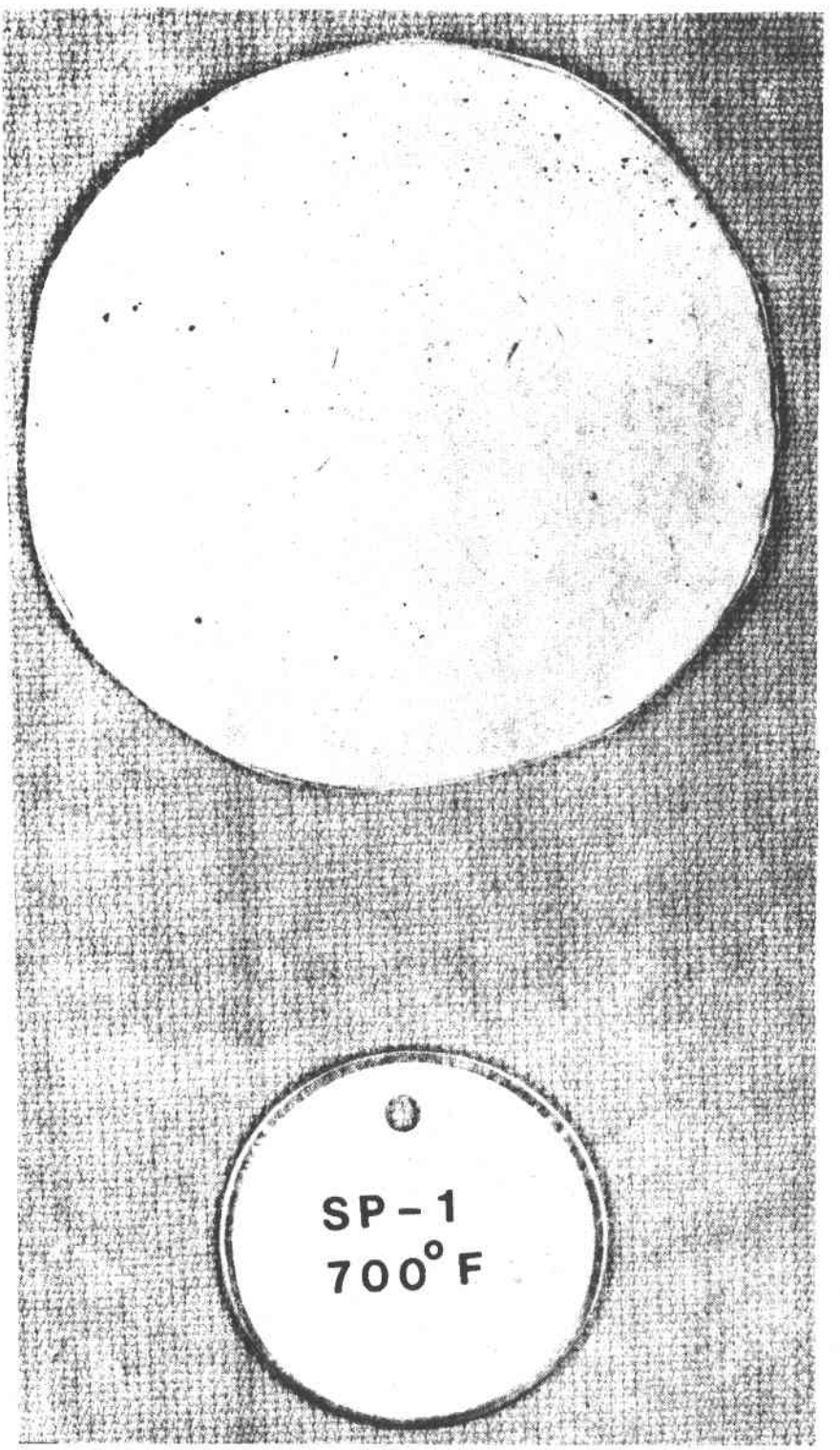

Figure A-5 Particulates Collected from Tube Sections 1 thru 8, Molten Salt Loop

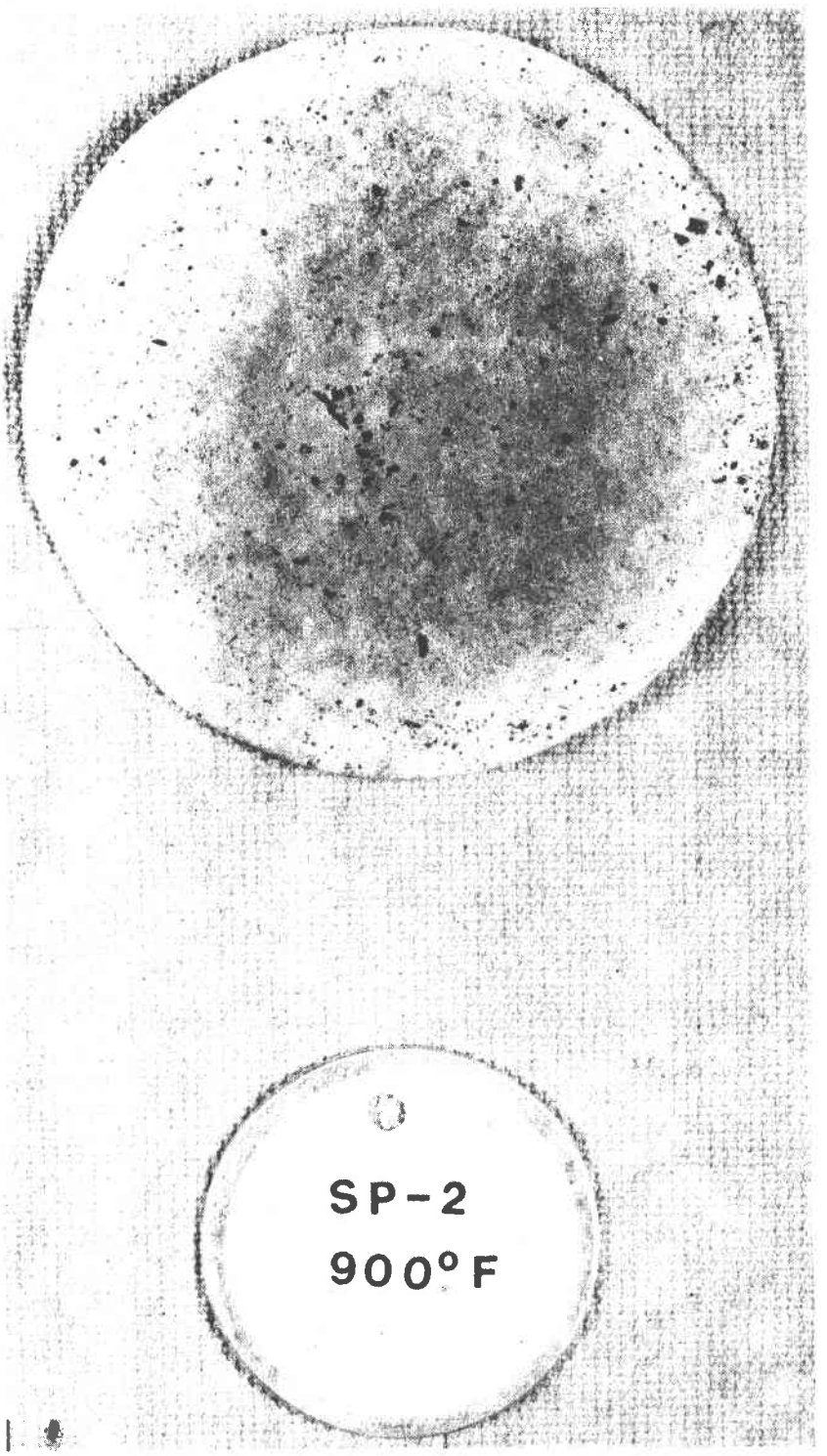

Figure A-6 Particulates Collected on Filter Paper From Sample Port 2 Tube Section Wash

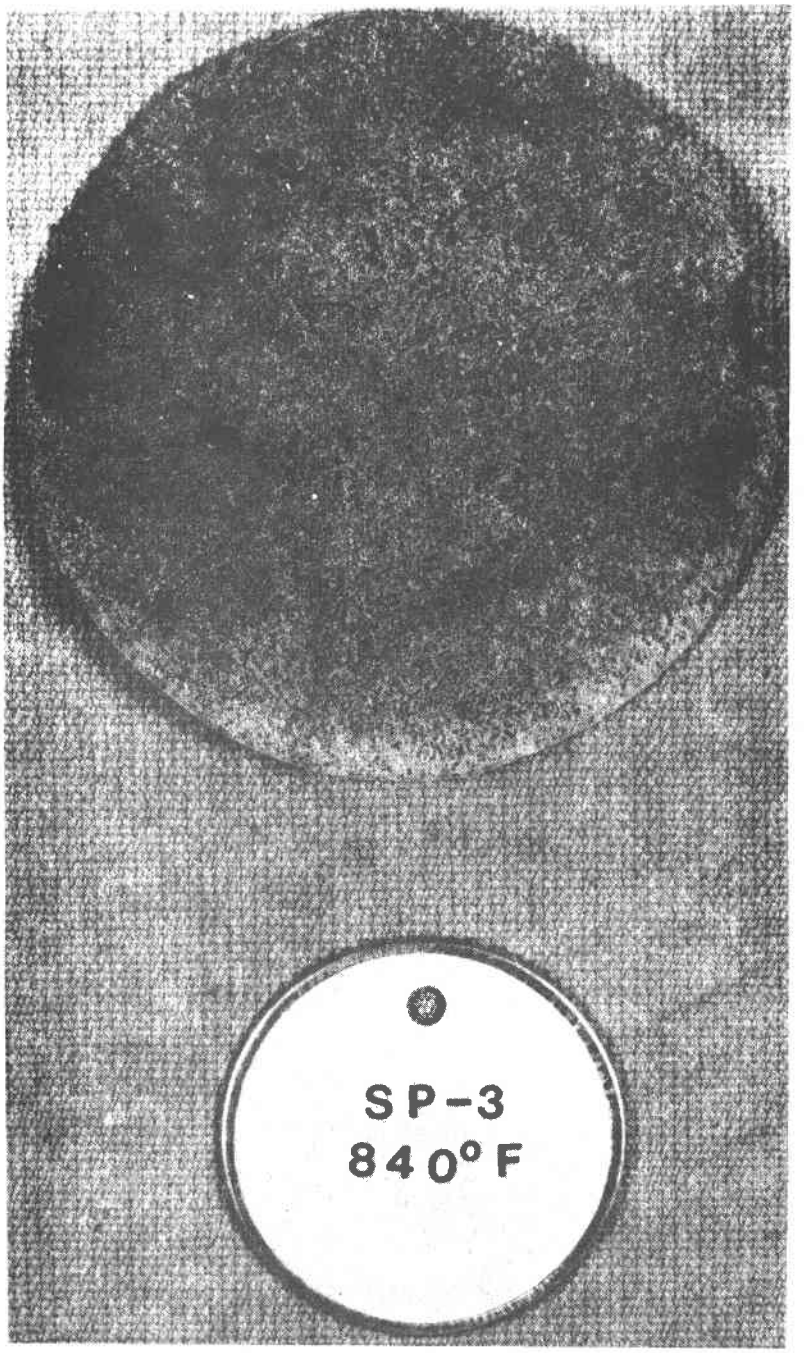

Figure A-7 Particulates Collected on Filter Paper From Sample Port 3 Tube Section Wash

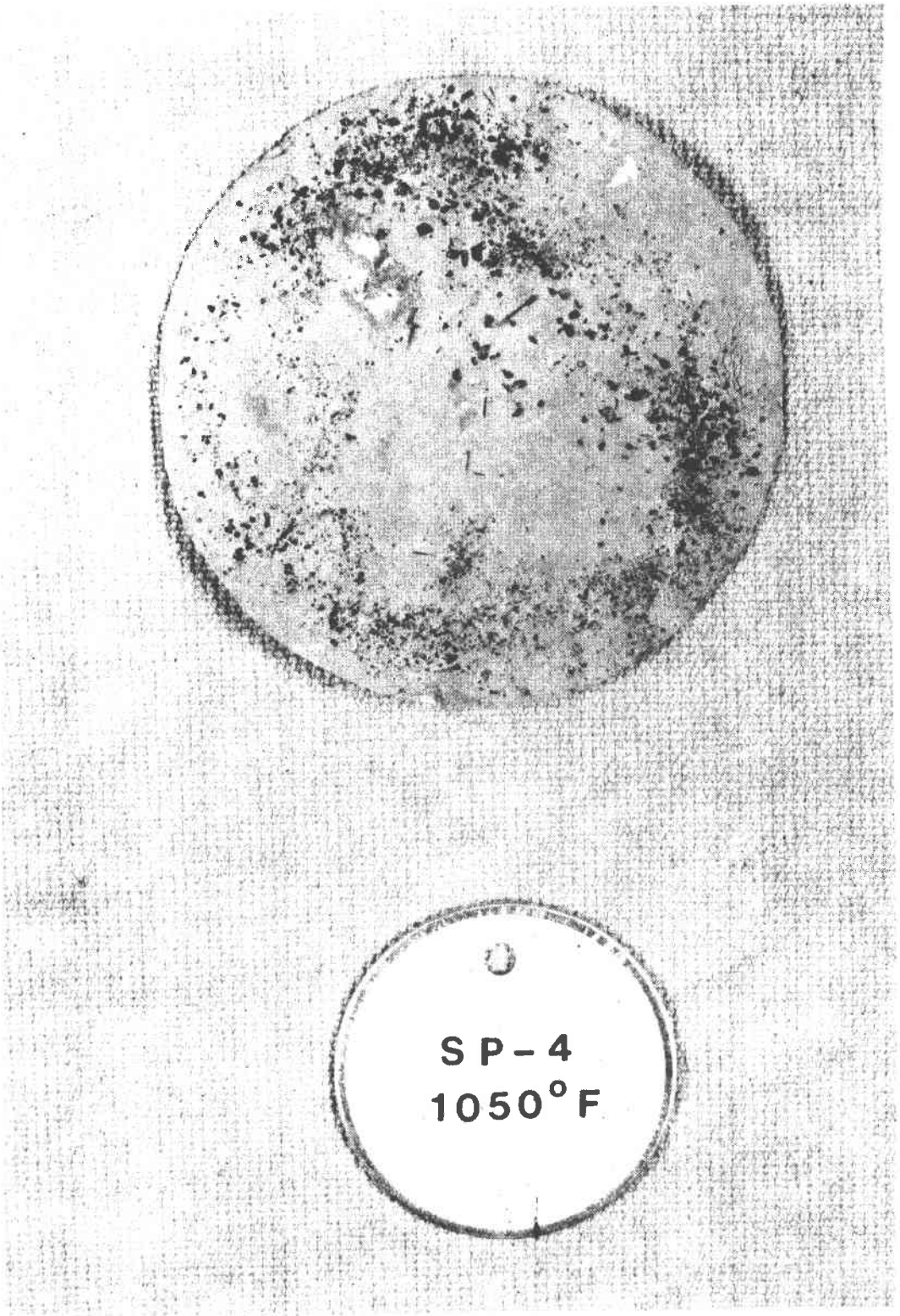

Figure A-8 Particulates Collected on Filter Paper From Sample Port 4 Tube Section Wash

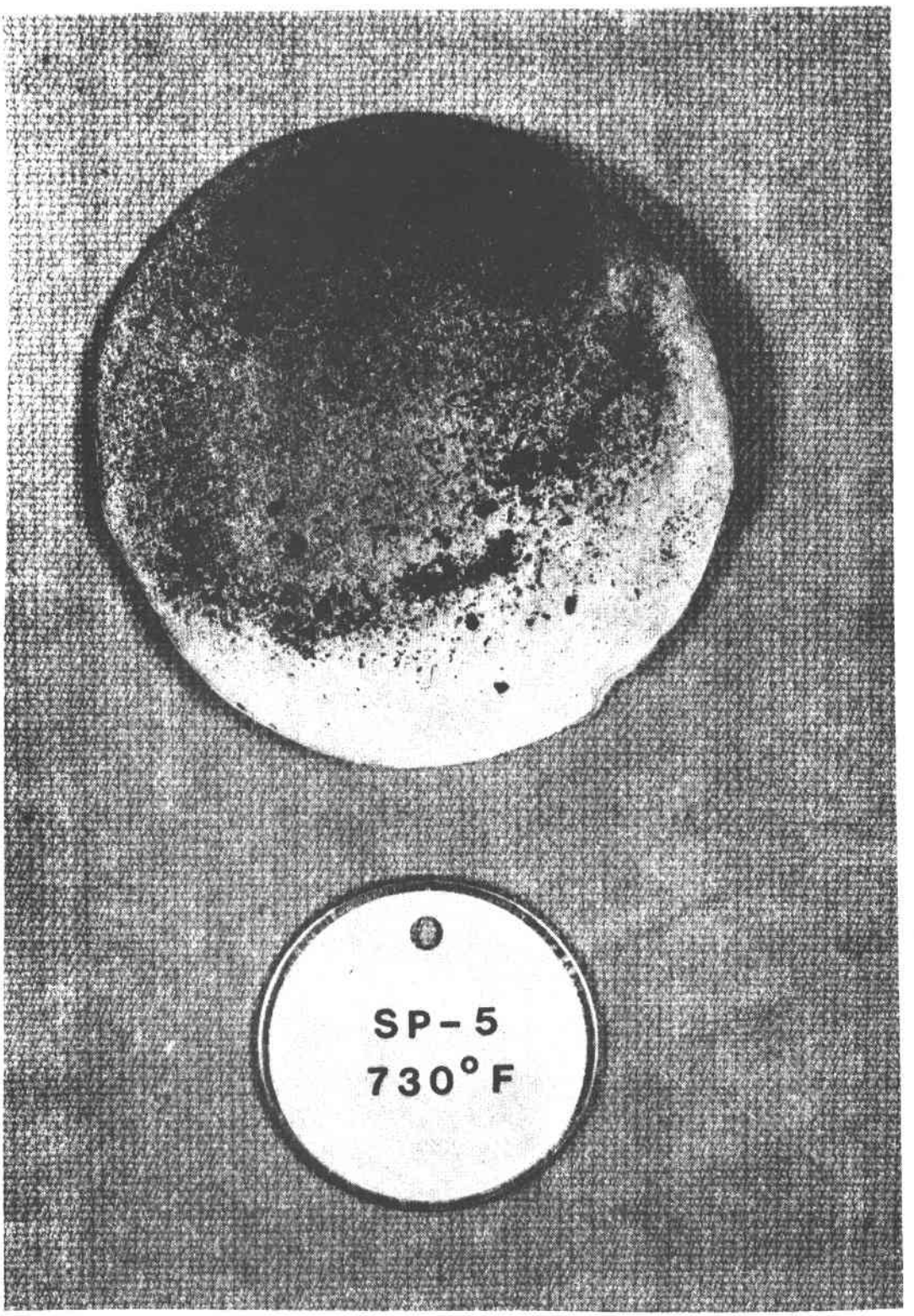

Figure A-9 Particulates Collected on Filter Paper From Sample Port 5 Tube Section Wash

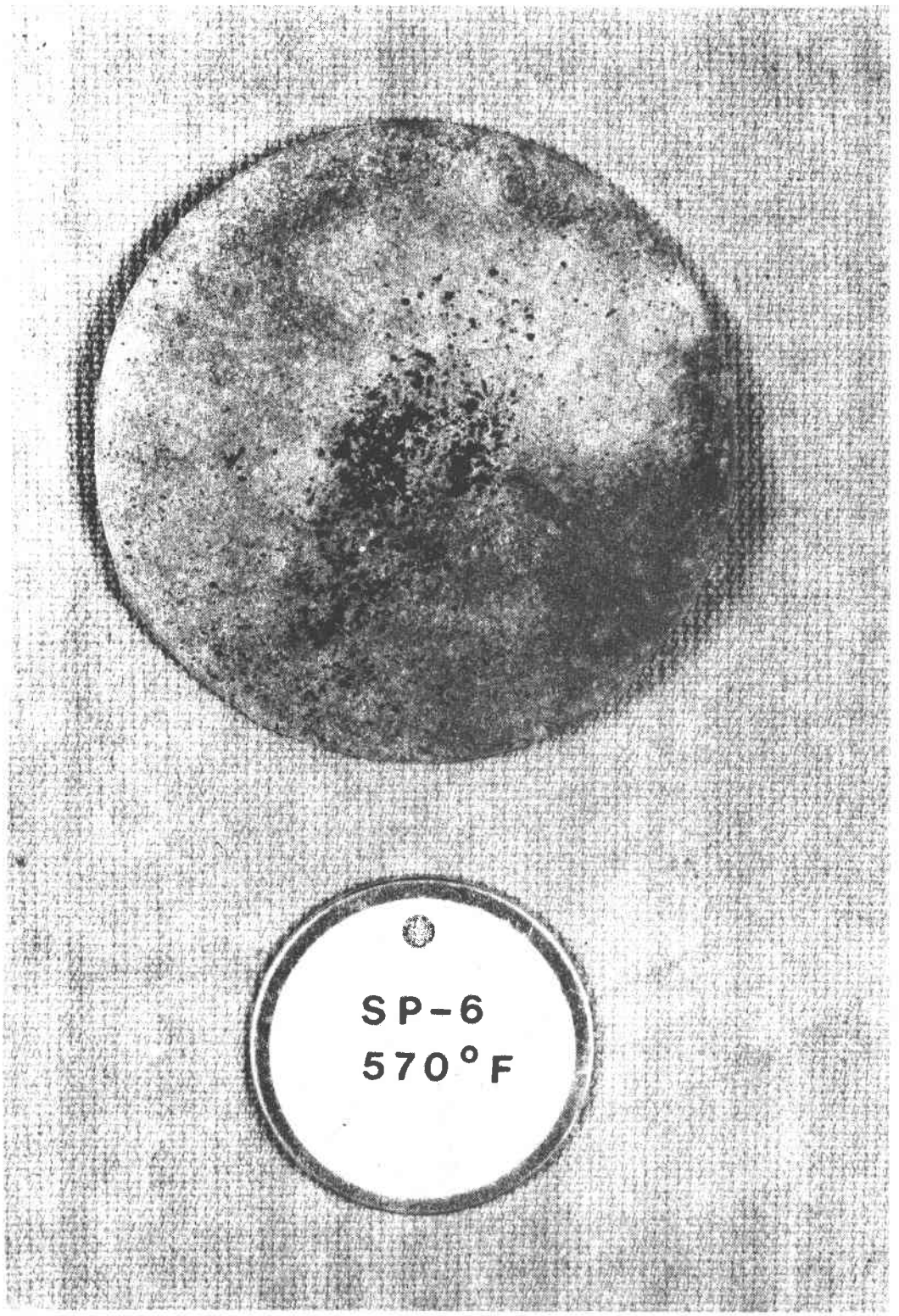

Figure A-10 Particulates Collected on Filter Paper From Sample Port 6 Tube Section Wash

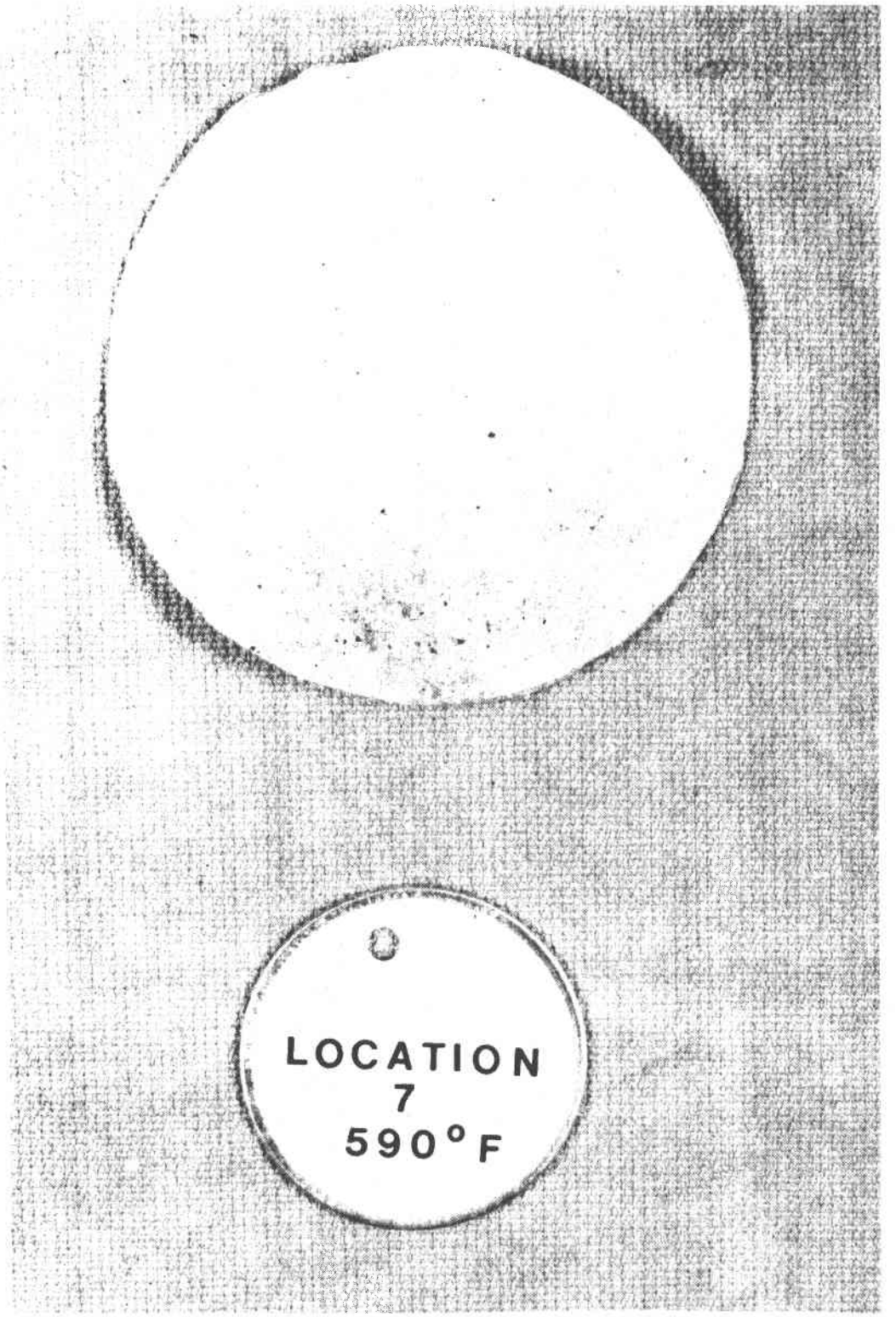

Figure A-11. Particulates Collected on Filter Paper From Sample Port 7 Tube Section Wash

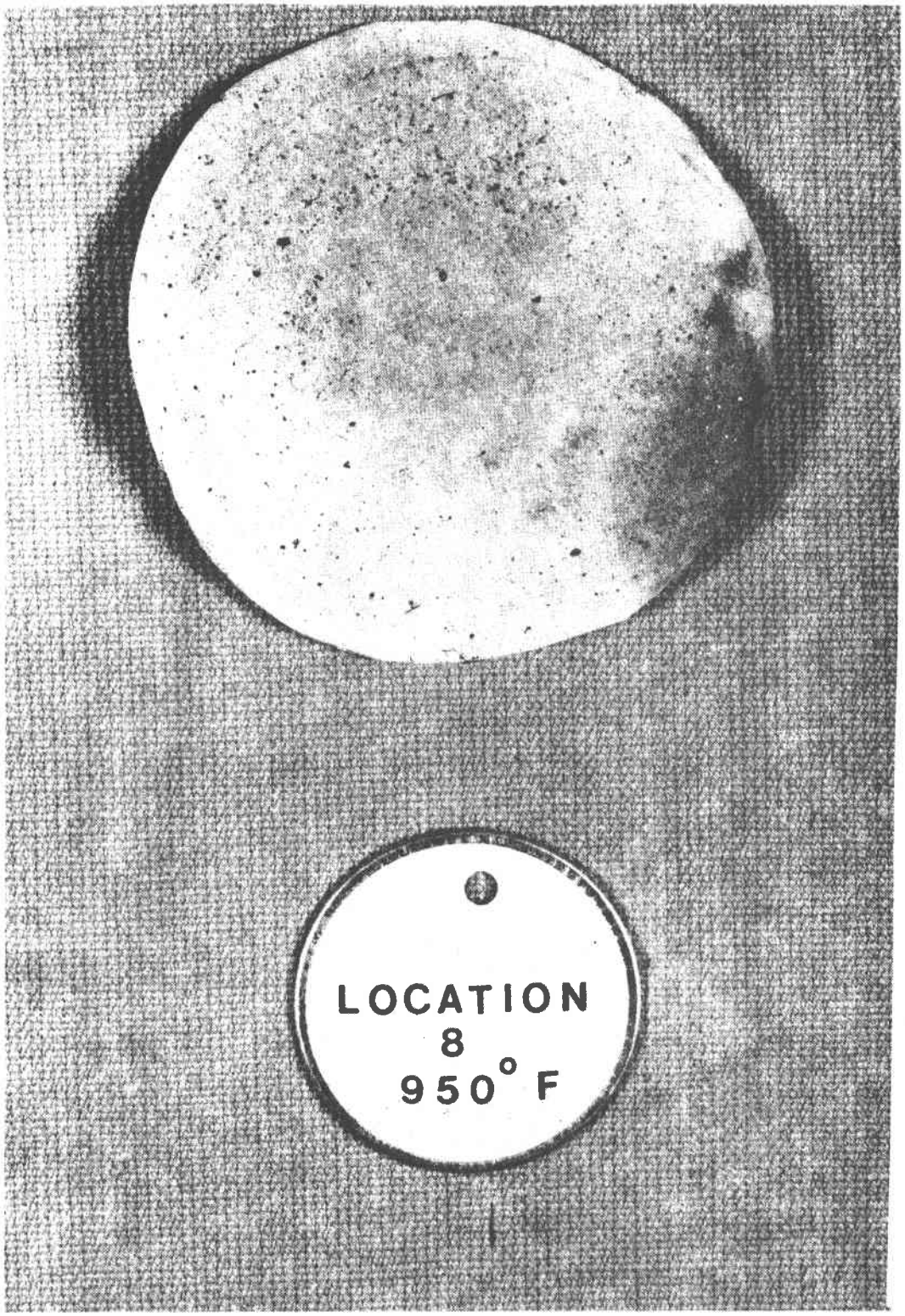

Figure A-12 Particulates Collected on Filter Paper From Sample Port 8 Tube Section Wash

Table A-1 Weight Change vs Time for I800 at 357°C and 482°C in Flowing Molten Salt Loop

ALLOY SPECIMEN WEIGHT CHANGE

DATA (mg/cm^2), MOLTEN SALT PUMPED LOOP

	Alloy: Incoloy 800			Sample Port: 1 ▲ Temperature: 357°C		
	Exposure Interval (K Hrs, nom [1])					
Specimen Number	0-1	1-2	2-3	3-4	4-5	5-6
10	-0.19	-0.19	0.02	-0.15	0.17	-0.11
9	-0.11	-0.06	0.00	0.04	-0.06	-0.04
8	-0.19	-0.02	0.02	-0.08	0.08	-0.02
7	-0.15	-0.02	0.02	-0.02	0.02	-0.06
6	-0.13	0.02	0.02	0.00	0.02	-0.04
5	-0.04	0.04	0.00	0.00	0.00	-0.04
4	-0.04	0.02	-0.02	0.00	0.00	0.00
3	-0.08	0.00	0.00	0.00	0.04	0.00
2	-0.08	0.23	-0.19	0.04	-0.02	0.02
1	-0.08	-0.06	0.00	0.02	0.06	-0.04
$\bar{X}$	-0.11	0.00	-0.01	-0.02	0.03	-0.03
σ	0.06	0.11	0.06	0.06	0.06	0.04

1 Actual Intervals:
1=1, 2=2, 3=3, 4=3.86, 5=4.719, 6=5.715 K Hrs

ALLOY SPECIMEN WEIGHT CHANGE

DATA (mg/cm^2), MOLTEN SALT PUMPED LOOP

	Alloy: Incoloy 800			Sample Port: 2 ◆ Temperature: 482°C		
	Exposure Interval (K Hrs, nom [1])					
Specimen Number	0-1	1-2	2-3	3-4	4-5	5-6
20	-0.81	-0.11	-0.02	0.00	0.04	-0.02
19	-0.59	-0.02	0.04	0.02	0.04	0.02
18	-0.47	-0.02	0.04	0.02	0.04	0.04
17	-0.40	-0.04	0.08	0.04	0.04	0.04
16	-0.34	0.00	0.00	0.06	-0.04	0.02
15	-0.15	-0.06	-0.02	0.04	0.02	0.02
14	-0.15	-0.13	0.08	0.04	0.02	0.02
13	-0.11	-0.15	0.08	0.02	0.04	-0.02
12	-0.23	-0.04	-0.13	-0.04	0.13	-0.02
11	-0.40	0.00	-0.17	-0.08	0.19	-0.04
$\bar{X}$	-0.37	-0.06	0.00	0.01	0.05	0.01
σ	0.22	0.05	0.09	0.04	0.06	0.03

1 Actual Intervals:
1=1, 2=2, 3=3, 4=3.86, 5=4.719, 6=5.715 K Hrs

Table A-2 Weight Change vs Time for I800 at 440°C and 566°C in Flowing Molten Salt Loop

ALLOY SPECIMEN WEIGHT CHANGE DATA (mg/cm^2), MOLTEN SALT PUMPED LOOP

Alloy: Incoloy 800				Sample Port: 3 ■ Temperature: 440°C		
	Exposure Interval (K Hrs, nom [1])					
Specimen Number	0-1	1-2	2-3	3-4	4-5	5-6
21	N/A	0.85	0.87	-0.34	-0.84	-1.42
22	N/A	-0.30	-0.04	-0.02	-0.93	-1.95
23	N/A	-0.85	-1.12	-0.15	-1.51	-0.93
24	N/A	-0.32	-0.32	-0.04	-0.02	-0.87
25	N/A	0.00	-0.13	-0.04	-0.08	-0.68
26	N/A	-0.15	-0.70	-0.02	-0.15	-0.68
27	N/A	-0.42	-0.13	-0.04	-0.23	-0.79
28	N/A	-0.38	-0.08	-0.06	-0.59	-0.53
29	N/A	-0.28	-0.25	-0.04	-0.28	-0.30
30	N/A	-0.32	-0.19	-0.23	0.02	-0.42
$\bar{X}$	N/A	-0.39	-0.38	-0.10	-0.46	-0.86
σ	N/A	0.27	0.38	0.11	0.50	0.49

1 Actual Intervals:
1=1, 2-2, 3-3, 4-3.86, 5=4.719, 6=5.715 K Hrs
N/A-Not Available

ALLOY SPECIMEN WEIGHT CHANGE DATA (mg/cm^2), MOLTEN SALT PUMPED LOOP

Alloy: Incoloy 800				Sample Port: 4 ✱ Temperature: 566°C		
	Exposure Interval (K Hrs, nom [1])					
Specimen Number	0-1	1-2	2-3	3-4	4-5	5-6
31	0.32	0.06	0.13	0.06	0.02	0.04
32	0.53	0.06	-0.06	-0.02	0.00	-0.11
33	0.34	0.15	-0.11	0.08	-0.02	0.00
34	0.89	0.17	-0.04	-0.04	-0.04	-0.08
35	0.30	-0.04	-0.15	0.13	0.02	0.00
36	0.64	0.11	-0.15	-0.04	0.02	-0.08
37	0.38	0.11	-0.11	0.00	0.04	0.02
38	1.23	0.21	-0.04	-0.02	0.02	-0.13
39	0.42	0.34	-0.04	0.02	0.08	-0.06
40	0.93	0.15	-0.17	-0.15	-0.04	-0.04
$\bar{X}$	0.60	0.13	-0.07	0.00	0.01	-0.05
σ	0.32	0.10	0.09	0.08	0.04	0.05

1 Actual Intervals:
1=1, 2=2, 3=3, 4=3.86, 5=4.719, 6=5.715 K Hrs

Table A-3 Weight Change vs Time for A570 at 288°C and 371°C in Flowing Molten Salt Loop

ALLOY SPECIMEN WEIGHT CHANGE

DATA (mg/cm^2), MOLTEN SALT PUMPED LOOP

Alloy: A-570				Sample Port: 5 ✕ Temperature: 371°C		
	Exposure Interval (K Hrs, nom [1])					
Specimen Number	0-1	1-2	2-3	3-4	4-5	5-6
A	N/A	-0.57	0.13	-0.02	N/A	0.13
B	N/A	-0.32	0.13	0.02	N/A	-0.34
C	N/A	-0.95	0.21	0.04	N/A	0.06
D	N/A	-0.49	0.08	0.02	N/A	0.11
E	N/A	-0.47	0.17	0.02	N/A	-0.47
F	N/A	-0.51	0.21	0.02	N/A	-0.83
G	N/A	-0.49	0.06	-0.02	N/A	-0.36
H	N/A	-0.72	0.17	0.00	N/A	-0.15
I	N/A	-0.51	0.13	-0.08	N/A	-0.08
J	N/A	-1.46	0.15	-0.04	N/A	-0.21
$\bar{X}$	N/A	-0.65	0.14	0.00	N/A	0.21
σ	N/A	0.33	0.05	0.04	N/A	0.30

1 Actual Intervals:
1=1, 2-2, 3-3, 4-3.86, 5=4.719, 6=5.715 K Hrs
N/A-Not available

ALLOY SPECIMEN WEIGHT CHANGE

DATA (mg/cm^2), MOLTEN SALT PUMPED LOOP

Alloy: A-570				Sample Port: 6 O Temperature: 288°C		
	Exposure Interval (K Hrs, nom [1])					
Specimen Number	0-1	1-2	2-3	3-4	4-5	5-6
K	N/A	-0.74	-0.45	-0.34	-0.13	0.00
L	N/A	-0.47	-0.66	-0.19	0.32	-0.02
M	N/A	-0.59	-0.45	-0.25	0.28	0.02
N	N/A	-0.66	-0.66	-0.34	0.38	0.02
O	N/A	-0.57	-0.36	-0.47	0.38	0.00
P	N/A	-0.49	-0.53	-0.13	0.38	-0.04
Q	N/A	-0.51	-0.38	-0.28	-0.02	-0.08
R	N/A	-0.45	-0.34	-0.30	-0.04	-0.02
S	N/A	-0.49	-0.49	-0.21	-0.15	-0.02
T	N/A	-0.72	-0.51	-0.34	-0.23	-0.02
$\bar{X}$	N/A	-0.58	-0.48	-0.29	0.12	-0.02
σ	N/A	0.10	0.11	0.10	0.25	0.03

1 Actual Intervals:
1=1, 2=2, 3=3, 4=3.86, 5=4.719, 6=5.715 K Hrs
N/A-Not available

APPENDIX B

SUPPORTING DATA FOR SECTION IV-A

APPENDIX B - LIST OF TABLES

APPENDIX B - LIST OF FIGURES

Table B-1 Nominal Compositions of Test Materials

Comp. %	RA330	I800	A286	316L	321	347	A570	A516	A387 Grade 11
Ni	35	32.5	24	12	11	11	-	-	0.10
Cr	19	21	13	17	18	18	-	-	1.2
Fe	43	46	61	68	68	68	100	100	96.96
Si	1.25	0.50	0.40	1.00	1.00	1.00	-	0.23	0.61
Mn	1.50	0.80	1.00	2.00	2.00	2.00	0.50	0.78	0.52
C	.05-.08	.05	.08	.08	.08		.25	.20	0.12
Other			+1.90 Ti	Mo=(.03)	+Ti	+Co+Ta			Mo 0.46
Density (mg/cm^3)	8050	7995	7930	7980	7950	8110	7870	7870	

Table B-2 Average Coupon Weight Change (mg/cm^2), in 1000 Hour Intervals, for I800 After Trace Contaminant Molten Salt Exposure at 579°C

Chemical Dopant (Symbol)	Average Coupon Weight Change, MG/CM^2											
	1000 Hours			2000 Hours			3000 Hours			4000 Hours		
	PM	W	Wc	PM	W	Wc	PM	W	Wc	PM	W	Wc
0.5% NaOH (O)	0.83	0.86	2.36	0.84	1.03	2.50	0.93	1.21	2.93	1.03	1.34	3.00
0.26% K_2CO_3 (C)	0.63	0.66	2.34	0.77	0.85	2.73	0.91	1.03	3.27	1.00	1.15	3.35
0.35% Na_2SO_4 (S)	0.61	0.57	1.98	0.75	0.85	2.27	0.84	0.93	2.67	0.97	1.02	2.91
0.25% NaCl (H)	0.43	0.43	1.56	0.61	0.80	1.79	0.70	0.87	2.31	0.71	0.96	2.63
.50% NaCl (I)	0.45	0.44	1.98	0.65	0.93	2.46	0.79	1.24	2.94	0.86	1.37	3.39
BLANK (B)	0.59	0.62	1.83	0.79	0.85	2.18	0.89	0.98	2.57	1.00	1.13	2.69
MAX. SPEC. (Σ)	0.54	0.67	2.40	0.56	0.90	2.68	0.72	1.09	3.31	0.80	1.23	3.52

PM = Parent Metal
W = Weld
Wc = Weld, Crevice

Table B-3 Average Coupon Weight Change (mg/cm^2), in 1000 Hour Intervals, for RA330 After Trace Contaminant Molten Salt Exposure at 579°C

Chemical Dopant (Symbol)	Average Coupon Weight Change, MG/CM^2											
	1000 Hours			2000 Hours			3000 Hours			4000 Hours		
	PM	W	Wc	PM	W	Wc	PM	W	Wc	PM	W	Wc
0.5% NaOH (O)	1.69	2.83	4.71	1.87	2.92	5.07	1.84	2.56	4.65	1.83	2.30	4.29
0.26% K_2CO_3 (C)	1.70	2.18	3.58	1.90	2.32	3.94	1.89	2.25	4.29	1.86	2.17	3.97
0.35% Na_2SO_4 (S)	1.41	2.04	3.34	1.67	2.33	3.67	1.85	2.52	4.22	1.80	2.37	4.23
0.25% NaCl (H)	0.32	0.43	1.05	0.45	0.60	1.44	0.47	0.61	1.75	0.42	0.60	1.87
).50% NaCl (I)												
BLANK (B)	1.22	1.43	2.88	1.26	1.86	3.31	1.27	1.84	3.71	1.35	1.91	3.55
MAX. SPEC. (Σ)	1.39	1.79	3.46	1.49	2.13	3.66	1.66	2.14	3.87	1.73	2.23	4.07

PM = Parent Metal
W = Weld
Wc = Weld, Crevice

Table B-4 Average Coupon Weight Change (mg/cm^2), in 1000 Hour Invervals, for 347 After Trace Contaminant Molten Salt Exposure at 579°C

Chemical Dopant (Symbol)	Average Coupon Weight Change, MG/CM^2											
	1000 Hours			2000 Hours			3000 Hours			4000 Hours		
	PM	W	Wc	PM	W	Wc	PM	W	Wc	PM	W	Wc
0.5% NaOH (O)	2.00	2.15	3.46	4.01	4.18	6.21	5.71	5.19	7.90	1.39	3.57	4.68
0.26% K_2CO_3 (C)	1.07	1.36	2.14	3.05	3.63	5.07	5.34	5.44	7.69	6.56	5.85	8.96
0.35% Na_2SO_4 (S)	1.40	1.80	5.22	2.92	3.29	6.93	4.29	4.35	8.60	4.76	5.63	10.38
0.25% NaCl (H)	0.46	0.50	1.17	0.63	0.71	1.38	0.90	0.99	1.74	1.17	1.20	1.94
).50% NaCl (I)												
BLANK (B)	0.85	1.09	1.48	1.97	2.93	3.83	2.51	3.87	4.98	3.74	4.62	5.05
MAX. SPEC. (Σ)	1.09	1.29	1.98	1.98	2.47	3.80	1.30	2.29	4.45	-15.32	-8.14	-4.76

PM = Parent Metal
W = Weld
Wc = Weld, Crevice

Table B-5 Average Coupon Weight Change (mg/cm^2), in 1000 Hour Intervals, for 316L After Trace Contaminant Molten Salt Exposure at 579°C

Chemical Dopant (Symbol)	Average Coupon Weight Change, MG/CM^2											
	1000 Hours			2000 Hours			3000 Hours			4000 Hours		
	PM	W	Wc	PM	W	Wc	PM	W	Wc	PM	W	Wc
0.5% NaOH (O)	1.07	0.98	1.76	1.37	1.28	2.61	1.44	1.62	2.80	1.56	1.60	2.98
0.26% K_2CO_3 (C)	0.90	0.74	1.24	1.46	1.69	2.34	1.64	1.84	2.62	1.66	1.78	2.55
0.35% Na_2SO_4 (S)	0.82	0.67	1.68	1.14	1.55	2.56	1.37	1.89	3.00	1.46	1.80	2.94
0.25% NaCl (H)	0.88	0.77	1.33	1.01	0.92	1.59	1.34	1.27	2.13	1.27	1.08	1.96
).50% NaCl (I)												
BLANK (B)	0.97	0.67	1.43	1.24	1.54	2.37	1.40	1.66	2.57	1.48	1.71	2.60
MAX. SPEC. (Σ)	0.61	0.71	1.56	0.98	1.15	2.14	1.14	0.99	2.41	0.96	0.77	2.28

PM = Parent Metal
W = Weld
Wc = Weld, Crevice

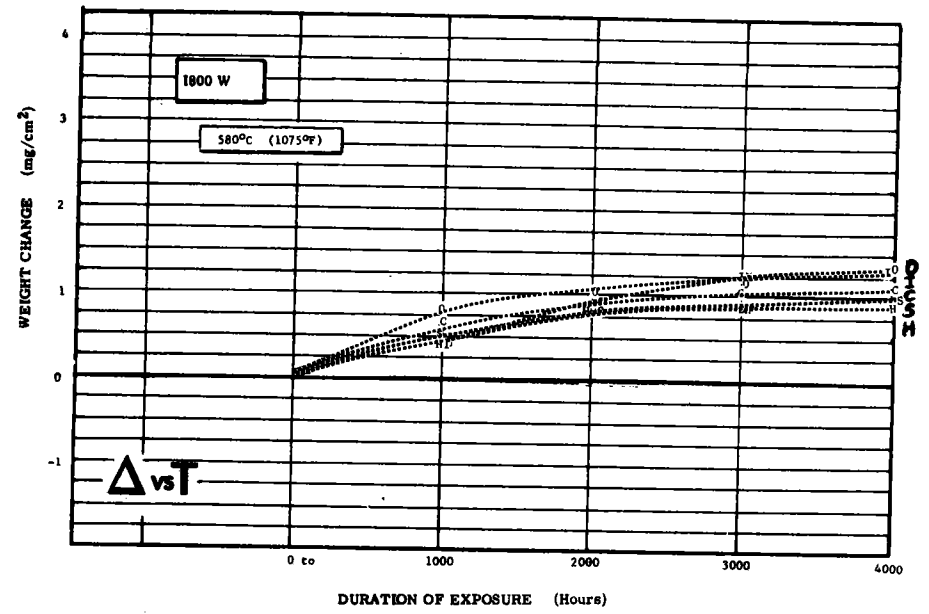

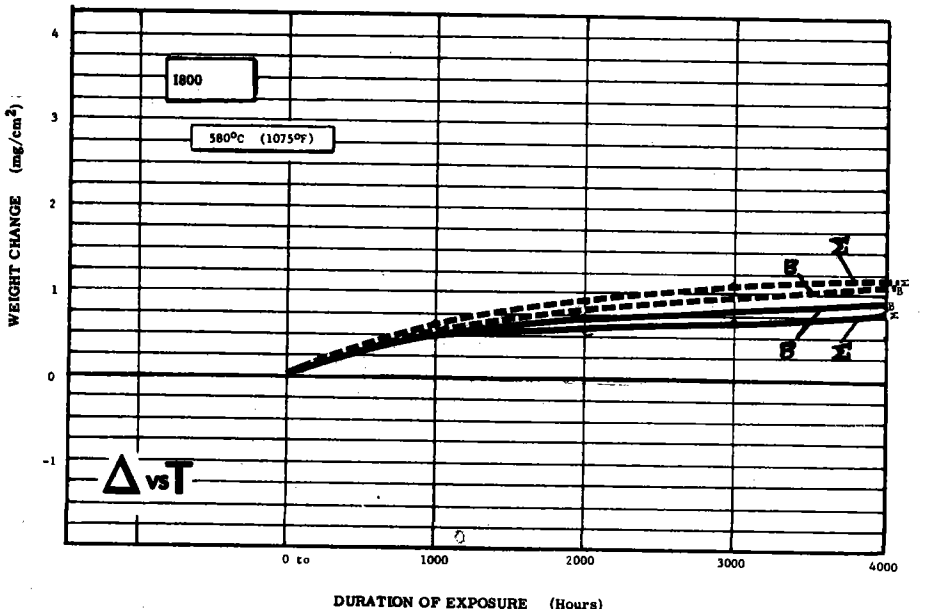

KEY: O : 0.50 Wt % OH^-
C : 0.26 Wt % $CO_3^=$
S : 0.35 Wt % $SO_4^=$
H : 0.25 Wt % Cl^-
I : 0.50 Wt % Cl^-
B : Blank Salt
$\sum$: Sum of All Contaminants

Figure B-1 Weight Change vs Time for I800 Welded Metal Coupons in 580°C (1075°F) Molten Salt with Different Trace Contaminants

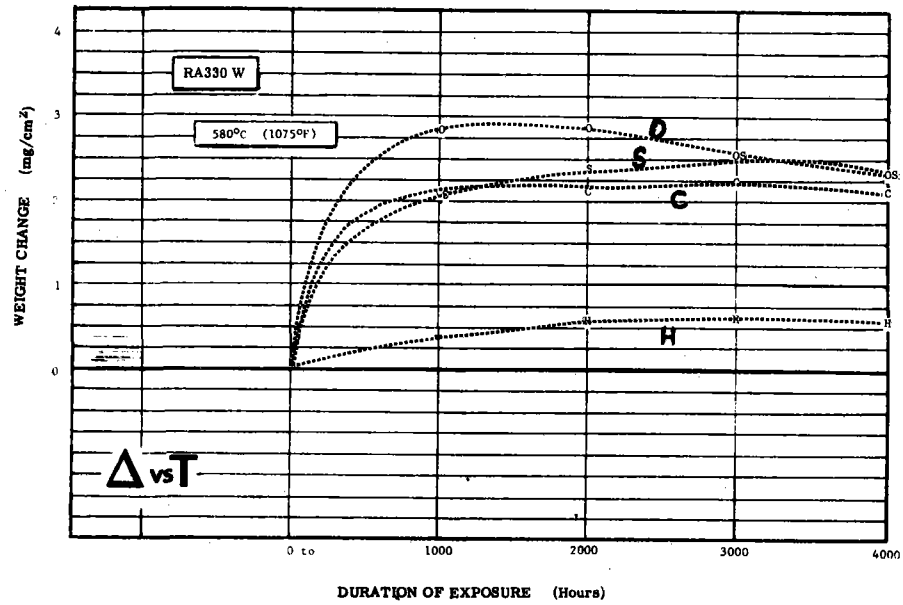

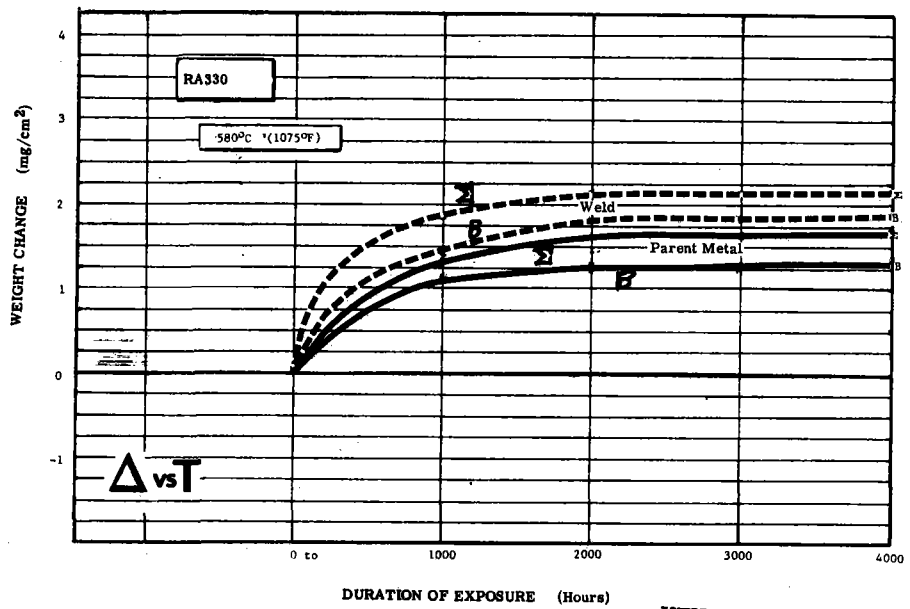

KEY: O : 0.50 Wt % OH^-
C : 0.26 Wt % $CO_3^=$
S : 0.35 Wt % $SO_4^=$
H : 0.25 Wt % Cl^-
I : 0.50 Wt % Cl^-
B : Blank Salt
Σ : Sum of All Contaminants

Figure B-2 Weight Change vs Time for RA330 Welded Metal Coupons in 580°C (1075°F) Molten Salt with Different Trace Contaminants

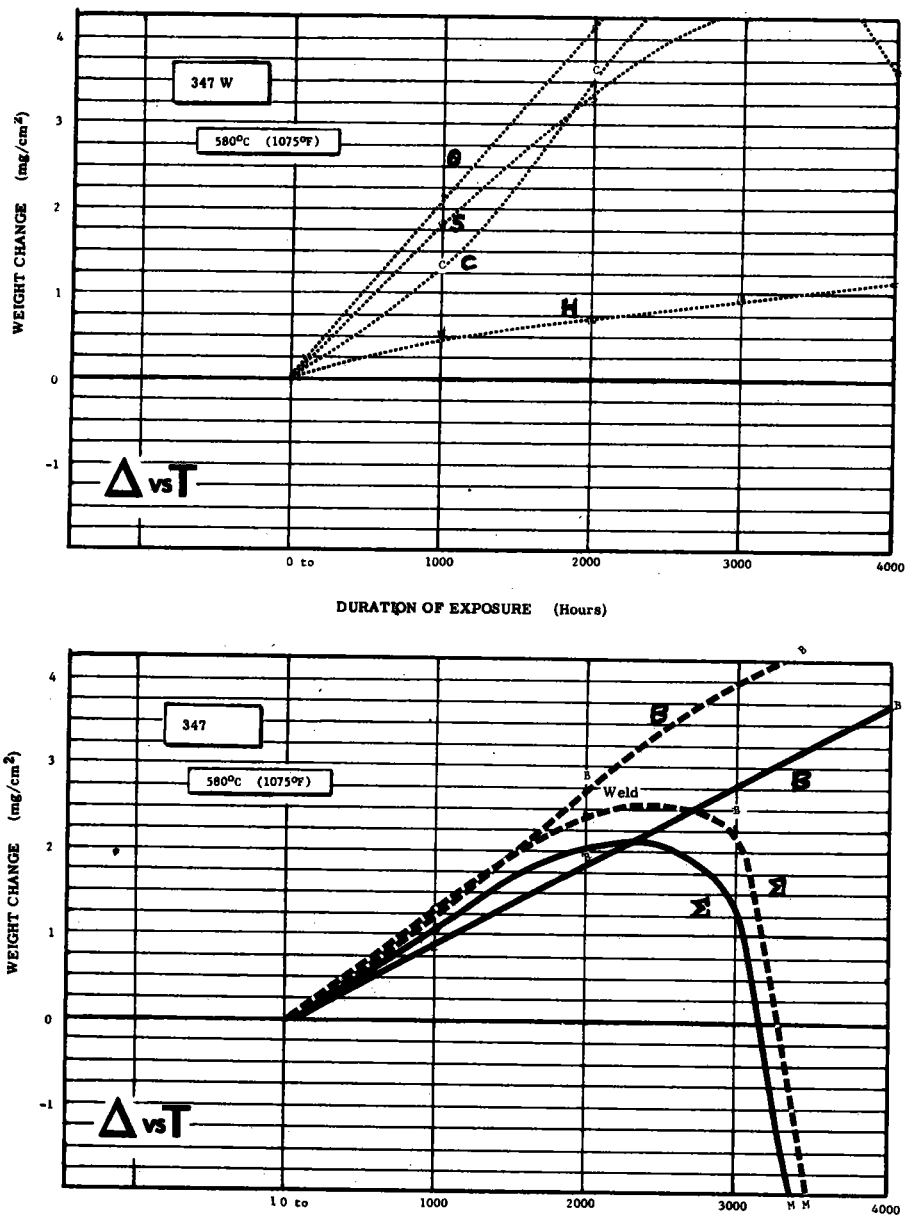

KEY : O : 0.50 Wt % OH^-
C : 0.26 Wt % $CO_3^=$
S : 0.35 Wt % $SO_4^=$
H : 0.25 Wt % Cl^-
I : 0.50 Wt % Cl^-
B : Blank Salt
Σ : Sum of All Contaminants

Figure B-3 Weight Change vs Time for 347 Welded Metal Coupons in 580°C (1075°F) Molten Salt with Different Trace Contaminants

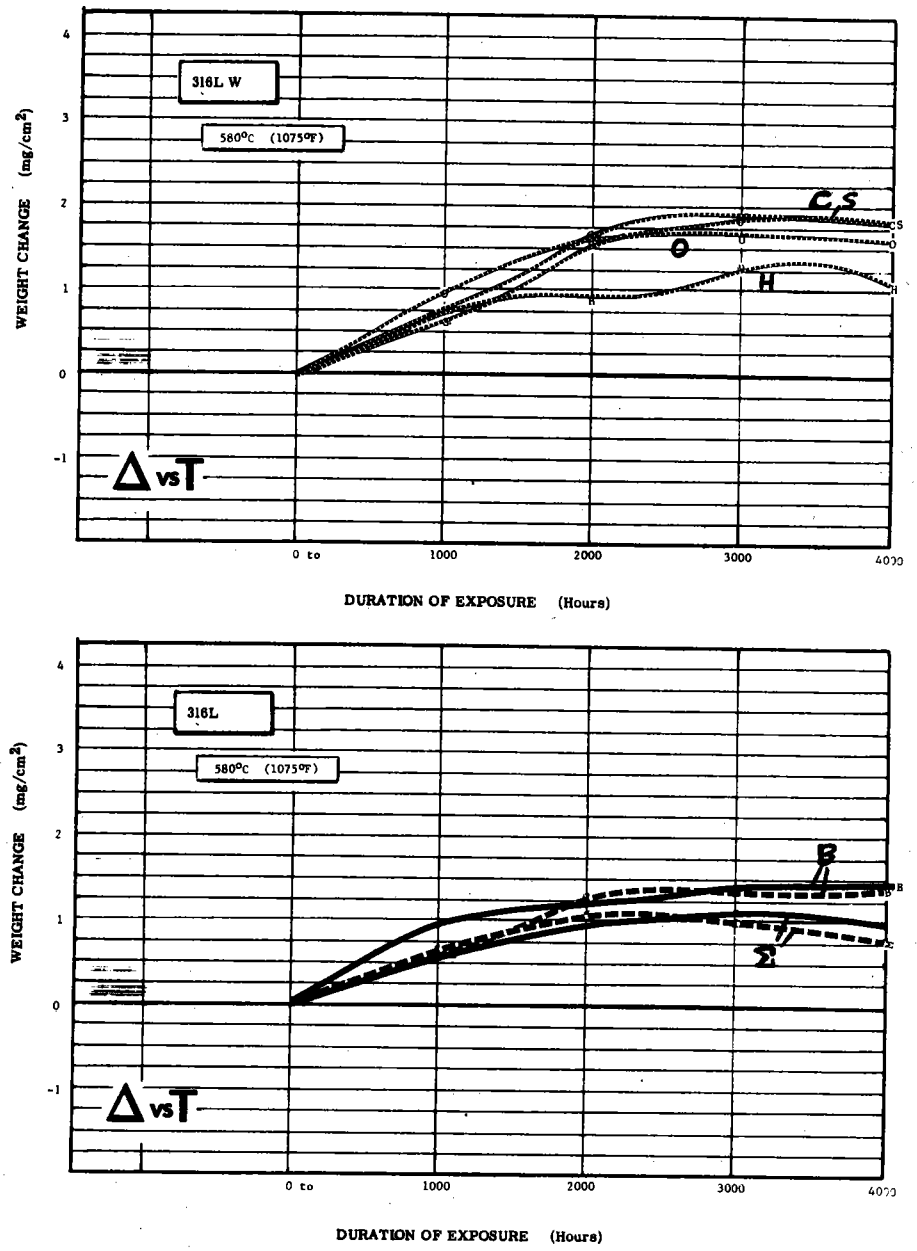

KEY: O : 0.50 Wt % OH^-
C : 0.26 Wt % $CO_3^=$
S : 0.35 Wt % $SO_4^=$
H : 0.25 Wt % Cl^-
I : 0.50 Wt % Cl^-
B : Blank Salt
Σ : Sum of All Contaminants

Figure B-4 Weight Change vs Time for 316L Welded Metal Coupons in 580°C (1075°F) Molten Salt with Different Trace Contaminants

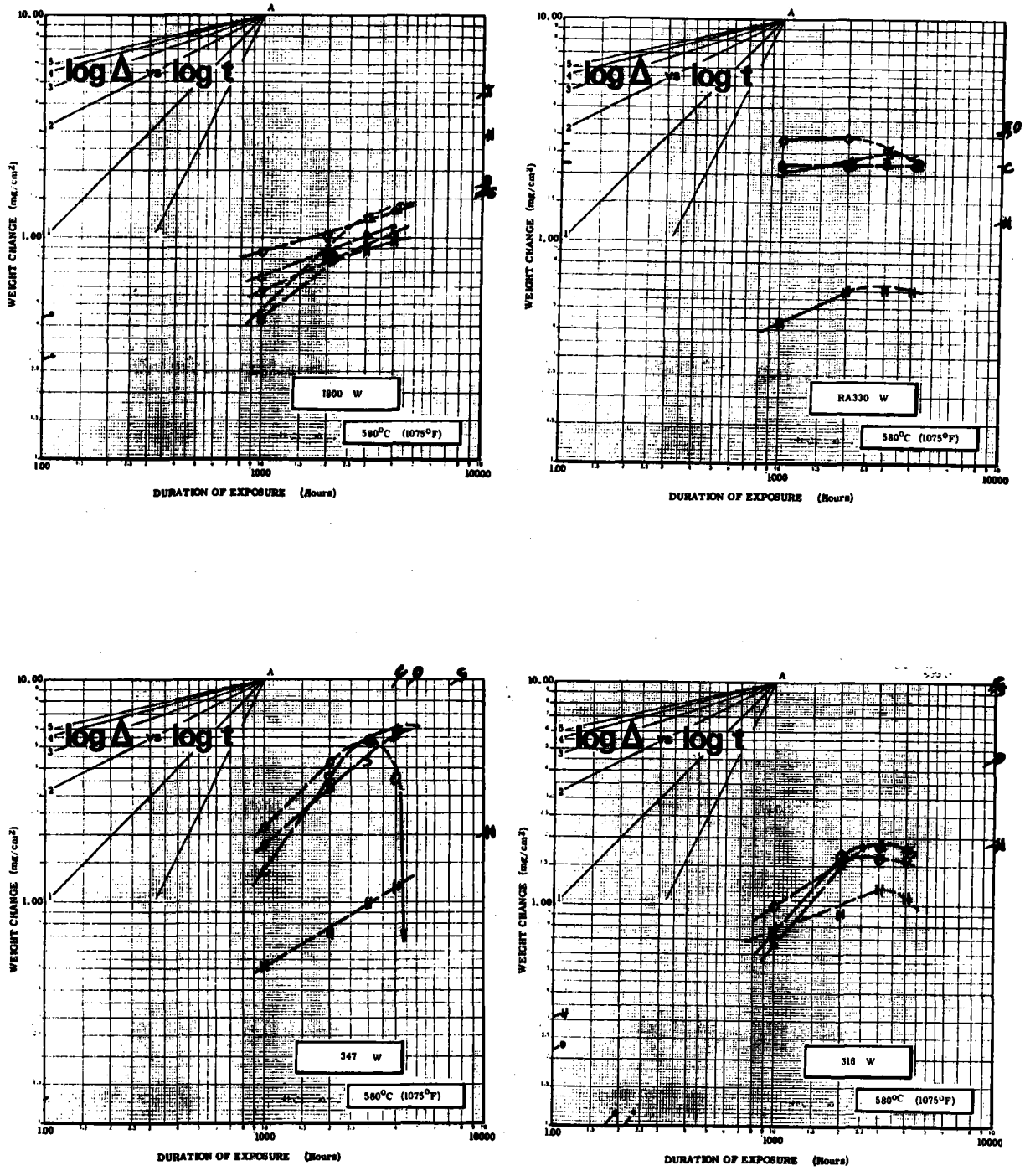

KEY : O : 0.50 Wt % OH^-
C : 0.26 Wt % $CO_3^=$
S : 0.35 Wt % $SO_4^=$
H : 0.25 Wt % Cl^-
I : o.50 Wt % Cl^-

Figure B-5 Log Weight Gain vs Log Time for I800, RA330, 347 and 316L Welded Coupons After 580°C (1075°F) Molten Salt Exposure (With Different Trace Contaminant Conditions)

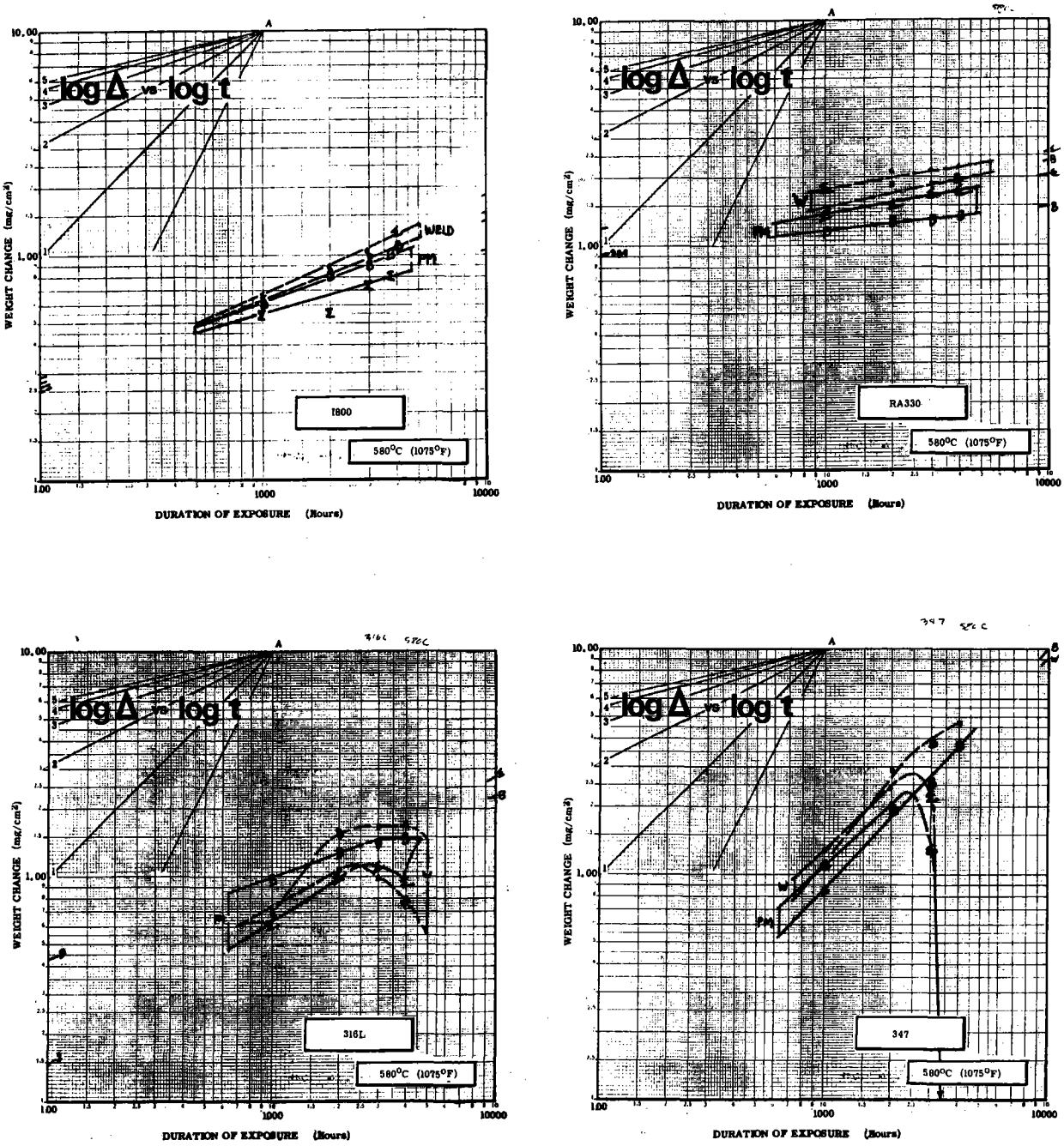

KEY : O : 0.50 Wt % OH^-
C : 0.26 Wt % $CO_3^=$
S : 0.35 Wt % $SO_4^=$
H : 0.25 Wt % Cl^-
I : 0.50 Wt % Cl^-
B : Blank Salt
Σ : Sum of All Contaminants

Figure B-6 Log Weight Gain vs Log Time for I800, RA330, 347 and 316L Welded and Parent Metal Coupons After Blank Salt and Sum of All Trace Contaminant Exposures

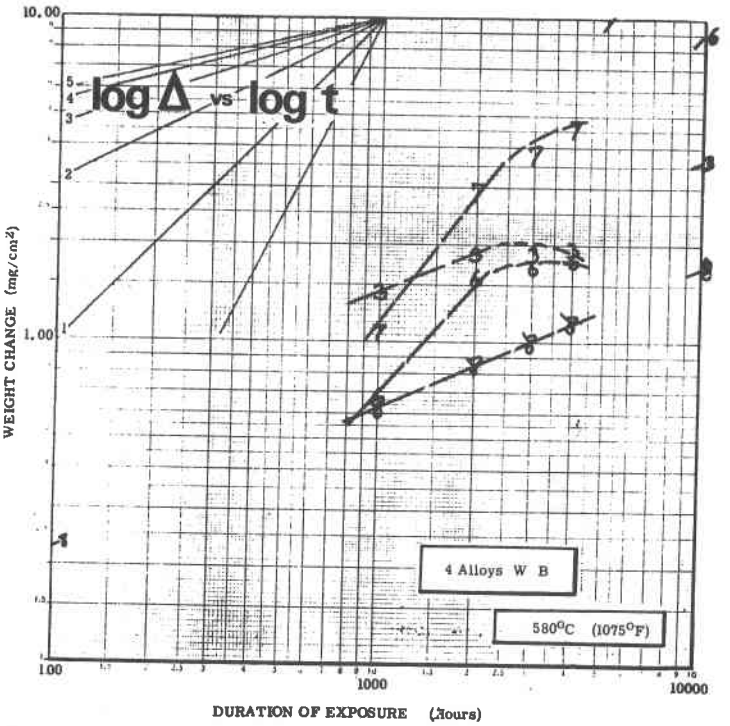

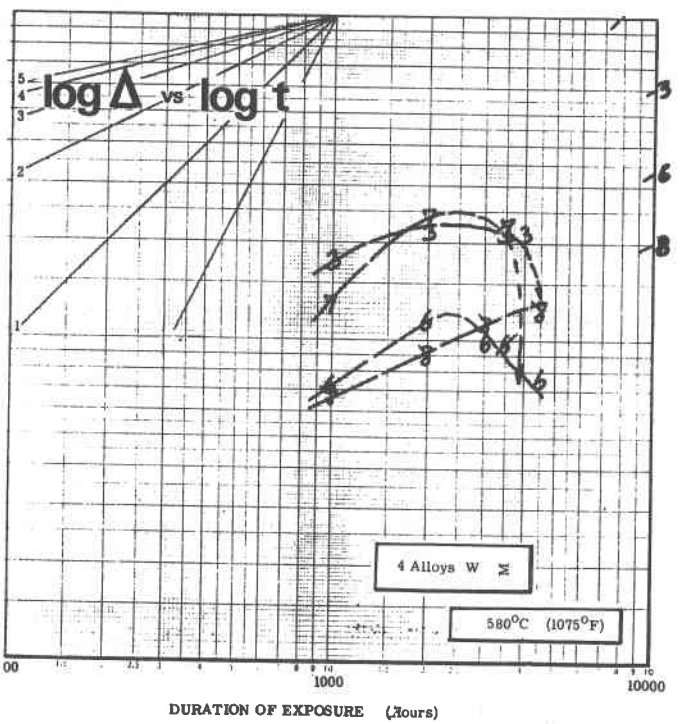

KEY : 3 : RA330
6 : 316L SS
7 : 347 SS
8 : I800

Figure B-7 Comparison of Log Weight Gain (Δ) vs Log Time (t) for Welded High-Nickel and High-Chromium Alloys Exposed to Blank Salt and Sum of all Contaminant Exposures

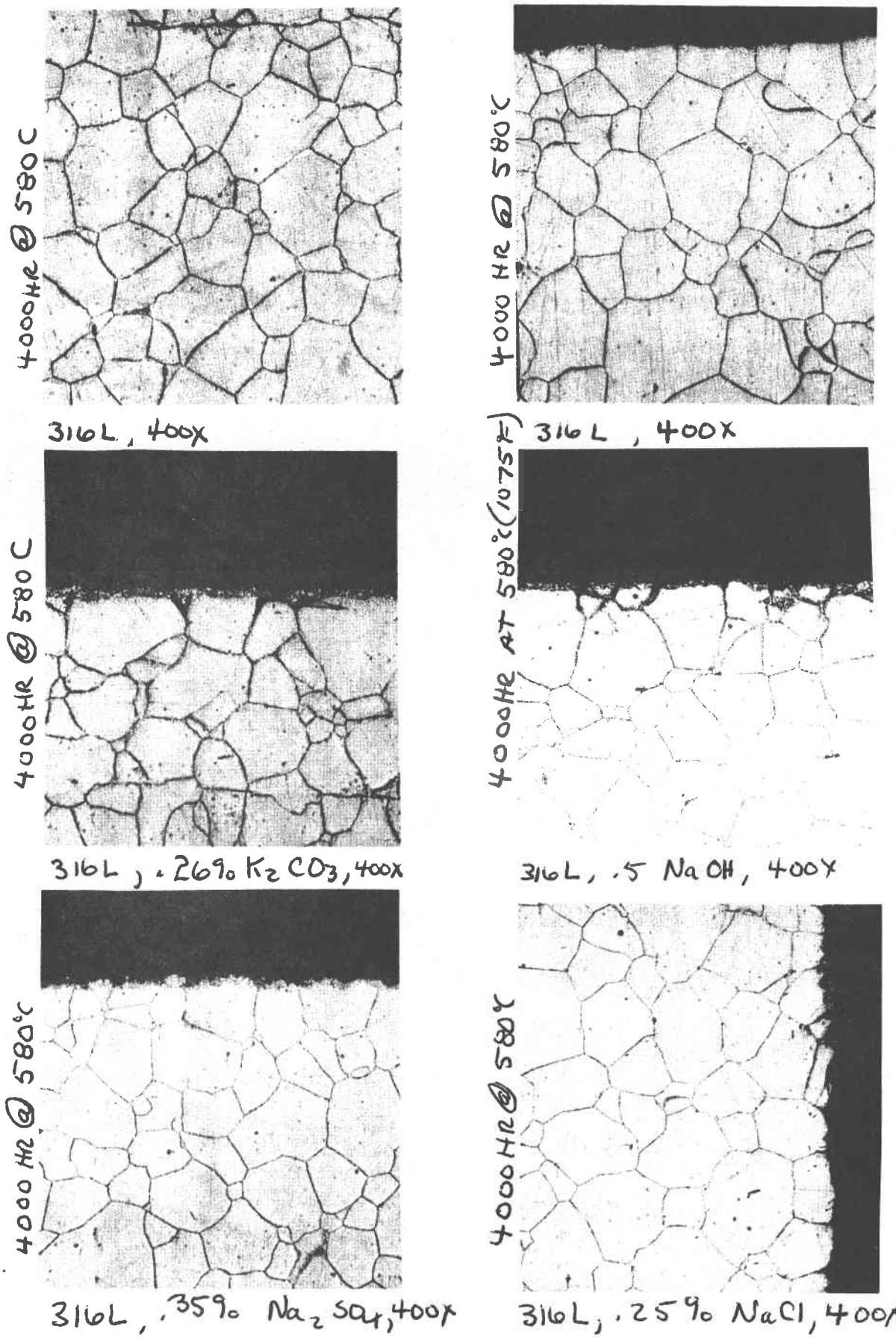

Figure B-8 Micrographs of Parent Metal 316L Coupons Exposed to Different Trace Contaminant Additions in 580°C Molten Salt After 4000 Hours

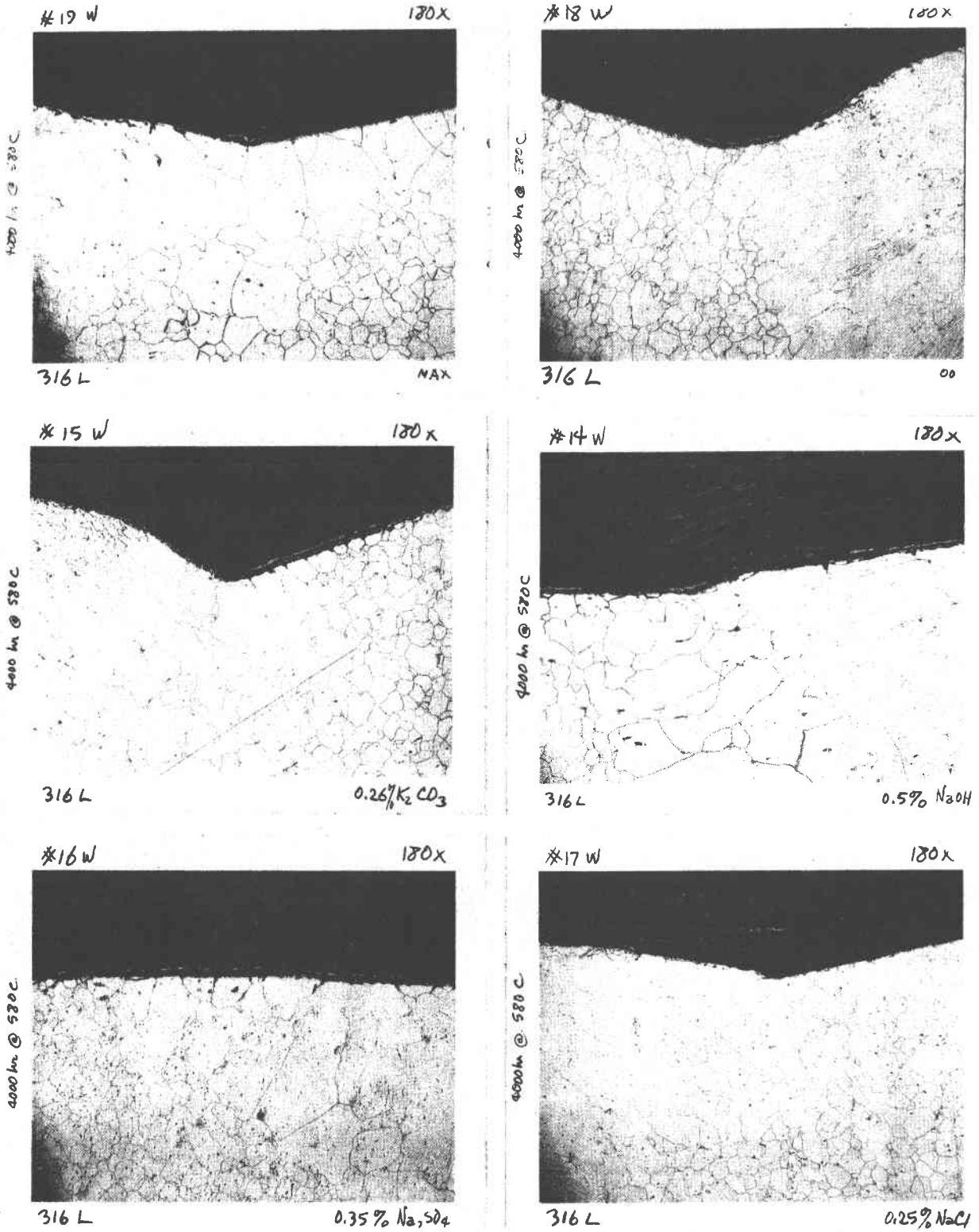

Figure B-9 Micrographs of Welded 316L Coupons Exposed to Different Trace Contaminant Additions in 580°C Molten Salt After 4000 Hours

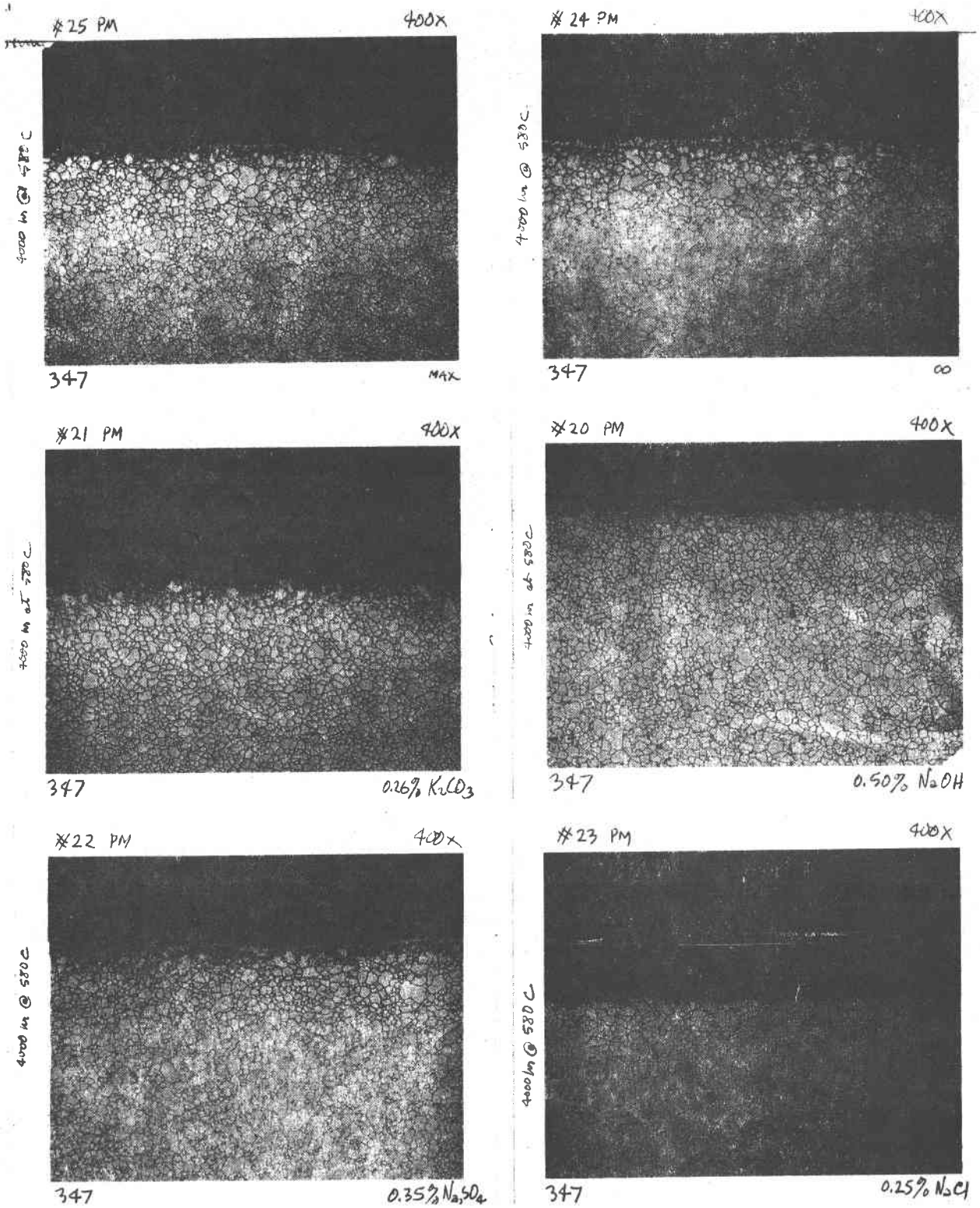

Figure B-10 Micrographs of Parent Metal 347 Coupons Exposed to Different Trace Contaminant Additions in 580°C Molten Salt After 4000 Hours

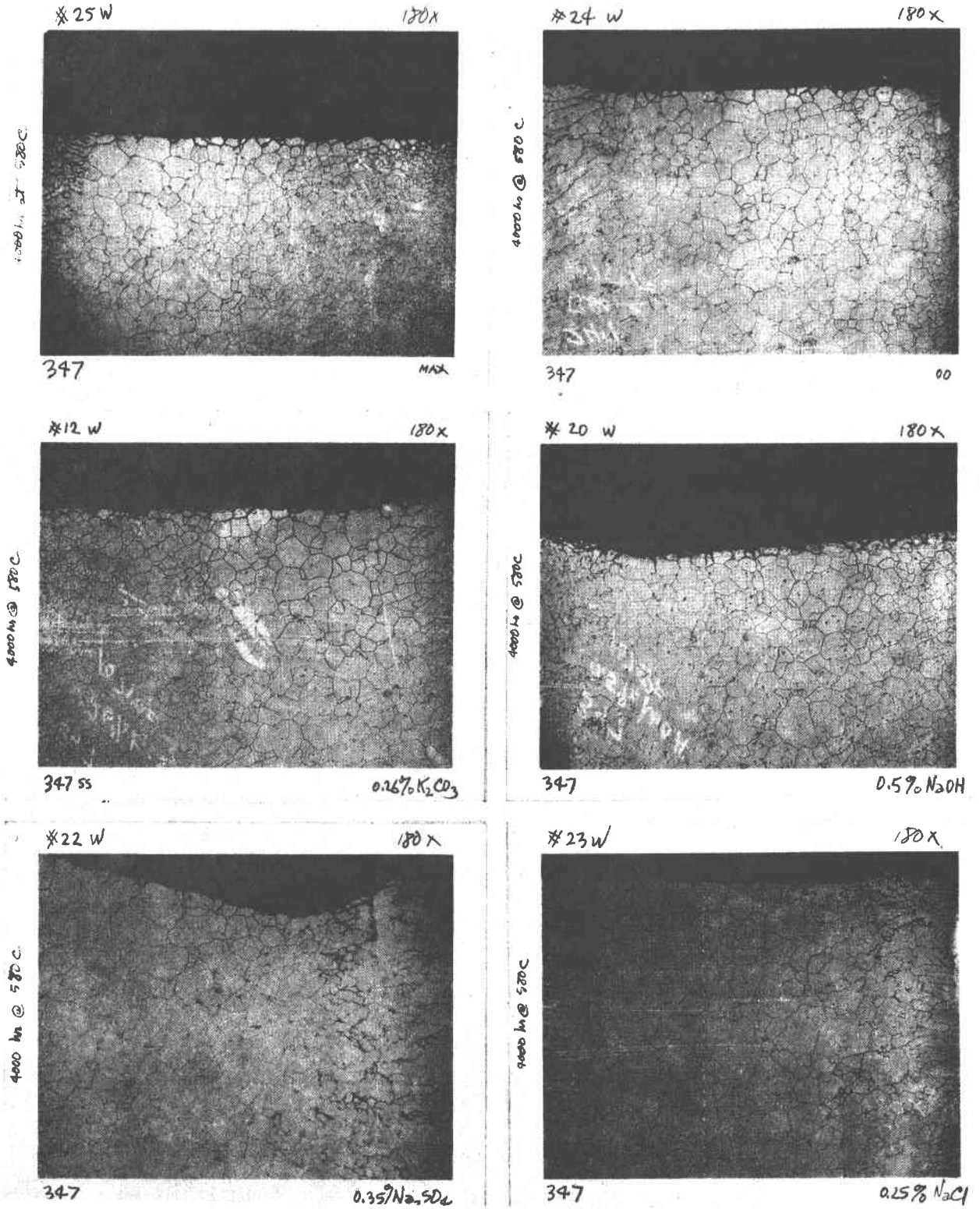

Figure B-11 Micrographs of Welded 347 Coupons Exposed to Different Trace Contaminant Additions in 580°C Molten Salt After 4000 Hours

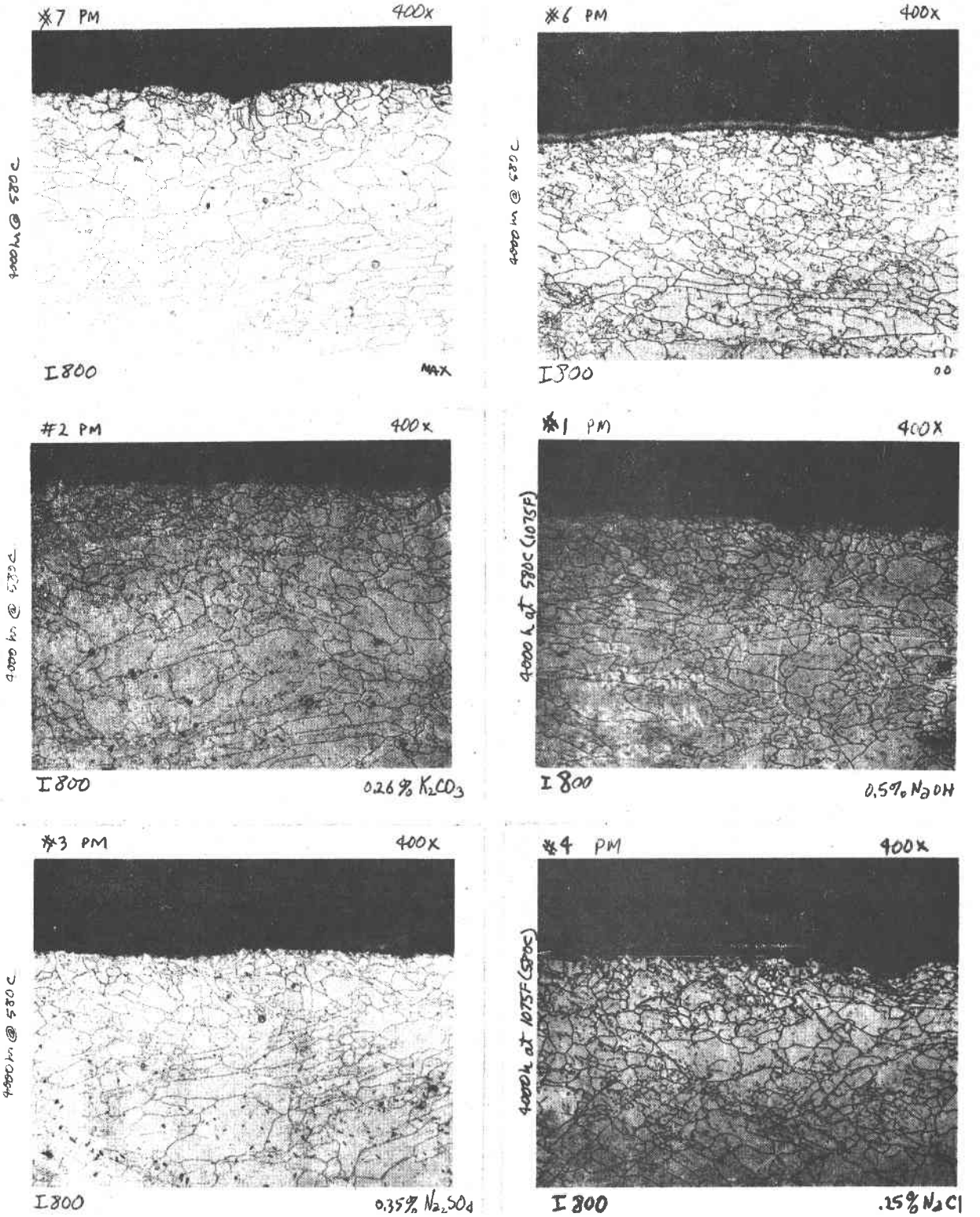

Figure B-12 Micrographs of Parent Metal I800 Coupons Exposed to Different Trace Contaminant Additions in 580°C Molten Salt After 4000 Hours

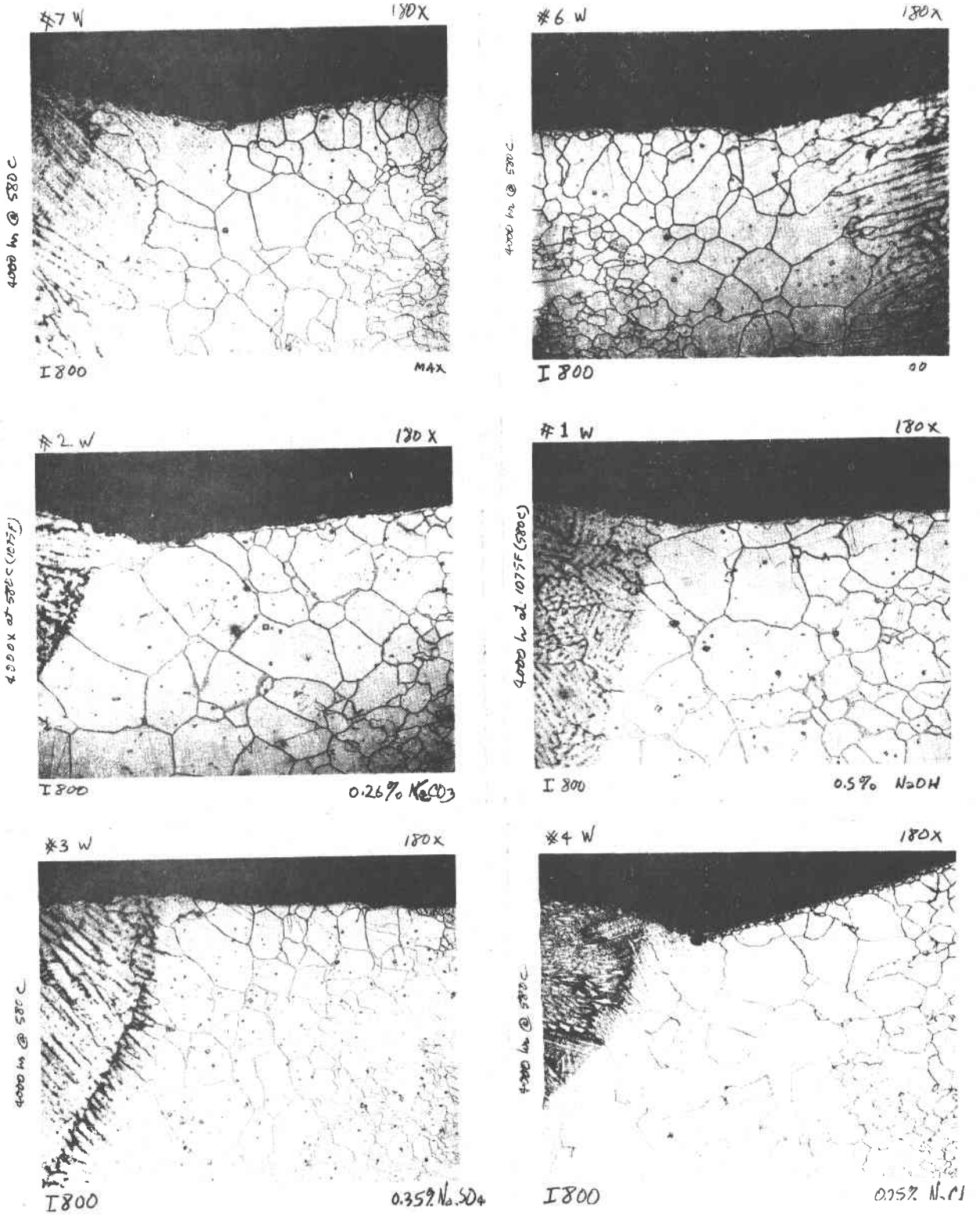

Figure B-13 Micrographs of Welded I800 Coupons Exposed to Different Trace Contaminant Additions in 580°C Molten Salt After 4000 Hours

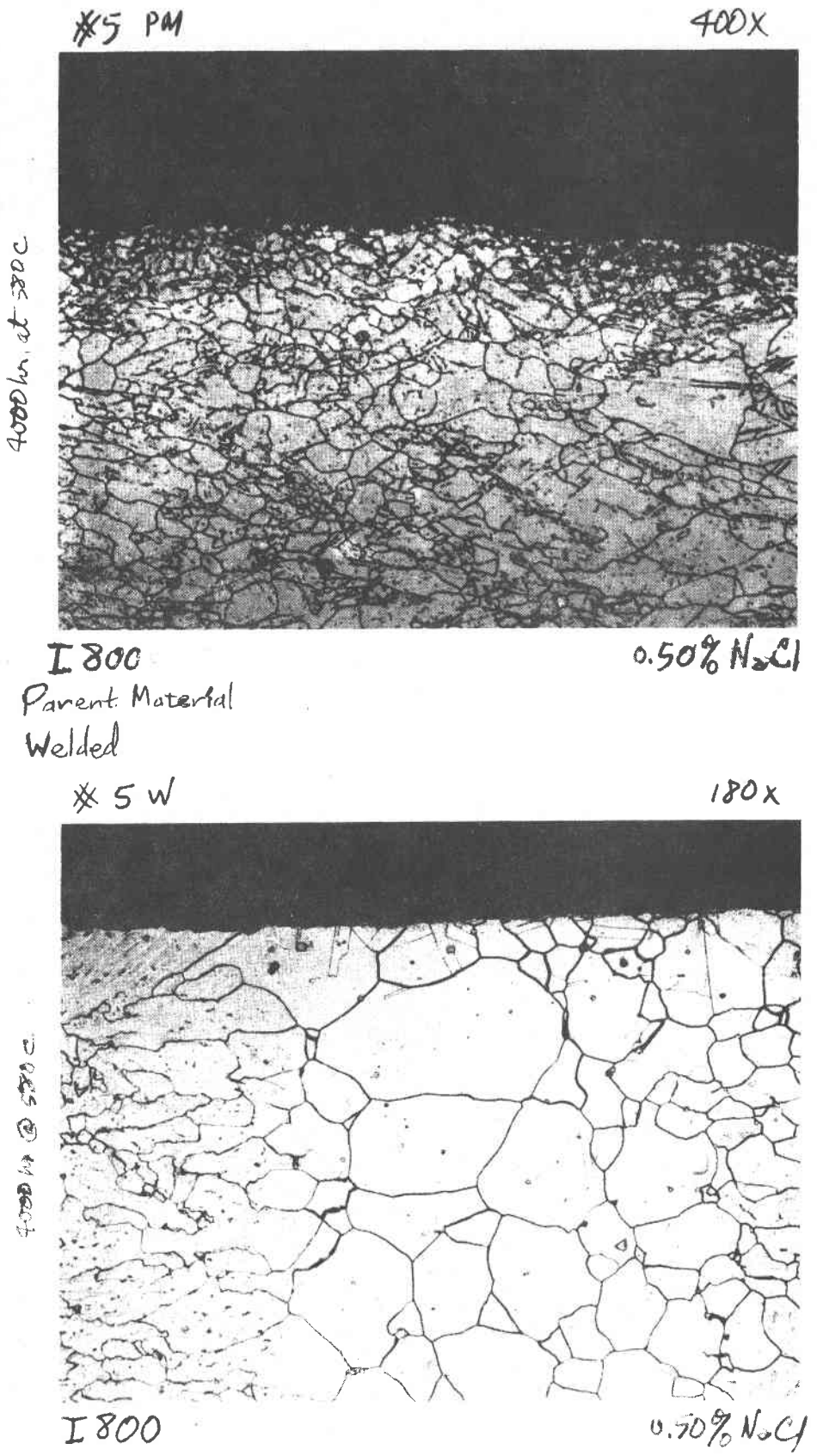

Figure B-14 Micrographs of Parent Metal and Welded I800 After 4000 Hour Exposure to 0.50 Wt % NACL in 580 C Molten Salt

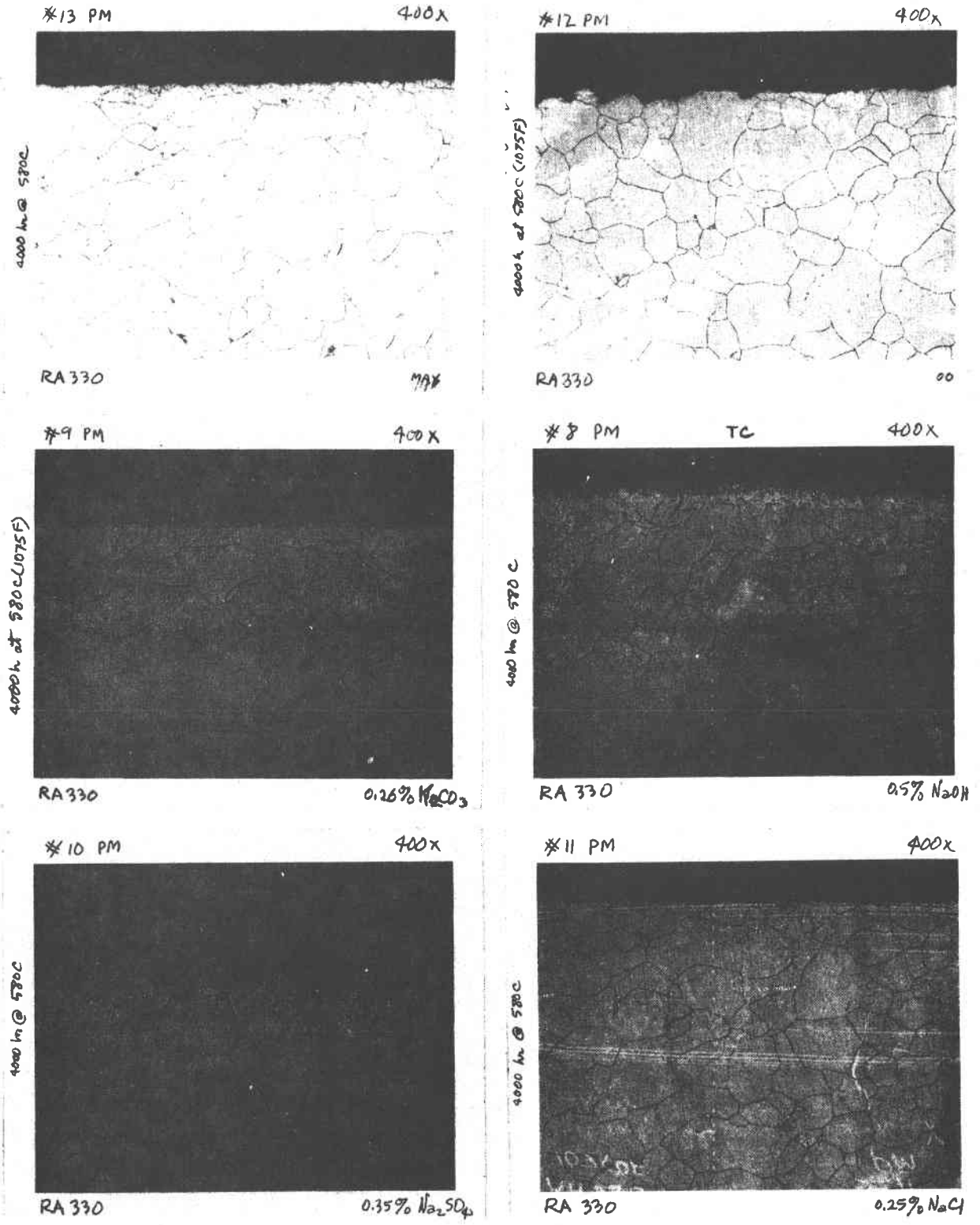

Figure B-15 Micrographs of Parent Metal RA330 Coupons Exposed to Different Trace Contaminant Additions in 580 C Molten Salt After 4000 Hours

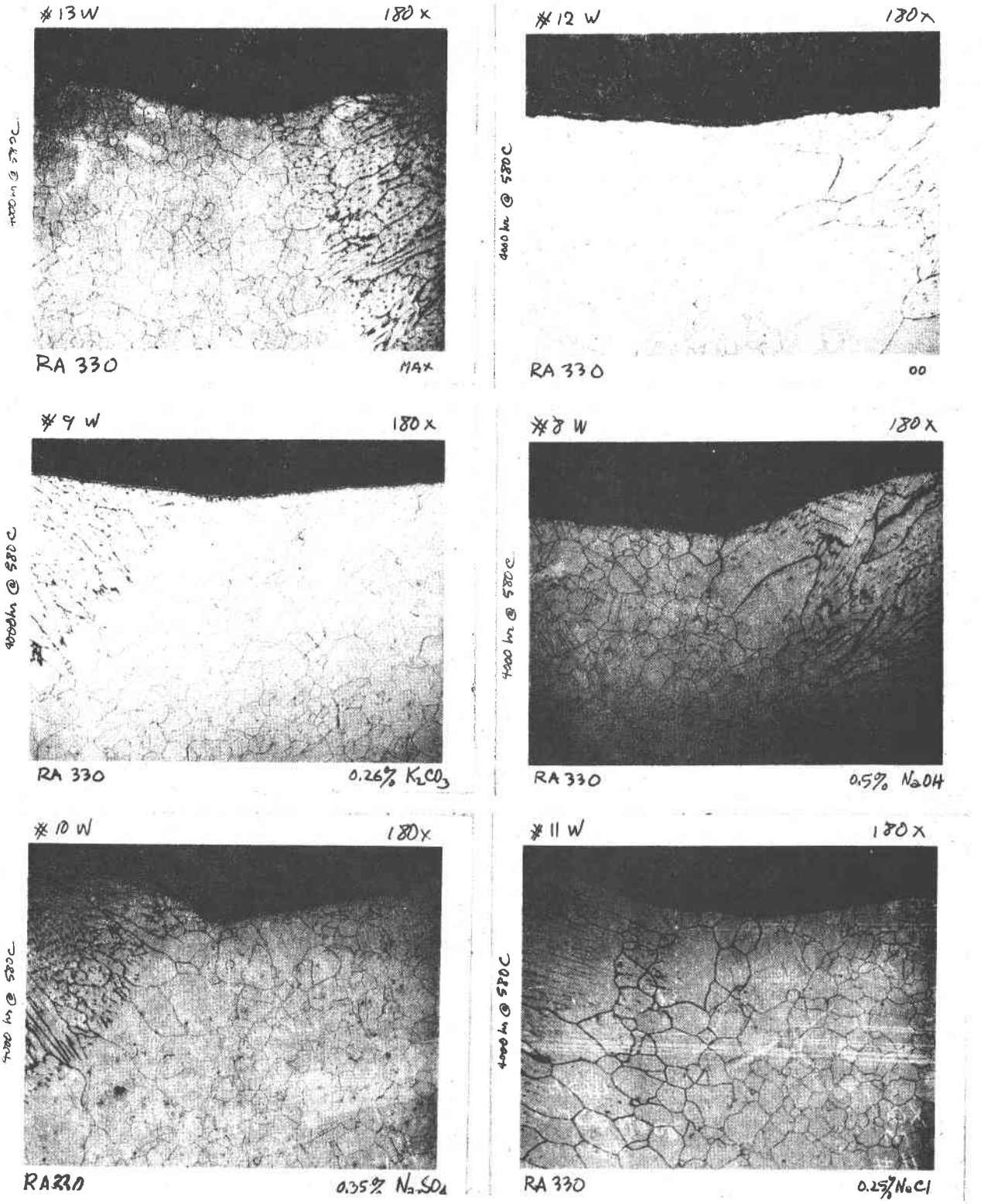

Figure B-16 Micrographs of Welded RA330 Coupons Exposed to Different Trace Contaminant Additions in 580 C Molten Salt After 4000 Hours

Table B-6 Average Coupon Weight Change (mg/cm^2), in 1000 Hour Intervals, for A387 After Trace Contaminant Molten Salt Exposure at 288°C

Chemical Dopant (Symbol)	Average Coupon Weight Change, MG/CM^2											
	1000 Hours			2000 Hours			3000 Hours			4000 Hours		
	PM	W	Wc	PM	W	Wc	PM	W	Wc	PM	W	Wc
0.5% NaOH (O)	0.37	0.68	----	0.91	1.06	----	1.79	1.82	----	2.11	2.09	----
0.26% K_2CO_3 (C)	0.40	0.05	----	-0.05	-0.22	----	0.65	0.15	----	0.72	0.15	----
0.35% Na_2SO_4 (S)	0.71	0.33	----	0.37	0.01	----	1.11	0.54	----	1.16	0.49	----
0.25% NaCl (H)	0.41	0.42	----	1.33	0.14	----	2.02	0.76	----	2.36	0.91	----
).50% NaCl (I)	0.49	0.25	----	0.76	0.55	----	1.42	1.00	----	1.57	1.11	----
BLANK (B)	0.54	0.33	----	0.58	0.56	----	1.20	1.01	----	1.34	1.16	----
MAX. SPEC. (Σ)	0.27	0.22	----	1.22	1.67	----	1.96	2.17	----	2.23	2.32	----

PM = Parent Metal
W = Weld
Wc = Weld, Crevice

Table B-7 Average Coupon Weight Change (mg/cm^2), in 1000 Hour Intervals, for A570 After Trace Contaminant Molten Salt Exposure at 288°C

Chemical Dopant (Symbol)	Average Coupon Weight Change, MG/CM^2											
	1000 Hours			2000 Hours			3000 Hours			4000 Hours		
	PM	W	Wc	PM	W	Wc	PM	W	Wc	PM	W	Wc
0.5% NaOH (O)	0.28	-.10	----	0.34	-.08	----	0.41	.04	----	0.52	0.20	----
0.26% K_2CO_3 (C)	0.16	0.25	----	0.30	0.14	----	0.25	0.19	----	0.35	0.26	----
0.35% Na_2SO_4 (S)	0.31	0.03	----	0.54	0.18	----	0.59	0.21	----	0.69	0.30	----
0.25% NaCl (H)	0.29	0.10	----	0.72	0.11	----	0.76	0.16	----	1.02	0.27	----
).50% NaCl (I)	0.27	0.31	----	0.85	0.96	----	1.03	0.47	----	1.33	0.61	----
BLANK (B)	0.13	0.20	----	0.35	0.18	----	0.35	0.29	----	0.41	0.32	----
MAX. SPEC. (Σ)	0.41	.08	----	0.73	0.28	----	0.92	0.41	----	1.10	0.61	----

PM = Parent Metal
W = Weld
Wc = Weld, Crevice

Table B-8 Average Coupon Weight Change (mg/cm^2), in 1000 Hour Intervals, for A570 After Trace Contaminant Molten Salt Exposure at 399°C

Chemical Dopant (Symbol)	Average Coupon Weight Change, MG/CM^2											
	1000 Hours			2000 Hours			3000 Hours			4000 Hours		
	PM	W	Wc	PM	W	Wc	PM	W	Wc	PM	W	Wc
0.5% NaOH (O)	2.47	2.52	2.20	3.51	3.60	3.17	4.15	4.28	3.80	Test Discontinued		
0.26% K_2CO_3 (C)	2.69	2.32	3.24	2.76	2.40	3.55	1.07	2.24	2.09	Test Discontinued		
0.35% Na_2SO_4 (S)	3.05	2.53	2.60	-0.66	1.47	1.01	-2.50	0.42	0.36	Test Discontinued		
0.25% NaCl (H)	2.32	4.30	3.04	2.87	1.28	-0.57	3.20	3.07	0.04	Test Discontinued		
).50% NaCl (I)	2.49	5.83	1.68	3.07	-0.27	-2.49	3.50	2.17	-0.41	Test Discontinued		
BLANK (B)	2.45	2.32	3.45	3.37	3.34	4.70	3.42	3.67	4.95	Test Discontinued		
MAX. SPEC. (Σ)	1.61	1.42	2.50	2.62	2.56	4.28	3.24	3.22	5.06	Test Discontinued		

PM = Parent Metal
W = Weld
Wc = Weld, Crevice

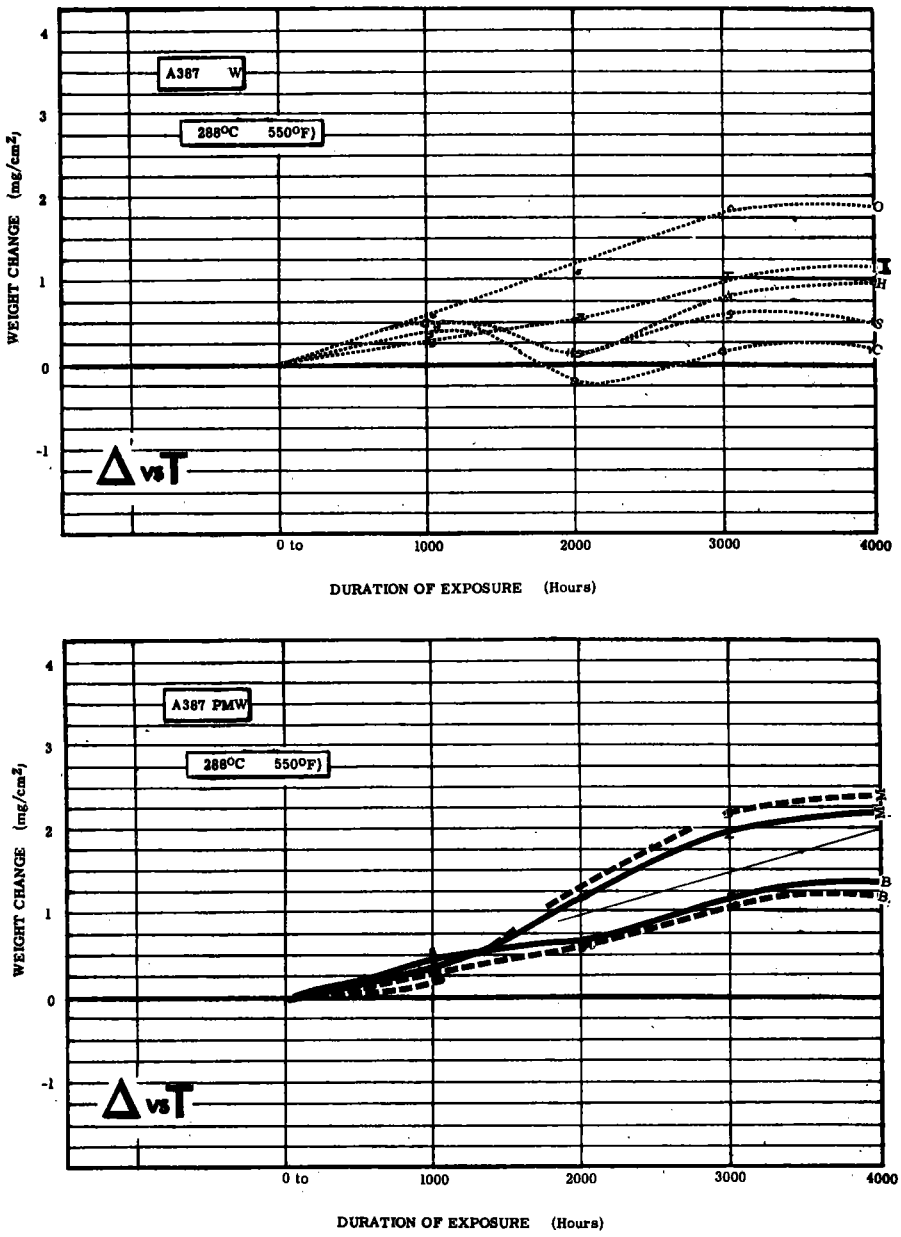

KEY: O : 0.50 Wt % OH^-
C : 0.26 Wt % $CO_3^=$
S : 0.35 Wt % $SO_4^=$
H : 0.25 Wt % Cl^-
I : 0.50 Wt % Cl^-
B : Blank Salt
Σ : Sum of All Contaminants

Figure B-17 Weight Change vs Time for Welded A387 From Trace Contaminant Tests at 288°C (550°F)

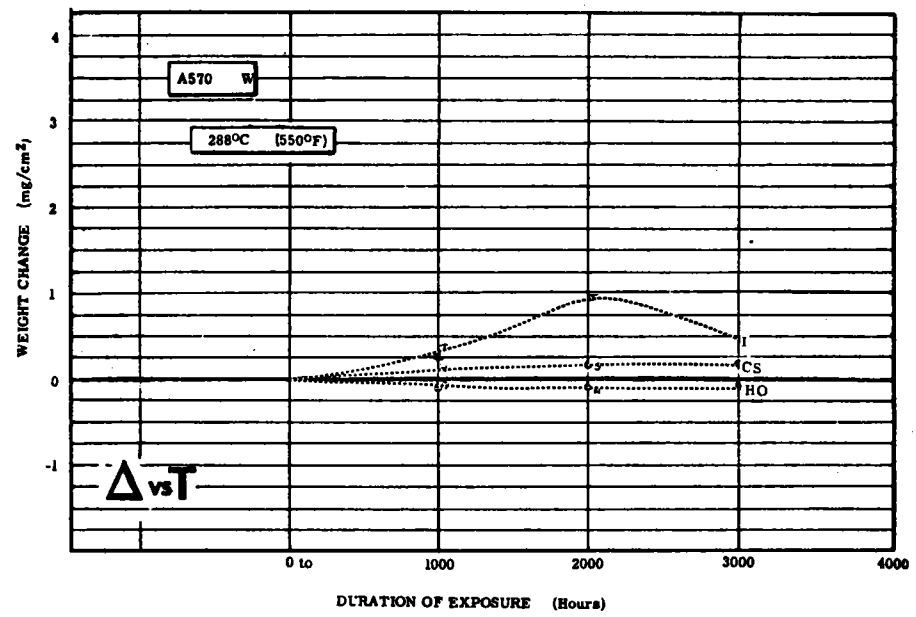

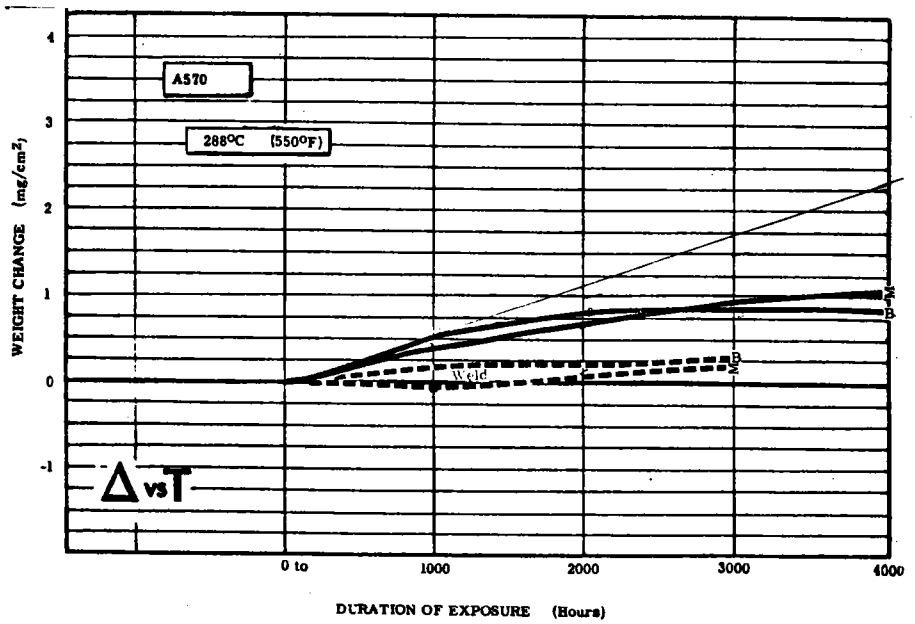

KEY: O : 0.50 Wt % OH^-
C : 0.26 Wt % $CO_3^=$
S : 0.35 Wt % $SO_4^=$
H : 0.25 Wt % Cl^-
I : 0.50 Wt % Cl^-
B : Blank Salt
Σ : Sum of All Contaminants

Figure B-18 Weight Change vs Time for Welded A570 From Trace Contaminant Tests at 288°C (550°F)

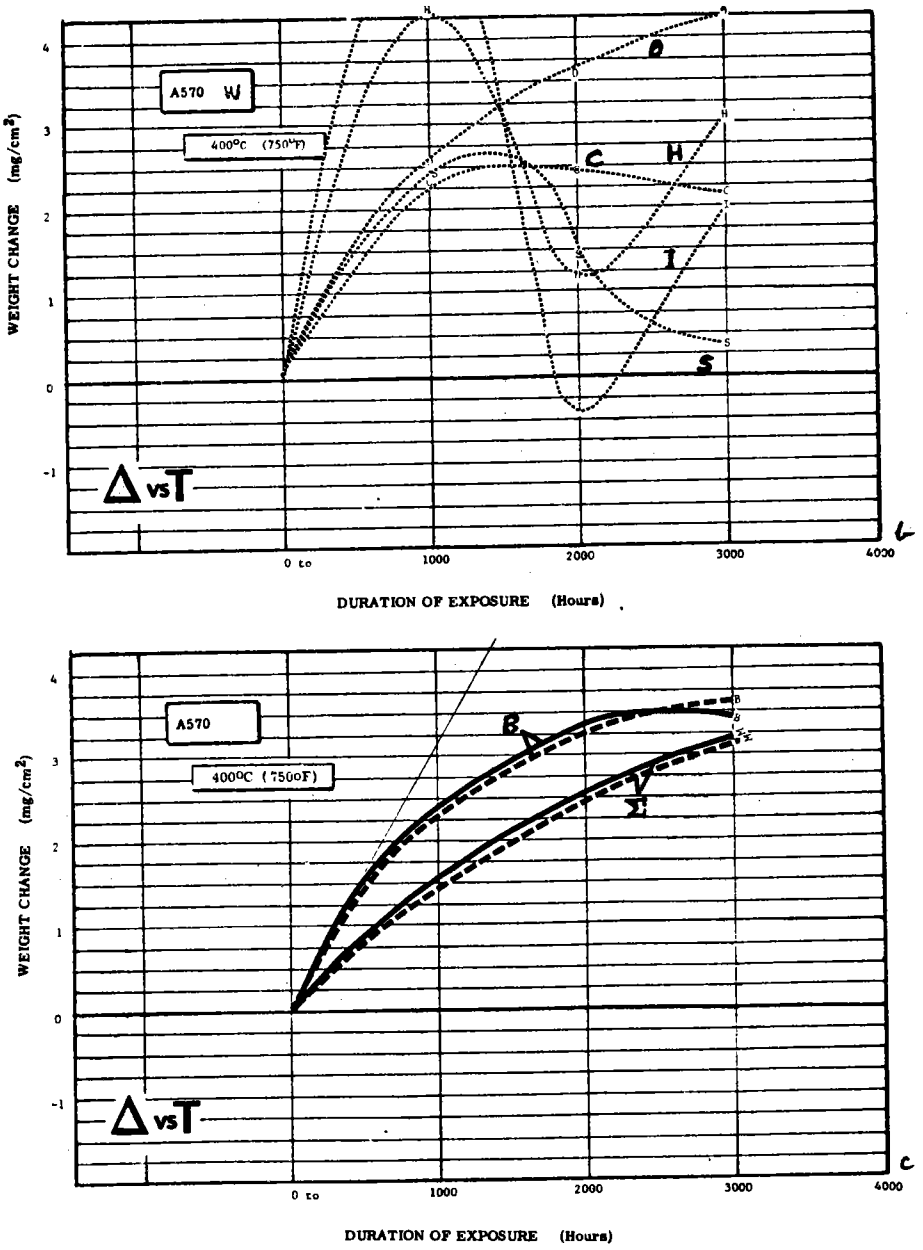

KEY:
- O : 0.50 Wt % OH^-
- C : 0.26 Wt % $CO_3^=$
- S : 0.35 Wt % $SO_4^=$
- H : 0.25 Wt % Cl^-
- I : 0,50 Wt % Cl^-
- B : Blank Salt
- Σ : Sum of All Contaminants

Figure B-19 Weight Change vs Time for Welded A570 From Trace Contaminant Tests at 400°C (750°F)

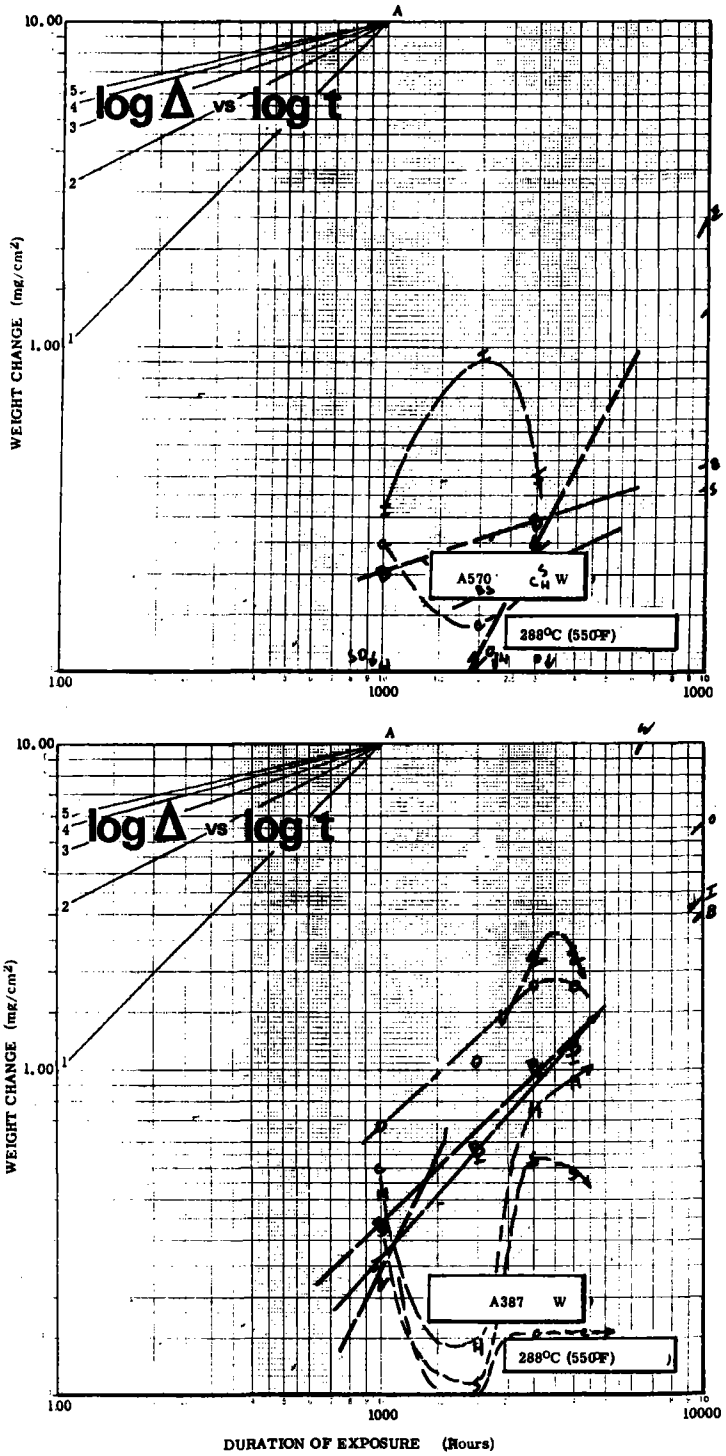

KEY:
- O : 0.50 Wt % OH^-
- C : 0.26 Wt % $CO_3^=$
- S : 0.35 Wt % $SO_4^=$
- H : 0.25 Wt % Cl^-
- I : 0.50 Wt % Cl^-
- B : Blank Salt
- Σ : Sum of All Contaminants

Figure B-20 Log Δ-Log t Plots for Welded A570 and A387 After Trace Contaminant Additions to 288°C Molten Salt

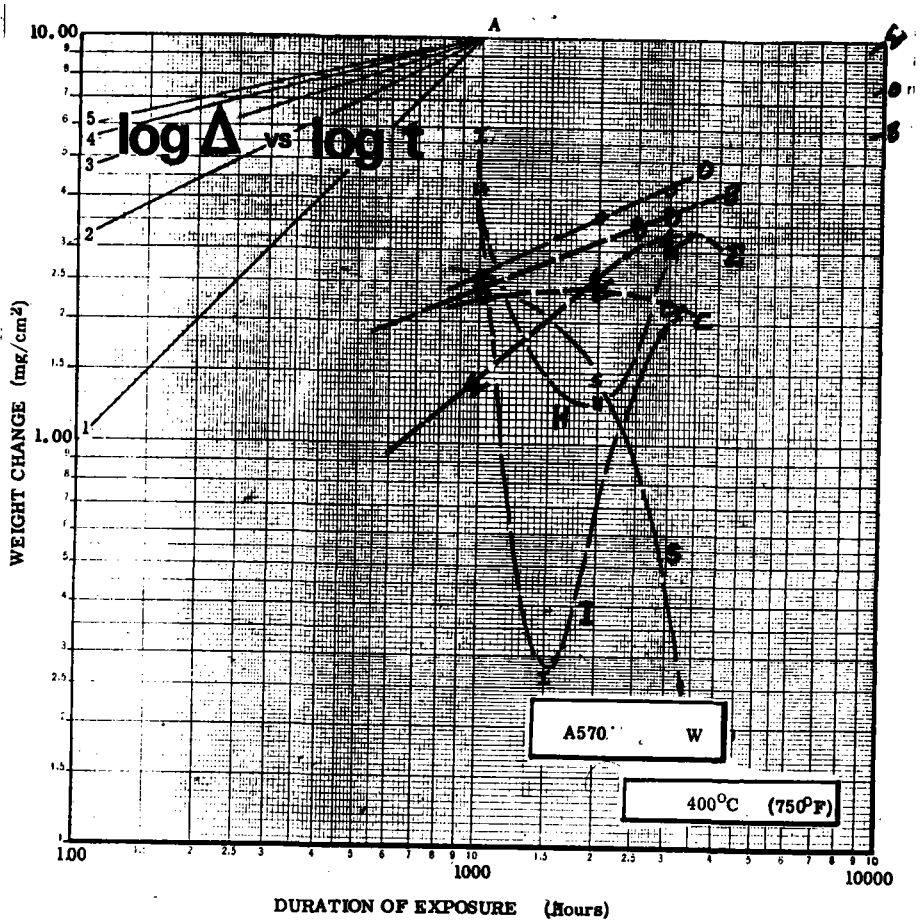

KEY:
O : 0.50 Wt % OH^-
C : 0.26 Wt % $CO_3^=$
S : 0.35 Wt % $SO_4^=$
H : 0.25 Wt % Cl^-
I : 0.50 Wt % Cl^-
B : Blank Salt
Σ : Sum of All Contaminants

Figure B-21 Log Δ-Log t Plots for Welded A570 After Trace Contaminant Additions to 400°C Molten Salt

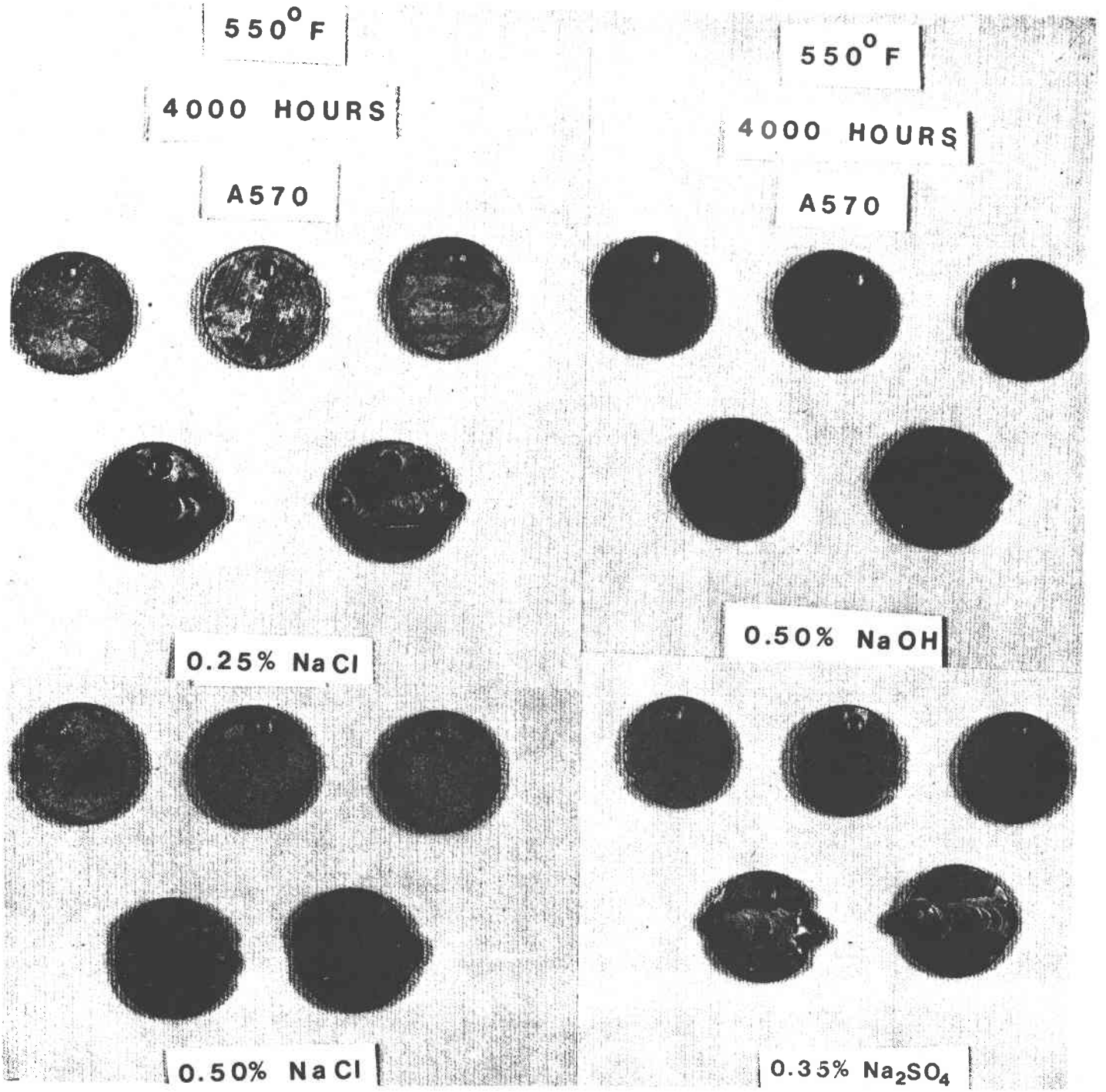

Figure B-22 Photographs of A570 After 4000 Hours Exposure to 288°C (550°F) Molten Salt with Cl^-, OH^-, and $SO_4^=$ Trace Additions

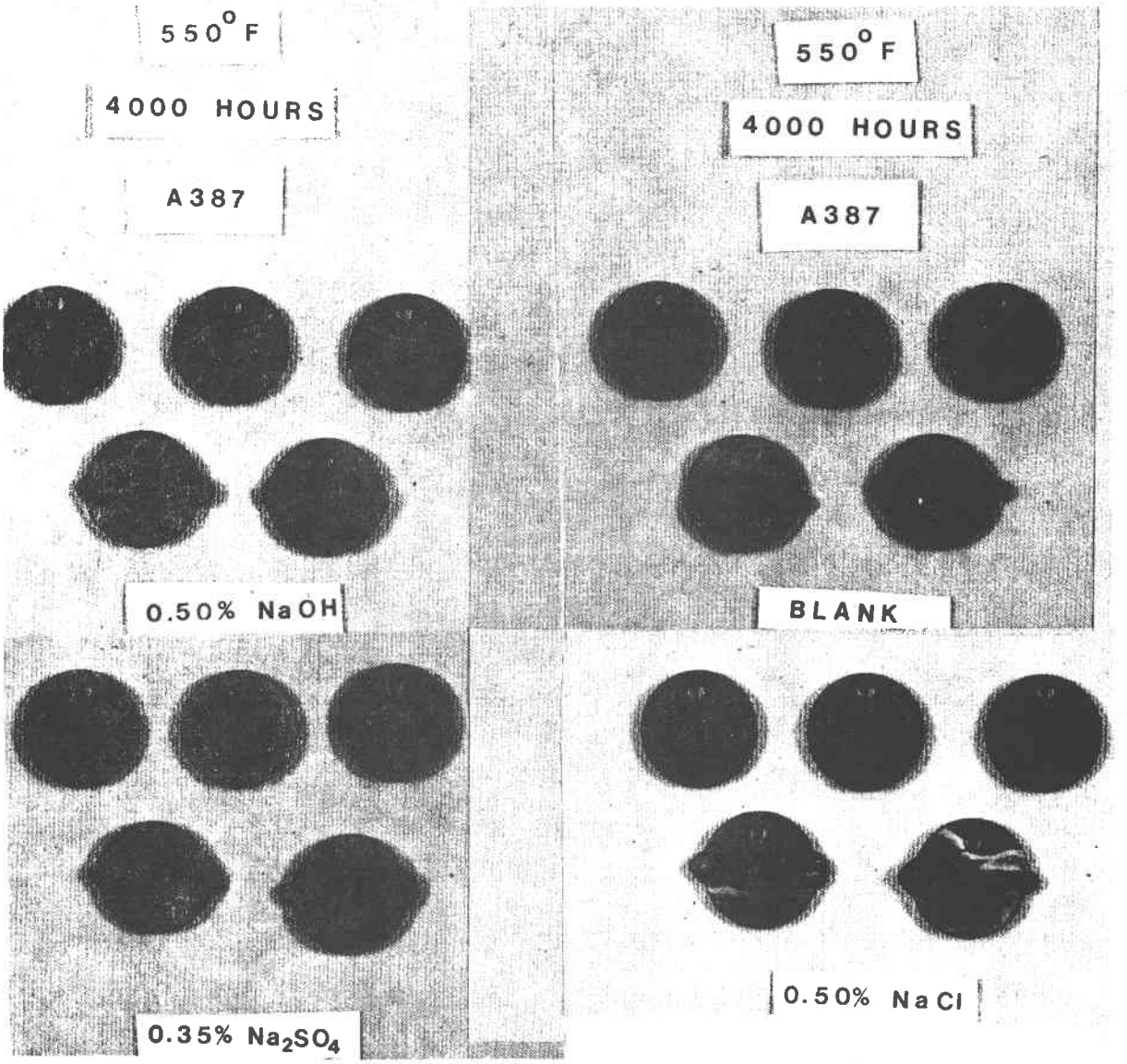

Figure B-23 Photographs of A387 After 4000 Hours Exposure to 288°C (550°F) Molten Salt With Cl^-, OH^-, $SO_4^=$ and No Trace Additions

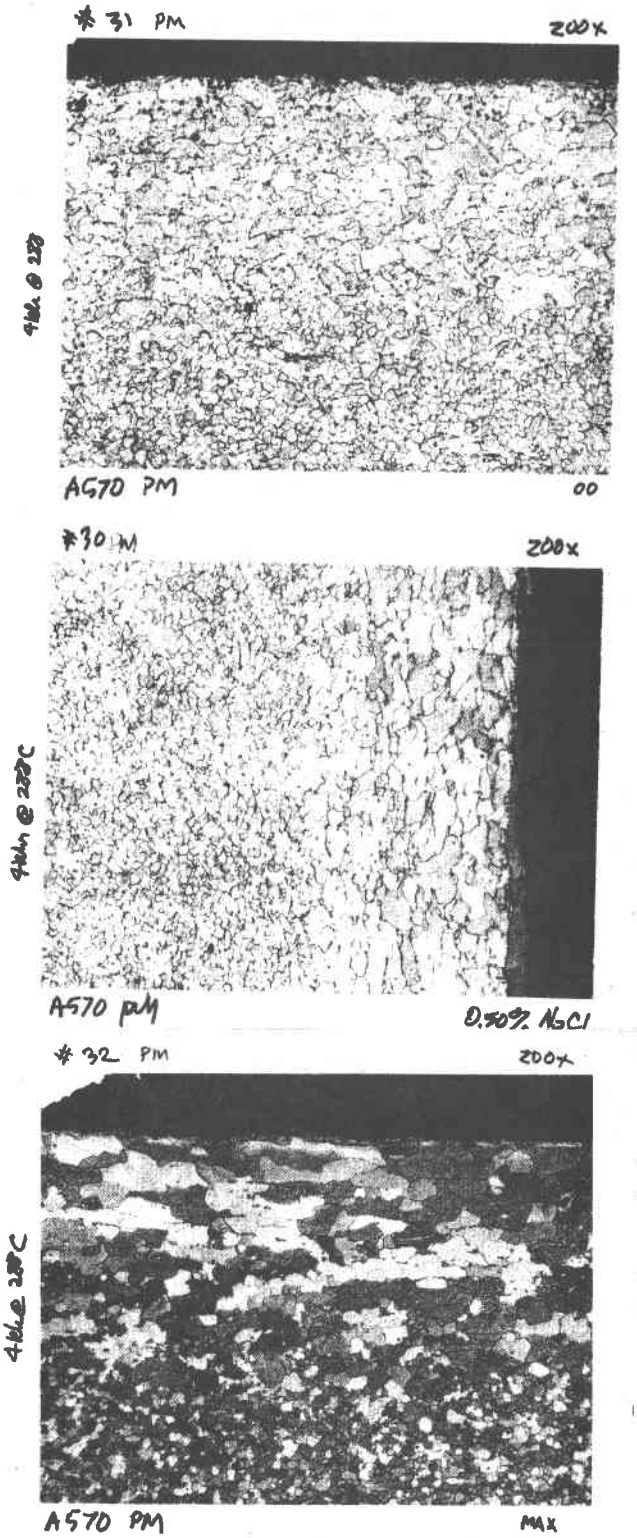

Figure B-24 Micrographs of Parent Metal A570 After 4000 Hours Exposure to 288°C (550°F) Molten Salt with Cl^-, Sum of All Contaminants and No Trace Contaminant Additions

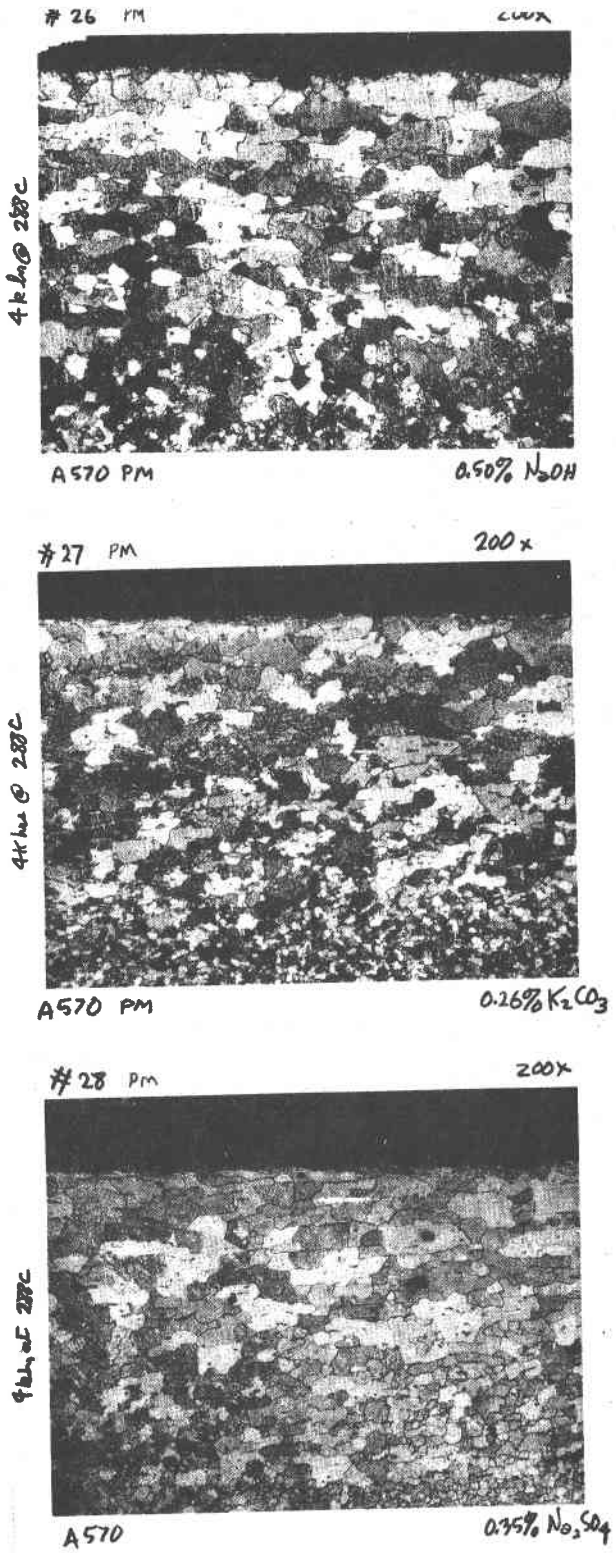

Figure B-25 Micrographs of Parent Metal A570 After 4000 Hours Exposure to 288°C (550°F) Molten Salt With OH^-, $CO_3^=$ and $SO_4^=$ Trace Contaminants

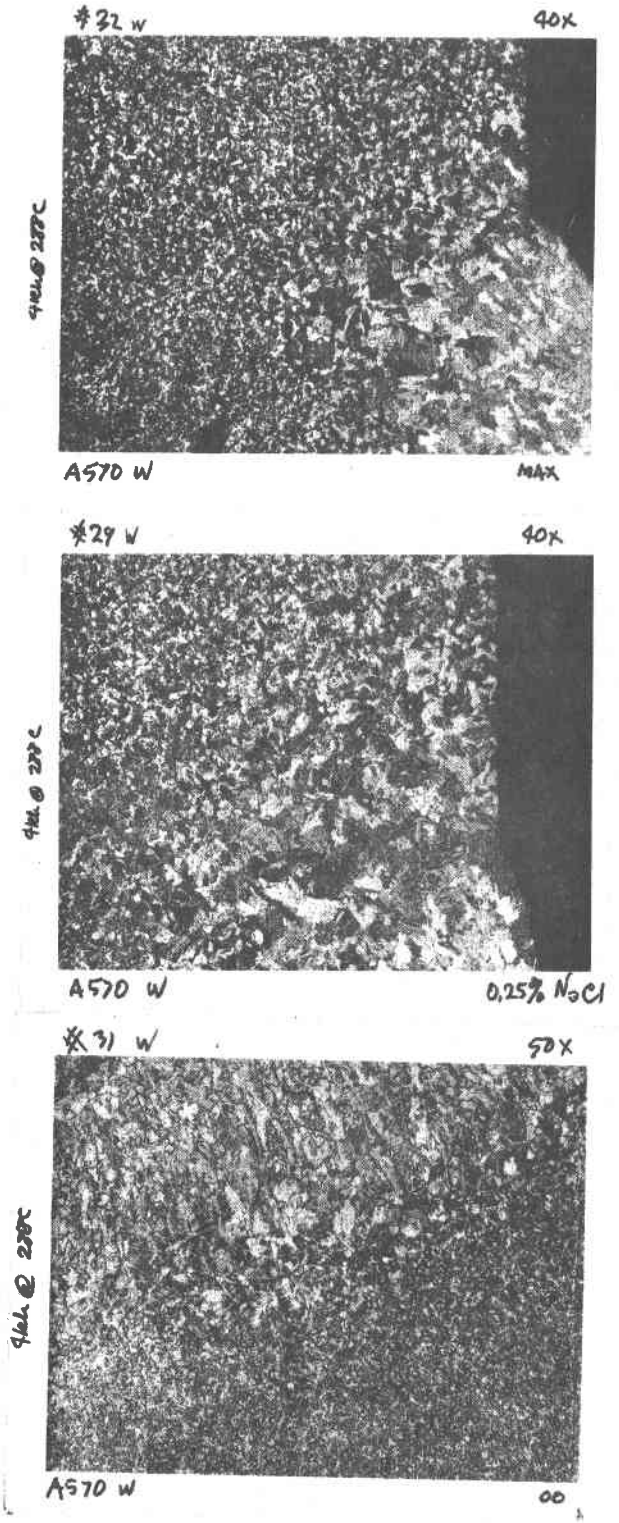

Figure B-26 Micrographs of Welded A570 After 4000 Hours Exposure to 288°C (550°F) Molten Salt With Cl^-, Sum of All Contaminants and No Trace Contaminant Additions

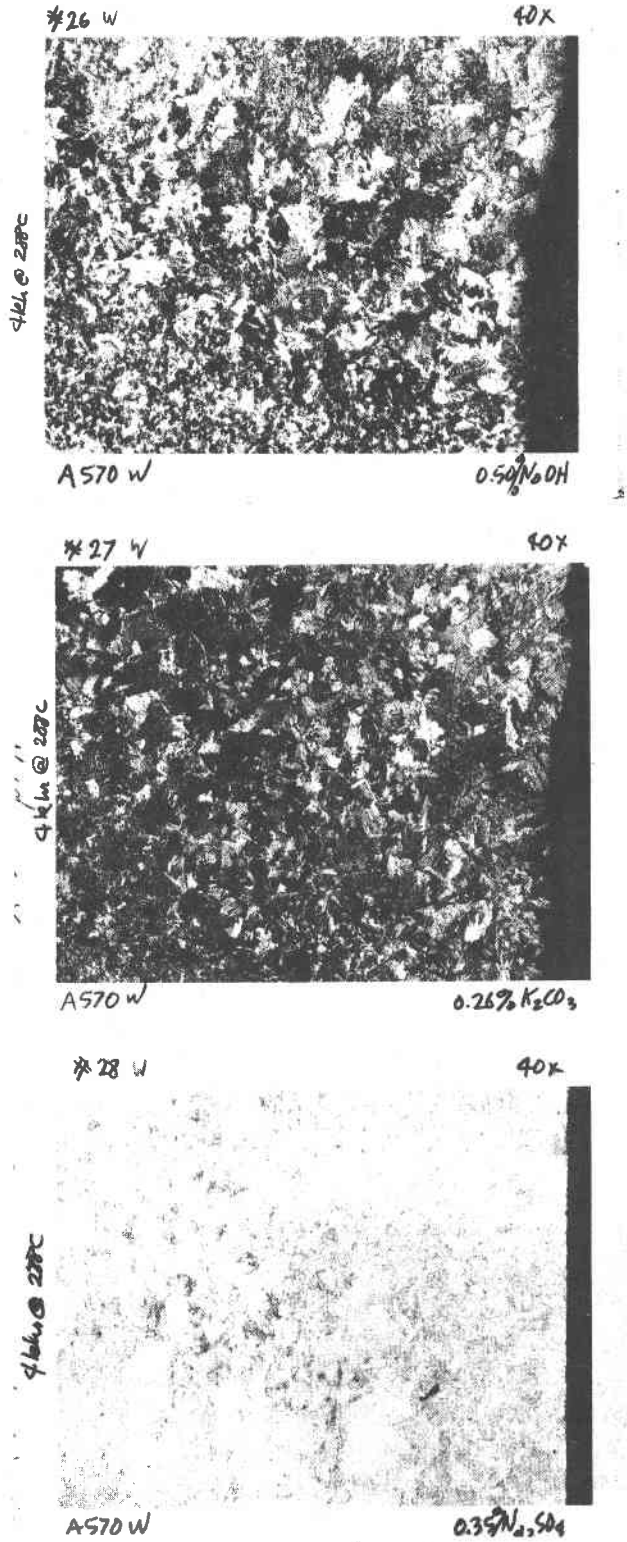

Figure B-27 Micrographs of Welded A570 After 4000 Hours Exposure to 288°C (550°F) Molten Salt with OH^-, $CO_3^=$ and $SO_4^=$ Trace Contaminants

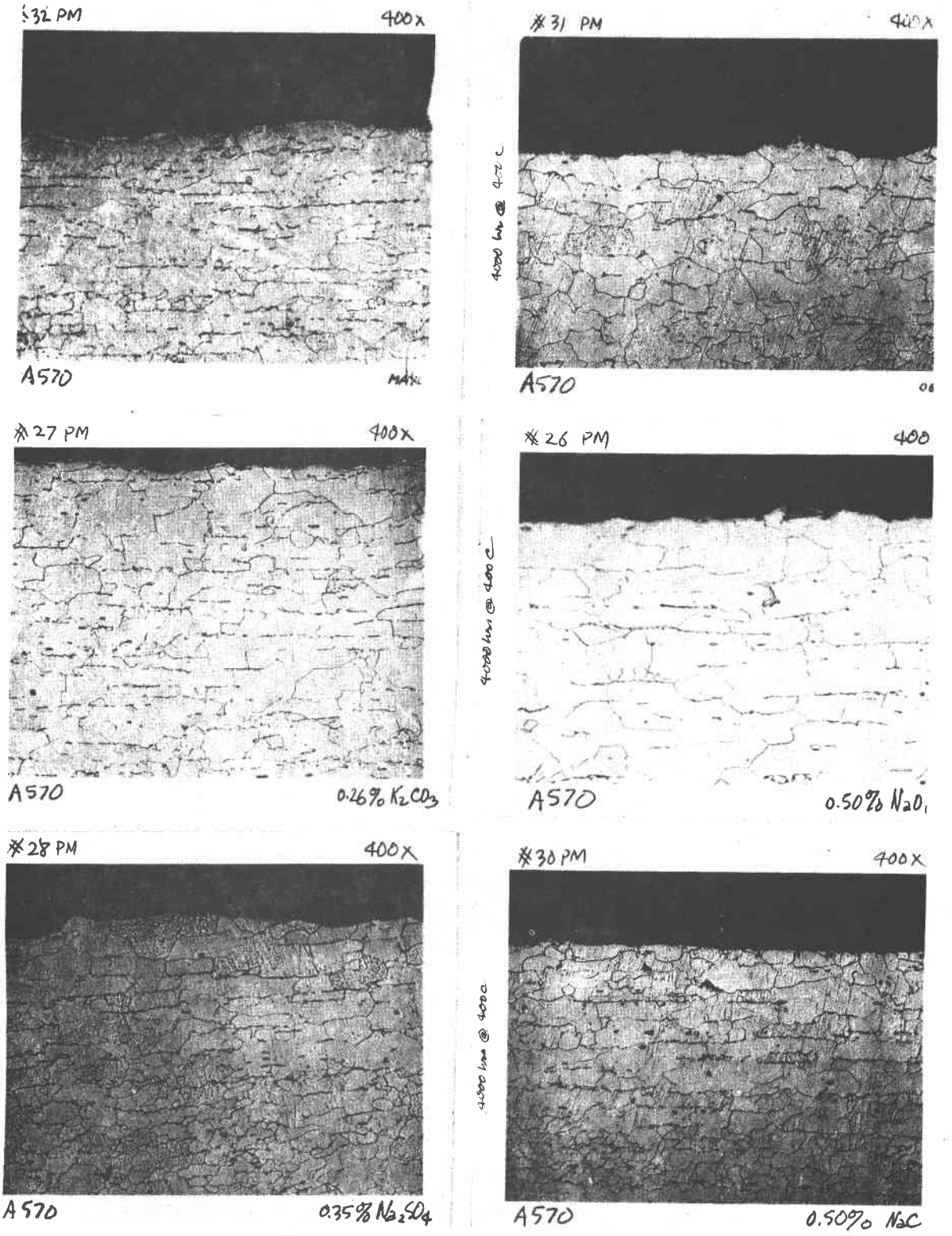

Figure B-28 Micrographs of Parent Metal A570 Coupons After Exposure to 399°C (750°F) Molten Salt for 4000 Hours (All Trace Contaminant Conditions)

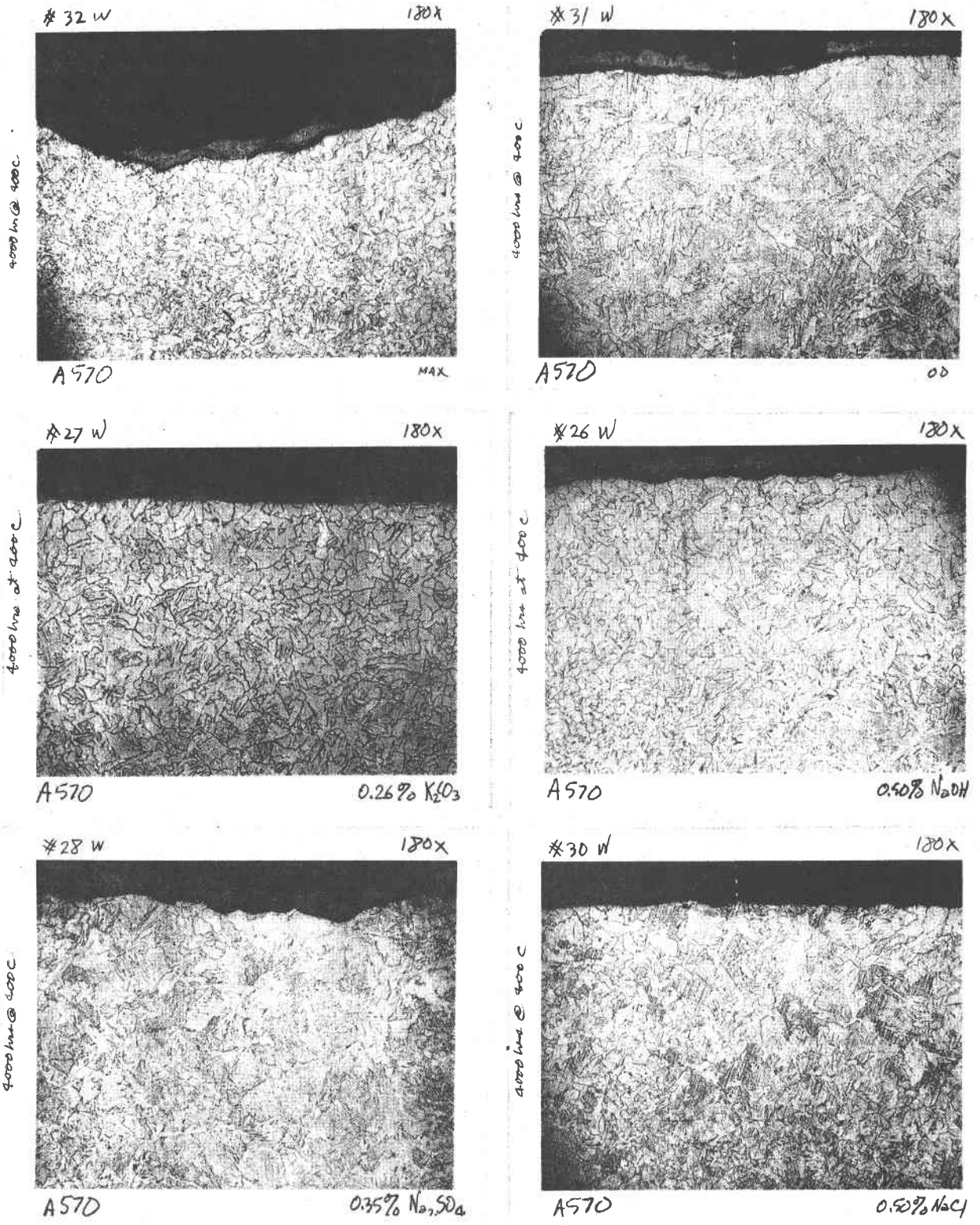

Figure B-29 Micrographs of Welded A570 Coupons After Exposure to 399°C (750°F) Molten Salt for 4000 Hours (All Trace Contaminant Conditions)

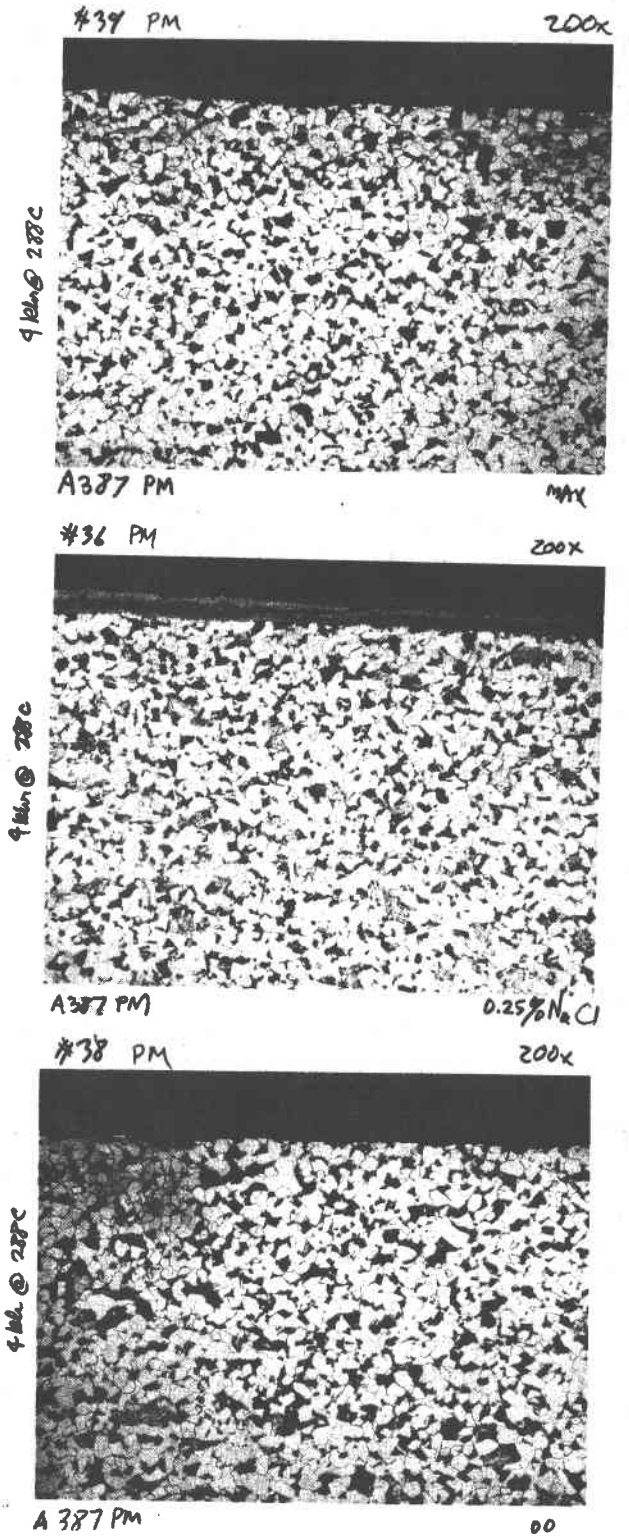

Figure B-30 Micrographs of Parent Metal A387 Coupons After Exposure to 288°C (550°F) Molten Salt With Cl^-, Sum of All Contaminants and No Trace Additions, for 4000 Hours

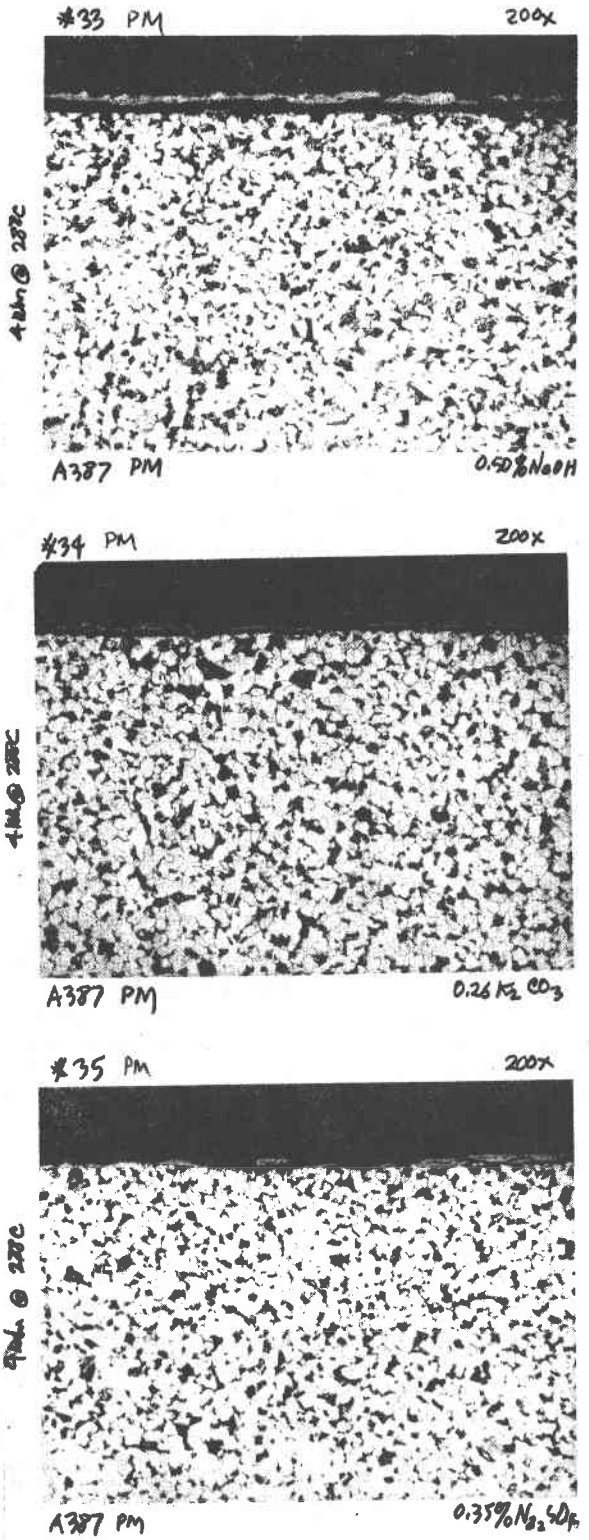

Figure B-31 Micrographs of Parent Metal A387 Coupons After Exposure to 288°C (550°F) Molten Salt With OH^-, $CO_3^=$, and $SO_4^=$ Trace Contaminants

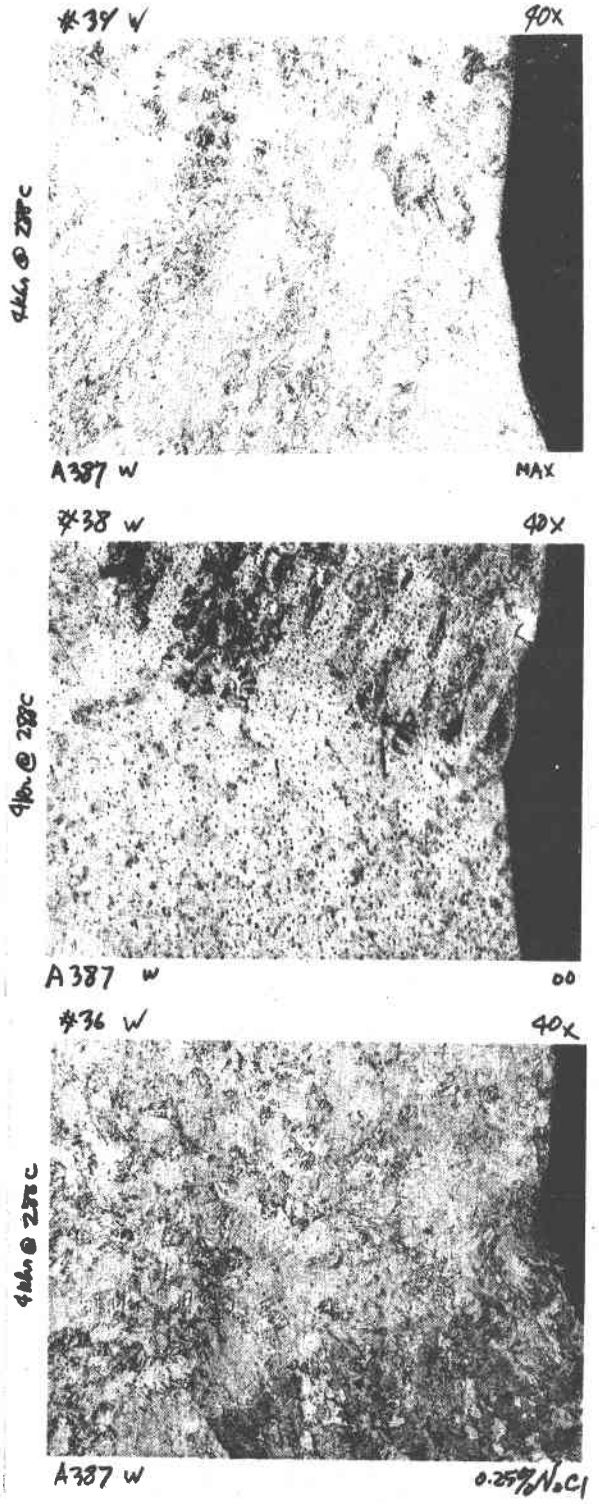

Figure B-32 Micrographs of Welded A387 Coupons After kxposure to 288°C (550°F) Molten Salt With Cl^-, Sum of All Contaminants and No Trace Contaminant Additions for 4000 Hours

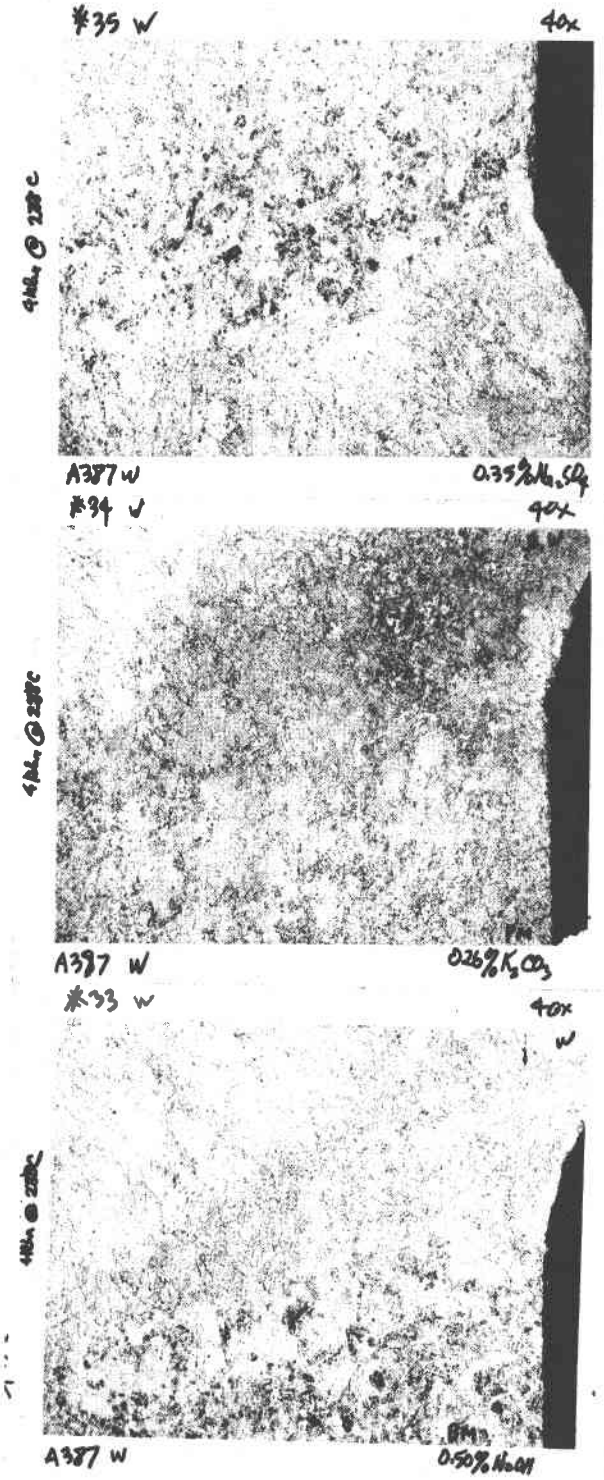

Figure B-33 Micrographs of Welded A387 Coupons After Exposure to 288°C (550°F) Molten Salt With OH^-, $CO_3^=$, and $SO_4^=$ Trace Contaminants for 4000 Hours

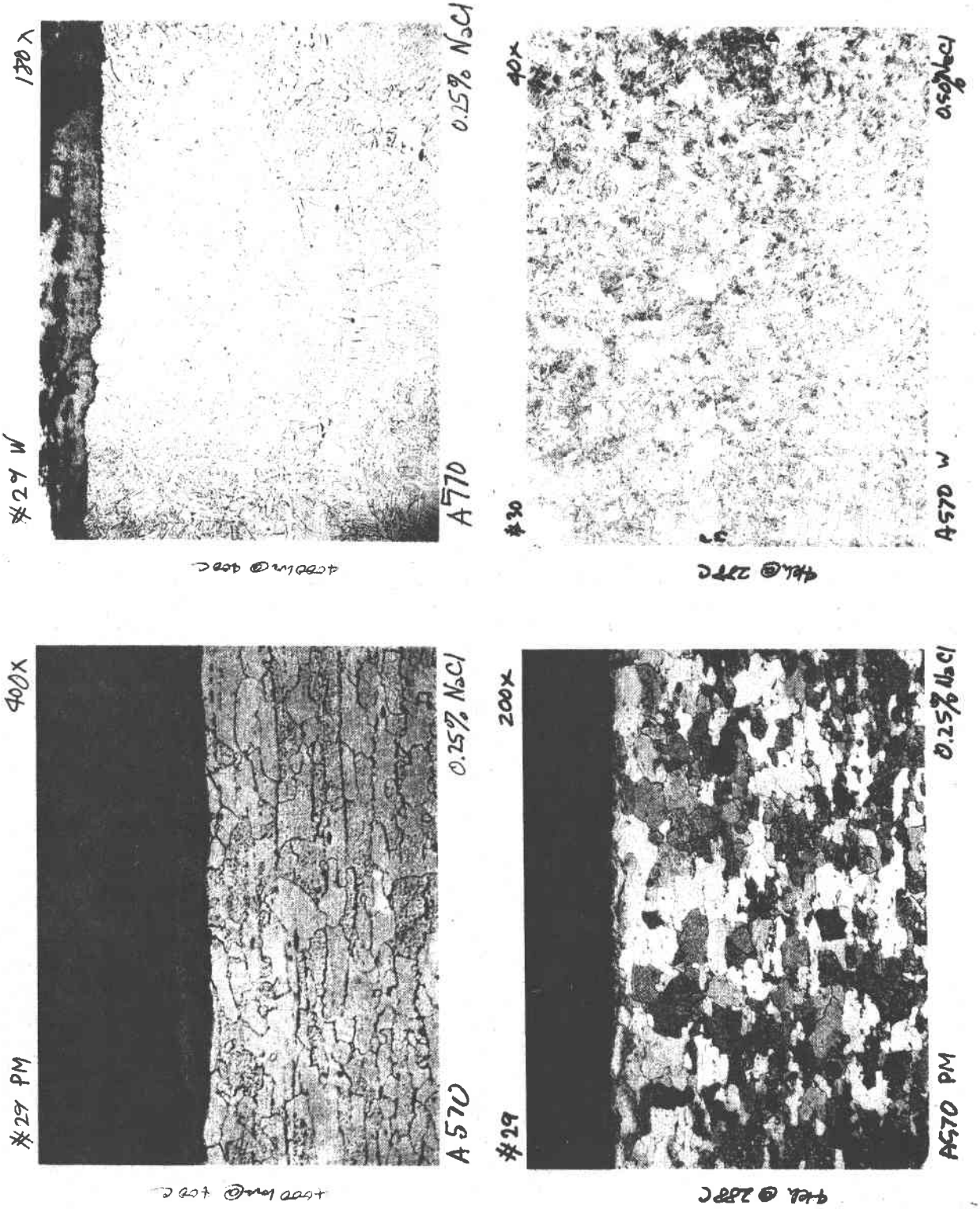

Figure B-34 Comparison of Cl^- Trace Contaminant Additions on Oxide Formation of A570 After Exposure to 288°C and 400°C Molten Salt for 4000 Hours

Description of 30-year Extrapolation Technique for Predicting Metal Loss

Figure B-35 shows a graphical representation of the observed oxidation behavior of materials. As shown, the behavior incorporates cycles of oxide growth and exfoliation with the total metal loss determined by a combination of actual weight loss (via dissolution or micro-sloughing) and metal loss due to oxide conversion.

In general during the oxide growth stage, a protective film is formed which effectively protects the metal from dissolution but allows load-bearing metal loss via metal conversion to oxide. During the exfoliation or flaking cycle, the amount of metal loss is proportional to the amount of oxide lost, since it is a compound of iron and oxygen. The metal loss during oxide conversion is determined by the stoichiometry of the oxide compound formed (see Table B-9). This assumes there is no selective dissolution of alloy elements during the oxide exfoliation cycle. This was confirmed from the dynamic loop results at the temperatures studied, with the exception of I800 at 482°C (900°F) where Cr depletion was observed. Molten salt is a relatively benign environment as compared to acid solutions, where dissolution may be the controlling mechanism.

The oxidation behavior observed in this investigation was of three general types, marked a, b, and c on Figure B-36. It should be noted that these three types of weight gain-loss behaviors were all parts of a generalized behavior, but highly alloy-, temperature-, and salt composition dependent. In addition, the test duration period also dictated the type of extrapolation method employed to predict 30-year metal loss. These methods yield only a rough estimate of the metal loss (to be used primarily for comparison purposes) which is probably conservative, since it assumes a worst-case behavior.

Method a:

For linear Δ-t results (i.e., 347 SS, Figure IV-5), the slope $mg/cm^2/hr$ at the test duration is found and multiplied by 263,000 hr to give a total extrapolated 30 year weight gain (linear extrapolation), i.e.,: 347 PM in $C\ell^-$ (Figure IV-5)

$$\text{slope } \left(\frac{mg/cm^2}{hr}\right) = \frac{1.13 \text{ mg/cm}^2}{4000 \text{ hr}} = 2.83 \times 10^{-4} \frac{mg/cm^2}{hr}$$

$$2.83 \times 10^{-4} \frac{mg/cm^2}{hr} \times 263{,}000 \text{ hr} = 75 \text{ mg/cm}^2$$

Using the conversion factor for 347 in Table B-9, column 2 (weight gain):

$$75 \text{ mg/cm}^2 \times 0.00335 \text{ mm/mg/cm}^2 = 0.25 \text{ mm}$$

Method b:

For parabolic-cubic Δ-t weight gain behavior, the method of extrapolation assumed complete exfoliation to bare metal (see Figure B-37) with no time allowed for exfoliation. Log Δ-log t graphical representation of the Δ-t

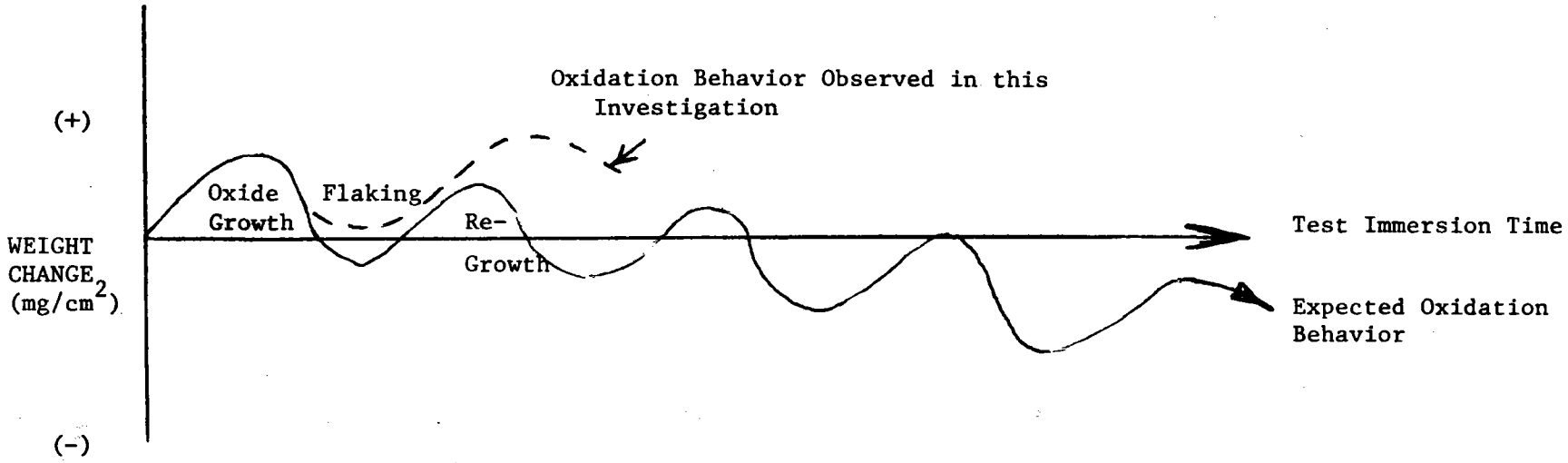

Figure B-35 Expected and Observed Weight Gain-Weight Loss Oxidation Behavior

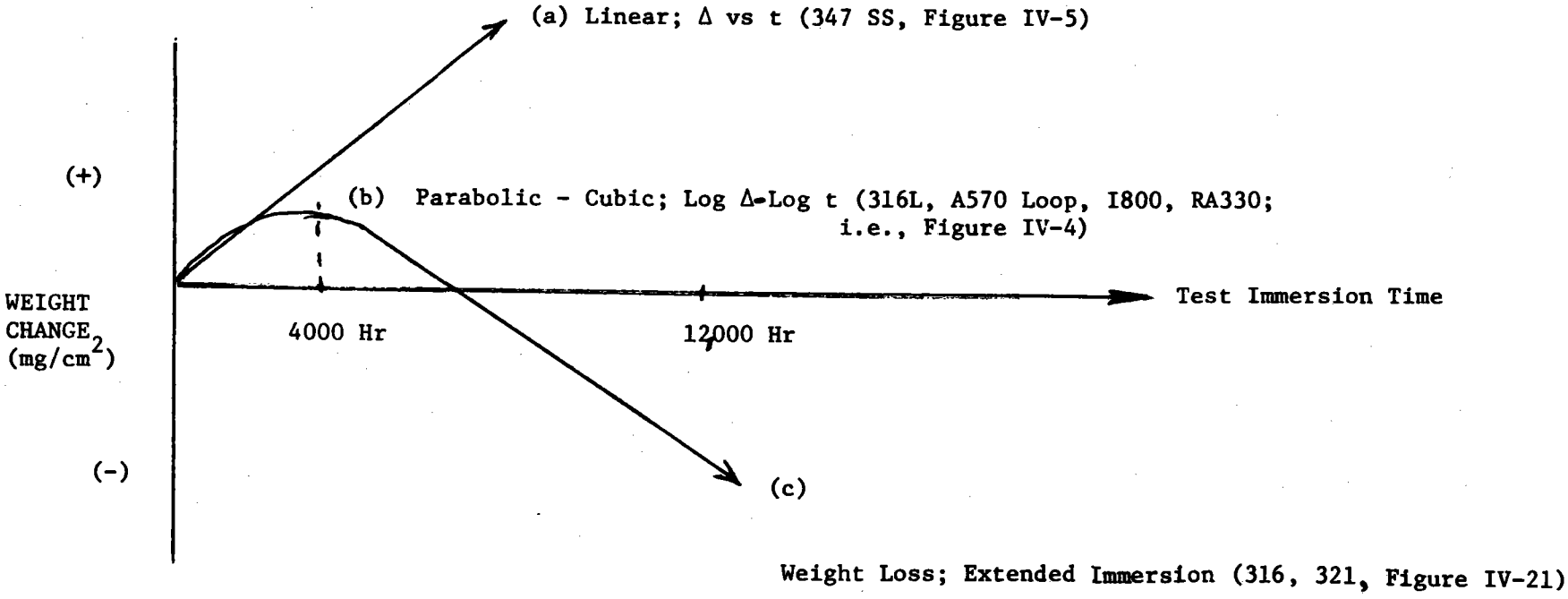

Figure B-36 Three Types of Extrapolations Used

plots was used to determine the peak weight gain Δ_p and weight gain period t_p. The use of these log-log plots simplified the determination of the peak (Δ_p) of the parabolic-cubic curves (see Figure B-38). Once Δ_p and t_p were found, the number of weight gain cycles N was calculated:

$$N = \frac{263{,}000 \text{ hr}}{t_p \text{ (hr)}}$$

The total weight gain/30 years was then determined by

$$\text{Weight gain (mg/cm}^2\text{)/30 years} = \Delta_p \text{ (mg/cm}^2\text{)} \times N$$

By mathematical manipulation this technique reduces to determining the slope (Δ_p/t_p) at the attainment of a level weight gain and then extrapolating to 30 years. After the total weight gain/30 years is calculated, the conversion factor for weight gain (Table B-9) is used to produce metal reduction.

i.e.,: I800 PM in $C\ell^-$ (Figures IV-4 and IV-6)

$$\left.\begin{aligned} t_p &= 3000 \text{ hr} \\ \Delta_p &= 0.7 \text{ mg/cm}^2 \end{aligned}\right\} \quad \text{Figure IV-6}$$

$$N = \frac{263{,}000 \text{ hr}}{3000 \text{ hr}} = 105 \text{ weight gain cycles}$$

$$\text{Weight gain (mg/cm}^2\text{)/30 years} = 0.7 \text{ mg/cm}^2 \times 105 \text{ cycles} = 74 \text{ mg/cm}^2$$

$$\text{Metal thickness reduction} = 74 \text{ mg/cm}^2 \times 0.00335 \frac{\text{mm}}{\text{mg/cm}^2} = \underline{\underline{0.25 \text{ mm}}}$$

Method c:

This is typified by continual drastic weight loss with time, after an initial oxide growth, such as seen in the extended immersion and fluid loop results.

For the extended immersion tests, after an initial weight gain (oxide growth) up to 4000 hr, an exended weight loss occurred. The method of analysis used was (1) the worst case linear weight loss slope extrapolated to 30 years; (2) average weight loss using maximum weight loss and time; and (3) Method b.

For 316 stainless steel (Figure IV-21),

$$\frac{\Delta \text{ wt loss}}{\Delta t} = \frac{20 - 7.5 \text{ (mg/cm}^2\text{)}}{11{,}000 - 7000 \text{ (hr)}} = 0.00313 \text{ mg/cm}^2\text{/hr}$$

for 30 years 821.9 mg/cm^2

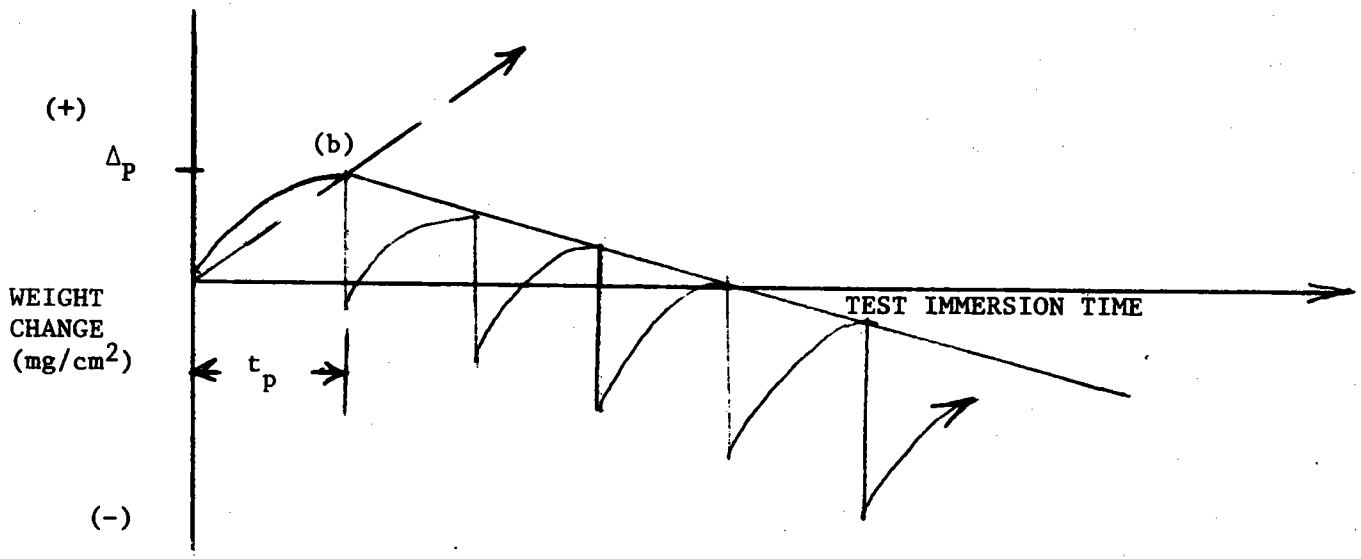

Figure B-37 Graphical Method (b) of Weight Gain Extrapolation

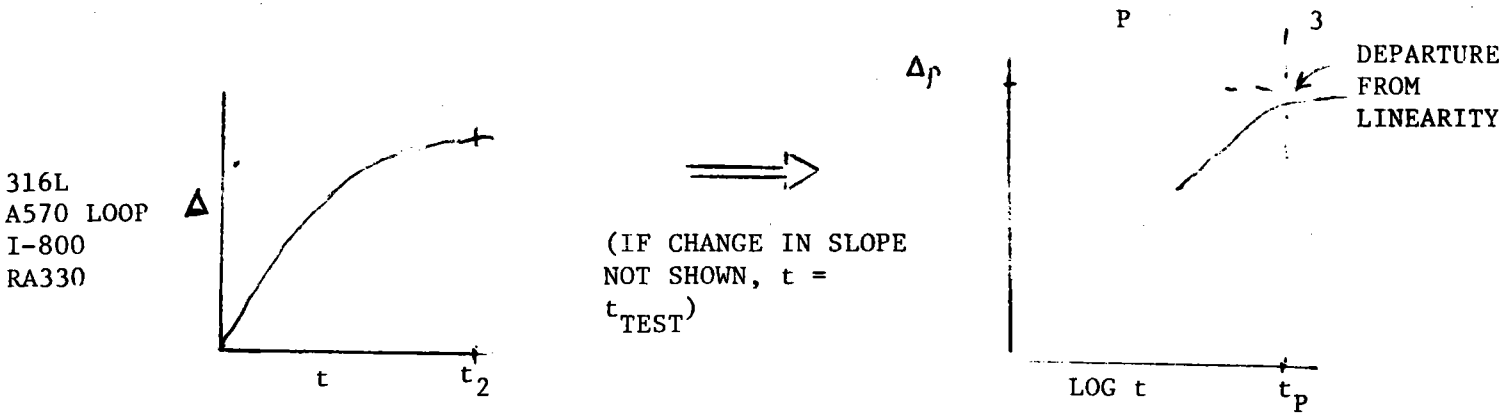

Figure B-38 Method (b) of Weight Gain Extrapolation

Metal reduction (using Table B-9, column 1),

$$821.9 \text{ mg/cm}^2 \times .00126 \frac{\text{mm}}{\text{mg/cm}^2} = 1.03 \text{ mm}$$

$$\frac{\Delta \text{ Wt loss}}{\Delta t} / 30 \text{ years} = 488 \text{ mg/cm}^2$$

$$\text{Metal reduction} = 488 \text{ mg/cm}^2 \times .00126 \frac{\text{mm}}{\text{mg/cm}^2} = .61 \text{ mm}$$

Table B-9 Table of Alloy Constants Used to Convert Weight Gain/ Loss into Metal Thickness Reduction

ALLOY	WEIGHT LOSS[1] mm of Metal Removal per 1 mg/cm^2 of Metal Loss by Actual Weight Loss	WEIGHT GAIN[2] mm of Metal Loss by Conversion to 1 mg/cm^2 of Oxide by Oxide Formation
I800	0.00125	0.0035
316L	0.00125	0.0035
316	0.00126	0.0035
347	0.00123	0.0035
A286	0.00126	0.0035
A570	0.00127	0.0035
A516	0.00127	0.0035
A387	0.00127	0.0035
RA330	0.00124	0.0035

Description of Calculations of Above Conversion Factors:

1) Metal removal by actual weight loss (assuming negligible oxide formation):

For example, for A570, (≈100 wt % Fe) $\rho_{A570} \approx \rho_{Fe} = 7.86 \text{ gm/cm}^3$

For a 1 cm^2 surface area, there is 7.86 gm/cm of material:

$$7.86 \frac{\text{gm}}{\text{cm}} \times \frac{\text{cm}}{10 \text{ mm}} = .768 \frac{\text{gm}}{\text{mm}} \times 1000 \frac{\text{mg}}{\text{gm}} = 786 \frac{\text{mg}}{\text{mm}}$$

$0.00127 \frac{\text{mm}}{\text{mg}}$ of A570 linear metal loss.

2) Metal removal by conversion to an oxide by weight gain:

For example for A570 (≈100 wt % Fe), it is assumed that Fe_3O_4 is the prevalent oxide formed.

For a weight gain of 1 mg/cm^2 (oxygen, main component of weight gain)

- the percent of Fe in Fe_3O_4 is ~72.4%
- the percent of O in Fe_3O_4 is ~27.6%

(by atomic weight ratios).

To find the mass/unit area of Fe corresponding to a 1 mg/cm weight gain (of oxygen):

$$0.276 \times (\text{Wt of } Fe_3O_4/cm^2) = 1 \text{ mg/cm}^2$$

$$\text{so Wt of } Fe_3O_4/cm^2 = 3.618 \text{ mg/cm}^2$$

$$0.724 \times (\text{Wt of } Fe_3O_4/cm^2) = \text{Wt of Fe/cm}^2$$

so Wt of Fe_3O_4/cm^2 = 2.619 mg/cm^2 for a 1 mg/cm^2 weight gain due to oxygen incorporation in the oxide.

From 2), 1 mg/cm of weight gain (oxygen) corresponds to a 2.619 mg/cm conversion of Fe from the metal substrate. Therefore, the linear metal loss corresponding to 2.619 mg/cm^2 of Fe is

$$2.619 \text{ mg/cm}^2 \times \frac{\text{cm}^3}{7.86 \text{ gm}} \times \frac{\text{gm}}{1000 \text{ mg}} \times \frac{10 \text{ mm}}{\text{cm}} = 0.0033 \text{ mm}$$

1 mg/cm^2 of weight gain from oxygen incorporation in the form of Fe_3O_4 translates into a metal conversion of 2.62 mg/cm^2 of Fe or a metal reduction of 0.0033 mm.

This assumes that Fe_3O_4 is the only oxide formed. For I800, 316, 316L, 347, A286, and RA330, the oxides also include Cr_2O_3 and NiO_2, which are lighter, resulting in less metal loss. We have conservatively assumed for this analysis, however, that all of the oxide is Fe_3O_4, as the resulting difference is very small.

APPENDIX C - LIST OF FIGURES

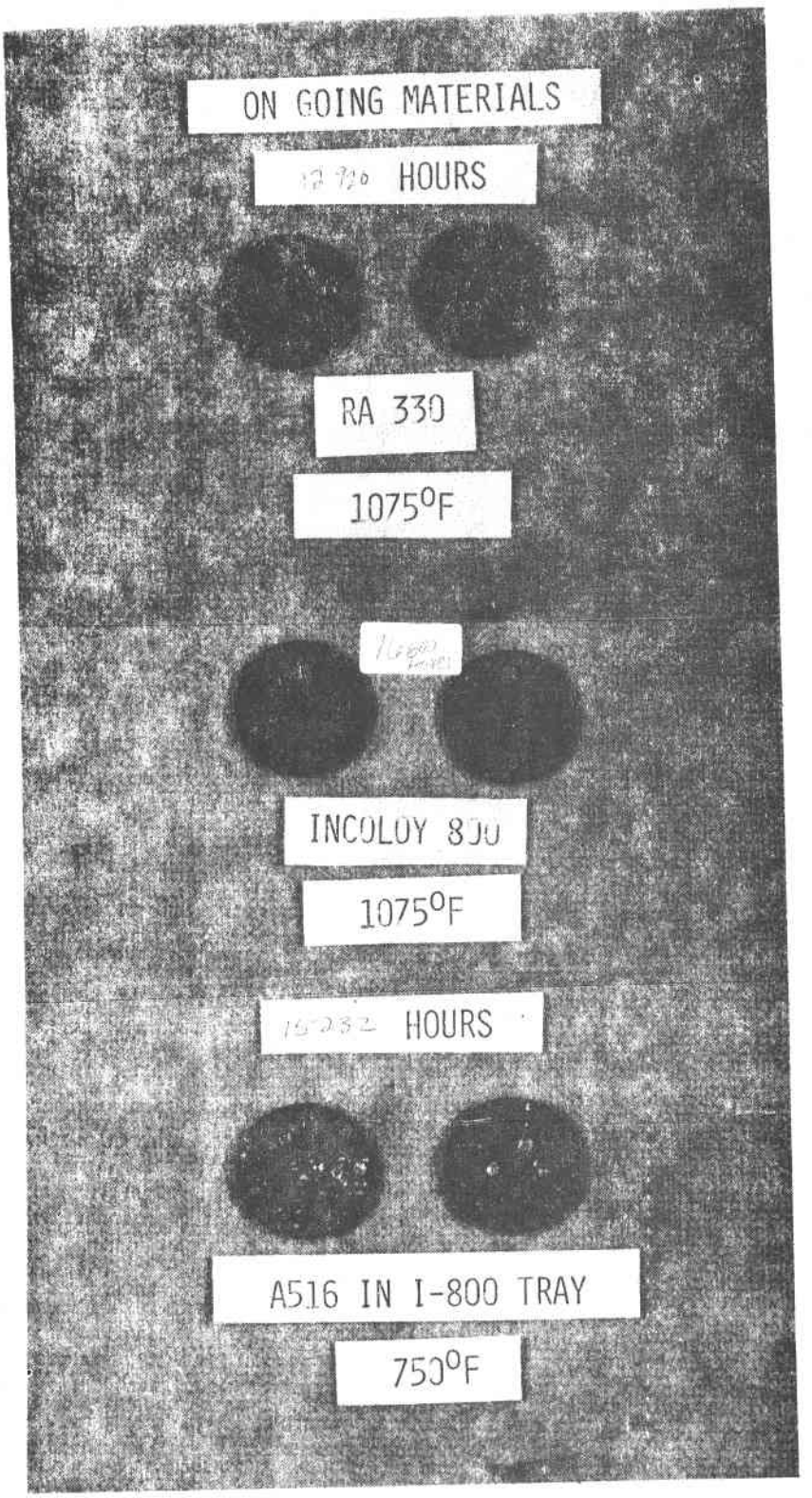

Figure C-1 *Photographs of RA330, I800 and A516 (in I800 Tray) Parent Metal Coupons After Extended Immersion Molten Salt Exposure*

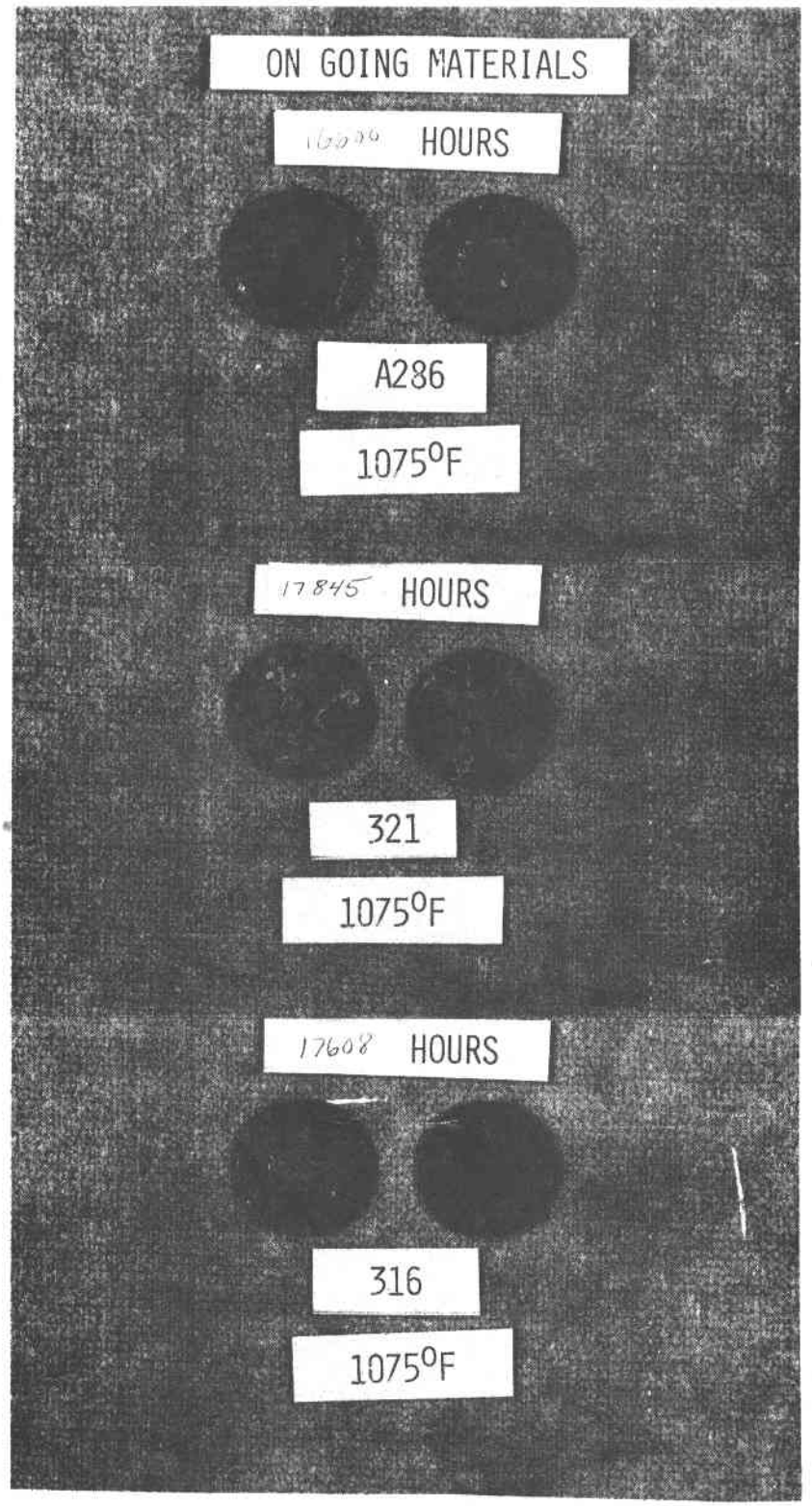

Figure C-2 Photographs of A286, 321 and 316 (In I800 Tray) Parent Metal Coupons After Extended Immersion Molten Salt Exposure

APPENDIX D

SUPPORTING DATA FOR SECTION IV-C

APPENDIX D - LIST OF FIGURES

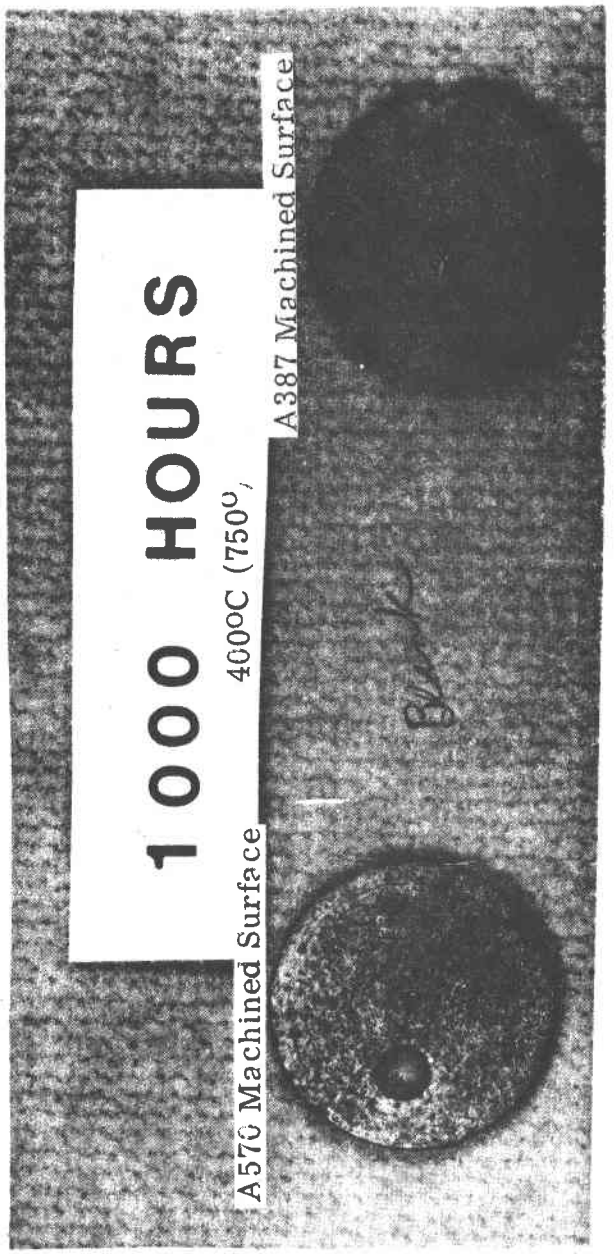

Figure D-1 Photographs of Machined Surfaces of Parent Metal A570 and A387 Coupons After 1000 Hour Molten Salt Exposure at 400°C (750°F)

APPENDIX E

SUPPORTING DATA FOR SECTION V-A

APPENDIX E - LIST OF FIGURES

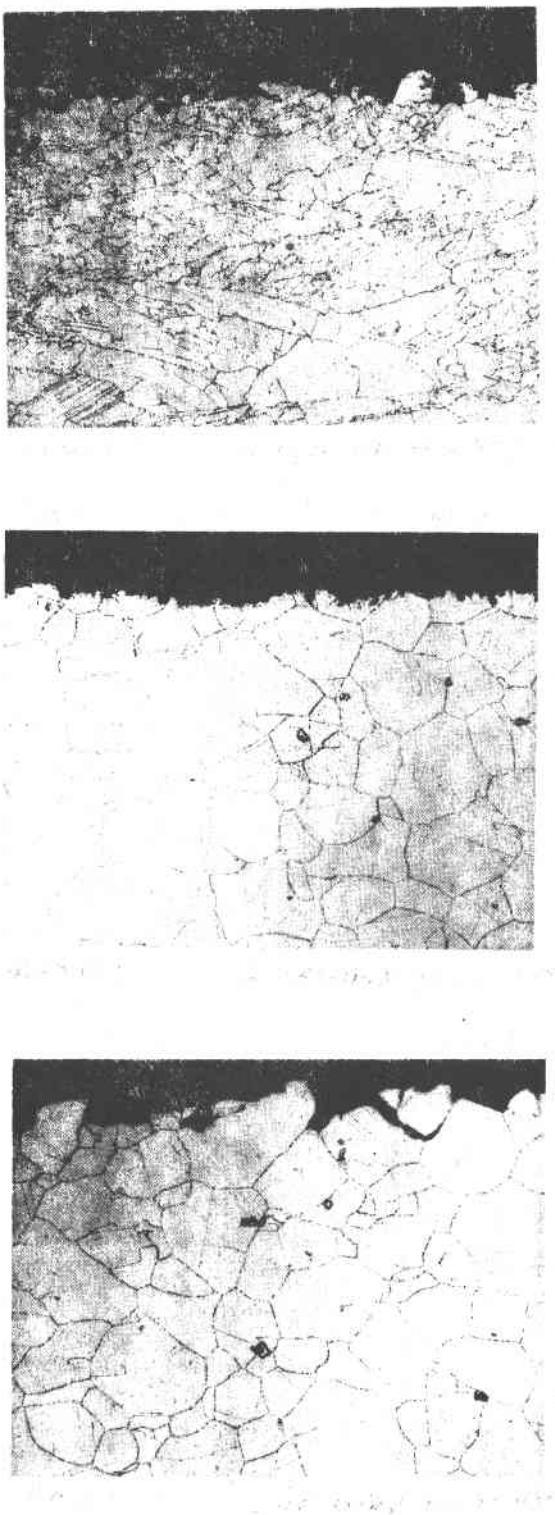

Figure E-1 Micrographs of I800 and RA330 Parent Metal Tensile Specimens With HNO -HF Acid Treatment After 8 Month Air and 9 Month Molten Salt Exposure at 580°C (1075°F)

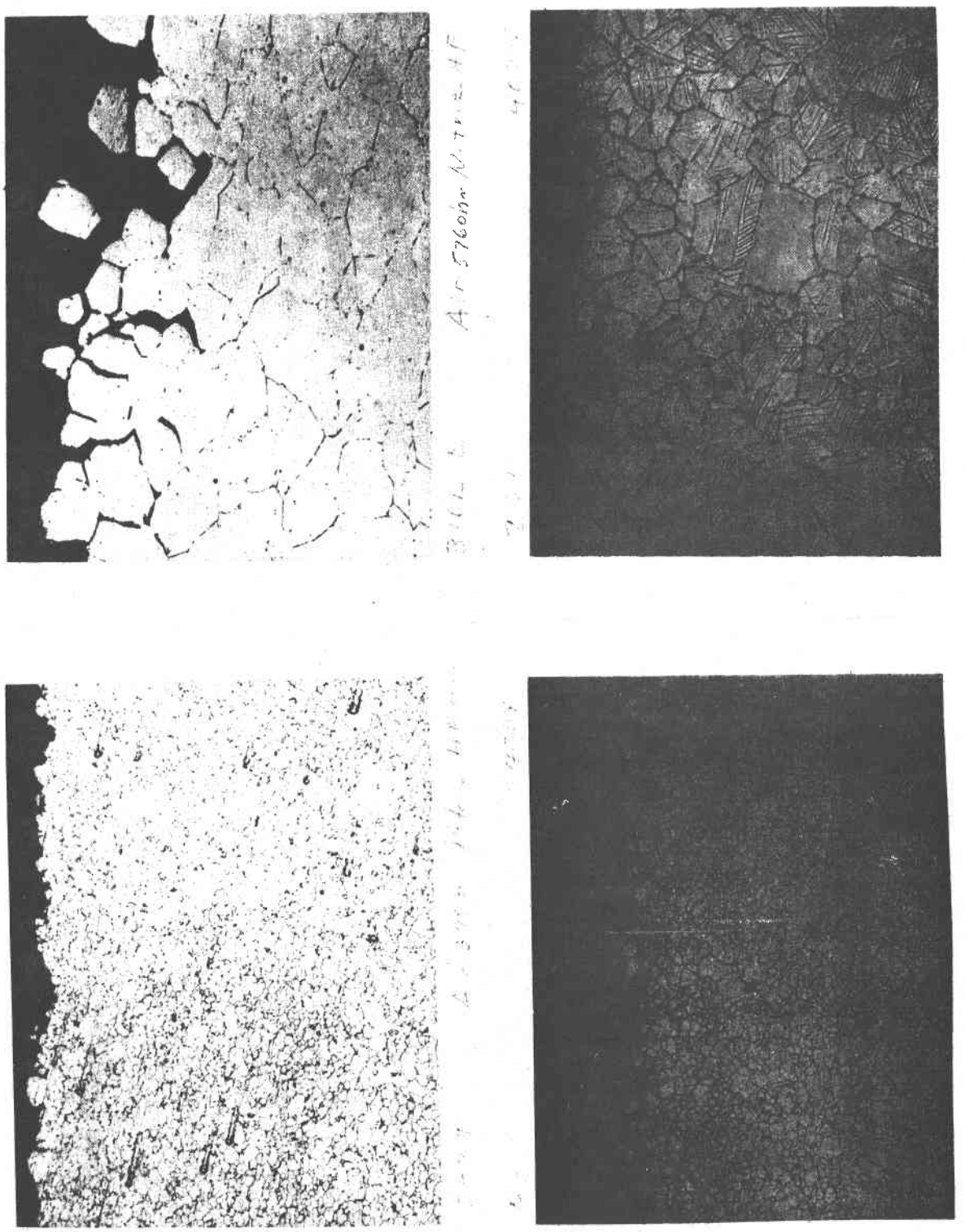

Figure E-2 Micrographs of 347 and 316L Parent Metal Tensile Specimens With HNO_3-HF Acid Treatment After 8 Month Air and 9 Month Molten Salt Exposure at 580°C (1075°F)

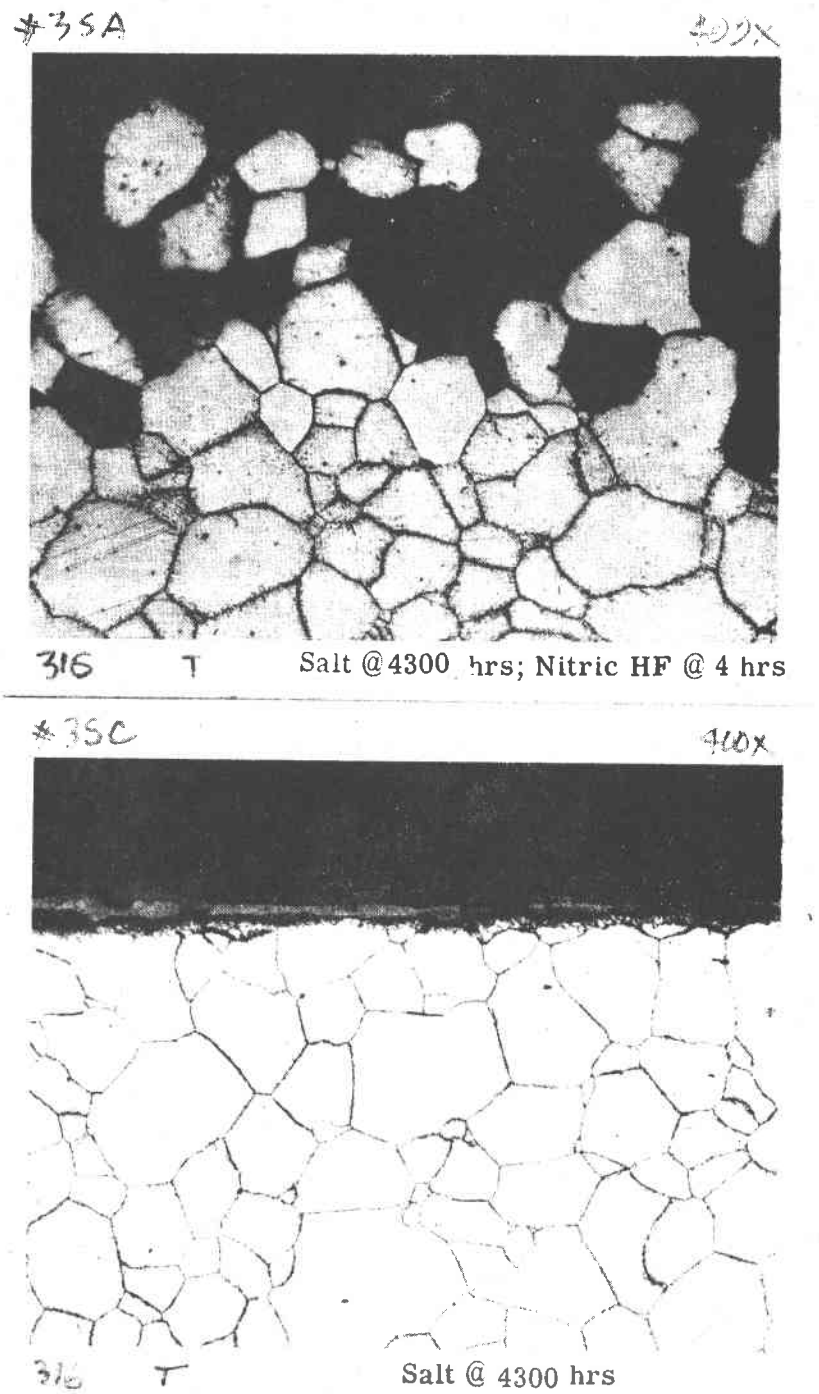

Figure E-3 Micrographs of 316 Parent Metal Tensile Specimens After 4300 Hour Salt Exposure at 580°C With and Without Prior HNO_3-HF Acid Treatment

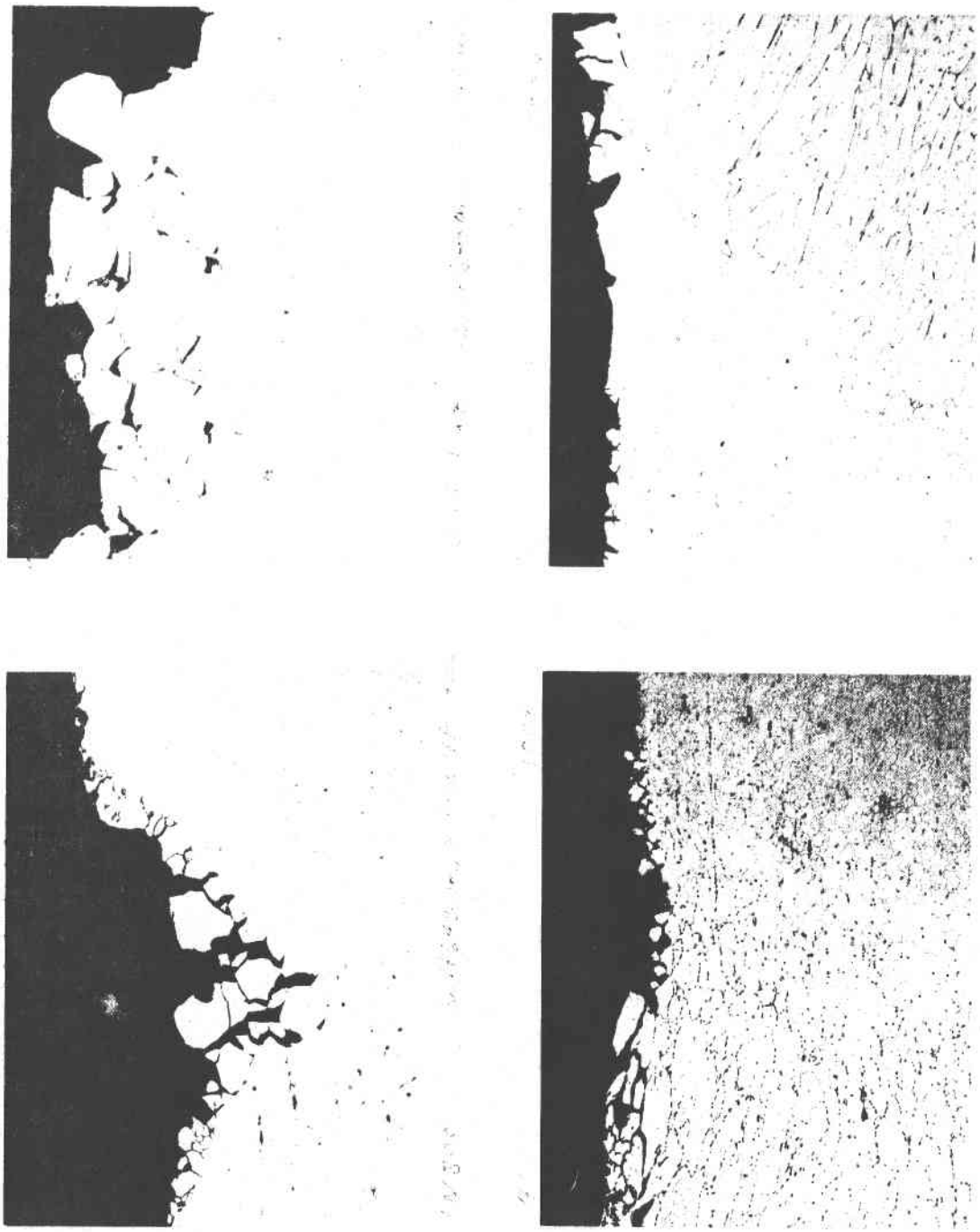

Figure E-4 Micrographs of Welded I800, RA330, 316L and 347 Tensile Specimens With HNO_3-HF Acid Treatment Before 9 Month 580°C Salt Exposure

APPENDIX F

SUPPORTING DATA FOR SECTION IV-B

APPENDIX F - LIST OF FIGURES

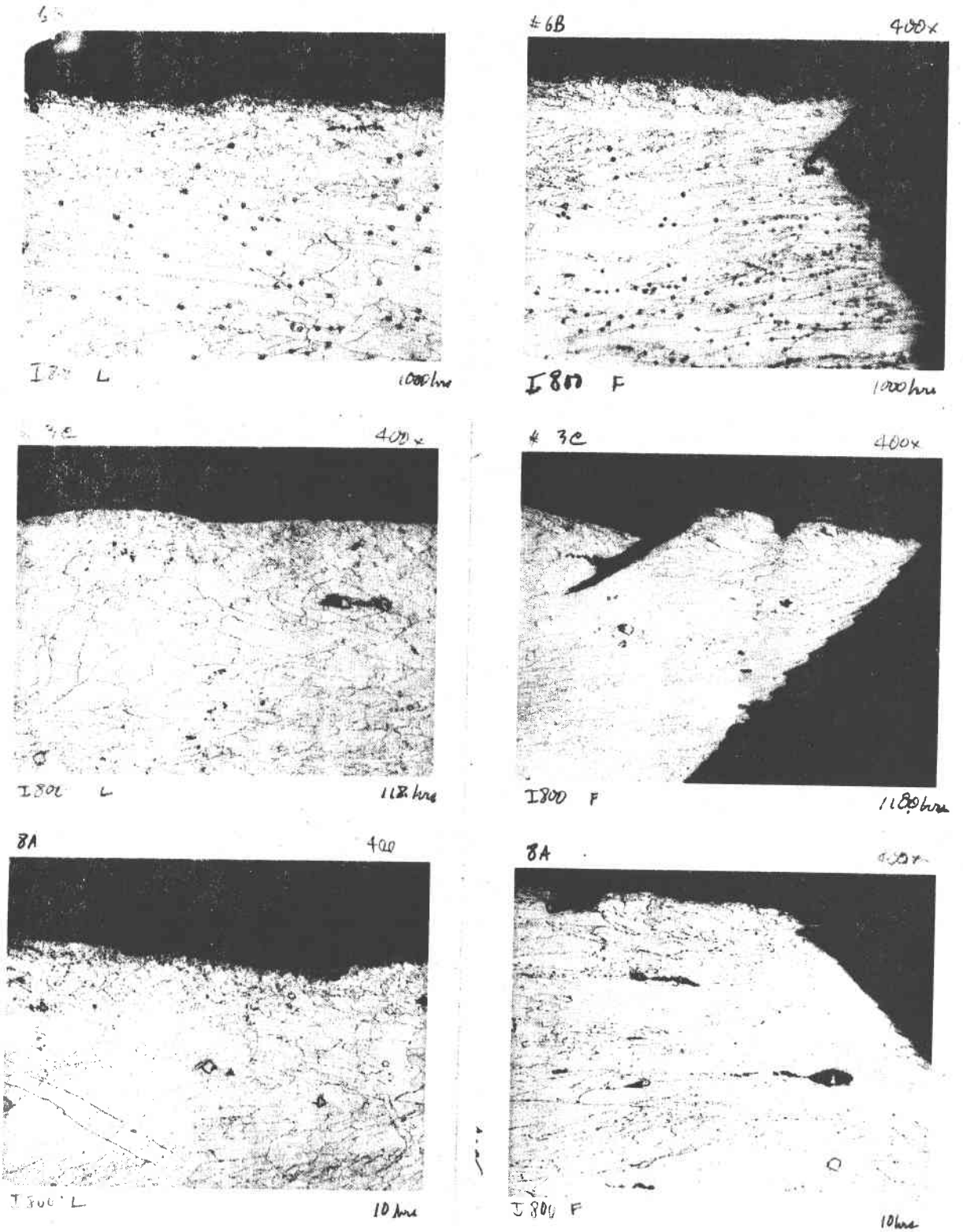

Figure F-1 Micrographs of I800 Parent Metal Creep Specimens (In Molten Salt) After Room Temperature Tensile Testing, as a Function of Creep Loading Time

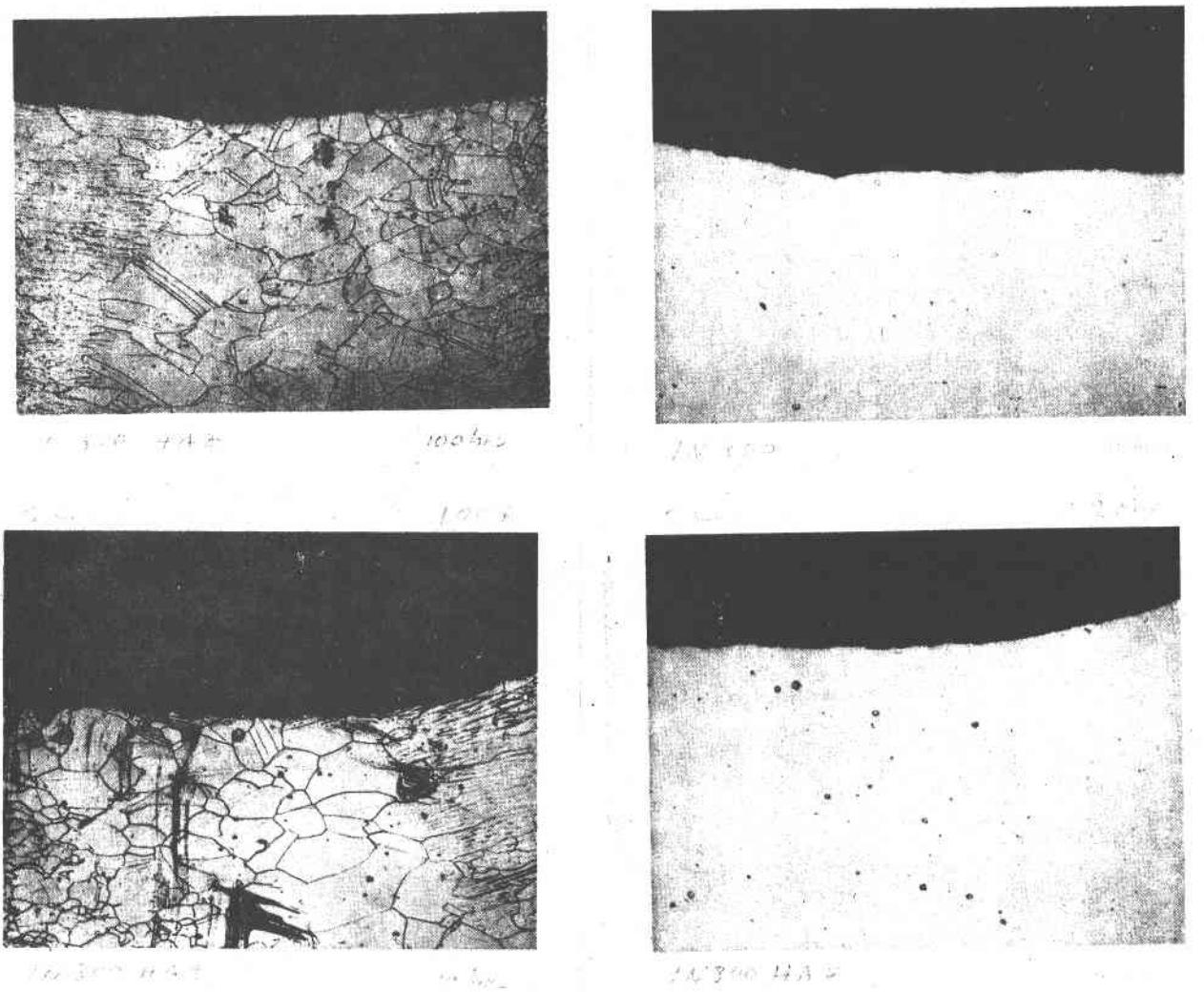

Figure F-2 Micrographs of I800 Welded Metal Creep Specimens (In Molten Salt) After Room Temperature Tensile Testing, as a Function of Creep Loading Time

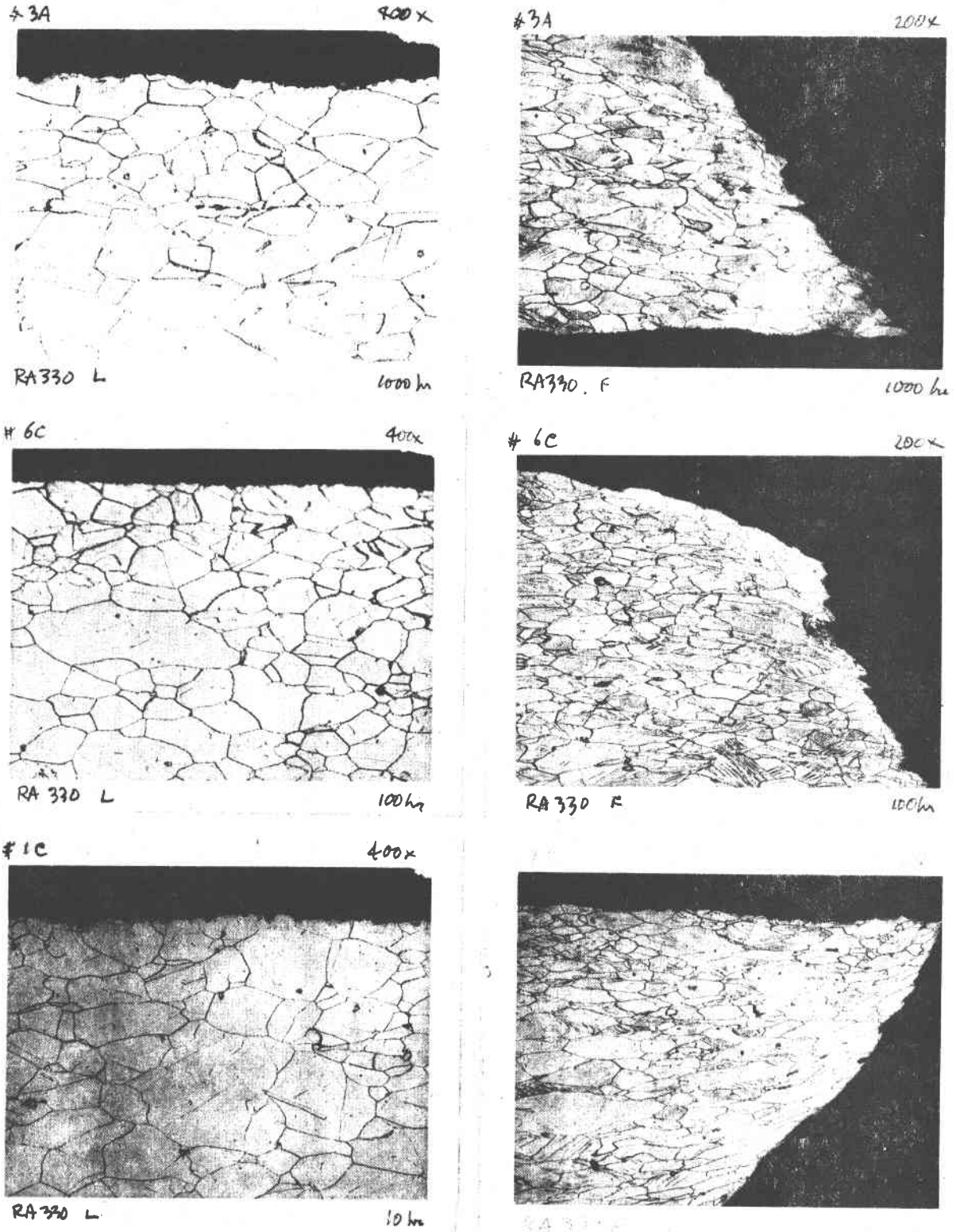

Figure F-3 Micrographs of RA330 Parent Metal Creep Specimen (In Molten Salt) After Room Temperature Tensile Testing, as a Function of Creep Loading Time

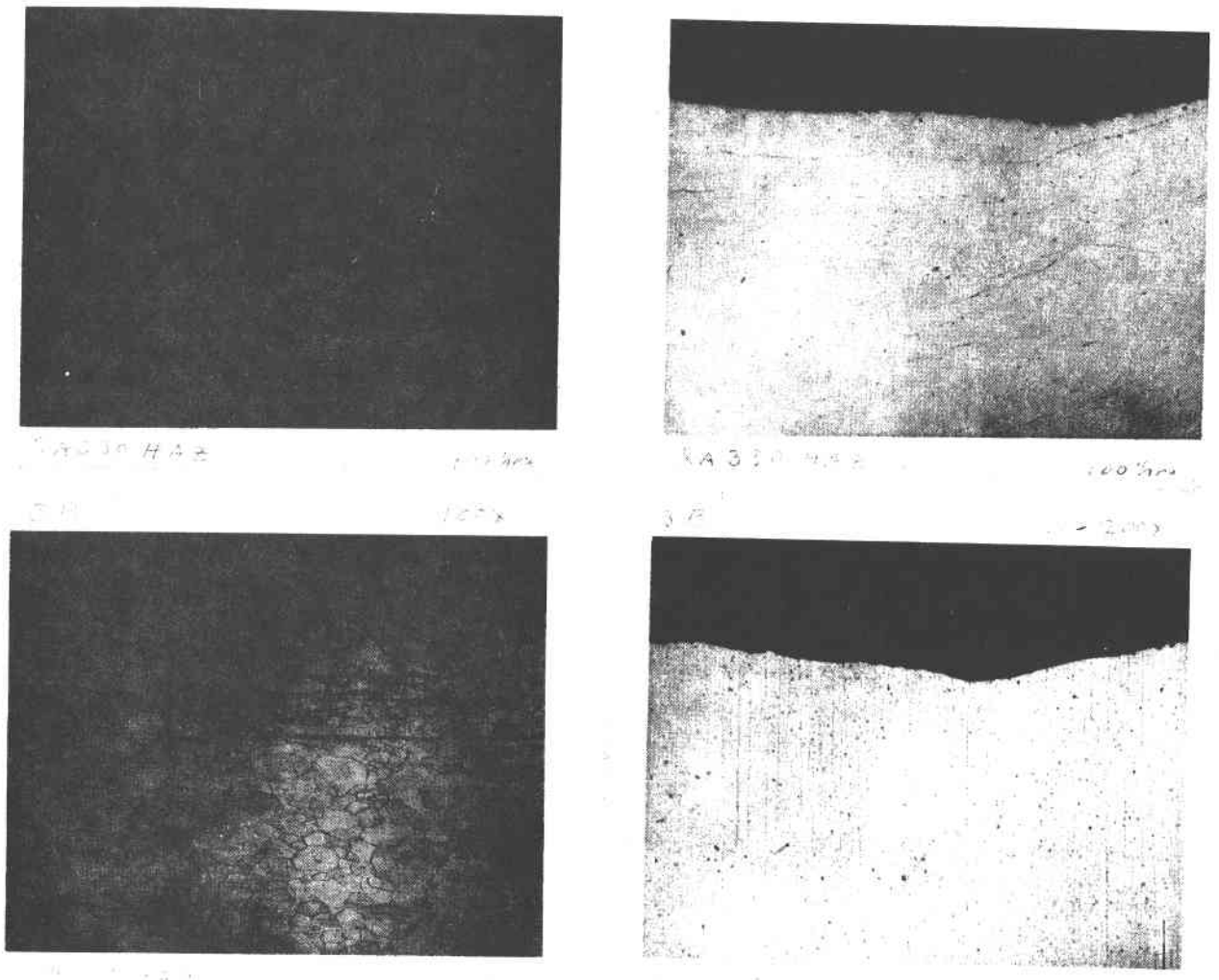

Figure F-4 Micrographs of RA330 Welded Metal Creep Specimens (In Molten Salt) After Room Temperature Tensile Testing, as a Function of Creep Loading Time

APPENDIX G

SUPPORTING DATA FOR SECTION V-D

APPENDIX G - LIST OF FIGURES

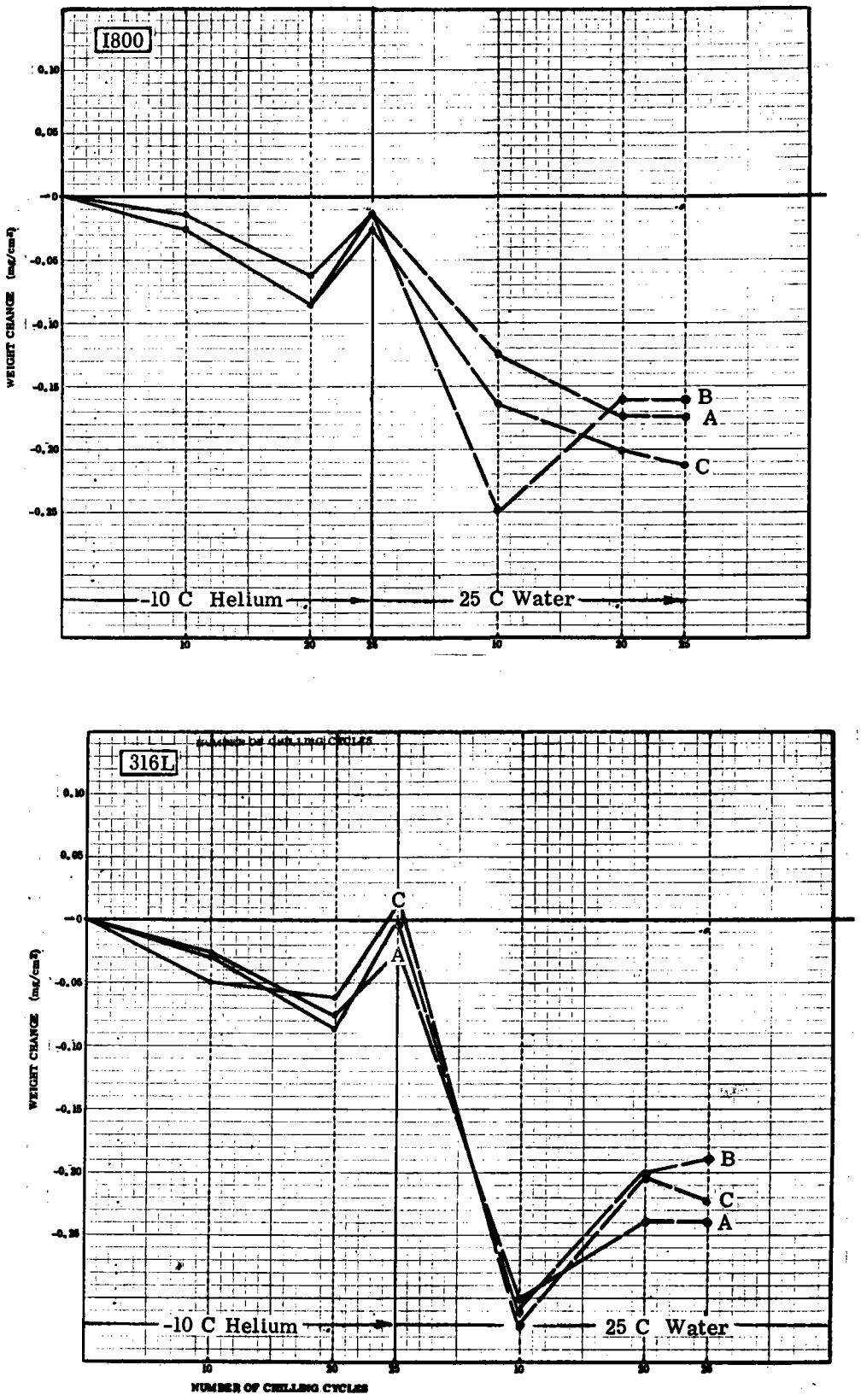

Figure G-1 Weight Change vs Number of Chilling Cycles for Thermal Cycling of I800 and 316L

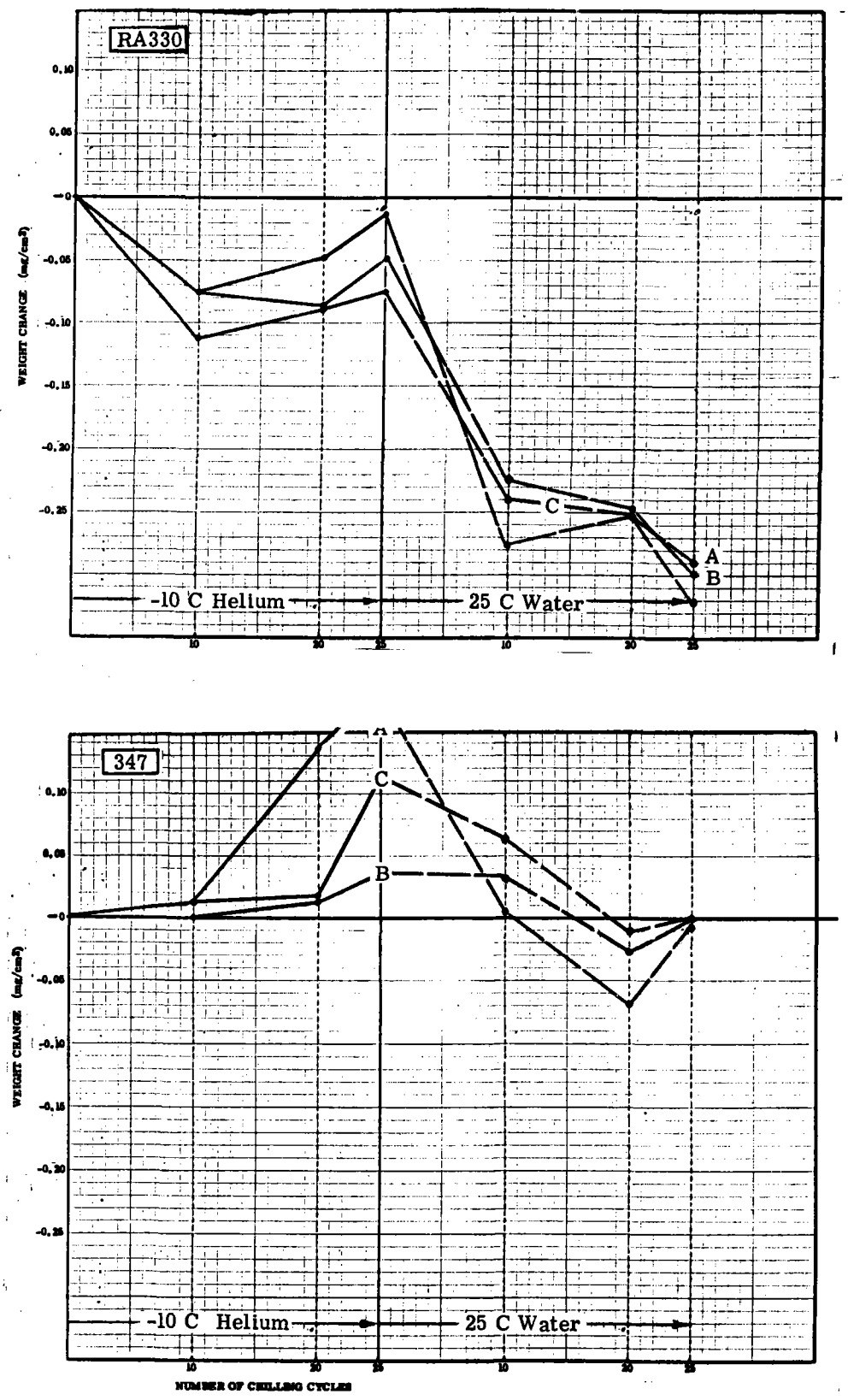

Figure G-2 Weight Change vs Number of Chilling Cycles for Thermal Cycling of RA330 and 347

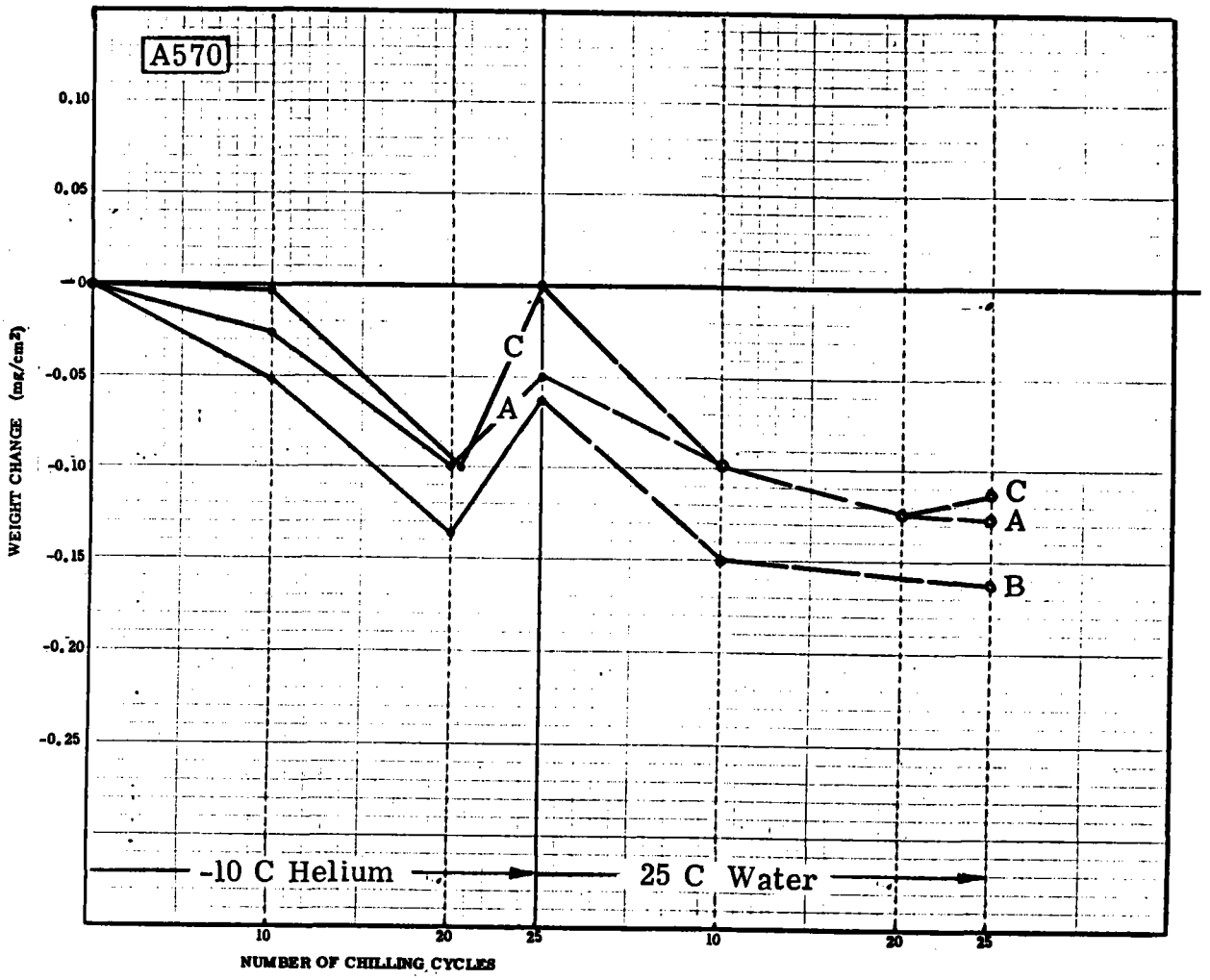

Figure G-3 Weight Change vs Number of Chilling Cycles for Thermal Cycling of A570

UNLIMITED RELEASE
INITIAL DISTRIBUTION

UC-62E

U. S. Department of Energy
Forrestal Building
1000 Independence Avenue, S.W.
Washington, D.C. 20585
Attn: H. Coleman
C. Carwile
K. Cherian
C. Mangold
M. Scheve
T. Wilkins

U. S. Department of Energy
P. O. Box 5400
Albuquerque, NM 87115
Attn: G. Pappas
J. Weisiger

U. S. Department of Energy
1333 Broadway
Oakland, CA 94612
Attn: R. Hughey
G. Katz
W. Lambert

University of California
Department of Electrical and
Computer Engineering
Davis, CA 95616
Attn: M. Soderstrand

University of Houston
Solar Energy Laboratory
4800 Calhoun
Houston, TX 77704
Attn: A. Hildebrandt

Aerospace Corporation
2350 El Segundo Blvd.
El Segundo, CA 90245
Attn: P. Munjal

ARCO Power Systems
7061 S. University, Suite 300
Littleton, CO 80122
Attn: F. Blake
D. Gorman

Arizona Public Service Company
P. O. Box 21666
Phoenix, AZ 85036
Attn: J. McGuirk
E. Weber

Babcock and Wilcox
91 Stirling Avenue
Barberton, OH 44203
Attn: G. Grant
I. Hicks
D. Smith

Badger Energy, Inc.
One Broadway
Cambridge, MA 02142
Attn: C. A. Bolthrunis

Bechtel Group, Inc.
P. O. Box 3965
San Francisco, CA 94119
Attn: G. W. Braun
J. Darnell

Black and Veatch Consulting Engineers
P. O. Box 8405
Kansas City, MO 64114
Attn: J. C. Grosskreutz
J. E. Harder

Boeing Engineering and Construction Co.
P. O. Box 3707
Seattle, WA 98124
Attn: R. B. Gillette

Burns & McDonnell
P. O. Box 173
Kansas City, MO 64141
Attn: M. Soderstrum

California Energy Commission
1111 Howe Avenue, MS-70
Sacramento, CA 95825
Attn: D. Pierson

Combustion Engineering, Inc.
1000 Prospect Hill Road
Windsor, CT 06095
Attn: C. R. Buzzuto

IEA/SSPS
c/o DFVLR
Apartido 19, Tabernas
Almeria, Spain
Attn: C. Selvage

El Paso Electric Company
P. O. Box 982
El Paso, TX 79946
Attn: J. E. Brown

Electric Power Research Institute
P. O. Box 10412
Palo Alto, CA 94303
Attn: E. DeMeo

Foster Wheeler Development Co.
12 Peach Tree Hill Road
Livingston, NJ 07039
Attn: S. F. Wu
R. Zoschak

Georgia Institute of Technology
Atlanta, GA 30332
Attn: C. T. Brown

Gibbs and Hill, Inc.
393 Seventh Avenue
New York, NY 10001
Attn: J. J. Jimenez

Institute of Gas Technology
Suite 218
1825 K. Street, N. W.
Washington, D. C. 20036
Attn: D. Glenn

Martin Marietta
P. O. Box 179, L#0450
Denver, CO 80201
Attn: T. Heaton
T. Tracey

McDonnell Douglas
5301 Bolsa Avenue
Huntington Beach, CA 92647
Attn: C. Finch
L. Glover

Olin Chemicals Group
P. O. Box 2896
Lake Charles, LA 70624
Attn: J. Morgan

Olin Chemicals Group
120 Long Ridge Road
Stamford, CT 06904
Attn: F. N. Christopher
L. C. Fiorucci

Pacific Gas and Electric Company
3400 Crow Canyon Road
San Ramon, CA 94526
Attn: H. E. Seielstad

Pacific Northwest Laboratories
P. O. Box 999
Richland, WA 99352
Attn: B. Johnson
S. Hauser

Public Service Company of New Mexico
P. O. Box 2267
Albuquerque, NM 87103
Attn: A. Akhil

Rockwell International
Energy Systems Group
8900 De Soto Avenue
Canoga Park, CA 91304
Attn: T. Springer
A. Ullman

Solar Energy Industries Association
1156 5th Street, NW
Suite 520
Washington, D.C. 20005
Attn: C. LaPorta

Solar Energy Research Institute
1617 Cole Boulevard
Golden, CO 80401
Attn: J. Anderson
M. Murphy
L. Shannon

Southern California Edison
P. O. Box 800
Rosemead, CA 92807
Attn: J. N. Reeves
P. Skvarna
R. W. Williamson

Stearns-Roger
P. O. Box 5888
Denver, CO 80217
Attn: W. R. Lang

Stone & Webster Engineering Corporation
P. O. Box 1214
Boston, MA 02107
Attn: R. W. Kuhr

Westinghouse Electric Corporation
Advanced Energy Systems Division
P. O. Box 10864
Pittsburgh, PA 15236
Attn: J. R. Maxwell

D. G. Schueler, 6220
J. V. Otts, 6222
R. S. Claassen, 8000; Attn: D. M. Olson, 8100
A. N. Blackwell, 8200
D. L. Hartley, 8300
C. S. Selvage, 8000A
R. J. Gallagher, 8124
M. E. John, 8125
J. Kraabel, 8132
R. L. Rinne, 8220
L. Gutierrez, 8400; Attn: R. A. Baroody, 8410
A. C. Schuknecht, 8420
H. Hanser, 8440
J. F. Barham, 8460
J. B. Wright, 8450
A. C. Skinrood, 8452
D. N. Tanner, 8452
W. G. Wilson, 8453
J. B. Woodard, 8454
Publications Division 8265, for TIC (27)
Publications Division 8265/Technical Library Processes Division, 3141
Technical Library Processes Division, 3141 (3)
M. A. Pound, 8424, for Central Technical Files (3)